AZƏRBAYCAN RESPUBLİKASI ELM VƏ TƏHSİL NAZİRLİYİ
AZƏRBAYCAN DÖVLƏT NEFT VƏ SƏNAYE UNİVERSİTETİ

MINISTRY OF SCIENCE AND EDUCATION
REPUBLIC OF AZERBAIJAN
AZERBAIJAN STATE UNIVERSITY OF OIL AND INDUSTRY

“NEFTİN, QAZIN GEOTEXNOLOJİ PROBLEMLƏRİ VƏ KİMYA”
ELMİ-TƏDQİQAT İNSTİTUTUNUN

ELMİ ƏSƏRLƏRİ

SCIENTIFIC PROCEEDINGS

SCIENTIFIC RESEARCH INSTITUTE

“GEOTECHNOLOGICAL PROBLEMS OF OIL, GAS AND CHEMISTRY”

VOLUME 23 Number1

BAKU-2023

ISSN 2218-5054

Contents

Formation conditions of the deep structure and hydrocarbon potential of the South Caspian oil-gas province and the Persian Gulf

R.Y. Aliyarov, B.S. Aslanov, F.B. Aslanzadeh, A.V. Bagirli
[a]Scientific Research Institute "Geotechnological Problems of Oil, Gas and Chemistry", Dilara Aliyeva str.227, Baku AZ1010, Azerbaijan

Abstract
The distribution of huge hydrocarbon (HC) deposits on Earth is mainly observed in the junction zones of large tectonic elements. Similar regions are the Persian Gulf basins, Alaska, Venezuela, South Caspian province, etc. From the point of view of the global tectonics theory, oil formation occurs in the subduction zone of the lithospheric plates as a result of sublimation and thermolysis of substances carried into the ocean together with oceanic sediments. For the first time, without any evaluation, this idea was expressed by H. Hedberg in 1970. Later, this possible mechanism of oil formation at the level of general quantitative calculations was continued by O. G. Sorokhtin, S. A. Ushakov, V. V. Fedinsky, A. A. Abidov, A. V. Bally, V. P. Gavrilov, L. I. Lobkovski, V. E. Khain and others.
The Persian Gulf and the South Caspian Sea are areas where huge hydrocarbon deposits are collected. Hydrocarbon deposits are located where foreland seas overlap the former Gondwana margins: Mesopotamian fore depression (MFD) in the Persian Gulf, Pirallahi-Kelkor in the South Caspian. In addition, it is found in the northern peripheries of the active seismic zones of the Persian Gulf and the South Caspian: The Zagros fold system in the Persian Gulf and the Absheron-Balkhan uplift zone in the South Caspian.
These strips are also the richest oil and gas regions. Is this a coincidence or is it related to the geological evolution of the region? What is the nature of these unique deposits? Where did the oil come from, when, where and how did it move to its current layers? The article is devoted to answering such questions based on the analysis of existing geological and geophysical material.
Keywords: Persian Gulf, South Caspian, province, geodynamics, seismic geodynamics, physiographic model, Alpine-Himalayan seismic belt, segment, Arabian plate, Cambrian basement.

Keywords:.
*Corresponding author: Tel.: +994702292969
E-mail r.aliyarov@asoiu.edu.as

1. Introduction.

Based on the analysis and comparison of limited literature published on different websites at different times and by different authors, a "genetic link" (formation from the same source) has been established in the hydrocarbon composition of the South Caspian Persian Gulf. 2,3,18].
When people talk about the "black gold" of the world, the Persian Gulf comes to mind, which has about 70 billion tons of oil and 20 trillion recoverable hydrocarbon reserves. Calculations by researchers [9÷11] show that according to the model of organic oil and gas formation, the Persian Gulf reserves could produce no more than 7.5 billion tons of oil, which is less than 5% of geological oil. This factor indicates the absence of a single oil source of the Persian Gulf and South Caspian oil fields and the abiogenic nature of the oil reserves of the studied provinces.

The oil and gas provinces of the South Caspian megadepression and the Persian Gulf are elements of a single seismic geodynamic block clearly delineated by the modern seismic geodynamic map (Fig. 1, A and regional physiographic models Fig. 1, B). Geological and geophysical materials taken mainly from websites: tectonic, topographic-geodesy, physical, structural maps of different horizons, physiographic and seismic geodynamic models of different years, deep geological and geophysical sections, earthquake catalogs, etc. it supports the joint exploration of the South Caspian and the Persian Gulf.

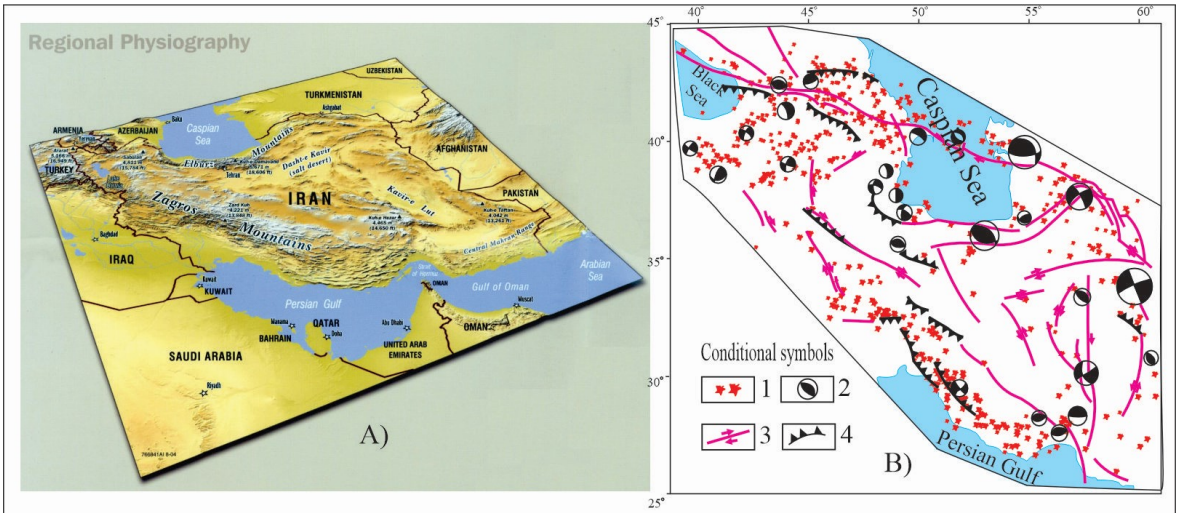

Figure 1. Physical-geographic geodynamic 3D model of the study area (A) and location map of deep-focus earthquake epicenters (B)

Fig. 1. A) Modern seismic geodynamics of the studied region; B) detailed digital (electronic) map (3D relief model). Conventional signs: 1 – earthquake epicenters, 2 – earthquake histograms (compression area is shown in black, extension is shown in white), 3 – transform faults, 4 – thrust sections. Image taken from http://old.ifz.ru/tecton and http://www.nationalsecurity.ru, modifications made by B.S. Aslanov.

2. The role of geodynamics in the formation of modern tectonics.

Located between the large Eurasian and Arabian lithospheric plates, the studied region is limited to a seismically active zone. The zone belongs to the Caucasian segment of the Alpine-Himalayan seismic belt (AHSB) and is characterized by a sharp contrast and intensity of magmatic processes, unusually high tectonic and geodynamic activity, mobility, migration, a wide network of multidirectional faults, minerals, including hydrocarbons.

The formation of the AHSB is related to the collision of the Arabian and Central Iranian plates. The segment covering Central Iran, Zagros, Makran and South Caspian is located east of the northern edge of the Arabian plate [4÷6]. The probable continuation of the northern branch of Neotethys is the Central Iranian microcontinent. It is characterized by Precambrian metamorphic basement and Vendian-Triassic platform cover. In the east, the meridional elongated Lut block stands out. According to the works [2÷15], the geodynamic evolution of this region is directly related to the north-eastern displacement of the Arabian plate, which began in the Mesozoic and continued throughout the Oligocene to the early Miocene. As a result, the Iranian plateau and the Elbrus mountains were formed, and at the same time, central Iran was separated from the Caspian Paleoben. Deformed blocks in the area between the South Caspian and the Black Sea (Fig. 2, A and

B) as well as adjacent low-order tectonic elements within the Persian Gulf and South Caspian basin are also the result of this displacement. Shifting movements continue to this day to one degree or another. These maps clearly show blocks of different scales, deep faults and landslides, and the role they play in supporting the neotectonic environment. The main stages of the development of the main tectonic elements of the region were determined in the Mesozoic history under the conditions of the horizontal movement of the Eurasian and Afro-Arabian continental plates, during which the Tethys paleocean water area gradually decreased until it completely disappeared.

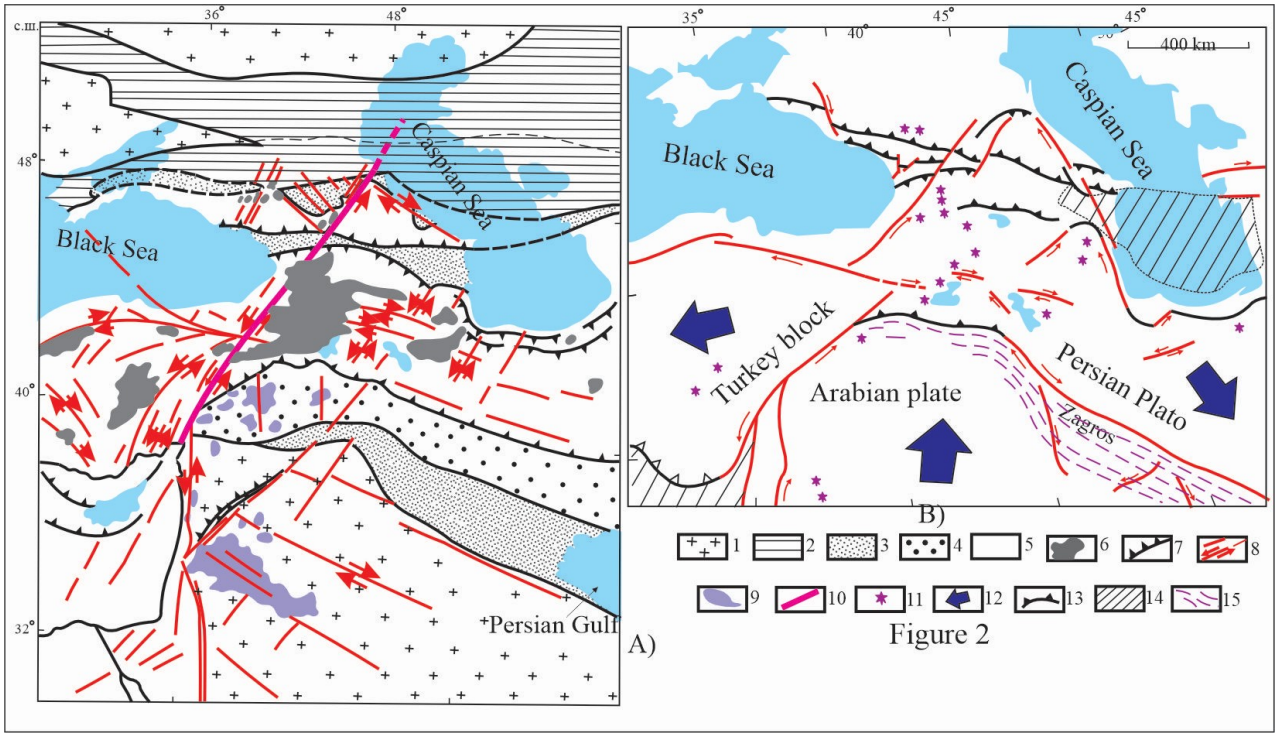

Figure 2

Fig. 2. A) Modern structural-geodynamic scheme (according to N.V. Koronovsky [7]) and B) fundamental tectonic features of the studied region (L.S. Smith-Roche [2]). Conventional signs: 1 – Precambrian plates, 2 – Epipaleozoic plates, 3 – advanced and intermountain plates, 4 – Submerged part of the Arabian plate, 5 – Main directions of relative movement of the Earth's crust (geoblocks, Alpine fold structures: a- proposed by the author of this article, b- proposed by the author of the works [7]), 6 – area of distribution of collision volcanism (Late Miocene-Anthropocene), 7 – impact force of geoblocks and main (main) directions, 8 – landslide faults and other faults (arrows relative shows movement), 9 – basaltic volcanism of the Arabian plate (mainly Quaternary), 10 – Agrahan-Tbilisi-Levantine left-lateral slip zone, 11 – collision zone volcanoes, 12 – oceanic crust, 13 – Zagros fold zone. The scheme was corrected by B.S. Aslanov.

Based on the general regularities of tectonic and magmatic evolution, it was determined that passive continental margin (PCM) conditions exist in this region in the Mesothetis. This region is the region where the PCM shelf is under the continental crust. The storage of most of the hydrocarbon resources in the PCM has been repeatedly noted by geologists A.I. Konyukhov, L.E. Levin, B.E. Khain, B.A. Sokolov, R.G. Garetsky, S.A. Ushakov and others. According to the data, 7/8 of all identified oil and gas reserves are linked to the PKM; only 1/8 of these reserves fall on the active continental margins (ACM). The ACM is formed where the oceanic crust sinks under the continent.

The complete closure of the Mesozoic Tethys Ocean occurs in the Cenozoic era, and subduction processes continue to this day in varying degrees in a number of places, for example, in the northern part of the South Caspian Sea (the Pre-Caucasus-Turkmen transform fault, as well as in the north of the Persian Gulf (the Zagros Mountains)). The periphery of the Tethys paleocean is regionally rich in oil and gas [16÷18]. The oil and gas provinces of the South Caspian and the Persian Gulf are located within its borders. The northeastern edge of the African-Arabian plate collided with the Iranian plate during the Cenozoic. The intense subsidence of this area of the Earth's crust is the result of the compression of the island arc systems of the southwestern periphery of the Tethys Ocean to the edge of the platform. The largest hydrocarbon reserves are concentrated in the layers existing on the edges of the continents during the closing of the oceans, primarily in the Jurassic and Cretaceous sediments, as well as in the oil and gas zones of the Persian Gulf during the Paleozoic (Permian).

Oil and gas basin of the Persian Gulf (OGBPG).

One of the unique regions of such a junction is the sedimentary basin of the Persian Gulf. 54% of all hydrocarbon reserves of the planet are concentrated here, and there are also more than twenty huge deposits, each of which has a reserve of 1 billion tons of oil and 1 trillion cubic meters of gas. The oil and gas basin of the Persian Gulf is located on the northern periphery of the Arabian-Nubian shield, in the junction zone with the folded mountainous Alpine belt. It is bounded to the north and northeast by the Zagros and Eastern Taurus structures, to the south and southwest by the South Arabian epirift uplift known as the Hadramaut Plateau, and to the west by the Aleppo uplift and folds. The eastern boundary of the basin is the obduction ophiolite complex of Oman structurally, the Persian Gulf basin is divided into a platform part corresponding to the northeastern slopes and foreland areas of the Arabian-Nubian shield (Fig. 3); Pre-Tharus dislocation zone, Mesopotamia and South Oman depressions. In the northern and eastern peripheral regions of the Arabian Craton, the thickness of the sediment cover varies from 1-2 to 4.5-7 km. In the Mesopotamian fore depression, the thickness of sedimentary rocks increases sharply, reaching 15 km in flooded areas. At the Oligocene and Miocene border, the closure of the Tethys Ocean took place, which was accompanied by the uplift of mountain fold belts (Zagros, Elburz and Caucasus mountains), and the formation of large and small foothills and inter-algae depressions. The tectonic events that led to the closure of the Tethys Ocean created a favorable structural background for the generation and accumulation of hydrocarbons, especially at several margins of the former passive Gondwana. Strong tectonic dislocations and the accumulation of sediment masses in large areas accelerated the processes of oil and gas formation in the sediments that once formed on the continental slopes and their foothills in the peripheral regions of the Tethys Ocean. Flows of liquid and gaseous hydrocarbons migrated from areas affected by folding and metamorphism to ancient shelves, where they filled traps and reservoirs formed in earlier stages. However, only the hydrocarbon deposits formed on the southern edge of the disappeared ocean have remained to this day (Persian Gulf and South Caspian). The Persian Gulf, with a basin depth of no more than 100 m, occupies the vast plain of the Tigris and Euphrates rivers adjacent to it from the northwest, as well as the coastal plains bordered by the gulf. The total area of the basin is 5063 thousand km^2, of which 4853 thousand km^2 is on land and only 213 thousand km^2 is in water. OGBPG is one of the five richest basins in the world (along with the Western Siberian, Western Canadian, Orinoco and North Caspian basins). It is unique in terms of primary recoverable hydrocarbon reserves (current reserves are more than 150 billion tons of standard fuel, 92-107 billion tons of oil, 50 trillion m^3 of gas;

primary hydrocarbon reserves are more than 180 billion tons, including oil - more than 130 billion tons, gas - 52 billion m^3). Estimates of Saudi Arabia's current oil and condensate reserves reach 36-42 billion tons. The oil reserves of Kuwait, Iran and Iraq are unique. In Iran, and in recent years in Qatar, large gas reserves have been discovered both on the coast and in the Gulf. A boundary (platform layer) type basin was formed at the junction of the ancient Arabian continental margin with the AHSB. The basin has a platform southwest and orogenic northeast frame and is sharply asymmetric. It covers the Mesopotamian fore depression and the gently sloping part of the Arabian plate - the pericraton, separated from the edge of the Arabian shield by a zone devoid of hydrocarbon deposits.

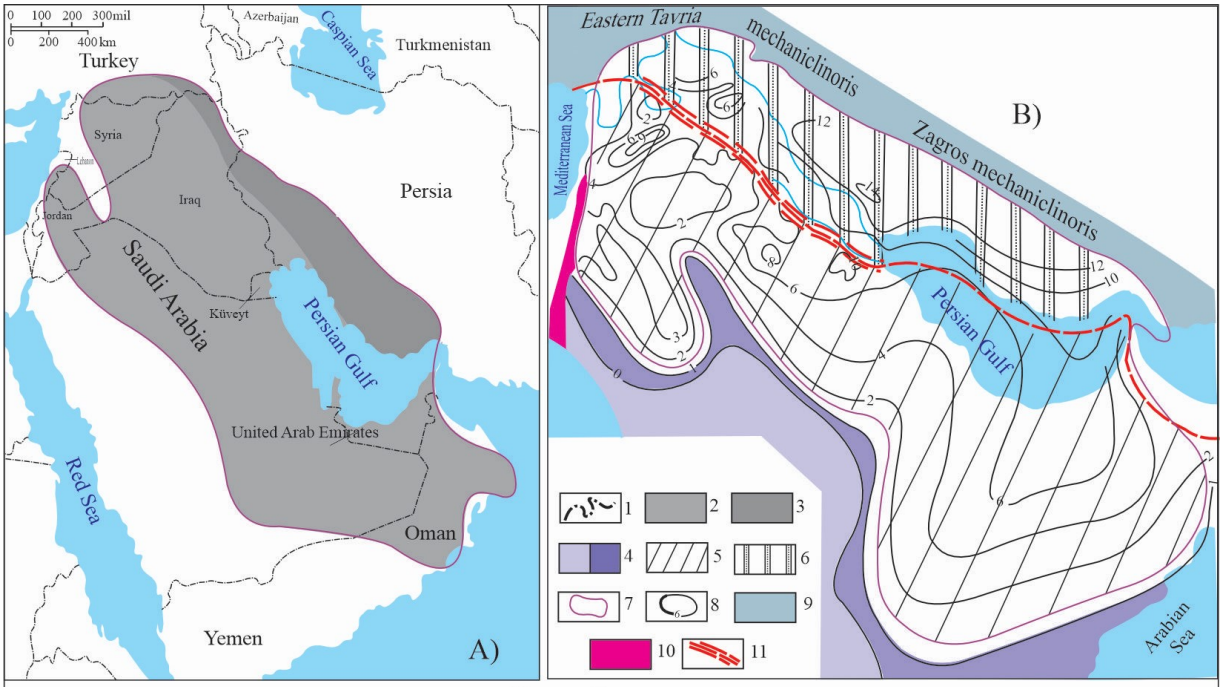

Figure 3

Fig. 3. A) Overview map of the sediment cover of the Persian Gulf; B) isopach map. Conventional signs: 1 – interstate boundary lines, 2 – saturated oil and gas area, 3 – rich oil and gas area, 4 – Nubian-Arabian shield under a thin sedimentary cover, 5 – Arabian plate, 6 – Predzagorsky regional depression, 7 – Persia boundary of the Gulf basin, 8 – isopachs of sediment cover, 9 – meganticlinoriums of Eastern Taros and Zagros, 10 – Eurasian sea rift, 11 – faults separating geotectonic areas within the Persian Gulf basin. The figure modified by B.S. Aslanov, retrieved from http://www.ipages.ru, http://www.nationalsecurity.ru.

Since the beginning of the 40s of the last century, OGBPG has taken a leading position among the oil-producing regions of the world. It is a province with a unique concentration of oil and gas (Fig. 3, A). It includes the Arabian Peninsula and Bahrain, Jordan, Iraq, southwestern Iran, Qatar, Kuwait, UAE, Oman, Saudi Arabia, most of Syria, and southeastern Turkey.

The province is bounded by a large asymmetric heterogeneous depression formed during long-term subsidence at the junction of the African-Arabian platform with the AHSB (Fig. 3, B). The main tectonic elements are the Arabian plate and the Mesopotamian fore depression, which form the platform and fold parts of the basin, respectively. The basis is Archaeo- Proterozoic. The maximum thickness of the sedimentary cover is 10-12 km in the deepest part of the basin, and the minimum

thickness is 2-2.5 km along its periphery (areas adjacent to the Arabian-Nubian shield) represented by sediments from the Vendian to the Quaternary.

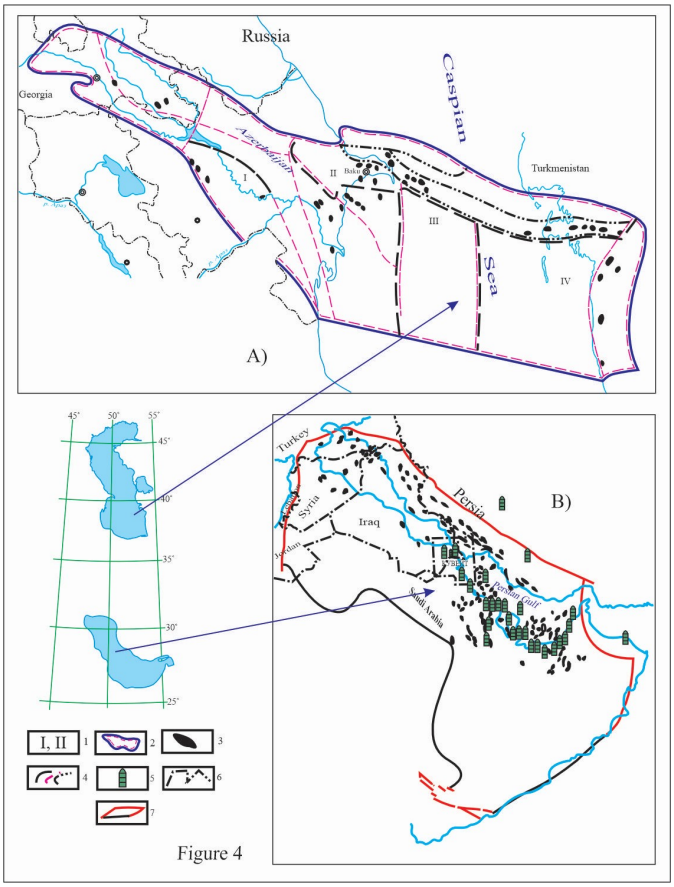

Fig. 4. Oil and gas provinces: A) South Caspian; B) Persian Gulf. Conventional signs: 1 – oil and gas fields within the South Caspian province: I – Gobustan-Kur, II – Absheron-Balkhan, III – Central-South Caspian, IV – Western Turkmen; 2 - the border of the South Caspian oil and gas region, 3 - oil and gas structures, 4 - the border of oil and gas regions, 5 - large oil refineries, 6 - interstate border lines, 7 - the border of the Persian Gulf oil and gas basin. The figure edited by B.S. Aslanov, taken from http://www.biblioclub.ru (Persian Gulf) and http://www.mining-enc.ru (South Caspian Oil and Gas Province).

In the geological structure of OGBPG, the Paleozoic section is mainly sandy-clay. Permian, Mesozoic, Paleogene and Lower Miocene deposits are mainly represented by carbonate rocks. Neogene-Quaternary sediments are dominated by terrigenous type, among which the Middle Miocene salt layers with a thickness of up to 1 km are distinguished. The main oil and gas complexes are Permian, Upper Jurassic, Lower Cretaceous, Upper Cretaceous and Oligocene-Lower Miocene. Mesozoic deposits make up 3/4 of the proven oil reserves, the main gas reserves are concentrated in Permian and Cenozoic rocks. Most of the deposits are concentrated in the eastern sediments of the Arabian plate (Basra-Kuwait basin, Gaza structural terrace, Rub-al-Gali basin) and the Mesopotamian fore depression. Hydrocarbon accumulations in the Mesopotamian fore depression are mainly confined to the Oligocene-Lower Miocene (Asmari formation) and Upper Cretaceous limestones at a depth of 0.2-2.7 km. The main proven hydrocarbon reserves in the basin are located at a depth of 1-3 km. The maximum oil and gas reserves are in the 2-3 km

interval, and the maximum gas reserves are in the 3-5 km depth. Structure-type deposits are mainly multi-layered. Sediments in the Mesopotamian fore depression are confined by high-amplitude anticlinal folds running from northwest to southeast along the Zagros fold system (Fig. 4, B). A significant part of oil and gas fields is limited by salt diapirism structures. The density of oil is 820-990 kg/m3, medium density oil (855-860 kg/m3) prevails. More than 1,500 trillion cubic feet of gas reserves have been discovered in Permo-Triassic carbonates sealed by thick Triassic anhydrites in the Zagros fold system (southwest Iran), southern Persian Gulf (Iran, Qatar and Abu Dhabi) and Saudi Arabia. Oil production began in the Middle Jurassic in extensive depositional areas, with the main formation phase occurring locally in the early Middle Cretaceous. Large volumes of oil and gas have accumulated in several major regional arches and salt structures belonging to the Zagros fold system. Some of the gas was lost during folding because some anticlines collapsed. Other parts of the gas have passed into the undamaged anticlinal traps along with the light oil.

South Caspian Oil and Gas Province (SCOGP).

The region includes Azerbaijan, Eastern Georgia and Western Turkmenistan. The location and orientation of the oil structures is similar to that of the Persian Gulf (Fig. 4, A and B). Its area is more than 200 thousand km^2. It includes the Ghabirri-Acinohur, Yevlakh-Aghjabedi, Gobustan-Absheron, Lower Kura depression, the South Caspian oil and gas regions and the oil and gas regions of Western Turkmenistan. The most popular deposits are: Samgori-Patardzeul, Naftalan, Muradkhanli, Kirovdagh, Neftchala, Sabunchu-Balakhani, Ramani, Bibi-Heybat, Binagadi, Neft Dashlari, Shahdeniz, Azeri, Chirag, Umid, Nebitdag, Gorgandag, Okarem, etc. The first oil fields (Balakhani-Sabunchu-Ramany, Çelakan) were discovered in the middle of the 19th century. Systematic exploration of oil and gas began in the 20s of the 20th century. Tectonically, the SCOGP was formed as a result of regional subsidence associated with the main geostructural elements of the Zagros Mountains, the Dasht-Lut block, and the Turanian plate with similar geodynamic regimes, and is divided into a series of depressional structures: The Kura intermountain depression, consisting of the Upper, Middle and Lower Kura depressions, the South Caspian depression, which includes the South Absheron, Pahlavi-Gorgan and Elbrus depressions, and the West Turkmen, Balkhan-Kyzylgum depressions in the east. From the north, this system of depressions is adjacent to Shamakhi-Gobustan and Absheron depressions, which are other components of the megadepression (Fig. 4, A). The northern and northeastern border of the SCOGP is represented by the megathiclinorium of the Greater Caucasus and its underwater extension, the Absheron-Pribalkhan anticlinal uplift zone, and the south is the megathiclinorium of the Lesser Caucasus. In the east, the megadepression is adjacent to the Dziryulski outcrop of the crystalline basement. In different parts of SCOGP, the crystal foundation tends to collapse step by step. It is located at a depth of 4-6 km in the western part, 16 km in the Middle Kura Basin, up to 20 km in the Lower Kura depression, and more than 25 km in the South Caspian Basin. A gradual subsidence of the pre-Alpine substrate also occurs in the transverse direction from the Greater and Lesser Caucasus to the central part of the SCOGP. Among the special depressions are the buried uplifts of the pre-alpine bedrock and the deep faults that limit them. There is no doubt that the Lower Pliocene deposits in the South Caspian are productive layers, but the formation and migration of oil is still a matter of debate among researchers. The main petroleum complex of the South Caspian oil and gas province, which includes almost all proven oil and gas reserves, is the Pliocene "Productive" layer (PL) and its counterpart "red" layer (RL) in Western Turkmenistan.

The PL is represented by the alternation of sandy reservoirs and clayey caps with a total thickness of 1.2 to 4 km, and the RL is represented by a monotonous alternation of sandy-silty and clayey rocks with a thickness of 0.8-3 km. In the western part of the province, in the subsidence part of the Lesser Caucasus (Ganja oil and gas region) and in eastern Georgia, there is no MF, hydrocarbon deposits were discovered in the Maykop range deposits of the Oligocene-Lower Miocene and in the Upper Cretaceous rocks. The main areas of oil and gas production are limited to the Absheron-Balkhan oil and gas region of Azerbaijan and Western Turkmenistan. PL reservoirs in Absheron Peninsula deposits are represented by well-sorted quartz sands with high porosity and permeability values. Up to 40 oil and gas fields have been identified on the border. The deposits are bounded by brachyanticlinals, intensively dissected by numerous faults of varying amplitudes, compounded by mud volcanism.

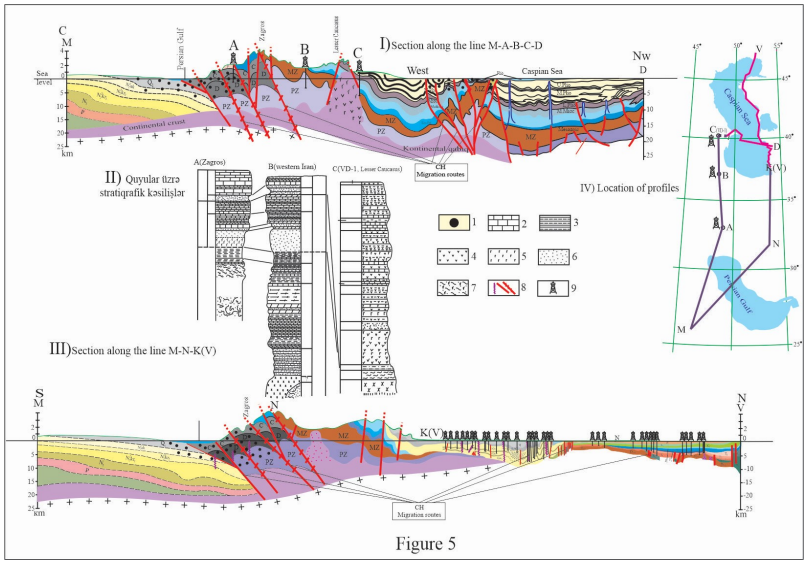

Figure 5

Fig. 5. Results of interpretation of geological and geophysical material in the study area: I) and III) geological sections; II) Comparison of stratigraphic sections from wells located on both sides of the Main Zagros (A and B) and in the Lesser Caucasus (C, SG-1); IV) location of profiles. Conventional signs: 1 – oil field (condensate or gas), 2 – limestones, 3 – clays, 4, 5 – volcanic rocks, 6 – coarse sands, 7 – fragments of intrusive rocks, 8 – deep faults and volcanoes, 9 – wells . The figure was compiled by B.S. Aslanov.

The composition of gas condensate is dominated by light hydrocarbons, the amount of paraffin, tar and asphaltenes is insignificant. The density of the condensate is 729-813 kg/m^3, which means that the oil here is lighter than in the Persian Gulf. The Western Turkmen depression is the eastern part of SCOGP. It is filled with very thick Mesozoic and Cenozoic sediments. Only within the Western Turkmen basin, the thickness of the Neogene reaches 5-6 km. The oil and gas fields of the Western Turkmen Basin are associated with the sandy-clay layers of the Pliocene. Based on the theory of lithospheric plates, by comprehensively analyzing the geodynamic transformations, geological evolution, tectonic structure of the main lithospheric plates of SCOGP and OGBPG (geoblocks of the Alpine fold belt), comparing the oil and gas bearing structures, and as a result of the interpretation of existing geological and geophysical materials, we made profile sections in two directions reflecting their structures, which have determined the geological structure of the research region. (Fig. 5, I and III). These sections clearly show both the deep and surface tectonic setting of

both provinces. At this time, a structural-tectonic discrepancy is clearly observed. It should be noted that for the Caspian region, we used existing sections collected from multiple wells. (Fig. 5, IV, red color). The surface geological structure of the Persian Gulf (oil and gas formations) is complicated by the Zagros Mountains, and the South Caspian Sea by the Absheron-Balkhan uplift zone

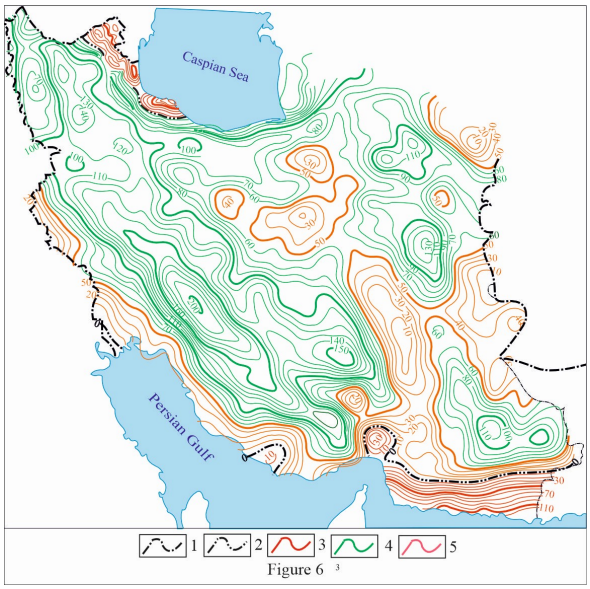

Fig. 6. Structural map of the Moho boundary (thickness of the Earth's crust). The map was compiled based on seismological data [11]. Conventional signs: 1 – isohypses along the ceiling of the Moho boundary, 2 – interstate boundary.

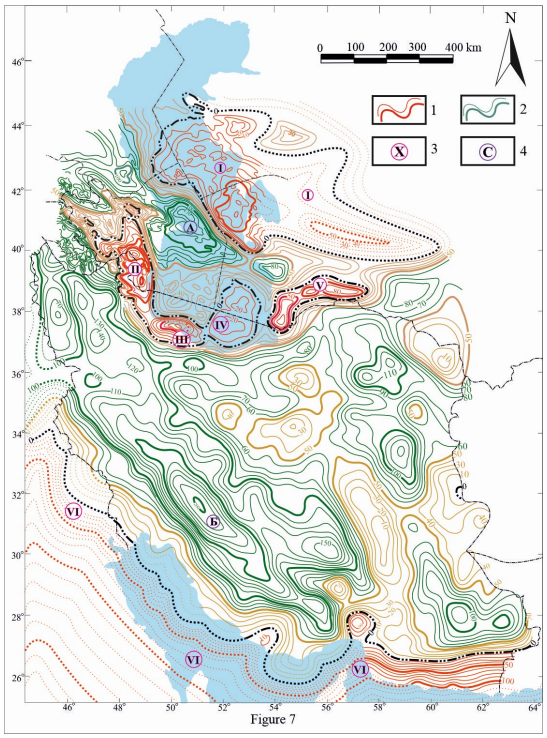

Fig. 7. Gravimetric map [14] (σ=2 300 kg/m^3 on Bouguet anomaly of Iran) Conventional signs: 1 – boundary, 2 – zero isolates; Gravity field isolates: 3 – positive, 4 – negative and 5 – up to 50 mGal. The figure was edited by B.S. Aslanov.

This complexity was formed on the basis of compression and extension processes that continue to this day [9÷11]. In other words, the Absheron-Balkhan region, characterized as the development zone of the Paleogene-Miocene fold, is tectonically complicated by the Alpine syncline, the Epihersin platform. The Zagros fold zone is complicated by a complex of Paleozoic, Mesozoic and Cenozoic sediments formed as a result of the collision of the Arabian and Eurasian plates at the end of the Mesozoic and the beginning of the Cenozoic. In addition, the Absheron threshold and the Zagros mountain move over deep depressions. Absheron is in the Pirallahi-Kalkor depression (PKD), and the Zagros mountain is in Mesopotamia. In addition, the Zagros Mountains are characterized with a ridge, which is 1300 km long, 250 km wide and 4.5 km high. This ridge, extending up to 350 km, consists of a thick (up to 8-10 km) sedimentary cover. By folding the passive edge of the Arabian plate, it gradually changes its movement from northwest to northeast. At the same time, the similar structures of the Persian Gulf and South Caspian oil fields are also clearly expressed. This once again shows that these oil provinces were formed in a single Paleo-Tethys basin, but were divided into Persian Gulf and South Caspian provinces in the process of evolution. On the schematic structural map (Fig. 6) along the surface of the Moho boundary, compiled from the seismological data of the last 50 years (the catalog of earthquakes that occurred in the studied region), two depressions located almost perpendicular to each other are distinguished: 400 km long and 56 km deep in the Zagros Mountains and northeast of the Iranian Plateau, and about 200 km long and 48 km deep within the Dasht-Lut block. Figure [15]. Between them, in the central part of Iran, at a depth of 40 km, there is a plain known as the "Iranian Plateau". Further north, in the South Caspian Sea, upwelling with an amplitude of 6 km is determined at a depth of 36 km. The depression in the northeastern Zagros Mountains and the Iranian Plateau is probably a component of the MFD and the depression within the Dasht-Lut block may represent a new tectonic unit in deep layers. (The Dasht-Lut block has an inversion structure). The geological structure of the South Caspian Sea in the deep layers is presented as a superimposed depression limited by the transitional tectonic regime (from the orogenic Alpine geosyncline and the Epihersian platform).

In order to analyze the obtained understanding of the geological structure of the studied region, the gravimetric map of Iran taken from [15] and added by us (Fig. 7) was analyzed. This map is based on a similar map within the oil and gas provinces of the South Caspian (Fig. 8). According to the gravimetric map of Iran, a gravity low with an intensity of up to 300 mGal extends along the Zagros Mountains. The geological interpretation of this minimum suggests that it is related to a deep tectonic structure. Because its parameters, that is, its size and intensity, cannot be explained by the folded structure of the Zagros and the structure of the Iranian plateau. In addition, the minimum in plan corresponds to the northeastern part of the MFD.

According to V. Zabanbark [19], the MFD is in the outer part of the Arabian platform, adjacent to the Zagros structure, the northeast side is protruding, and the southwest side is flat and has an asymmetric structure. The most intensive formation of tectonic structures is recorded in the parts that stretch parallel to the Zagros fold structure and develop relatively narrow folds. The depression itself was formed in the last stage of the Alpine folding. The dominant shear dislocations in the Zagros have caused disharmonic compression of the sedimentary layers. In the MFD, hydrocarbons are accumulated in Upper Cretaceous, Lower Cretaceous, Upper Jurassic, Middle Jurassic, and Upper Permian rock formations. Mesopotamia is the largest depression in the considered region, covering a distance of 2.5 thousand km from northwest to southeast. The width of the depression varies from 180 to 400 km, and the total thickness of the sediment cover in the most tilted (axial) part reaches 14-15 km. In the late Precambrian and Paleozoic periods, the ancient continental

masses existing in the territory of Iran were an integral part of the Arabian continental platform. Their separation in the Permian or Triassic indicates a belt of Zagros ophiolites bounded by the main Zagros fold line. PKD can be attributed to a similar geotectonic transformation. The MFD was formed at the border of the Arabian Platform with the Iranian Plateau. The PKD is bounded by the Epichersian Platform to the northeast and the Alpine fold to the southwest. But paradoxically, the dimensions of these bends are not comparable. It turned out that both depressions overlapped in older sedimentary basins. This is due to the fact that two tectonic stages are distinguished in the geodynamic evolution of the Persian Gulf and South Caspian basins: Initially, the region developed as part of the continental margin of Gondwana until it collided with the Eurasian continent. As a result of this collision, the Zagros zone and later the MFD, which once overlapped with the deep sea structure, were formed. In parallel, a similar evolution took place on the northern edge of the seismodynamic block, resulting in the formation of the PKD.

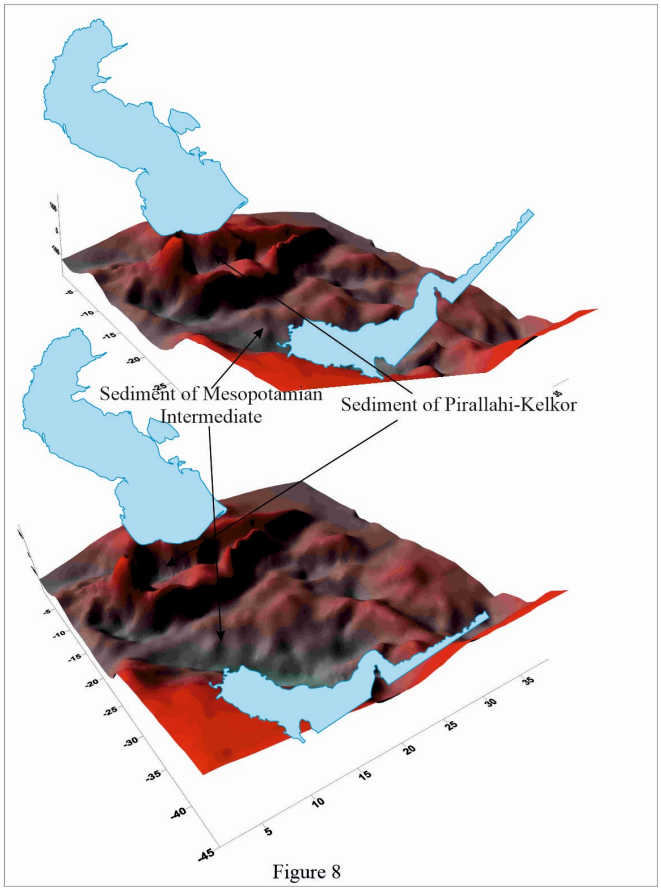

Fig. 8. Gravimetric map of the studied region (σ=2 300 kg/m^3 according to Bouguet anomaly). Conventional signs: 1- positive and 2- negative isolates of the gravity field, 3- gravity maxima: I - Middle Caspian-Turan, II - Mughan-Karabakh, III - Safiudrudsky, IV - South Caspian and V - North Kopetdag; 4 – gravity minima: A – Northern Absheron and B – Northern Zagros. The figure was compiled by B.S. Aslanov

We assume that this also explains the deep structure of OGBPG and SCOGP.

Comparing the gravimetric map (Fig. 6) and the structure map of the Moho surface, we assume that the deepest part of the MFD is located further north than previously thought, i.e. beneath the Zagros

Mountains. Just like in PKD. Thus, the deepest part is located in the northeast under the Absheron-Balkhan threshold.

This idea is well illustrated by the 3D model of the gravimetric map (Fig. 8) that we made using the SURFER program. Here you can clearly see how OGBPG and SCOGP are located: The tectonic structure of both provinces appears to be inversion, i.e. they are located in deep "basins". However, the formation of hydrocarbon potential is probably related to completely different geotectonic conditions, especially tectonic units. In our opinion, the hydrocarbons of the Persian Gulf are formed in the MFD, this process is influenced by the dynamics of three tectonic units: Arabian Plate, Dasht-Lut Block and Iranian Plateau. The hemechanism occurs as follows: when the Arabian plate moves in the northeast direction, the southeastern edge touches the Dasht-Lut block, and the block turns counterclockwise and compresses the Iranian plateau. As a result of these compressive forces, favorable conditions for the formation of hydrocarbons are created in the deep interior of the MFD. Subsequently, again due to these compressional forces, the hydrocarbons formed migrate along existing deep fractures into the oil and gas bearing structures of the Persian Gulf.

In the South Caspian, this process has a slightly different character. We assume that hydrocarbons in the South Caspian Sea are formed in the PKD depression as a result of the influence of geodynamic forces of three tectonic units: Iranian plateau, Dasht-Lut block and Turanian plate. The geomechanical process here is also related to the Arabian plate mechanism, that is, when the Arabian plate moves in the northeast direction, the southeast edge touches the Dashta-Lut structure, and the block passes through the Kopetdag mountain layer and touches the Turan plate, and the plate turns counterclockwise and compresses the South Caspian geosyncline. Since the deep structure of the South Caspian Sea is represented by an arcuate uplift along the Moho boundary, the center of compressive forces falls on the PKD. As a result, the deep underground of the PKD creates favorable conditions for the formation of hydrocarbons. Later formed hydrocarbons migrate along existing deep fractures into the oil and gas bearing structures of the South Caspian region. The movement of geodynamic blocks in the study area was studied and analyzed in [4], which is consistent with the geomechanism described above.

3. Conclusion

Thus, based on existing geological and geophysical data, earthquake catalogs, comparative analysis of hydrocarbon composition and evolutionary processes of geotectonic formation, we briefly analyze the structural-tectonic structure, seismogeodynamic characteristics, and come to the following conclusion:

1. The hydrocarbon potential of the OGBPG and SCOGP is connected with the rift system of the Tethys Ocean and is formed in the PCM. The migration and generation routes in the study area are as follows:

– in the South Caspian oil and gas region, in the pre-Caucasian-Turkmen fault and inside the Persian Gulf;

– In the deep fractures of the Zagros support system;

2. Oil and gas provinces of the Persian Gulf and South Caspian have existed as PCM during most of their evolution (late Paleozoic to Miocene), but the northern part (South Caspian Sea) has been more active than the south (Persian Gulf);

3. After the collision of two opposing edges of the Tethys, they turned into modern basins typical of the fusion zones of ancient cratons with younger mountain-fold structures;

4. Most of the accumulation of hydrocarbons in these provinces is the result of degassing that occurred during the second stage of basin evolution, when the folds (MFD and AKP) overlapped at the edges of the former Gondwana;
5. From the point of view of the global tectonics theory, the formation of oil occurred as a result of sublimation and thermolysis of substances carried along with ocean sediments to the subduction zone of lithospheric plates;
6. The difference of the geological and tectonic structure of the named provinces is related to the seismic geodynamic evolution.

Conflict of interest

The authors declare that they have no conflict of interest in relation to this research.

4. References

1. Mamedov P.Z. 2010. Tectonotypes of paleobasins of the Caucasus-Caspian region and the main stages of the evolutionary development of the South Caspian megabasin // Catalog of seismic forecast observations on the territory of Azerbaijan, Baku, pp. 127-139(in Russian).
2. Smith-Rouch L.S., 2006, Oligocene–Miocene Maykop/Diatom Total Petroleum System of the South Caspian Basin Province, Azerbaijan, Iran, and Turkmenistan: U.S. Geological Survey Bulletin 2201-I, 27 p.
3. Bordenave M.L**.** 2008. The origin of the Permo-Triassic gas accumulations in the Iranian Zagros Foldbelt and contiguous offshore areas: a review of the Palaeozoic petroleum system // Journal of Petroleum Geology. - Vol.31, № 1. - p.3-42: ill., tab. - Bibliog.: p.40-42.
4. Koronovsky N.V. 2006. Block dynamics in the territory of Eastern Anatolia, the Caucasus, Iran and Zagros according to GPS data, p.58 (in Russian).
5. A. Ghasemia, C.J. Talbotb. 2005. New tectonic scenario for the Sanandaj–Sirjan Zone (Iran). Journal of Asian Earth Sciences. p.1–11.
6. N. Ebadati, A. Adib. 2010. Geodynamics Evolution of the Oil Traps in Southern Regions of Zagros Due to Closing of Neotethy The st International Applied Geological Congress, Department of Geology, Islamic Azad University - Mashad Branch, Iran, 26-28 April.
7. N. Quarrie. 2004. Crustal scale geometry of the Zagros fold–thrust belt. Iran, Journal „Structural Geology“, p.519–535.
8. M. Bahrami, M. Sahraeyan, K. Taherkhani. 2012. Microfacies and Sedimentary Environments of Dalan Formation at Surmeh Mountain, Folded Zagros Zone, Southwestern Iran International Journal of Basic and Applied Sciences, 1 (4) p.380-389.
9. H. Shafaii Moghadam, J. Robert Stern, M. Rahgoshay. 2010**.** The Dehshir ophiolite (central Iran): Geochemical constraints on the origin and evolution of the Inner Zagros ophiolite belt. Geological Society of America Bulletin, p.1516-1547.
10. V. Regard, D. Hatzfeld, M. Molinaro, C. Aubourg, R. Bayer, O. Bellier5, F. Yamini-Fard, M. Peyret and M. Abbassi. 2010. The transition between Makran subduction and the Zagros collision: recent advances in its structure and Active deformation. "Special Publication - Geological Society of London 330", p 41-64.
11. F. Mouthereau, O. Lacombe, J. Vergés. 2012. Building the Zagros collisional orogen: Timing, strain distribution and the dynamics of Arabia/Eurasia plate convergence Contents lists available at SciVerse ScienceDirect “Tectonophysics 532–535” p.27–60.

12. L. Csontos, Б. Sasvбri, T. Pocsai, L. Kysa, Azad T. Salae, A. Ali. 2012. Structural evolution of the northwestern Zagros, Kurdistan Region, Iraq: Implications on oil migration. GeoArabia, v. 17, p.81-116.
13. J. Vergés, E. Saura, E. Casciello, M. Fernàndez, A. Villaseñor, I. Jiménez-munt, D.García-Castellanos. 2001. Cambridge University Press. Geol. Mag.: p.1-23.
14. A. Zamani, N. Hashemi 2000. A comparison between seismicity, topographic relief, and gravity anomalies of the Iranian Plateau. Department of Geology, College of Sciences, Shiraz University, Shiraz, Iran."Tectonophysics 327" p.25-36.
15. M. Mokhtari, A. M. Farahbod, C. Lindholm, M. Alahyarkhani, H. Bungum. 2004. Iranian Int. J. Sci. 5(2), p.223-244.
16. Zabanbark A., Kazmin V.G., Lobkovsky L.I.. 2010 Ancient continental margins and a comparative analysis of their oil and gas potential. Reports of the Academy of Sciences, 2010, volume 431, no. 3, pp. 365–368.
17. Zapivalov N. P. 2008. Offshore oil - a new milestone for humanity // Oil industry. No. 6. p.54–58.
18. Khain V. E., Sokolov B. A. 1994. The role of fluid dynamics in the development of oil and gas basins // History of oil in sedimentary basins. Ed. B.A. Sokolova. M.: Moscow State University Publishing House.
19. A. Zabanbark. 2011. Distribution of large oil and gas fields - a source of hydrocarbon degassing (Persian Gulf basin). Moscow, Proceedings of the Institute of Oceanology named after. P.P. Shirshov, RAS, pp. 133-138.

Prediction of porosity in mountain rocks

R.Y. Aliyarov[a], J.N. Aslanov[a], R.K. Mekhtiyev[a], N.R.Agazade[b], V.M. Durmushov[a]

[a]Scientific Research Institute "Geotechnological Problems of Oil, Gas and Chemistry", Dilara Aliyeva str.227, Baku AZ1010, Azerbaijan
[b] Department of Industrial Machines, Azerbaijan State Oil and Industry University, 20 Azadlig Avenue, Baku AZ1010, Azerbaijan

Abstract: Porosity is one of the most important parameters when studying groundwater. The porosity parameter is used to estimate storage and travel times in aquifers and aquifers. Studies use seepage theory to determine the thickness and variation of rocks. The percentage of voids in a substance is called its porosity. To calculate porosity, it is needed to divide the volume of voids by the material's total volume to get the percentage.

***Keywords**:* porosity, mountain rocks, displacement modulus, leakage theory, seepage theory.
*Corresponding author: Tel.: +99451-790-99-79
E-mail address: camaladdin.aslanov@asoiu.edu.az

1. Introduction

Over the past few years, progress in predicting the elastic properties of porous materials over the entire porosity range has been closely related to the power law empirical relationship of Phani and Niyogi.

$$\mu = K_p \left(1 - \frac{P_{\mu o}}{P_{\mu w}}\right)^f \quad (1)$$

where μ-is the effective displacement modulus of the material with porosity p, K_p-modulus of displacement of solid material, $P_{\mu w}$- porosity where the effective displacement modulus becomes zero and f - is a parameter that depends on the atomic morphology of the porous material and the geometry of the pores [1]. These parameters are from Wagh et al. mentioned by [2]. A fit of experimental data to equation 1 is often obtained when $P_{\mu w}$ = 1 [1, 3], and this fit does not accurately explain the data. In recent experimental work, either $P_{\mu w} \equiv 1$ is better used [4–6] or the linearized model (f ≡ 1) [7] by Lam et al., where $P_{\mu w}$ is assumed to be the initial dust porosity.

2. Methodological part

The empirical relationship shown in equation is the same as any collation theory equation for the behavior of shear modulus with displacement and porosity. In addition, the capability of the seepage model for the displacement modulus of porous materials will be demonstrated and the results discussed. The particles of porous materials are made of powders and their size and shape can vary significantly. Different pores can be achieved by changing technological parameters such as external pressure, temperature or time during powder solidification. Compaction begins just by touching the dust particles and progresses to low porosity with the formation and growth of pores between the particles. As a result of the subsequent closing of the pore channels, the process of pore elimination occurs. Usually three different porosity ranges can be defined, for example Danninger et al. [8] observed the following porosity ranges for sintered iron:

1. porosity ≤ 3%: fully isolated pores with almost spherical or elliptical shape
2. porosity ≥ 20%: complex-shaped fully interconnected pores
3. when the porosity is between 3% and 20%, both isolated and interconnected pores are present in varying amounts.

This indicates that dust coupling is a contact problem generally studied by seepage theory [9]. According to the seepage theory, there is a critical volume fraction, called n_c - seepage threshold, at which the solid phase forms a continuous network covering the entire system. The geometrical, physical and mechanical properties of the system at and above the leakage limit behave as follows.

$$\mu \propto (n - n_c)^f \quad n \geq n_c \quad (2)$$

Here, μ -is the special one under study, and n is the volume fraction of the solid body. Material and f is the theoretically predicted critical exponent for the object under study. The theory of seepage shows that the values of critical exponents are universal, that is, they do not depend on the structure and geometric properties of the system, but on the size of the problem. On the other hand, the value of the seepage threshold depends significantly on the structure. Experimental values of the seepage threshold in the three-dimensional (3D) structure were as high as 0.06% vol and 60% vol.

When porosity is used instead of powder volume fraction in Equation 2,

$P_{\mu o}$ = 1−n,

$$P_{\mu o} \leq P_{\mu w} \text{ for } \mu \propto (P_{\mu w} - P_{\mu o})^f \quad P_{\mu o} \leq P_{\mu w} \text{ for} \quad (3)$$

the formula is obtained. Thus, equation 3 must satisfy the con boundary. E = E_0; At $P_{\mu o}$ = 0, it can be expressed as follows:

$$\mu = K_p \left(1 - \frac{P_{\mu o}}{P_{\mu w}}\right)^f \quad \text{for } P_{\mu o} \leq P_{\mu w} \quad (4)$$

3. Results and discussion

The resulting equation (4) is the same as equation (1). Leakage theory predicts f = 2.1 for the displacement modulus in 3D [12]. This value is determined for a finite cluster or when all dimensions of the system tend to infinity. In a continuum, however, this universal behavior is often affected by the finite size of the system, thus yielding a characteristic rather than a critical one. This means that the characteristic index for all porous materials should be almost the same. On the other hand, the value of the filtration threshold depends on the size, shape, distribution and preparation method of the powder. Here, experimental data from different sources are combined in an attempt to obtain a wider range of porosity for the material under study, thus leading to unrealistic values of the pc compatibility parameters.

If we apply the obtained equation in determining the porosity of formation rocks in the case that the oil is full of product:

$$\mu(X) = K_p\left(\frac{P_{\mu w} - P_{\mu o}}{P_{\mu w}}\right)^2$$

Data statistics are given in table 1:

Table 1.

Kp	Pμ Dry	Pμ Water	Pμ Oil
0.01	28.00215609	28.06902632	28.06138849
0.02	18.56439005	18.62162559	18.61655848
0.04	12.30750149	12.35400671	12.35064508
0.05	10.78207279	10.82522932	10.82228368
0.07	8.831781873	8.870116177	8.86770254
0.12	6.415595781	6.446916571	6.445162308
0.24	4.253301857	4.277029962	4.275866145
0.26	4.056133838	4.07908848	4.077978524
0.28	3.88174283	3.903999858	3.902937545

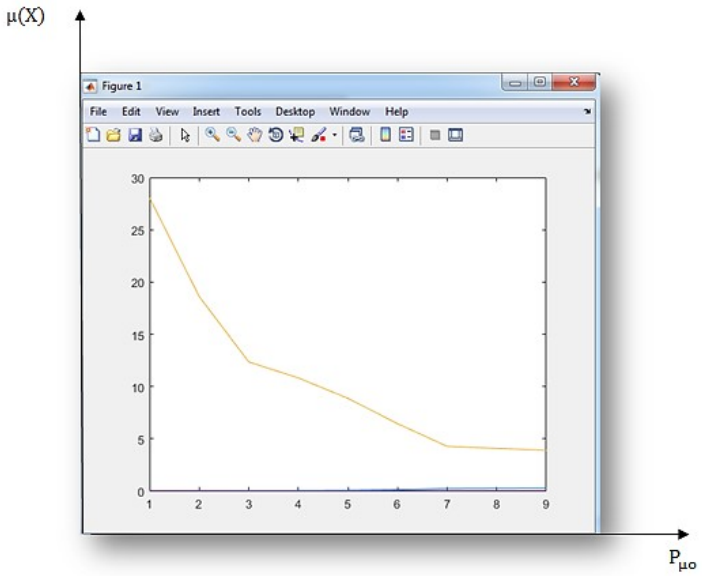

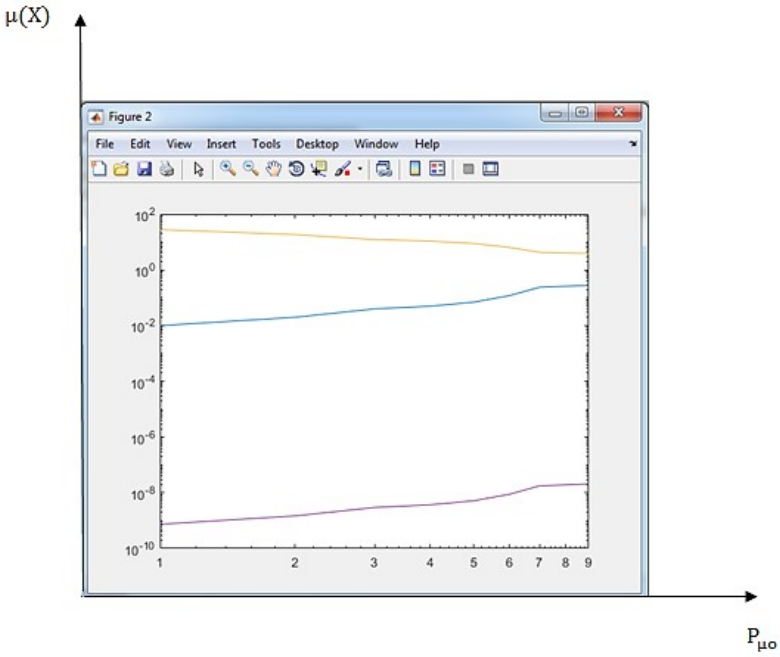
μ(X)
Figure 2
File Edit View Insert Tools Desktop Window Help
10^{2}
10^{0}
10^{-2}
10^{-4}
10^{-6}
10^{-8}
10^{-10}
1 2 3 4 5 6 7 8 9
$P_{\mu o}$

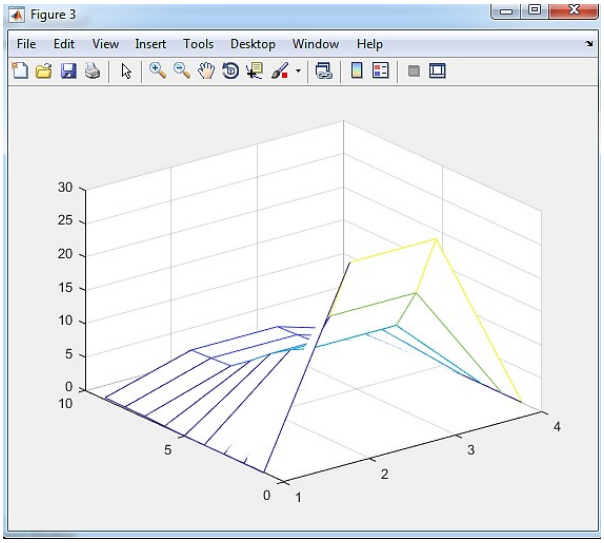
Figure 3
File Edit View Insert Tools Desktop Window Help
30
25
20
15
10
5
0
10
5
0
1
2
3
4

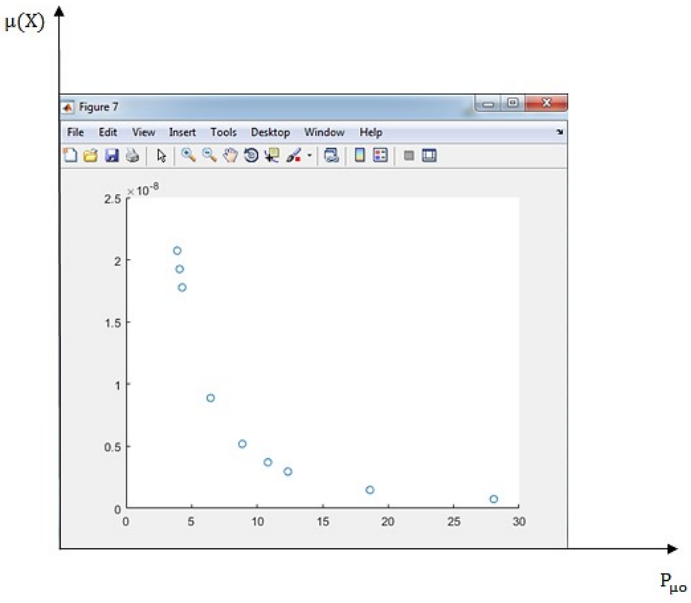
μ(X)
Figure 7
File Edit View Insert Tools Desktop Window Help
$\times 10^{-8}$
2.5
2
1.5
1
0.5
0
0 5 10 15 20 25 30
$P_{\mu o}$

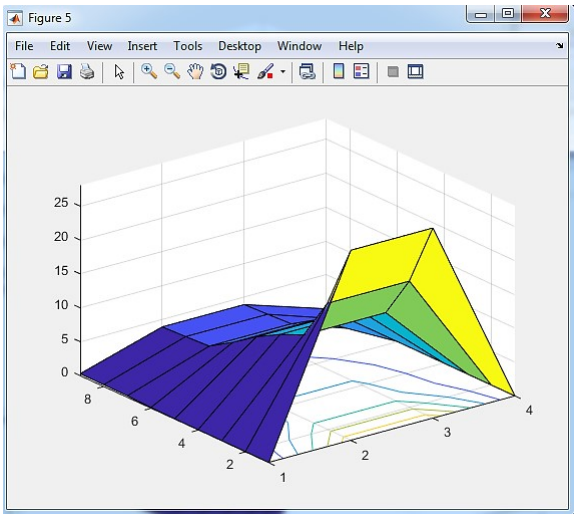

Kp	PW	PO	EX
0,01	28,06902632	28,06138849	7,4043e-10
0,02	18,62162559	18,61655848	1,4809e-09
0,04	12,35400671	12,35064508	2,9617e-09
0,05	10,82522932	10,82228368	3,7022e-09
0,07	8,870116177	8,86770254	5,1830e-09
0,12	6,446916571	6,445162308	8,8852e-09
0,24	4,277029962	4,275866145	1,7770e-08
0,26	4,07908848	4,077978524	1,9251e-08
0,28	3,903999858	3,902937545	2,0732e-08

KP(1-(PO/PW) EX=KP*(1-(PO/PW))^2;
>> KP = 0.01;
>> PO = 28.06138849;
PW = 28.06902632;
>> EX=KP*(1-(PO/PW))^2;
>> plot(PO,PW)
>> EX=KP*(1-(PO/PW))^2;

3. Conclusion

1. Fuzzy set theory in predicting rock porosity has 4 times more accuracy than classical methods.

2. The values of the porosity of the displacement modulus in dry, water and oil environments were determined by the theory of fuzzy sets.

Conflict of interest

The authors declare that they have no conflict of interest in relation to this research.

4. References

1. Aslanov, J.N., Mammadov, G.A., Ahmadov, A.H.S.A., Huseynli, Z.S., Hamidova, G.A., Agazade, N.R. Calculation of sealing efficiency in cylindrical parts// International Journal on Technical and Physical Problems of Engineering, 2023, Vol. 15, Issue 3, pp. 247–255.
2. Aslanov, J.N., Mammadov, G.A., Mamedov, V.T. Stress-Strain State of Sealing Rubber Membranes at Large Deformations// Journal of Applied Mechanics and Technical Physics, 2020, Vol. 61, Issue 2, Pages 286 - 291. https://doi.org/ 10.1134/S0021894420020157
3. Kırkayak, Y., Ayyıldız T. Porosity prediction based on conventional and geostatistical image computation, Lower to Middle Eocene siliciclastics in the Tuz Gölü Basin (Central Anatolia, Turkey) // Marine and Petroleum Geology, 2022, Vol. 143, pp. 102-240. https://doi.org/10.1016/j.marpetgeo.2022.105821
4. Zhu, W., Wu, S., Yin, Z., Han, T., Wu, Y., Liu, Y., Feng, W., Luo, Y., Cao, C. Braided river delta outcrop architecture: a case study of Triassic Huangshanjie Formation in Kuche depression, Tarim Basin, NW China // Petroleum Exploration and Development, Vol. 43, Issue 3, June 2016, Pages 528-536. https://doi.org/10.1016/S1876-3804(16)30062-3
5. Mineo, S., Giovanna, P. Nondestructive rock porosity estimation by InfraRed Thermography applied to natural stones. Construction and Building Materials, Vol. 342, Part B, 1 August 2022, 127950. https://doi.org/10.1016/j.conbuildmat.2022.127950
6. Michael, J.H., Fabian B.W., Heng, Z., Tao, X., Griffiths, L., Andrea, A.V., Vaire, E. The tensile strength of volcanic rocks: Experiments and models // Journal of Volcanology and Geothermal Research, Vol. 418, October 2021, 107348. https://doi.org/10.1016/j.jvolgeores.2021.107348
7. Reimus, P.W., Callahan, T.J., Ware, S.D., Marc, J.H., Counce, D.A. Matrix diffusion coefficients in volcanic rocks at the Nevada test site: Influence of matrix porosity, matrix permeability, and fracture coating minerals. Journal of Contaminant Hydrology, Vol. 93, Issues 1–4, 15 August 2007, Pages 85-95. https://doi.org/10.1016/j.jconhyd.2007.01.017
8. Rashid, F., Glover, P.W.J., Lorinczi, P., Collier, R., Lawrence, J. Porosity and permeability of tight carbonate reservoir rocks in the north of Iraq. Journal of Petroleum Science and Engineering, Vol. 133, September 2015, Pages 147-161. https://doi.org/10.1016/j.petrol.2015.05.009
9. Bollerman, T., Yuan, T., Kulenkampff, J., Stumpf, T., Fischer, C. Pore network and solute flux pattern analysis towards improved predictability of diffusive transport in argillaceous host rocks. Chemical Geology, Vol. 606, 20 September 2022, 120997. https://doi.org/10.1016/j.chemgeo.2022.120997
10. Yanbin, C., Enlong, L., Yanyang, Y., Huiwu, L., Peishuai, C. A binary-medium-based constitutive model for porous rocks // International Journal of Rock Mechanics and Mining Sciences, Vol. 164, April 2023, 105345. https://doi.org/10.1016/j.ijrmms.2023.105345
11. Xianglan, L., Cai, L., Shaowen, L., Xudong, L. Thermal Properties of Evaporitic Rocks and their Geothermal Effects on the Kuqa Foreland Basin, Northwest China // Geothermics, Vol. 88, November 2020, 101898. https://doi.org/10.1016/j.geothermics.2020.101898
12. Bertrand, L., Geraud, Y., Diraison, M. Petrophysical properties in faulted basement rocks: Insights from outcropping analogues on the West European Rift shoulders // Geothermics, Vol. 95, September 2021, 102144. https://doi.org/10.1016/j.geothermics.2021.102144

Application of nanotechnology for regulation the rheophysical properties of water-oil emulsions

H.Kh.Malikov, A.A.Suleymanov, E.A.Mirzayev

Research Institute "Geotechnological Problems of Oil, Gas and Chemistry", ASOIU, 20 Azadlig Ave., Baku, AZ-1010 Azerbaijan

Abstract.

In this paper, application of nanoparticles for regulation of rheophysical properties of water-oil emulsions were considered.

The effect of Al_2O_3 nanoparticles on the rheological characteristics of the emulsion is shown by the results of laboratory experimental research.

As a result of the application of the proposed technology for downhole oil demulsification, well productivity increased.

Keywords: water-oil emulsions, rheology, nanotechnology, Al_2O_3 nanoparticles, downhole demulsification.

*Corresponding author. Tel.:+994506447759

E-mail address: h.malikov@gpogc.az

1. Introduction

The problem of stable water-oil emulsions separation is very important for oilfields at the final stage of well production.

The well production process has a considerable influence on the cost of oil production. Therefore, an individual approach to the problem of deemulsification is necessary not only for different fields, but even for each wells [1].

The process of splitting water-oil emulsions depends on many factors: oil properties (oil density, viscosity, component composition, etc.); properties of formation water (mineralogical composition); the presence of solid particles (clay, gum, etc.); the presence of natural emulsifiers and stabilizers, etc. [2-7].

Various methods of breaking water-oil emulsions are used: thermal, chemical reagents at high temperature, gravity separation (sedimentation), filtration separation, centrifugation, ultrasonic separation, electric effect, magnetic effect, etc.

The main method of field preparation of oil is thermochemical deemulsification and a lot of chemical reagents are used that reduce the surface tension between oil and water.

The modern synergetic approach to the oil demulsification process is based on the application of a combined physicochemical effect.

A promising and actual approach to increase the efficiency of the deemulsification process of highly viscous and stable water-oil emulsions is the joint application of nanotechnologies and physicochemical effects [8].

In this paper, application of Al_2O_3 nanoparticles for regulation the rheophysical properties of water-oil emulsions was considered.

2. Experimental Apparatus and Methodology

It is proposed to apply Al_2O_3 nanoparticles for water-oil emulsion separation. To this, nanoparticles are previously dissolved in a specific reagent.

Later, two test cells filled with 5% sulfate solution prepared in water were taken. 5% Al_2O_3 nanoparticles was added to one of the test cells. Both test cells were hermetically sealed and the contents were thoroughly mixed. Then, the mixture inside both test cells is separately added to equal amounts of emulsions taken from one well.

The mixture in the test cell with added Al_2O_3 nanoparticles separated for 3 min and the separation was observed by gas bubbles. In the second test cell, the separation time took several hours. It should be noted that the amount of oil released in the test cell with added nanoparticles is significant.

The reaction was carried out a second time, and at this time the composition of the mixture was taken in the following ratio: Al_2O_3 nanoparticles - 22.3% of composition; specific reagent 33.1%; H_2O was 44.6%. $6 \cdot 10^3$ g of specific reagent and $8 \cdot 10^{-6}$ m^3 of water were used for every $4 \cdot 10^3$ g of nanoparticles during the field experiment carried out.

As a result of the reaction, hydrogen release is observed at an intense rate. Then the resulting solution was added to the water-oil emulsion. As a result, the emulsion was separated in 5-10 minutes.

As a result of laboratory studies, the optimal component composition of the mixture was determined: 0.01% Al_2O_3 nanoparticles, 0.99% reagent.

The viscosity of oil and emulsions was determined by keeping the given temperature constant for 10 minutes using a rotary viscometer. The average value of the velocity gradient was 0.56 m/sec.

The dependence of the dynamic viscosity of emulsion and oil taken from well show on figure 1.

Due to the fact that the viscosity of the oil is smaller than viscosity of the emulsion, as a result of the application of the proposed methodology, the volume of produced oil increases.

Thus, the rheological characteristics of the viscometric studies conducted on the emulsion oil sample taken from the well allow us to conclude that adding 0.01% of Al_2O_3 nanoparticles, the viscosity of the studied system is significantly reduced and the emulsion, to the elements of which it is composed (water and to oil) is broke.

The effects of nanoparticles on the change of the oil structure were studied.

Processing of emulsion oils by the proposed method results to the transition of oil from non-Newtonian to Newtonian fluid character.

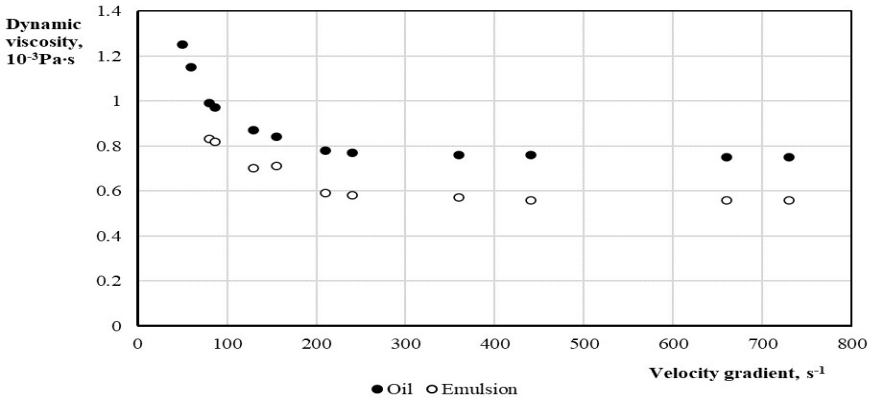

Fig.1. Dynamic viscosity of oil and emulsion (T=25°C)

3. **Field Case**

It is necessary to have information about the viscosity of degassed water-oil emulsions at different temperatures in the high dilution range (10-60%).

Let's analyze the effect of the proposed reagent on the viscosity of the water-oil emulsion.

Figure 2 shows the dynamic viscosities of the emulsions with different percentages of water and oil taken from well, as well as measurements of the viscosity of pure oil during decomposition by reagent and Al_2O_3 nanoparticles.

It can be seen that the presence of 5% water causes the viscosity of the break emulsion to decrease relative to the oil viscosity. The viscosity of water and 5% oil solution is already several cPs.

Figure 3 shows the measurements of the dynamic viscosity of the emulsion taken from the well until the demulsifier is introduced. The viscosity of the emulsion is significantly greater than the viscosities of water and oil. Comparisons of figures 2 and 3 show that the viscosity of the emulsion broken by the added reagent drops to the level of the comparable water viscosity. If we take into account that the produced liquid of well contains 60-80% water, it can be concluded that the fluid behaves like an ideal fluid.

Changing the rheological properties can result to an increase in liquid rate. However, maintaining the volume of injected gas at the previous level is accompanied by a decrease in liquid flow rate.

Thus, it is necessary to adjust the injected gas consumption to maintain the liquid rate of the well at a high level.

The effect of alkaline waste, dust and chemical preparation on the rheological properties of water-oil emulsion was studied. Figure 4 shows the dynamic viscosity of the emulsion taken from the well before and after the introduction of alkaline residue, as well as the dynamic viscosity of the combination of the emulsion with alkaline waste, aluminum powder and chemical preparation. It can be seen from the picture that the injection of alkali waste reduces the viscosity of the oil by half. The injection of Al_2O_3 nanoparticles dissolved in the alkali waste and the chemical preparation reduces the viscosity of the oil by four times.

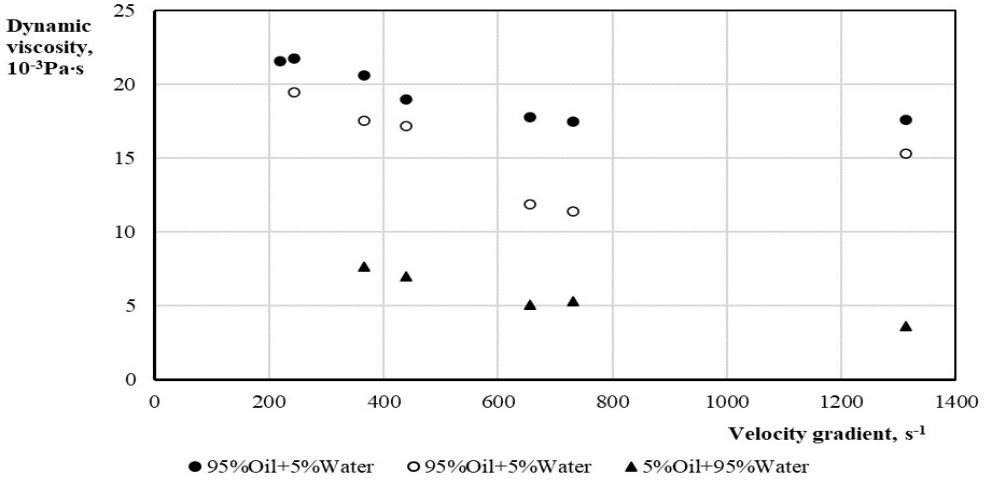

Fig.2. Dynamic properties of emulsions during decomposition.

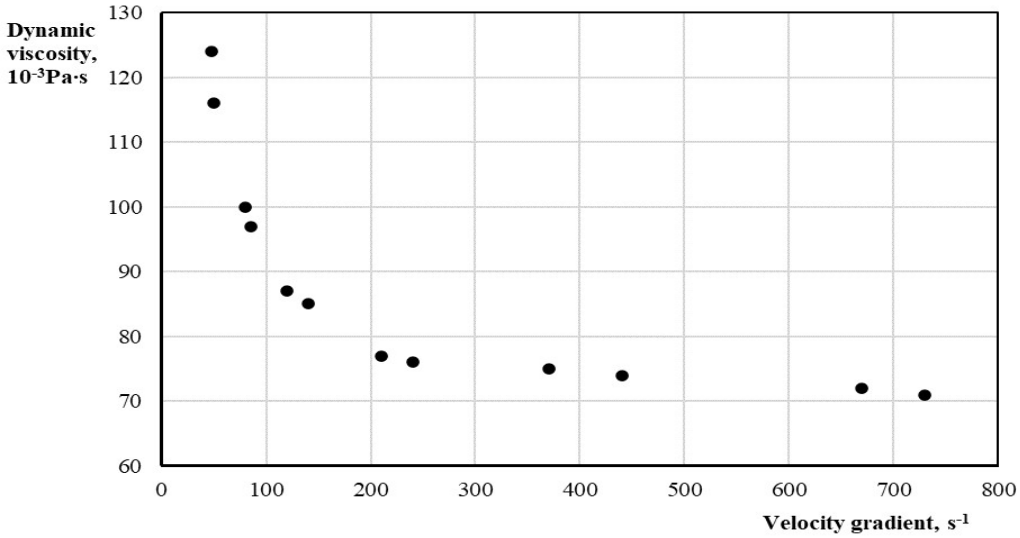

Fig.3. Viscosity of the emulsion.

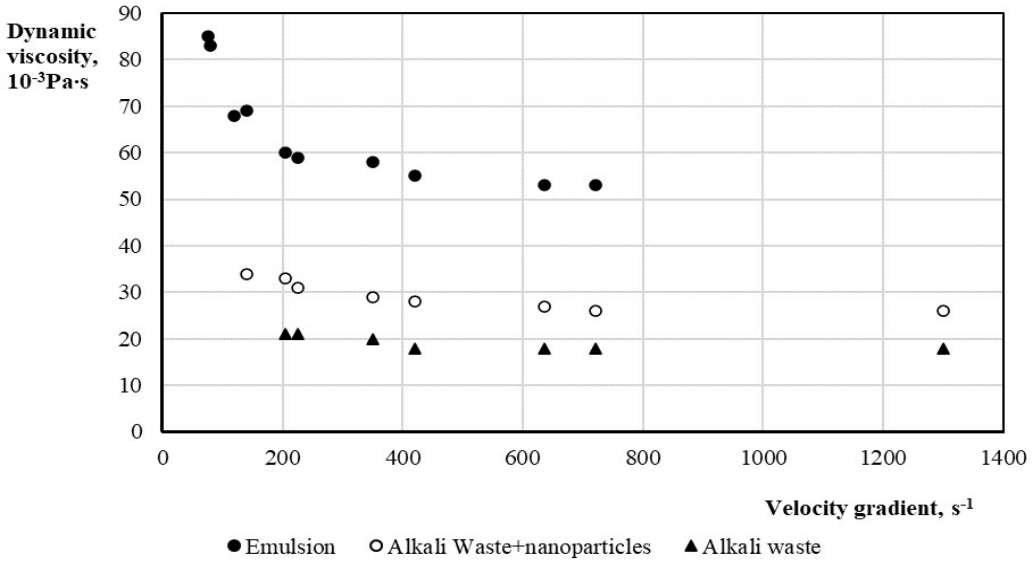

Fig.4. Effect of alkaline waste and nanoparticles on the dynamic viscosity of the emulsion

The developed technology for breaking water-oil emulsion with Al_2O_3 nanoparticles was tested in production well (table 1)

Table 1.

Change of parameters of a well during application of Al_2O_3 nanoparticles

Days	Method of influence	Pressure, bar	Liquid, t	Oil, t	Water, t	Oil fraction
1	Emulsion breaker	53				
2	Emulsion breaker	53				
3	Emulsion breaker	53	58	8	50	0.137931
4	Emulsion breaker	53	56	8	48	0.142857
1	Emulsion breaker+nanoparticles	53				
2	Emulsion breaker+nanoparticles	52	74	11	63	0.148649
3	Emulsion breaker+nanoparticles	51	70	10	60	0.142857
4	Emulsion breaker+nanoparticles	52				
5	Emulsion breaker+nanoparticles	52				
1	Nanoparticles	52	70	10	60	0.142857
2	Nanoparticles	53				
3	Nanoparticles	53	56	8	48	0.142857
4	Nanoparticles	55	55	8	47	0.145455
5	Nanoparticles	53	54	7	47	0.12963
6	Nanoparticles	53				
7	Nanoparticles	53	54	7	47	0.12963
8	Nanoparticles	53				
9	Nanoparticles	53	47	7	40	0.148936
10	Nanoparticles	53	61	9	52	0.147541
11	Nanoparticles	53	48	7	41	0.145833
12	Nanoparticles	53	46	6	40	0.130435
13	Nanoparticles	53	46	5	41	0.108696
14	Nanoparticles	53				
1	Emulsion breaker	52	58	9	49	0.155172
2	Emulsion breaker	52				
3	Emulsion breaker	47	59	8.8	50	0.149153
4	Emulsion breaker	48	60	8.8	50	0.146667
5	Emulsion breaker	48	59	8.5	50.5	0.144068
6	Emulsion breaker	48	58.3	8.3	50	0.142367
1	Emulsion breaker+nanoparticles	49	60	9	51	0.15
2	Emulsion breaker+nanoparticles	48	62	9	53	0.145161
3	Emulsion breaker+nanoparticles	49	63	8.8	54.2	0.139683
4	Emulsion breaker+nanoparticles	48	62	8.6	53.4	0.13871
5	Emulsion breaker+nanoparticles	48	64.4	9.02	55.38	0.140062
6	Emulsion breaker+nanoparticles	49	67	10.22	56.78	0.152537
7	Emulsion breaker+nanoparticles	49	70.2	10.44	59.76	0.148718
8	Emulsion breaker+nanoparticles	47.3	68	10.15	57.85	0.149265
9	Emulsion breaker+nanoparticles	49	71	8.325	62.675	0.117254
10	Emulsion breaker+nanoparticles	49	61	9	52	0.147541
1	Nanoparticles	49.4	60	9	51	0.15
2	Nanoparticles	51	57	8	49	0.140351
3	Nanoparticles	51.2	57	8	49	0.140351
4	Nanoparticles	52	57	7.4	49.6	0.129825

Application of offered nano-technology increase oil production by 25 tons in two weeks.

4. Conclusions

The influence of nanoparticles on the rheological characteristics of oil-water emulsions was shown.

A technology for downhole demulsification using Al_2O_3 nanoparticles has been proposed.

Application in an oil field showed the effectiveness of the proposed technology and increased the productivity of production wells.

Conflict of interest

The authors declare that they have no conflict of interest in relation to this research.

Acknowledgments: This work was supported by the Azerbaijan Science Foundation-**Grant AEF-MCG-2023-1(43)-13/07/2-M-07**

5. References

1. Mirzajanzadeh A., Hasanov M., Bahtizin R. Modeling of oil and gas production processes// ICR. Moscow. 2004.

2. Sun N., Shen L., Sun H., Hu J. pH Responsiveness of Microwave Polymer-Type Modified Magnetic Nanoparticles for Synergistic Emulsion-Breaking Effect on Thick Oil// SPE J. 28 (05): 2619–2628. 2023.

3. Mierez J., AlTammar M.J., Alruwaili Kh.M. Review of Recent Research Related to Ultrasonic Technologies for Well Productivity Enhancement// The 57th U.S. Rock Mechanics/Geomechanics Symposium, Atlanta, Georgia, USA, June 2023. ARMA-2023-0477.

4. Adewunmi A.A., Kamal M.Sh., Gbadamosi A., Patil Sh. Natural Extracted Waste Materials for Breaking Crude Oil Emulsion// SPE Western Regional Meeting, Anchorage, Alaska, USA, May 2023, SPE-213007-MS.

5. Adewunmi A.A., Kamal M.Sh., Gbadamosi A., Patil Sh. Demulsification of Heavy Crude Oil Emulsion Driven by Natural Materials // Middle East Oil, Gas and Geosciences Show, Manama, Bahrain, February 2023, SPE-213624-MS.

6. Vu H.H., Rangponsumrit M., Hoang N.D. et al. Identification of Downhole Emulsion in a Light Oil Development and Demulsifier Injection for Increasing Production.// International Petroleum Technology Conference, Bangkok, Thailand, March 2023, IPTC-22754-EA.

7. Alamoudi S.M., Alwani M.A. Enhancing Upstream Oil Water Separation Efficiency Through Microwave Energy//. ADIPEC, Abu Dhabi, UAE, October 2022, SPE-211297-MS.

8. Sun N., Chang X., Sun H. et al. Study on the Coupling Effect of Microwave and Magnetic Nanoparticles on Oil Droplet Coalescence.// SPE J. 27 (05): 3051–3062. 2022.

Influence of transverse magnetic field on the process of sand settlement in water

A. M. Mamed–Zade, H.Kh. Malikov, T.H. Malikov

Scientific Research Institute of Geotechnological Problems of Oil, Gas and Chemistry, ASOIU, 20 Azadlig Avenue. Baku, AZ-1010 Azerbaijan

Keywords: transverse magnetic field, magnetic field strength, solid particles, sand, test tube.
*Corresponding author. Tel.: +994 506761101
E-mail address: a.mammadzade45@gmail.com

1. Introduction

During the oil production process, a constant transverse field is use to increase oil productivity. This field also affects the movement of the mixture of gas - water - oil - solid particles in the production wellbore. In this case, complex processes of interaction of each fragment with others occur, one of which is the precipitation of solid particles from the mixture. Rock fragments that make up the reservoirs of the oil reservoir represent the main part of the solid particles: sand, clay, mica, etc.
Modeling the process of flow movement in a production wellbore and studying, the influence of the sand fraction on this process is very difficult. The complexity increases due to the creation of a stable emulsion, through which it is difficult to observe the process of emulsion separation and sedimentation of solid particles.
Therefore, decided to follow world practice, in which the behavior of a complex system considered as a set of simple ones. Examine them separately and establish the areas of magnetic fields that lead to a positive result in each case. By comparing the intervals of successful magnetic field strengths of each fraction, the most acceptable one for the system selected.
Numerous studies show that the magnetic field has a significant effect on clay particles; however, plugs in the wellbore contain a large percentage of sand fractions. Therefore, it decided to study the influence of a magnetic field on the process of sand deposition, since clay particles relatively well carried away by an upward flow of liquid.
In our studies, transverse constant magnetic fields were use. It is known, that an alternating magnetic field with an oscillation frequency of 50 Hz does not produce a noticeable effect, while a constant magnetic field increases oil recovery from a porous medium. Therefore, in all subsequent studies a constant magnetic field was use.

2. Methodological part

In this work, we study the effect of a transverse magnetic field in the strength range H = 0 – 176 000 A/m on the process of sedimentation of sand particles in water.
For this purpose, an experimental setup was created, consisting of an electromagnet, in the core of which a 78 mm long slot was cut. Since the results of studies of the transverse and longitudinal magnetic fields were supposed to be compared in the future, the magnetic field intensity gradient in both cases should have been the same. This was achieved by placing the test tube with the sample in the same gap of the electromagnet. In the case of a transverse magnetic field, the magnet poles were located in the horizontal plane; with a longitudinal field – in the vertical plane. Using a power source, a direct current of various voltages supplied to the electromagnet and the magnetic field

strength determined using a Teslameter at three points A;B;C. İn the figures, the magnetic field strength corresponds to the value in the middle of the gap - along the axis of the test tube (point C in Fig. 1).

The experiments were carried out as follows. A test tube 77.5 mm high was filled with 50% sand and 50% water; the test tube was tightly sealed to prevent water evaporation and the concentration of the water and sand fractions remained constant. In this case, the size of sand particles was in the range of 10 – 20 microns.

Before the experiment, the test tube was shaken so that the separated sand formed a uniform mixture of sand in water. The test tube was left in a vertical position and the appearance of the interface between the water and the sand fraction was observed. Sand settlement was observed by tracing the interface. The settling rate of sand particles was calculated by dividing the distance traveled at the interface level by the settling time, which was determined using a stopwatch.

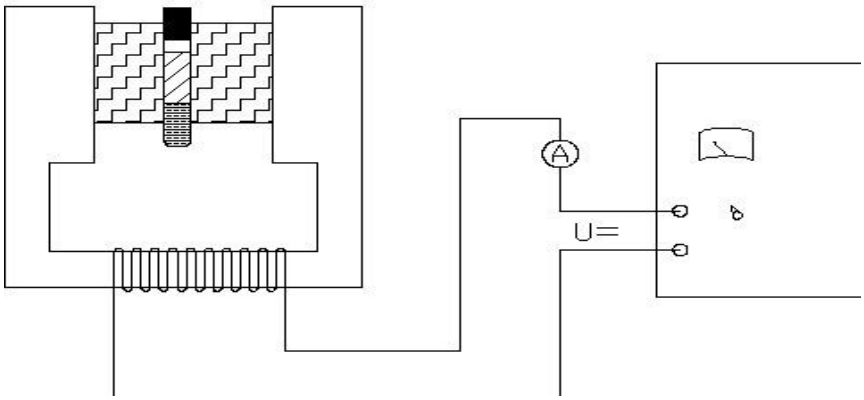

Figure 1. Scheme of the experimental setup.

To determine the influence of a magnetic field on the subsidence process, a comparison base is needed, which is the subsidence rate of sand particles in the absence of a magnetic field. The settling rate of sand particles in the absence of a magnetic field was determined by placing a test tube in a mesh metal screen. This is done in order to eliminate the influence of the Earth's magnetic field on the subsidence rate. The resulting curve is a reference, it is shown in Fig. 2.

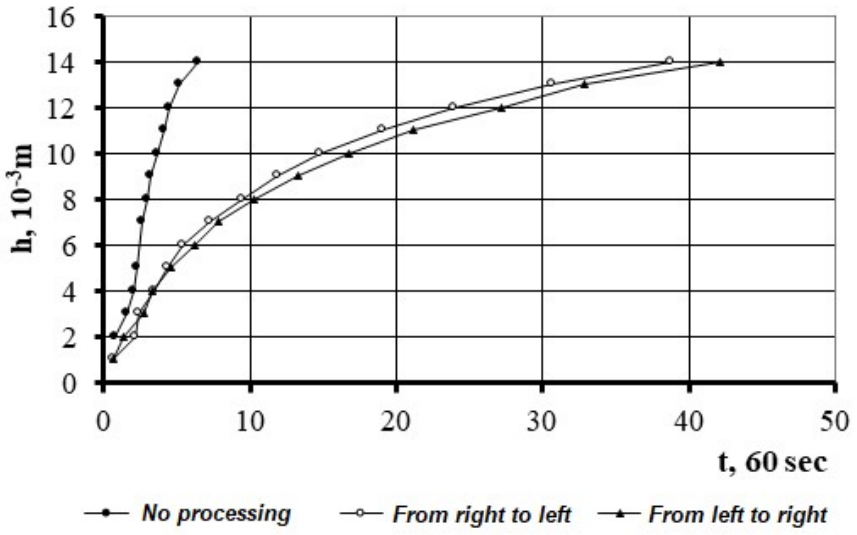

Figure 2. Dynamics of sand subsidence.

Fig. 2 also shows the sand subsidence curves in the presence of a magnetic field with a strength of 152 00 A/m. It follows from the figure that in this case the process of settling sand particles can be divided into two stages:

- main – in which the sand is separated from the water and settles to the bottom of the test tube (section I);
- final – in which further repacking of layered sand particles occurs (section II).

From Fig. 2 it follows that in the absence of a magnetic field, the final stage (sand repacking) takes approximately the same time as the particle settling stage. In both periods, the rate of change in the interface of the "water-porous medium" system is approximately the same.

Subsequently, the magnetic field strength was increased, the experiment was carried out again, and the settling rate of the particles was measured. The magnetic field strength varied from 0 to 176 000 A/m. In order to eliminate the influence of residual magnetization on the process of sedimentation of sand particles, the magnetic field strength was changed in an increasing manner. Based on the data obtained, the average speed for various stages of sedimentation of sand particles was calculated. The obtained values of average velocities of descent without an external field were compared with the average values of velocities of subsidence, and a conclusion was drawn about the influence of the created magnetic field.

A similar procedure was carried out for different magnetic field strengths. The settling rate of sand particles was studied in two directions of the magnetic field:

1. The magnetic field lines are directed perpendicular to the direction of particle settling, the N pole was on the left, and the S pole was on the right.
2. The magnetic lines of force are directed in the opposite direction, that is, the N pole was on the right, and the S pole was on the left.

The results of the average sedimentation rate of sand particles are shown in Fig. 3,4.

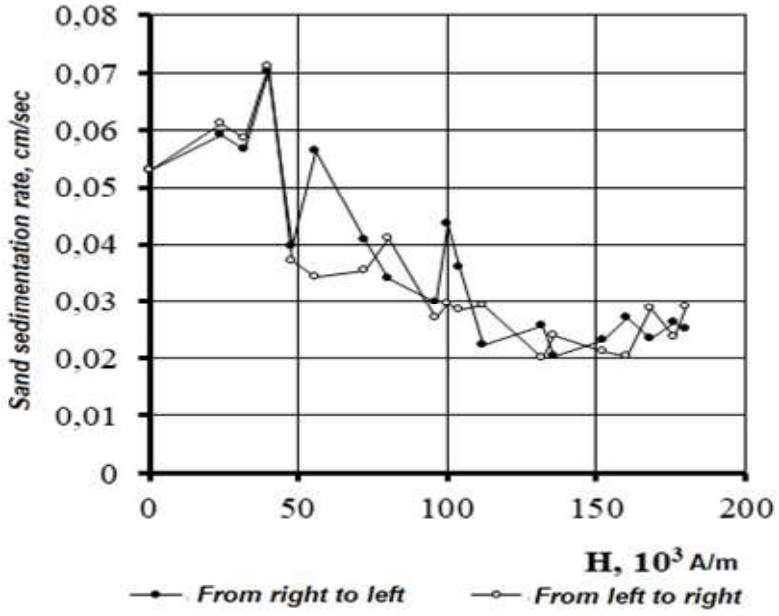

Figure 3. Dependence of the rate of sedimentation of sand in water on the strength of the transverse magnetic field.

3. Results and discussion

In the region (I) of sand particle separation, the following is observed. When the direction of the magnetic field, when the N pole was on the left and S on the right, is perpendicular to the settling of sand in the range of magnetic field strength 24 000 – 40 000 A/m, an increase in the settling rate of sand particles is observed by 15% at the end of the interval compared to the settling rate of sand in absence of a magnetic field, which was 0.053 cm/s Further, the settling rate of sand particles uniformly decreases, however, there is a surge in speed at a magnetic field strength of 56 000 A/m, which increases the settling rate. Another surge in the increase in the sedimentation rate of sand particles is observed in the range of 100 000 – 104 000 A/m, with a general tendency for the sedimentation rate to decrease. This increase in rate reaches approximately twice the average rate of decrease in subsidence.

At a magnetic field strength of 114 000 A/m, the subsidence rate is reduced by 2 times compared to the subsidence process in the absence of a magnetic field. A further increase in the magnetic field strength does not lead to a significant change in the sedimentation rate of sand particles up to 176 000 A/m. In this case, the curve of the dependence of the settling rate on the magnetic field strength throughout its entire length has periodic bursts in the settling rate of particles with a small amplitude. The minimum value of sand subsidence speed is 0.022 cm/s at a magnetic field strength of 112 000 A/m.

In the case when the direction of the magnetic field is opposite to that discussed above, that is, the N pole was on the right, and the S pole was on the left. The settling speed of particles in the magnetic field strength range of 24 000 - 4 0000 A/m, an increase in the settling speed is observed by an average of 15% at the end of the interval.

Further, the settling rate of sand particles drops sharply and, at a magnetic field strength H = 46 000 A/m, decreases by 30% compared to the settling process in the absence of a magnetic field, which is 0.053 cm/s. A further increase in the magnetic field strength to 132 000 A/m leads to a gradual decrease in the rate of deposition of sand particles. In this case, the curve of the dependence of the settling rate of sand particles on the magnetic field strength throughout its entire length is smooth. In the range of 132 000 – 160 000 A/m, the settling speed of particles is two times less than the settling speed in the absence of a field.

In the range of 160 000 – 176 000 A/m, there is a slight increase in the particle sedimentation rate by an average of 10% compared to the minimum sedimentation rate. The minimum value of the sand subsidence speed is 0.02 cm/s at a magnetic field strength of 132 000 A/m.

In region II of repacking of sand particles, the following is observed.

In the direction of the magnetic field, when N – was on the left, and S – on the right, perpendicular to the repacking of the sand. In the magnetic field strength range of 24000–40000 A/m, a slight decrease in the particle settling rate is observed. Further, the rate of sedimentation of sand particles drops sharply and, at a magnetic field strength of 56000 A/m, decreases by 4 times compared to the repacking process in the absence of a magnetic field.

A further increase in the magnetic field strength does not lead to a significant change in the rate of repacking of sand particles up to 176 000 A/m. In this case, the curve of the dependence of the subsidence rate on the magnetic field strength throughout its entire length has a wave character. The maximum deviation from the average subsidence rate, in some cases, is up to 0.05 cm/s. The minimum value of sand subsidence speed is 0.01 cm/s at a magnetic field strength of 132 000 A/m.

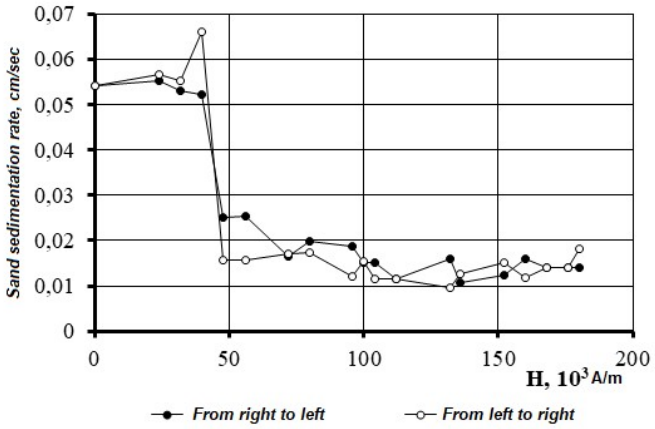

Figure 4. Dependence of the speed of redistribution of sand particles in water on the strength of the transverse magnetic field.

In the case when the direction of the magnetic field is opposite to that considered above, the repacking of sand particles in the magnetic field strength range of 24 000 – 40 000 A/m is observed to increase the settling speed of sand particles by 25% at the end of the interval. At a magnetic field strength of 48 000 A/m, the sedimentation rate decreases by approximately 4 times compared to the settling process in the absence of a magnetic field. A further increase in the magnetic field strength does not lead to a significant change in the sedimentation rate of sand particles up to 176 000 A/m. In this case, the curve of the dependence of the subsidence rate on the magnetic field strength throughout its entire length is smooth. The minimum value of the sand subsidence speed is 0.011 cm/s at a magnetic field strength of 136000 A/m.

`4. Conclusion

Summarizing the above, we can conclude that by changing the magnitude and direction of a constant transverse magnetic field, it is possible to regulate the process of sedimentation of sand particles: enhancing or slowing down this process when necessary in various oil production processes.

For example, an increase in the settling rate of particles is necessary during the primary processing of oil: in a separator, the rapid separation of the emulsion from sand leads to an increase in the productivity of treatment facilities.

Reducing the settling rate of particles is necessary when flushing wells or in the process of preventing the formation of plugs during the operation of sand-producing wells

If it is necessary that sand particles are suspended and better removed from the wellbore, then when using a transverse constant magnetic field, it is most preferable to place the N-pole of the magnet on the left and the S-pole on the right in the direction of flow. In this case, it is advisable to maintain the measured magnetic field in the measurement range of 132 000 – 176 000 A/m.

Conflict of interest

The authors declare that they have no conflict of interest in relation to this research.

5. References

1. Mirzajanzade A. Kh., Mamed – Zade A. M. (1990). Effect of clay mineral on fluid filtration in a porous mediym // Amsterdam: Elsevier Science Publishers B.V., Printed in Netherlands, Lithas, 24, 251–260.
2. Mirzajanzade A.Kh., Mamedzade A.M., Shakhverdiev A.H., Kuznetsov O.L. (1996). Geomagnite fields and oil and gas fields // Moscow: Geology of Oil and Gas 6, 4 – 7.
3. Mamed–Zade A. M. Nanotechnologies in oil production// Baku, 2010, 268p.
4. Mamed–Zade A. M. Nana technological basis of application of non-equilibrium effects of physical fields in oil & gas extraction // Baku, 2021, 207 p.
5. Mamed–Zade A. M. Application of a magnetic field to increase oil production // Estonia, Tallinn 2022 https://www.ester.ee/record=b5535873*est

Assessment of technological measures effectiveness based on the interpretation of pressure build-up curves using identification equations

A.V. Mammadov[a], A.V. Sultanova [a,b], R.M. Mammadov[a,b*]

[a] Department of Oil and Gas Engineering, Azerbaijan State Oil and Industry University, 20 Azadliq Avenue. Baku AZ1010, Azerbaijan
[b] Scientific Research Institute "Geotechnological Problems of Oil, Gas & Chemistry", 20 Azadliq Avenue., Baku AZ1010, Azerbaijan

Abstract.

Identification of hydrodynamic studies of wells is important in the control and management of various technological processes of oil production. One of the most used research methods in oilfield practice is taken by taking pressure recovery curves in production wells. Determination of the filtration characteristics of the formation by pressure buildup makes it possible to reasonably select wells under the influence, the method of the impact on the bottomhole zone itself, the necessary optimal operations, as well as to assess the degree of effectiveness of the geological and technological measures being carried out.

***Keywords**:* pressure build-up, production, identification equations, productivity index, unbiased criterion

[*] Corresponding author: Tel.: +99450-530-33-40
E-mail address: oilman25@mail.ru

1. Introduction

Hydrodynamic methods for assessing the effectiveness of impact on the bottom-hole zone of wells are based on model ideas about the nature of filtration flows and the geological structure of the formation.

Such, for example, are a priori ideas and assumptions about radial filtration, uniformity of the formation in thickness, invariability of the formation pressure at a certain specified distance from the well, etc. In a number of cases, mathematical research approaches and schemes are not adequate to the actual processes occurring during hydrodynamic testing of wells.

Considering this fact, when considering the method for selecting identification equations, one should not accept restrictions in favor of any particular type of mathematical models and simplifying assumptions about the physical properties of reservoirs and the geometric structure of the formation [3].

2. Methodological part

The recovery of pressure in the well is further accepted as a dynamic process, a complete description of which should be presented in the form of a functional relationship

$$\Delta P = \varphi\left(\frac{d\Delta p}{dt}, \frac{d^{\Delta} p}{dt^2}, ..., Q_0, Q_1(t)\right) \tag{1}$$

where $\Delta P = p_w(t) - p_w(0)$ is the current drawdown, measured from the initial pressure in the well; $Q_0(t)$ – initial flow rate of the well; Q_1 - inflow into the well after shutdown.

Below, the following are given as partial identification equations that approximately describe the complete equation (1):

$$\Delta P_1 = cQ_0 - bQ_1(t); \Delta P_2 = cQ_0 - bQ_1(1) + a_1\frac{d\Delta p}{dt}; \ \Delta P_2 = cQ_0 - bQ_1(1) + a_1\frac{d\Delta p}{dt} + a_2\frac{d^2\Delta p}{dt^2} \tag{2}$$

If the pressure in the well has almost been restored and the inflow has stopped, i.e. $Q(t) = \frac{d^i\Delta p}{dt^2} = 0, \quad i = 1,2,...,$ then equations (2) take the form

$$\Delta p = cQ_0 \tag{3}$$

If, when processing the results of pressure build-up observations in the resulting identification equation, the coefficients c and b differ significantly, this is explained by the non-linear nature of the inflow to the well in the corresponding flow rate range. To select an identification equation of optimal complexity, i.e. most adequate to the nature of pressure build-up in a given time interval, as well as to the accuracy and frequency of measurements, we apply the criterion of unbiasedness of the model proposed by Ivakhnenko A.T. [2]. In this case, the entire sample of observations of the current depression $\Delta p(t)$ in a certain time interval $(t_1; t_2)$ is divided into two alternating sequences – training (N_{tr}) and testing(N_{test}). At each observation point, the difference derivatives of the depression are calculated to the required order and the coefficients of the identification equations are determined using the least squares method at the points of the training and testing sequences, respectively

$$N_{tr}: \begin{array}{l} \Delta p_1 = cQ_0 - bQ_1(t) \\ \Delta p_2 = cQ_0 - bQ_1(t) + a_1\dfrac{d\Delta p}{dt} \end{array}$$

$$N_{test}.: \begin{array}{l} \Delta p^*{}_1 = c^*Q_0 - b^*Q_1(t) \\ \Delta p^*{}_2 = c^*Q_0 - b^*Q_1(t) + a^*{}_1\dfrac{d\Delta p}{dt} \end{array}$$

The criterion of unbiasedness of the k^{th} model is calculated:

$$\delta^k_{unbias} = \frac{1}{N}\sum_{i=1}^{N}\left[\Delta p_k(t_i) - \Delta p^*{}_k(t_i)\right] \tag{4}$$

$$N = N_{tr} + N_{test}$$

The summation in (4) is carried out over all observation points, including both the training and testing sequences. As the identification equations become more complex, the unbiased criterion δ^k_{unbias} first decreases and then begins to increase. The optimal complexity model is the one for which the minimum value corresponds δ^k_{unbias}. If, in the process of increasing the complexity of identification models, a stable minimum criterion δ^k_{unbias} is not obtained, the initial sample of the training and testing sequences should be changed [1,4].

3. Results and discussion

The pressure buildup of a well was processed according to the procedure given below. Current depression was measured for 750 minutes at intervals $\Delta t = 10$ min. The well production before shutdown was $Q_0 = 20\ m^3 / day$. Results are shown in Table 1.

The pressure buildup was processed under the assumption that there was no inflow into the well after shutdown, i.e. $Q_1(t) = 0$.

The points in the training sequence corresponded to:

N_{tr} : *t1=270 min., t3=310 min., t5=330 min., t7=370 min., ….*

The points in the testing sequence corresponded to:

N_{test} *: t2=290 min., t4=320 min., t6=350 min., t8=390 min., ….*

Difference derivatives at the corresponding points are calculated using the formulas:

$$\frac{\Delta p}{\Delta t} = \frac{\Delta p(t_0+\Delta t)-\Delta p(t_0)}{\Delta(t)};\ \frac{d^2\Delta p}{dt^2}(t=t_0) = \frac{\Delta p(t_0+\Delta t)-2\Delta p(t_0)+\Delta p(t_0-\Delta t)}{\Delta t^2};$$

$$\frac{d^3\Delta p}{dt^3}(t=t_0) = \frac{\Delta p(t_0+\Delta t)-3\Delta p(t_0)+3\Delta p(t_0-\Delta t)-\Delta p(t_0-2\Delta t)}{\Delta t^3} \qquad (5)$$

where Δt is the time interval between measurements of the current depression $\Delta p(t)$.

For example:

$$\frac{\Delta p}{\Delta t} = \frac{14,78-14,48}{10} = 0,3\cdot 10^{-4}\ \ MPa/\sec$$

$$\frac{d^2\Delta p}{dt^2} = \frac{14,78-2\cdot 14,48+14,14}{\Delta t^2} = -0,04\cdot 10^{-8}\ \ MPa/\sec^2$$

$$\frac{d^3\Delta p}{dt^3} = -0,04\cdot 10^{-12}\ \ MPa/\sec^3$$

Since the quantities $\frac{d^3\Delta p}{dt^3}$ are of the order of magnitude $\square 10^{-12}$, intermediate calculations when determining the coefficients of the identification equations should be carried out up to a value of the order of $\square 10^{-12}$.

To determine the k^{th} identification model using the least squares method, based on the points of the training and testing sequence, it is necessary to solve the following system of linear algebraic equations (for ease, the notation $a_0 = cQ_0$ is introduced). Based on the points of the training sequence

$$\sum_{r=0}^{k} a_r A_{rs} = B_s, \quad s = 0,1,2,...,k \qquad (6)$$

where the coefficients of matrix *A* and vector *B* are defined as follows

$$A_{00} = N_{tr},\ A_{0s} = \sum_{i-1}^{N_{tr}} \frac{d^s \Delta p}{dt^s}(t_i),\ s \geq 1;\ A_{rs} = \sum_{i=1}^{N_{tr}} \frac{d^r \Delta p(t_i)}{dt^r} \frac{d^s \Delta p(t_i)}{dt^s},\ r \geq 1,\ s \geq 1$$

$$B_0 = \sum_{i=1}^{N_{tr}} \Delta p(t_i);\ B_s = \sum_{i=1}^{N_{tr}} \Delta p(t_i) \frac{d^s \Delta p(t_i)}{dt^s},\ s \geq 1 \qquad (7)$$

In (7) the sums are carried out only over the points of the training sequence.
By points of the test sequence:

$$\sum_{r=0}^{k} a_r^* A_{rs}^* = B_s^*,\ s = 0,1,2,...,k;\ A_{00}^* = N_{test},\ A_{00}^* = \sum_{i=2}^{N_{test}} \frac{d^s \Delta p(t_i)}{dt^s};\ s \geq 1 \qquad (8)$$

$$A_{rs}^* = \sum_{i=2}^{N_{test}} \frac{d^r \Delta p(t_i)}{dt^r} \frac{d^s \Delta p(t_i)}{dt^s},\ r \geq 1,\ s \geq 1;\ B_{i=2}^* = \sum_{i=1}^{N_{test}} \Delta p(t_i);\ B_s = \sum_{i=2}^{N_{test}} \Delta p(t_i) \frac{d^s \Delta p(t_i)}{dt^s},\ s \geq 1$$

Thus, the minimum value of the unbiased coefficient was obtained for the model

$$\Delta p = a_0 + a_1 \frac{d\Delta p}{dt} = cQ_0 + a_1^* \frac{d\Delta p}{dt}$$

For the average value of the productivity coefficient we obtain:

$$K_{avg} = \frac{1}{2}\left(\frac{1}{c} + \frac{1}{c^*}\right) = \frac{1}{2}\left(\frac{Q_0}{a_0} + \frac{Q_0}{a_0^*}\right) = 9{,}87 \frac{m^3}{day \cdot MPa}$$

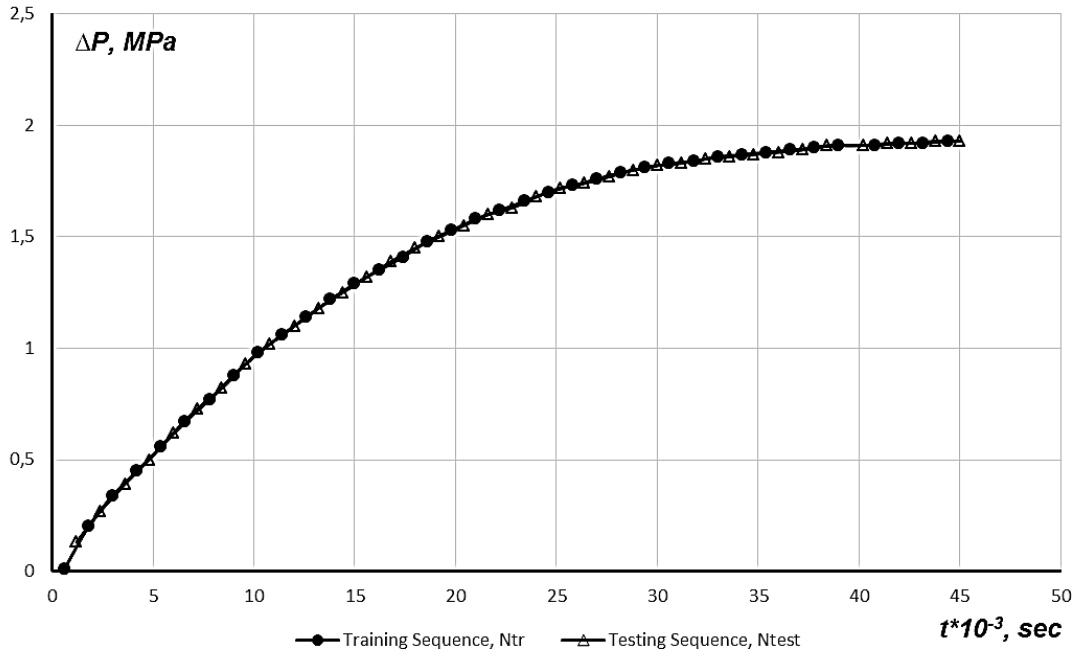

Fig. 1. Dependence curve ΔP=f(t)(Pressure Build-up Curve – Training and Testing Sequences)

Table 1

Results of PBC (Pressure Build-up Curve) processing

Training sequence, N_{tr}		***Testing sequence, N_{test}***	
t^{3}-10-, second	***ΔP*, MPa**	***t^{3}-10-, second***	***ΔP*, MPa**
0,6	0,01	1,2	0,13
1,8	0,2	2,4	0,27
3	0,34	3,6	0,39
4,2	0,45	4,8	0,5
5,4	0,56	6	0,62
6,6	0,67	7,2	0,73
7,8	0,77	8,4	0,82
9	0,88	9,6	0,93
10,2	0,98	10,8	1,02
11,4	1,06	12	1,1
12,6	1,14	13,2	1,18
13,8	1,22	14,4	1,25
15	1,29	15,6	1,32
16,2	1,35	16,8	1,39
17,4	1,41	18	1,45
18,6	1,48	19,2	1,5
19,8	1,53	20,4	1,55
21	1,58	21,6	1,6
22,2	1,62	22,8	1,63
23,4	1,66	24	1,68
24,6	1,7	25,2	1,72
25,8	1,73	26,4	1,74
27	1,76	27,6	1,77
28,2	1,79	28,8	1,8
29,4	1,81	30	1,82
30,6	1,83	31,2	1,83
31,8	1,84	32,4	1,85
33	1,86	33,6	1,86
34,2	1,87	34,8	1,87
35,4	1,88	36	1,88
36,6	1,89	37,2	1,89
37,8	1,9	38,4	1,91
39	1,91	40,2	1,91
40,8	1,91	41,4	1,92
42	1,92	42,6	1,92
43,2	1,92	43,8	1,93
44,4	1,93	45	1,93

The calculated value K_{avg} of the productivity coefficient coincides with the value of the productivity coefficient determined from the indicator diagram. The relative error does not exceed *3%*. It should be noted that the minimum of the unbiased criterion may correspond to different models depending on the selected interval for processing the pressure build-up curve. Regarding models, it is necessary to do the following: in the solution of the corresponding differential equation, terms of the $e^{e^{\omega t}}$, $\omega \succ 0$ form may be present. This is explained by the fact that the function of complete description of an object (1) in the general case depends on derivative depressions of a higher order than those considered in the proposed model. Therefore, when physically interpreting the coefficient $a_0 = cQ_0$, one should proceed from the conditions of smallness of the derivatives of depressions with respect to time, and not from solving the corresponding differential equation at $t \to \infty$.

4. Conclusions

Therefore, the calculation sequence when determining the productivity coefficient of a well using pressure build-up should be as follows:

- ✓ The points of the training and testing sequence are selected.
- ✓ Derivatives are calculated to the required order for the selected control points.
- ✓ From the system of linear algebraic equations (6-8), the coefficients a_i and a^*_i i.e. identification equations of the object are determined according to the training and testing sequences, respectively.
- ✓ For each model, the δ^k_{unbias} unbiased criterion is calculated using (4).
- ✓ Based on the stable minimum criterion δ^k_{unbias}, the most optimal model is selected.
- ✓ The average value of the productivity coefficient is determined by the formula $K_{avg} = \frac{Q_0}{2}\left(\frac{1}{a_0} + \frac{1}{a^*_0}\right)$

Conflict of interest

The authors declare that they have no conflict of interest in relation to this research.

5. References

1. Mirzajanzade A.Kh., Ametov I.M. Forecasting the field efficiency of methods of thermal action on oil reservoirs // M. Nedra. 1983, 205 p. [in Russian]
2. Ivakhnenko A.T., Zaychenko Y.L. Dmitrov V.V. Decision making based on self-organization // M., Soviet radio, 1976, 280 p. [in Russian]
3. Mikhaylov N.N. Information and technological geodynamics of borehole zones // M., Nedra, 1996, 349 p. [in Russian]
4. Shagiyev R.G. Study of wells by pressure build-up.// M., Nauka. 1998, 304 p. [in Russian]

Research of rheological characteristics of two-phase systems

T.S. Babayeva

Scientific Research Institute of Geotechnological Problems of Oil, Gas and Chemistry, ASOIU, 227 Dilara Aliyeva Ave., Baku, AZ-1010 Azerbaijan

Abstract.

Field practices shows that many wells that produce oil, gas and condensate in the final period watered. In this case, in the lift, in the pipeline, the capacitive system moves two-phase system, such as "water-oil".

Conducted a large literary analysis showed that insufficiently studied hydrodynamics of two-phase systems.

In this paper, based on laboratory and field data, proposed a new movement model emulsion systems. It was proposed a method for determining the basic indicators such systems. On the basis of this method, it was receipted a formula for determining the dynamic viscosity of such systems.

Keywords: emulsion, two-phase system, shear stress, velocity gradient, watercut.

Corresponding author. Tel.: +994 55 767 64 16

E-mail address: tamilla.babaeva.85@mail.ru

1. Introduction.

On the basis of laboratory studies, a mathematical equation for the movement of emulsion systems "water-oil" is proposed, in a wide range of changes in the water cut of the formation production. Taking into account this design scheme, expressions are proposed for determining the main indicators of emulsion systems, such as average speed, volumetric content of components, as well as the dynamic viscosity of the "water-oil" system.

In the technological processes of oil production, pipeline transport and processing, as a rule, there is a flow of a two-phase system (oil and formation water). Due to the fact that reservoir water is enriched with various surfactants during filtration in a porous medium [1], favorable conditions are created for the formation of direct and reverse water-oil emulsions in reservoir conditions, between which conversion is observed. In theoretical studies of these systems, methodological difficulties arise, the elimination of which is associated with the adoption of a number of assumptions both when considering the liquids themselves and when compiling models [5÷7].

The results of studies by domestic and foreign authors show that, in contrast to viscosity, when estimating the density of emulsion systems, it is possible to use the additivity rule [3, 4].

This uses the known values of the density of oil and water that form the emulsion, and their relative content. Other properties of stable emulsions depend to a greater extent on the conditions of their formation and the composition of the adsorption shell on the drops of the disperse medium.

Many authors note that there is still no more accurate method for calculating the dispersion of stable emulsions, and only methods for its experimental determination have been developed. It is difficult to determine the viscosity of stable emulsions. Only for very dilute emulsions (with a dispersed phase content of less than 0.05), it is sufficient to describe the dynamic viscosity of any emulsions by the Einstein equation [7].

With an increase in the content of the dispersed phase, the armoring shells on the drops affect the volume of the dispersed phase and the coagulation of the drops with the formation as a result of their merger.

In hydrodynamic calculations, it is impossible to take into account these factors and lead to the need to study the viscosity of oil-water emulsions of individual reservoirs and deposits. This requires obtaining numerous empirical formulas for the viscosity of stable emulsions, which have certain coefficients that must be determined empirically.

Some authors offer empirical formulas in a small range of the content of an individual phase or component [5,6,7].

In this work, the hydrodynamic properties of stable and unstable emulsions of the “water-oil” and “oil-water” types are investigated.

An unstable emulsion is a two-phase dispersed system consisting of two mutually insoluble liquids, so that one of them is distributed in the other in the form of droplets, on the surface of which there are no strong stabilizing shells. It should be noted that in stable emulsions, formation water itself has a stabilizing shell [2].

The conducted laboratory analyzes have shown that an unstable emulsion is formed in the turbulent regime of motion of at least one of the phases separately. Formation water has multimolecular layers of surfactants on the interface, which partially do not prevent crushing or coalescence of drops of one of the components. The first such proposal was made by Academician A.Kh.Mirzajanzade in 1948.

Our laboratory studies have shown that only with the steady motion of unstable emulsions of the "oil-water" type, a dynamic equilibrium is established between the processes of coagulation and crushing. During the transition to the laminar regime of motion of one of the phases or both phases, the separation of the constituent phases occurs [2].

An unstable emulsion is characterized by non-equilibrium rheological properties and dispersion. At the same time, it was found that simultaneously with the transition of laminar motion to turbulent, the nature of the distribution of velocities over the pipe section, as well as the nature of hydraulic resistance, change. The analysis showed that in the laminar regime of motion of emulsion systems, the distribution of velocities over the cross section has a parabolic character. It should be noted that the velocities are equal to zero directly at the walls, and as they move away from them, they continuously and smoothly increase, reaching a maximum on the pipe axis.

2. Methodological part.

Processing the experimental material, the authors came to the conclusion that, similarly to the phenomenon of shear in solids, the following relationship between stress and strain for emulsion systems was obtained:

$$\tau = \left(\mu \frac{du}{dr} \right)^n \qquad (1)$$

where τ is the tangential shear stress;

μ is the dynamic viscosity of the emulsion system;

$\frac{du}{dr}$ is the speed gradient.

Considering that

$$\tau = \frac{r}{2} \frac{\Delta P}{L} \qquad (2)$$

solving together equation (1) and (2) with respect to speed we have:

$$dU = \frac{1}{\mu}\left(\frac{\Delta P}{2L}\right)^{\frac{1}{n}} r^{\frac{1}{n}} dr \quad (3)$$

where r is the radius;

ΔP is the pressure drop;

L is the length of the area under consideration.

Integrating the differential equation, we get:

$$v = \frac{1}{\mu}\left(\frac{\Delta P}{2L}\right)^{\frac{1}{n}} \frac{n}{1+n}\left(R^{\frac{1+n}{n}} - r^{\frac{1+n}{n}}\right) \quad (4)$$

If $n = 1$, we have the Stokes equation.

The emulsion flow rate in the pipe can be found by summing up the elementary flow rates passing through the annular platforms and described by the following expression:

$$Q = \int_0^R v \cdot 2\pi r dr \quad (5)$$

Substituting its value instead of speed (4) and integrating, we get:

$$Q = \frac{\pi}{\mu}\left(\frac{\Delta P}{2L}\right)^{\frac{1}{n}} \frac{n}{3n+1} R^{\frac{3n+1}{n}} \quad (6)$$

For $n = 1$, from this equation we have the Poiseuille equation.

The average speed of emulsion systems is defined as

$$v_a = \frac{Q}{\omega} = \frac{1}{\mu}\left(\frac{\Delta P}{2L}\right)^{\frac{1}{n}} \frac{n}{3n+1} R^{\frac{n+1}{n}} \quad (7)$$

where ω is the cross-sectional area of the round pipe.

Solving this equation with respect to dynamic viscosity, we have:

$$\mu = \frac{n}{3n+1} \cdot \frac{\pi}{Q}\left(\frac{\Delta P}{2L}\right)^{\frac{1}{n}} R^{\frac{3n+1}{n}} \quad (8)$$

where n is a coefficient that depends on the water cut of the product.

To compare this formula and the calculation method with laboratory data, the measured dynamic viscosity was compared with the calculated one obtained by formula (8).

3. Results and discussion.

As can be seen from the graph, with a correlation coefficient of 0.88, with an average deviation of ±3%, the data fit well on a straight line with a slope of 45°, which shows the practical acceptability of this method for calculating the main indicators of water-oil emulsionsystems (Figure 1).

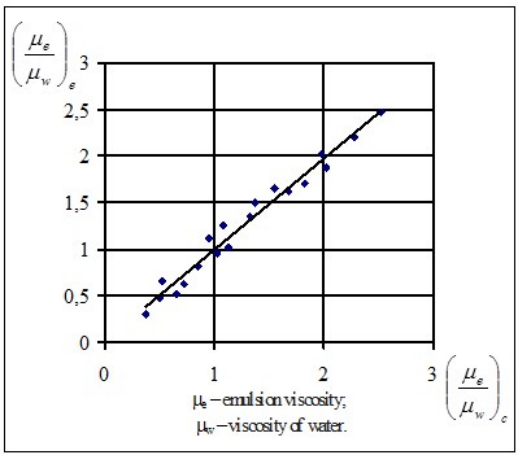

Figure 1. Comparison of laboratory data with calculated data

$\left(\frac{\mu_e}{\mu_w}\right)_e$ and $\left(\frac{\mu_e}{\mu_w}\right)_c$ – are the experimental and calculated value of the dimensionless viscosity.

1. Conclusion.

A method and model of emulsion systems during their movement in tubing and pipelines are proposed.The use of this method makes it possible to control the conditions for the formation and separation of direct and reverse emulsions in various technological processes.

Conflict of interest

The authors declare that they have no conflict of interest in relation to this research.

2. References

1. Mirzajanzadeh A.Kh. The expediency of preparing clay solution based on groundwater. // Azerbaijan Oil Industry. 1948. No. 11. P. 10-13 [in Russian].
2. Babayeva T.S. Non-traditional methods of determination of rheological parameters of water-oil emulsions and their consideration// Scientific Research Institute of Geotechnological Problems of Oil, Gas and Chemistry, "Scientific works", Baku - 2021.Volume XXI. P. 277-281[in Russian] .
3. Emtsev B.T. Technical hydromechanics // M.: Mashinostroenie, 1978. - 463 p.
4. Loitsyansky L.G. Mechanics of liquids and gases // 3rd ed. - M.: Nauka, 1970. - 904 p [in Russian].
5. Mansurov M.N. Research of transportable properties of oil-water emulsions// Ufa, 1977. - 132 p.
6. Chugaev R.R. Hydraulics. - L.: Energoizdat, 1982. - 682 p . [in Russian]
7. Emulsions. Textbook for high schools. Ed. F. Sherman//L.: Energoizdat, 1982. - 235 p [in Russian].

Experımental study of resıdual oıl compressıon from hydated sludge usıng a surface-actıve substance (sas) mıxture whıch ıs a non-sedıment solutıon ın the formatıon fluıd

Gasimli A.M., Aliyev E.N., Bayramova N.S., Yusubova N.A., Huseynova S.S.
Scientific Research Institute of Geotechnological Problems of Oil, Gas and Chemistry, ASOIU, 227 Dilara Aliyeva Ave., Baku, AZ-1010 Azerbaijan

Abstract

The irrigation method, which was once highly valued by oil workers and could increase oil recovery from fields, is currently unable to ensure full oil production from the reservoir. Especially when pumping into heterogeneous formations and fields with high-viscosity oil, this manifests itself in a small set of sweep coefficients. Upon completion of field development, it turns out that 40-70% of oil reserves remain unrecoverable. At this time, the remaining oil reserves are in such a state that they cannot be extracted by known processing methods.

Keywords:.

Corresponding author. Tel.: +994 50 6201516
E-mail address: elsan67@mail.ru

1. Introduction

It is known that the stage of development of the oil industry is characterized by the complexity of the operating conditions of the fields. The reason is that due to changes in the structure of oil and the characteristics of reservoirs, the reserves of the fields have become difficult to recover. As a result, there is a decrease in the volume of oil produced, a sharp increase in dilution, and a large number of highly productive fields are entering the final period of development. At present, in the development of oil fields, the most pressing problems are considered to be the involvement in active development of areas remaining outside of development - stagnant zones - and the exploitation of recoverable residual oil reserves. It is shown that this reserve is 160 million tons in onshore fields and 135 million tons in offshore fields.

The reason why most methods used to improve oil recovery from oil fields that have been in production for a long time cannot give the expected effect is that oil is retained in the pore channels due to capillary forces, the coefficients of movement of the compressive agents and the compressive agents are unfavorable, and reservoir reservoirs are heterogeneous.

2. Methodological part.

Methods of influencing the oil layer are either methods that affect the compression of the oil (various gases, alkalis, surfactants, etc.), or methods that provide an increase in the coverage coefficient of the layer with the working agent (polymer solutions, water-gas mixture, precipitant, etc.).

To increase the degree of oil compression, physicochemical methods are mainly used. Recently, some advantages have been observed in this area, and it has been possible to increase the oil compression ratio from 0.25-0.45 to 0.50-0.60. However, the application coverage ratio remains small, which does not allow achieving the desired level of oil production during field development.

Many years of experience in developing oil fields shows that water injected into the reservoir in most cases does not end up in low-permeability formations, but in formations with high

filtration properties. The volume of oil collected as a result of a decrease in the effectiveness of the impact method, which increases the dilution of the resulting product to 70-90%, is 35-40% of the balance reserve. On the other hand, severe dilution of the product indicates the ineffectiveness of physicochemical methods used to increase oil yield.

The results of the conducted theoretical studies showed that during the compression of oil by water in the well system, the pressure gradient changes several times, causing the current lines to be directed in a complex way, especially in fields with non-Newtonian oil, and the formation of stagnant zones [1,2]. Therefore, there is a great need to create a working agent that ensures the displacement of high-viscosity oil from the porous medium.

Recently, one of the most urgent problems facing the justification of the effective development system in fields is the problem of increasing the oil yield of fields with oil reserves that are difficult to extract. These deposits are mainly oil objects with small permeability of oil reservoirs (less than 0.05 mkm^2) and high oil viscosity (more than 10 mPa·s). When exploiting fields with hard-to-extract reserves, the use of known technology (various options of the irrigation method) does not ensure the elimination of the reasons preventing the increase of the oil yield of the formation. If the ratio of the viscosity of the oil in the formation to the viscosity of the injected water exceeds 15, the formation of the water-oil boundary becomes difficult. In such a situation, the movement of water-oil contact in the formation is disturbed, the coverage of oil with water decreases, the injected water finds its way and begins to move towards the production wells, and the formation of stagnant zones occurs in the formation.

Another reason is that the capillary forces formed as a result of surface exchange between the formation fluid and the porous medium keep the oil immobile in stagnant zones.

It is known that there are two types of residual oil. The first is the oil that is not covered by the entrapping agent in the stagnant zones and leeches. The reason for the formation of this type of oil is, first of all, that reservoirs of the formation have non-homogeneous permeability and are poorly covered by the impact. Mining experience has proven that if the permeability of two layers separated by a clay layer differs by several times, water does not enter the layer with low permeability. Such oil differs from compressed oil because it does not come into contact with the compressing agent.

The second residual oil is the oil remaining in the wetted areas of the reservoir. For such oil, the relationships of the rock-oil and injected fluid system play a major role, for example, the wetting nature of the rock surface.

Oil displacement from hydrophilic porous media is close to the "piston shapes" regime, and 90% of oil is recovered in the anhydrous period. Aqueous period is short in hydrophilic rocks, so when 0.5-1.5 pore volume of water enters, it is known that the obtained oil is fully hydrated. The oil in the formation completely covers the rock surface in a thin layer, and the residual oil accumulates in high pores. Water percolation occurs primarily in small and medium capillaries, from which oil is transferred to large capillaries in the form of droplets. In this case, saturation with residual oil is capillary-buried.

The adsorption of surface-active substance (SAS) on a solid surface depends on two main factors: the affinity of the SAS with the surface and the hydrophobicity of the SAS, which creates a hydrophobic effect. This effect is highly dependent on the structure of the SAS molecule – the solubility of SAS in water.

It has been confirmed that these effects play the main driving role of SAS adsorption if these surfaces are hydrophobic (because SAS molecules are adsorbed as a result of molecular contact on a hydrophobic surface).

At a highly polar surface and a small concentration of SAS, its molecules are oriented with polar groups on the surface.

Ametov I.M., Khavkin AY, Buchenkov LN note [3] that, regardless of the thickness of the oil layer absorbed on the rock, at the zero value of wetting, it becomes very strong. At any other values of cooling, the oil layer can change its thickness depending on the following expression (1):

$$\sigma_{S\text{-}W} - \sigma_{S\text{-}O} = \sigma_{W/O} \cos\theta \qquad (1)$$

where $\sigma_{S\text{-}W}$, $\sigma_{S\text{-}O}$, $\sigma_{W\text{-}O}$ surface tension at the solid-water, solid-oil and water-oil boundaries, respectively, θ - is the wetting angle.

The occurrence of the change is due to the fact that the differentiation of the oil layer into droplets occurs quickly, depending on surface tension on the one hand and viscosity on the other, the shape of the droplets is determined by formula (1), and the adhesion force is determined by formula (2):

$$A = \sigma_{W/O} (1+\cos\theta) \qquad (2)$$

This process is observed regardless of whether one of the compressing or compressing fluids wets the rock surface.

Currently, there are a large number of surfactants. According to their chemical structure, they are divided into two classes: ionogenic surface-active substances (ISAS) and nonionic surface-active substances (NSAS). The solubility of SAS in fresh, formation (alkaline or hard) and sea water is of great importance for its application in various technological processes of oil production. In particular, the fact that SAS dissolves in formation water without precipitation is of more interest. If the SAS solution forms a precipitate in contact with the oil while injecting the formation, then not only the active components of the SAS will decrease or completely disappear, but at the same time, pores may be blocked by the formed precipitates. This will lead to a decrease in the compactness of layer collectors.

Almayev RX shows that [4], despite the positive effect of non-ionogenic SAS solution on formation oil yield compared to water, its application to terrigenous rocks saturated with oil lowers the permeability of the porous medium.

It is known that we can reduce the effect of capillary forces by lowering the value of the surface tension coefficient formed at the water-oil boundary. For this purpose, recently various types of surfactants are added to the water injected into the formations, so that the surface tension value at the boundary between the formation oil and the injected water will decrease due to their influence, and as a result, it will be possible to remove most of the residual oil.

A solution of a concentrated alkaline reagent in water occupies a special place among the physico-chemical methods. The advantage of the alkaline solution is that it has a good oil-squeezing ability when the formation is injected, and it also increases the coverage of the formation as a result of lowering the surface tension in contact with the oil. In contact with the active components of the oil, a highly dispersed emulsion is formed at the compression front.

If we take into account that the active components of oil become soapy when using an alkaline solution, then the criterion for applying an alkaline solution to deposits is that the surface tension of the solution in contact with oil is sharply reduced.

The results of laboratory work conducted by various researchers [5,6] show that the main factors influencing the oil yield coefficient during the application of alkaline solution are the characteristics of water, rock and oil.

The water of the deposit, which makes it difficult to compress with an alkaline solution, has a high hardness (especially the presence of Ca and Mg ions). The hardness of the water reduces the surface activity of the alkaline solution.

It was confirmed that lowering of the surface tension by the alkaline solution depends on the presence of naphthenic acid in the oil.

Currently, SAS are used as a composition rather than as a separate product. This is considered more favorable both economically and physico-chemically. It has been proved that it is possible to replace SAS, which is often difficult to find and expensive, by means of a cheap composition [6].

If we talk about the mechanism of action of SAS, we should note that SAS added to water first of all reduces the surface tension at the oil-solution boundary. With a decrease in surface tension, the oil droplet undergoes easy deformation, less force is spent to pass through the narrowed pores of the reservoir, and the movement of the oil droplet in the reservoir increases.

SAS is a chemical compound that concentrates at the phase boundary and causes a decrease in surface tension. The main property of SAS is surface activity – its ability to reduce surface tension at the interface.

A solution of SAS in water increases the wetting of the rock surface. The wetting of the rock surface and the decrease in surface tension reduce the energy of contact of oil with the rock by 6-10 times. The solution of most SAS in water has a high oil-washing ability, and they have the ability to wash away the oil drop stuck to the rock surface in a thin layer.

Recently, the increase in the price of known SAS and the fact that most of them precipitate when dissolved in seawater and reservoir water have made it difficult to use them to increase reservoir oil yield. Therefore, alkaline waste (AW), which is the output product of the oil refinery, was used to increase the oil yield in Azerbaijan's fields [7]. However, in the AW, it gives sediment in formation and sea water. Currently, there are surfactants that are soluble in various waters without sedimentation. Therefore, it was decided to use a mixture of the substance with AW. First, the effects of the solutions of these substances in formation water separately on the surface tension at the boundary with oil were studied. For this purpose, samples of oil and reservoir water were brought from well No. 697 of "Absheronneft" Oil and Gas Production Department (OGPD). The viscosity of oil at room temperature is equal to 100 mPa·s. First, the surface tension at the boundary between oil and formation water was determined (13.5 mN/m). Then, 5% solution of AW [8] was mixed with the 1% solution of SAS in formation water, and the surface tension was determined to be 0.7 mN/m. It should be noted that the addition of 5% AW to a 1% solution of our selected SAS solution in formation water did not cause precipitation. This gave impetus to the use of the received composition to increase the oil yield of the formation. In the linear formation model, oil compression was carried out through reservoir water, and the oil compression coefficient was 0.18 in the dry period and 0.48 in the last period (Figure 1).

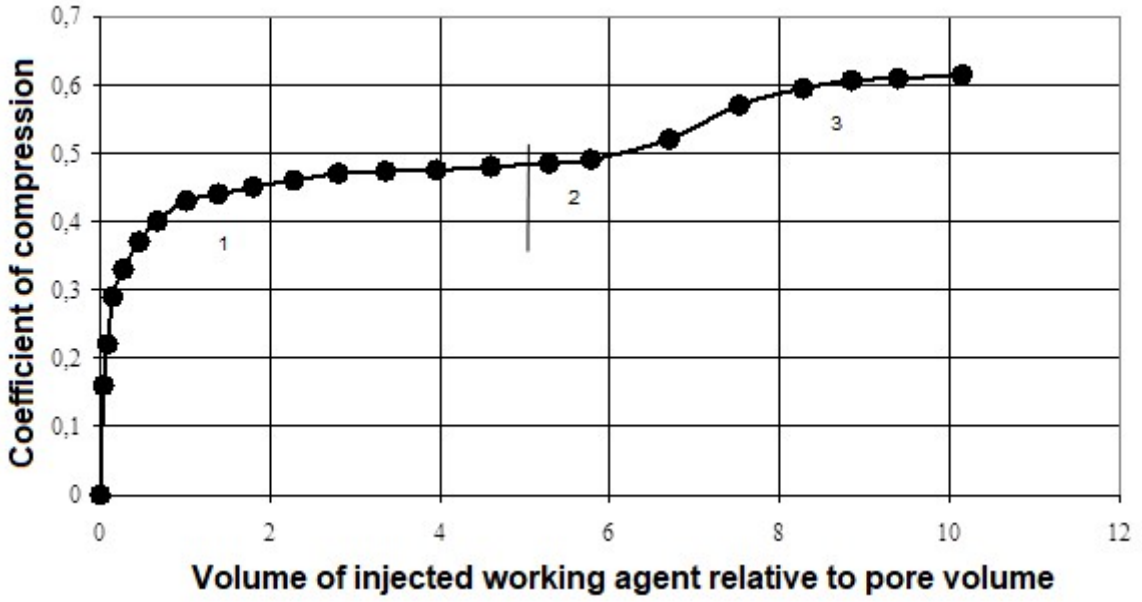

Figure 1. After forcing the oil through the formation water (1), the residual oil is again driven through the formation water (3) to form argate from the composition (2)

Using the developed composition for extracting residual oil from a wetted formation, 25% of the pore volume was injected into the reservoir model in the form of aragate (Figure 1 (2)), followed by continued injection of formation water. Injection of the pore volume of formation water after injection of aragat allowed to remove 14% of the remaining residual oil in the liquefied reservoir model (Figure 1 (3)).

3. Conclusion

As a result of the conducted experimental research, we can say that by using the composition obtained by adding 5% AW to a 1% solution of the selected SAS, which is a sediment-free solution in formation water, it was possible to remove a certain part of residual oil from the liquefied formation. This allows us to apply the results obtained in the real mining conditions.

Conflict of interest

The authors declare that they have no conflict of interest in relation to this research.

4. References

1.Levi B.I. и др. Development of oil fields using surface-active substances. // M.: Nedra, 1983. – 216 c.

2. Ibatullin R.R., Ibragimov N.G., Takhautdinov Sh.F. Enhanced oil recovery at a late stage of field operation //- M.: Nedra Business Center LLC.- 2004. - 292 p (In Russian).

3. Ametov I.M., Khavkin A.Ya., Buchenkov L.N. Enhanced oil recovery. New possibilities. //Oil Industry, No. 12, 1997, p. 30-32 (In Russian).

4. Almaev R.Kh. Influence of solutions of nonionic surfactants on phase permeability of oil-saturated rocks. //Нефтяное Хозяйство, No. 2, 1991, p. 18-21.

5. Gorbunov A.E., Zheltov Yu.V., Buchenkov L.I., Nazarov V.I. Alkaline effect on oil layers and its modification. // M. ВНИИОЕНТ, Обзорная информация, Серия Нефтепромысловое дело, 1985.

6. Surguchev M.L. Secondary and tertiary methods of increasing oil recovery layers // M. "Nedra", 1985, pp. 19-254.
7. Abasov M.T. и др. Additive to water injected into the oil layer// A.S. N 784411, Bul. Goskom po delam isobr. и откр. No. 44, 1980.
8. Latifov A. I., Gasimli AM Increasing formation oil yield by creating arada from a solution of alkaline waste in fresh water // Azerb. Oil Industry, Baku, 2005, N 4, p. 16-20.

Elimination of formation damage in the wellbore area and expansion of the well drainage area

[1]Y.Samedov, [2]J. Eyvazov

[1]ASOIU, 20 Azadlig Avenue. Baku, AZ1010
[2]Oil Gas Scientific Research Project Institute, SOCAR, 88a H.Zardabi str., Baku, AZ1012

Abstract
The exploration of unconventional oil and gas reservoirs is a prominent global trend today. Achieving cost-effective and efficient hydrocarbon production from these reservoirs necessitates advanced technologies. One such technology that has been employed in the oil and gas industry for many decades is hydraulic fracturing. It is used to create highly conductive channels within formations characterized by extremely low permeability values. The successful implementation of hydraulic fracturing hinges on the development of an effective fracturing design. This design is crucial to achieving the anticipated production outcomes from unconventional reservoirs, including tight gas, shale gas, coal bed methane, and reservoirs with very low permeability. Key parameters for the success of hydraulic fracturing operations include the determination of the optimal fracturing rate, fracture height, and the selection of propping agents. These factors collectively contribute to the efficiency and productivity of hydraulic fracturing activities in unconventional reservoirs.

Keywords: Formation damage, well stimulation, hydraulic fracturing, drainage area, tubing diameter, skin factor
*Corresponding author. Tel.: +994 559672223
E-mail address: jabrayil.eyvazov88@gmail.com (J.M.Eyvazov)

1. Introduction.

Formation damage refers to the phenomenon in which the permeability of the subsurface formation near the wellbore decreases. There are various factors that can lead to formation damage, which will be explored later. The decrease in permeability in the wellbore region has a direct impact on the overall productivity of the well. This reduction is often attributed to the blocking of pore throats in the vicinity of the wellbore, causing a decrease in the available flow area.
Turbulent flow in the well is another factor contributing to the reduction in the flow area. When turbulent flow occurs, it leads to a significant pressure drop in comparison to laminar or Darcy flow. The pressure drop associated with turbulent flow is notably higher, which results in a further

reduction in wellbore permeability. This complex interplay of factors underscores the importance of understanding and managing formation damage in well operations.

2. The Skin factor.

The skin factor is a crucial measure of the impact of formation damage on well performance. Formation damage typically results in a reduction in permeability around the wellbore. The accompanying figure illustrates the ideal pressure profile of a well, highlighting the influence of formation damage (represented by the yellow line) on creating an additional pressure drop.

The skin factor (s) can take on various values, and its interpretation is as follows:

Positive skin factor, s > 0: When a damaged zone near the wellbore leads to a reduced permeability (k_skin) compared to the formation's original permeability (k), the skin factor is positive. The magnitude of the skin factor increases as the damaged zone's permeability (k_skin) decreases and as the depth of the damage (r_skin) increases.

Negative skin factor, s < 0: When the permeability around the well (k_skin) is higher than that of the formation (k), a negative skin factor is indicated. This negative skin factor suggests an improved wellbore condition, often associated with measures to enhance permeability near the well.

Zero skin factor, s = 0: A skin factor of zero signifies that no alteration in permeability around the wellbore is observed, implying that k_skin equals the formation's original permeability (k).

The skin factor is a valuable metric for evaluating the influence of formation damage on well performance and is a critical parameter in wellbore management and optimization.

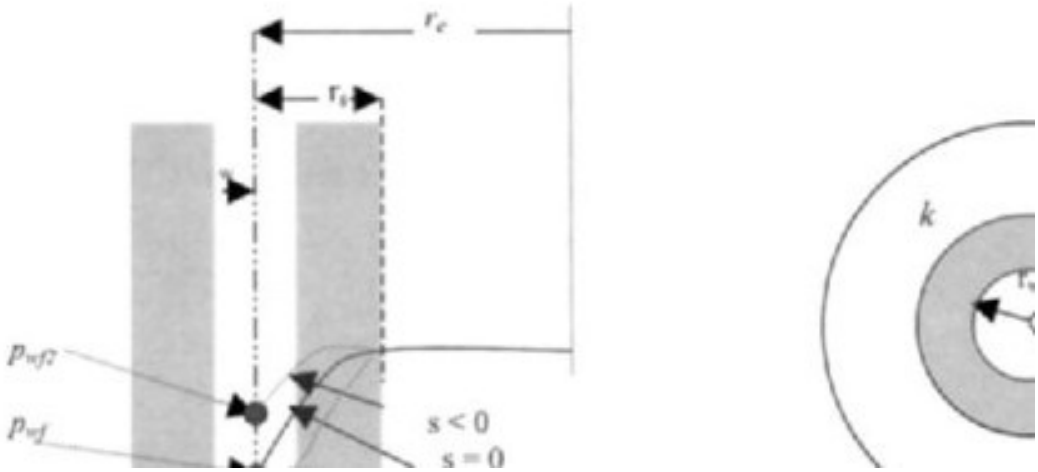

Figure1: Effect of the skin on pressure profile around wellbore

$$S_d = \frac{2\pi k_0 h \Delta P_d}{q_0 \mu_0} = \left(\frac{k_0}{k_d} - 1\right) \ln\left(\frac{r_d}{r_w}\right).$$

h -formation height

q_0 - oil flow rate

μ_0 - oil viscosity

S_d - formation damage skin

k_0 - formation permeability to oil

k_d - damaged permeability to oil

ΔP_d - extra pressure drop due to formation damage

Formation damage skin is directly related to the ratio of the original permeability to the damaged permeability. As this ratio increases, the skin factor also increases, signifying greater formation damage.

Stimulation in the context of oil wells refers to a set of operations carried out to optimize productivity. This technique is of paramount importance in the production process, as it encourages the flow of hydrocarbons from the reservoir rocks to the wellbore, given that the hydrocarbons are situated within the pores of the reservoir rock. Stimulation also encompasses methods aimed at improving the natural permeability of undisturbed rock formations housing the reservoir, making it economically viable for oil production. Permeability is the rock's ability to conduct fluids, including oil and water. Stimulation technologies can be applied to increase the reservoir's permeability to a level that allows for enhanced oil production rates.

One of the well stimulation techniques is hydraulic fracturing, which is employed to boost well productivity. In hydraulic fracturing, a fracturing fluid or pumping fluid, typically composed of a mixture of water and sand, is injected into the formation under high pressure.

This article delves into the influence of hydraulic fracturing on well productivity, with reference to a real well example using the Prosper model. The project explores how oil and gas production behavior is affected in various scenarios, including the base case, a 30-degree deviation angle, and a 45-degree deviation angle. Furthermore, the study investigates how different parameters, such as tubing diameters and skin factor, impact oil and gas production, aiming to determine the optimal well production rates. In practice, the well in question is somewhat deviated, and the study conducts a sensitivity analysis to identify optimal parameters for future wells and to assess production outcomes under different trajectories.
PVT parameters are as following in this well:

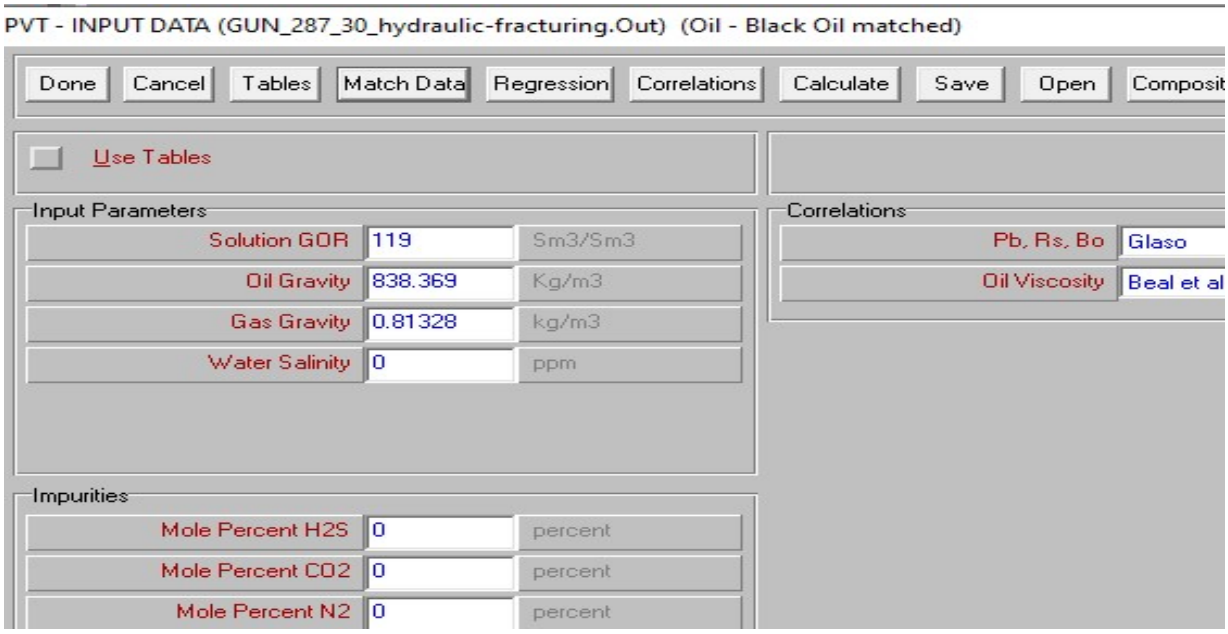

Figure 2: PVT parameters for the well-reservoir model

PVT - Match Data (GUN_287_30_hydraulic-fracturing.Out) (Oil - Black Oil matched)

Done | Main | Cancel | Reset | Copy | Clip | Import | PVTP Import | Transfer

PVT Match data

Table 1

Temperature	68 deg C
Bubble Point	277.176 BARa

	Pressure BARa	Gas Oil Ratio Sm3/Sm3	Oil FVF m3/Sm3	Oil Viscosity centipoise
1	1	0	1.0309	2.41353
2	8.618	4.26	1.0441	2.10595
3	17.237	9.1	1.0572	1.99951
4	34.474	17.54	1.0786	1.82365
5	86.184	40.66	1.1325	1.40926
6	137.895	65.01	1.1875	1.10401
7	172.369	81.96	1.2248	0.94854
8	189.606	90.66	1.2437	0.88249
9	206.843	99.47	1.2627	0.82313
10	241.316	117.53	1.301	0.72155
11	258.553	126.74	1.3203	0.67808

Figure 3: PVT test results for the well-reservoir model

The initial reservoir conditions for this well include a reservoir pressure of 350 bar and a reservoir temperature of 68°C.

To enhance the permeability around the wellbore, hydraulic fracturing has been employed. The following are the relevant reservoir and technical parameters for the hydraulic fracturing operation.

Inflow Performance Relation (IPR) - Input Data

Done | Validate | Cancel | Reset | Help | Calculate | Report | Plot | Export | Test Data | Sensitivity | Transfer Data | Sand Failure

Hydraulically Fractured Well Model

Reservoir Permeability	113	md
Reservoir Thickness	26.6	m
Drainage Area	77494.3	m2
Dietz Shape Factor	1.96133	Calculate Dietz
WellBore Radius	0.07	feet
Time	1	days
Reservoir Porosity	0.2	fraction
Fracture Height	30.48	m
Fracture Half Length	9.144	m
Dimensionless Fracture Conductivity	5000	

Figure 4: Input parameters for the hydraulic fracturing model in Prosper

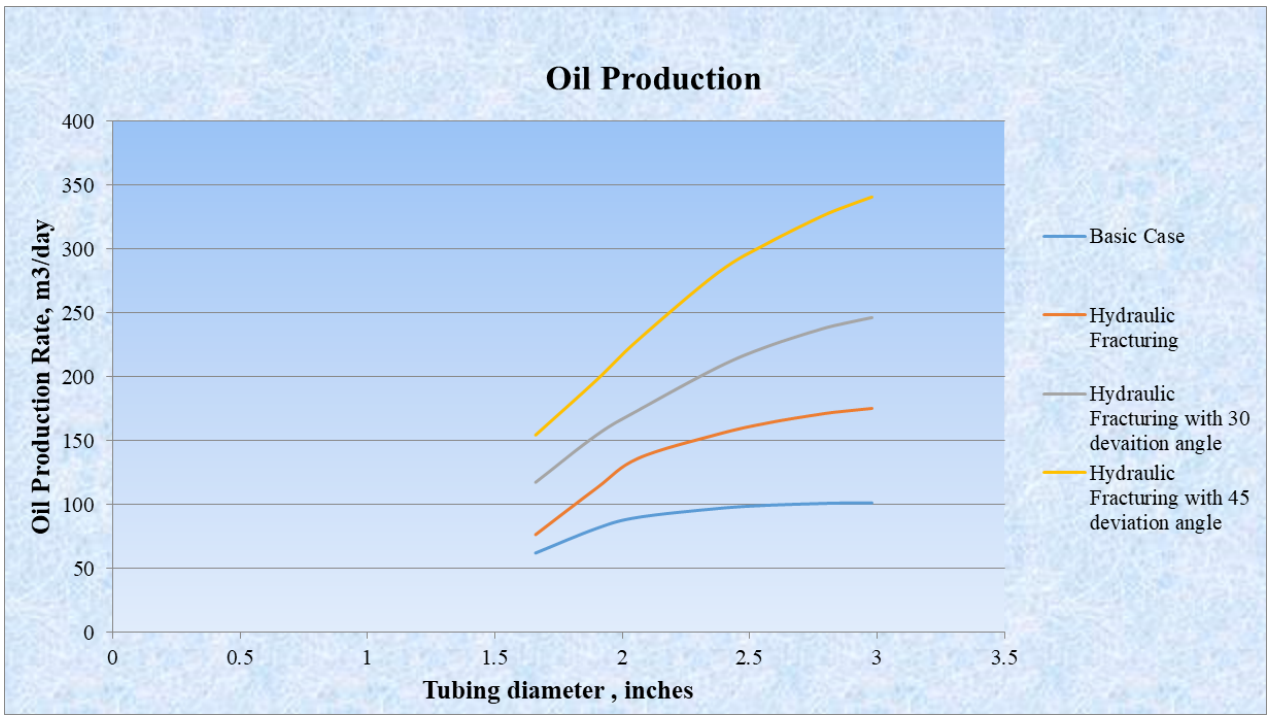

Figure 5: The daily oil production rate varies depending on the chosen tubing diameter.

Different tubing diameters can significantly impact the rate at which oil is produced from a well. This variation is a critical consideration in well optimization and reservoir management. It demonstrates that when a tubing diameter of 2.98 inches is selected, the daily oil production rate significantly increases to 340.8 cubic meters per day (m3/day) when employing the hydraulic fracturing method in the case of a 45-degree deviation angle. In contrast, the base case yielded a daily oil production rate of 101.4 m3/day. This comparison highlights the substantial improvement in oil production achieved through hydraulic fracturing with the specified tubing diameter under the given conditions**.**

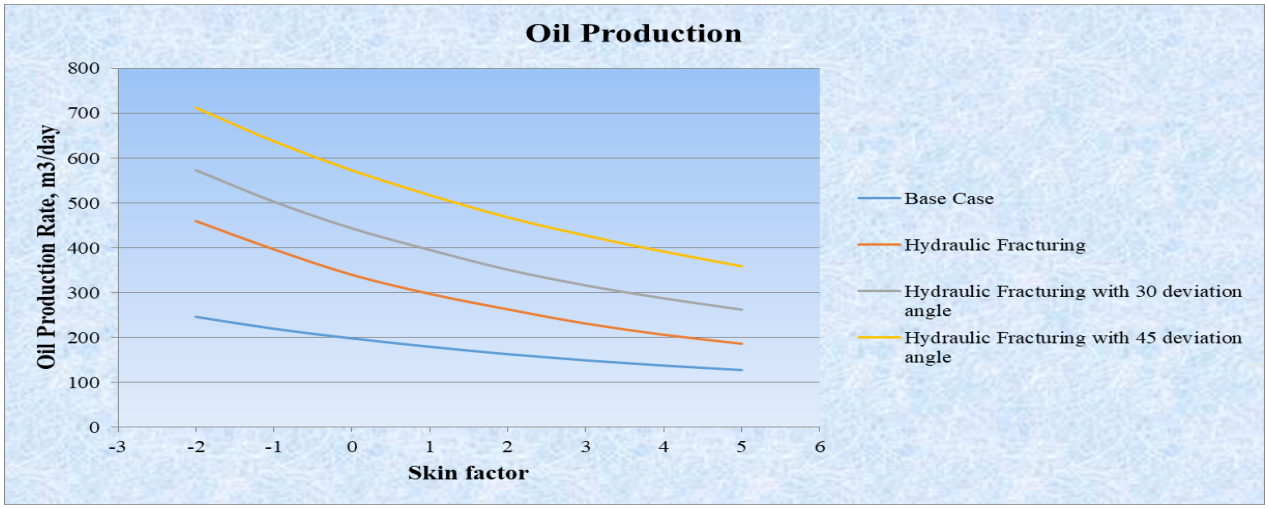

Figure 6: The daily oil production rate varies with different skin factors.

The skin factor is a key parameter that can influence the productivity of a well. Changes in skin factor can have a notable impact on the rate at which oil is produced from a well. Understanding

how different skin factors affect oil production is essential for well management and reservoir optimization.

Figure 6 depicts that when a negative skin factor of -2 is selected, the daily oil production rate significantly increases to 711.6 cubic meters per day (m3/day) when employing the hydraulic fracturing method in the case of a 45-degree deviation angle. In contrast, the base case yielded a daily oil production rate of 245.8 m3/day. This comparison highlights the substantial improvement in oil production achieved through hydraulic fracturing with a negative skin factor under the given conditions.

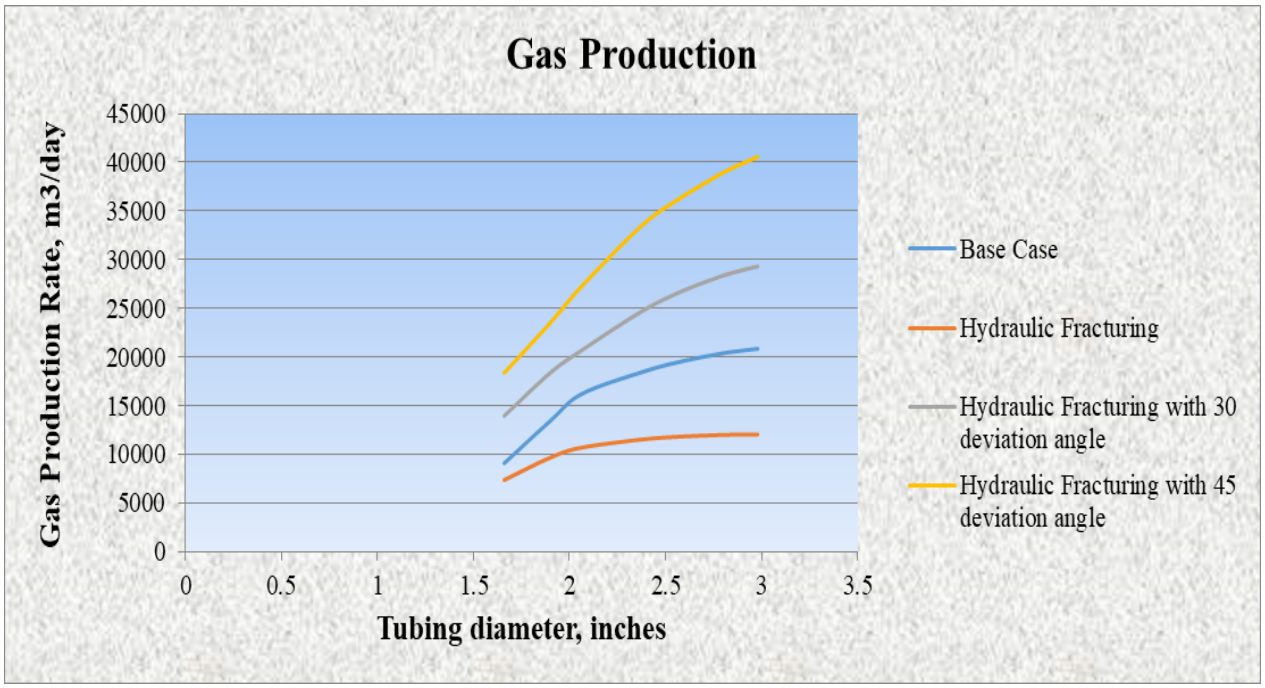

Figure 7: The daily gas production rate can vary depending on the choice of tubing diameter.

Different tubing diameters can have a significant impact on the rate at which natural gas is produced from a well. This variation is an important consideration in optimizing well performance and reservoir management, especially when aiming to maximize gas production.

Figure 7 illustrates that when a tubing diameter of 2.98 inches is chosen, the daily gas production rate significantly increases to 18,388 cubic meters per day (m3/day) when employing the hydraulic fracturing method in the case of a 45-degree deviation angle. In contrast, the base case yielded a daily gas production rate of 7,398.5 m3/day. This comparison underscores the substantial improvement in gas production achieved through hydraulic fracturing with the specified tubing diameter under the given conditions.

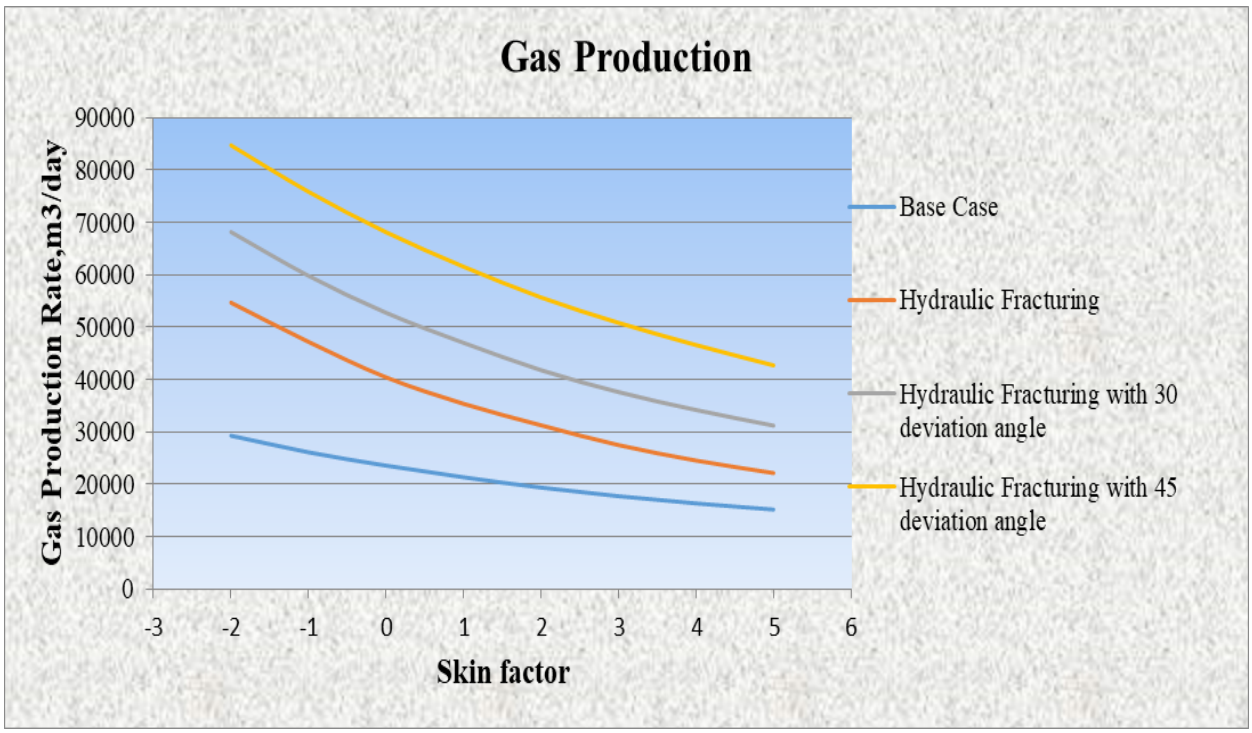

Figure 8: The daily gas production rate can vary with different skin factors.

Figure 8 demonstrates that when a negative skin factor of -2 is selected, the daily gas production rate significantly increases to 84,681.9 cubic meters per day (m3/day) when employing the hydraulic fracturing method in the case of a 45-degree deviation angle. In contrast, the base case yielded a daily gas production rate of 29,245.8 m3/day. This comparison highlights the substantial improvement in gas production achieved through hydraulic fracturing with a negative skin factor under the given conditions.

3. Conclusion

In conclusion, hydraulic fracturing proves to be an effective method for creating fractures in the rock formation, which stimulates the flow of natural gas or oil and increases the recoverable volumes. Choosing a deviation angle in well completion allows for a more extensive coverage of the drainage area compared to a vertical well. Additionally, in a deviated well, the pressure around the wellbore is higher than in a vertical well. The selection of a larger tubing diameter further enhances the extraction of oil and gas from the well. Through sensitivity analysis, the research has successfully determined the optimal tubing diameter and the targeted skin factor around the wellbore, which are critical factors in maximizing production.

Conflict of interest

The authors declare that they have no conflict of interest in relation to this research.

4. References

1. Reservoir Stimulation Ahmed S.Abou -Sayed
2. Jabrayil Eyvazov, Natig N.Hamidov. The effect of hydraulic fracturing length to the well production // Journal of Physics Conference Series 2594(1):012022. DOI: 10.1088/1742-6596/2594/1/012022

3. Robert S. Schechter, W.A (Monty) Moncrief Endowed Chair in Petroleum Engineering. “Oil Well Stimulation”, 2013. “Origins of the formation Damage”, page 121-129,246-249
4. Tulparkhan Salavatov, Hajı Malikov, Jabrayıl Eyvazov. Removing formation damage around wellbore by hydraulic fracturing method and increasing well drainage area // Geotechnological Problems of Oil, Gas and Chemistry Scientific Research-Scientific Papers. XX volume.2020. pp 235-241
5. Zhai, F, A and C. A new tool for multi & multi-well hydraulic fracture modeling // SPE-173367-MS (2015)
6. Jabrayil Eyvazov, Natig N.Hamidov .The Effect of Different Hydraulic Fracturing Width to the Well Production // International Journal of Oil, Gas and Coal Engineering2023; 11(4): 74-78http://www.sciencepublishinggroup.com/j/ogcedoi: 10.11648/j.ogce.20231104.12ISSN: 2376-7669 (Print);

About one of methods for determining the true parameters of the gas-liquid flow in risers

Ismayılov Sh.Z., Ismayilov G.G., Ismayilova P.Sh.
Azerbaijan State Oil and Industry University

Annotation.
In oil and gas production, multiphase gas-liquid flows are very typical for risers of fountain and gas lift wells. In the article, a new approach for estimating the real parameters of multiphase flows is proposed, taking into account the phase shift, and the possibility of their determination based on the macroscopic parameters is shown.

Keywords: multiphase flow, gas lift riser, flow parameters, structural mode, phase shift.
*Corresponding author. Tel.: +994502016674
E-mail:

1. Introduction.

It is very important to correctly assess the true characteristics of those flows in order to solve engineering problems related to multiphase flows, to perform hydrodynamic calculations in accordance with thermo-baric conditions in the viewed (researched) section of the lifting pipes. The analysis shows that important parameters such as the real density of the mixture, the real volume capacity of the phases, which characterize such flows, depend to a great extent on the slippage (relative speed) of individual phases, as well as the cross-sectional migration [1-6].

2. Formulation of the problem and solving methods.

In general, the study and determination of the true gas capacity parameter for gas-liquid mixtures has been the subject of research by many scientists, but in many cases, it has concluded with contradictory results. Thus, a number of researchers have emphasized that the real gas capacity (φ) increases with the increase of the relative velocity of the gas phase (displacement relative to the liquid), and some of them have emphasized the decrease of the φ parameter with the increase of the relative velocity of the gas. There were also scientists who claimed that the mentioned dependence

does not exist at all and that this effect occurs only at values of speed greater than 2 m/s. The analysis shows that, indeed, the problem of determining the drift factor of gas (bubbles and its germs) for the purpose of estimating the real gas capacity, although there are currently a number of analytical and semi-empirical formulas for determining the velocity of gas bubbles in multiphase flows, solving engineering problems it also necessitates and conditions the construction of simpler models based on well data and dependent on macroscopic parameters [2, 7, 8].

It is known that the relative velocity of gas in vertical pipes can be described by the interaction of Froud (*Fr*), Reynolds (*Re*) and We (*Weber*) criteria. According to these criteria, the diameter of the gas bubbles, the surface tension and the diameter of the pipe have the greatest effect on the relative velocity of the gas. The degree of influence of the last two parameters on the relative speed depends on the dispersion of the system. It happens when the diameter of the pipe, mainly the size of the bubbles (plug) is the same size as the diameter of the pipe. Since the laboratory tests were carried out in small diameter pipes ($<10^{-3}$ *m*), and the diameter of mining pipelines is relatively large, some of the obtained results may not be sufficiently justified. The question of determining the value of the diameter for gas bubbles in the risers in mining practice is also a very problematic issue.

Depending on the volume capacity of the liquid and gas phases in the fountain and gaslift risers, it is possible to have a liquid or gas phase as a dispersion phase. If we take into account that these processes occur with the change of pressure gradients both along the riser (longitudinally) and along the cross-section of the pipe, then the question of determining the true parameters for multiphase flows becomes even more relevant. Taking into account the above, the calculation of the real parameters of multiphase flows (the real density of the mixture, the real gas capacity and the relative velocity of the gas) was considered on the example of a gas lift (Fig. 1), and for this purpose, the operational data of gas lift wells were used (tables 1 and 2).

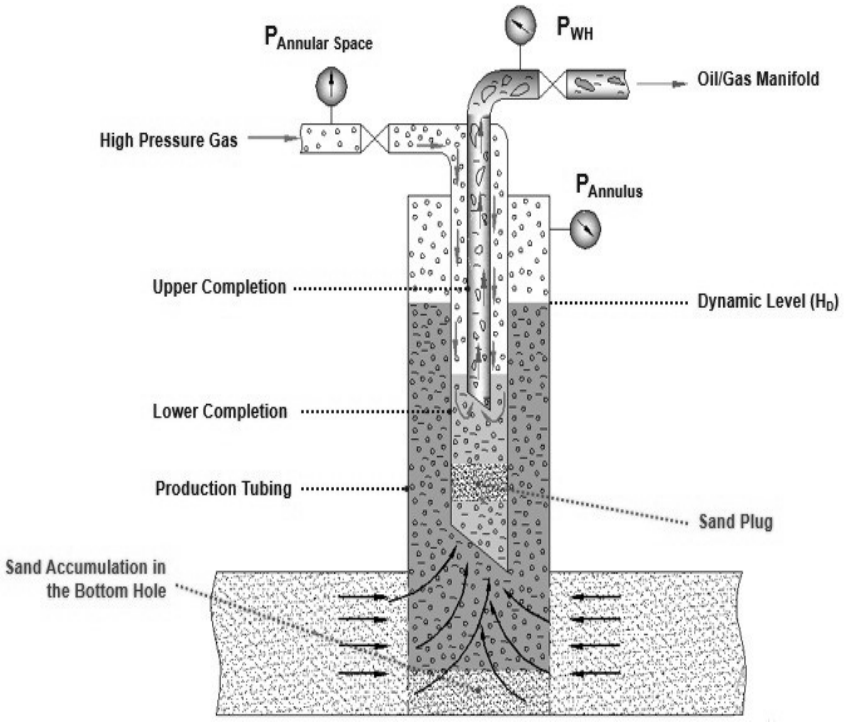

Figure 1. Scheme of the fountain or gas lift riser

Table 1

Tubing of the first and second row of wells in the Gunashli field (Submersible Platform -15) and information about changes in production (28.04.2022)

Well №	Row I		Row II		Production, t/day		Gas, ths. m^3/day		Gas factor (GOR) m^3/t	Gas consumption for 1 t oil
	73 mm	114 mm	48 mm	73 mm	Q_{oil}	Q_{water}	Injection	Production		
93	1358	1514	1199	1001	47.0	7.0	18.0	25.2	153.2	383.1
98	1547	1482	1100	1304	9.0	1.0	12.0	17.2	578.3	1334.6
220	1561	1466	595	1203	34.1	82.9	17.0	26.7	284.4	498.4
235	1468	1548	901	1303	37.0	24.0	17.0	26.5	256.6	459.3
237	1328	1591	901	1496	47.0	0	20.0	26.5	138.4	425.8
248	2305	703	1802	604	46.0	15.9	20.5	29.0	184.7	445.4
271	1260	1620	695.4	1503.6	35.0	1.0	17.0	34.8	508.8	485.9
272	1390	1405	1202	1201	37.0	1.0	21.0	36.6	421.6	567.6
274	1877	940	1496	706	34.1	1.0	6.0	34.5	836.9	176.2
275	1470	1488	805	1297	39.0	18.0	26.5	59.0	833.1	679.3
277	1348	1489	997	604	34.0	0	14.0	51.4	1099.0	411.4
279	1400	1492	698	1357	83.0	0	21.0	29.9	107.3	253.1
281	1509	575	1700	205	17.1	1.0	18.0	28.3	604.4	1056.2
283	1566	1444	1153	1252	9.0	1.0	27.0	34.2	800.7	3002.8
285	1356	1552	805	1302	35.0	0	23.0	31.9	254.1	656.8
294	876	1997	403	1974	57.0	0	19.0	28.5	166.6	333.2
431	2260	1081			20.0	0	31.5	44.0	624.6	1573.9

Table 2

Pressure and production changes in wells in the Gunashli (Submersible Platform-15) field

Well №	$P_{wh.}$ atm	$P_{ann.sp.}$ atm	$P_{annulus.}$ atm		Diameter of choke.mm	$Q_{oil.}$ m^3/day	$Q_{gas.}$ m^3/day
98	18/19	20	30		10	10.3	15400
220	34/38	90/92	152		11	124.1	25800
235	46/64	96/100	140		8	67.7	25000
271	17/20	49	53		14	40.8	33700
274	19/24	53	58		15	40.8	33800
98	18/19	20	30		10	10.0	15700
220	34/38	90/92	156		11	124.6	25800
235	46/64	96/100	142		8	68	26000
271	17/20	49	53		14	41.0	33700
274	19/24	53	58		15	41.5	33500
98	18/19	20	30		10	10.5	15700
220	34/38	90/92	156		11	124.4	25800
235	46/64	96/100	142		8	68.6	27000
271	17/20	49	53		14	41.9	33700
274	19/24	53	58		15	42.0	33500
237	18/20	58	65		15	58.0	25800
281	21/22	43	53		11	21.6	25900

To calculate the actual density (ρ) of the mixture in the riser. the following formula was used based on the actual well data:

$$\rho_{act} = \frac{P_{op} - P_{buf}}{g \cdot h} \quad (1)$$

where P_{op} - working pressure;

P_{buf} – buffer pressure (it can also be wellhead pressure);

h is the length of the gas lift.

If we take into account that the density of the mixture is determined by the expression $\rho_{act}=\rho_{liq}(1-\varphi)+\rho \cdot \varphi$ based on the true gas capacity (φ) according to the rule of additivity. then we get the following expression for determining φ:

$$\varphi = \frac{\rho_{liq} - \rho_{act}}{\rho_{liq} - \rho_{gas}} \quad (2)$$

where ρ_{liq} and ρ_{gas} are the liquid and gas phase densities. respectively.

It is known from experience that the real gas capacity is $\varphi<\beta$ during the vertical movement from bottom to top due to the displacement of gas relative to the liquid in the fountain (gas lift) riser. Taking into account the slippage factor. the following expression can be written for the determination of the actual gas capacity:

$$\varphi = \frac{Q_{gas}}{Q_{gas} + Q_{liq} + Q_{slip}} \quad (3)$$

where Q_{slip} is the slippage consumption of gas;

Q_{gas} and Q_{liq} - gas and liquid consumption in the riser at medium pressure and temperature. respectively.

From the last expression. we get to calculate the consumption of slipped gas:

$$Q_{slip} = \frac{1-\varphi}{\varphi} \cdot Q_{gas} - Q_{liq} \quad (4)$$

Taking the average pressure in the gas lift as the arithmetic mean and taking into account the static level at the wellhead. the following expression can be written to determine gas consumption (Q_{cons}) under normal conditions:

$$Q_{cons} = (Q_{liq} + Q_{slip}) \cdot \frac{(P_{op} + P_{buf}) \cdot P_{buf}}{2P_0 \cdot (P_{op} - P_{buf})} \quad (5)$$

where P_0- is normal atmospheric pressure.

From the last statement. we get the following formula for the determination of Q_{slip}:

$$Q_{slip} = \frac{Q_{cons}}{A} - Q_{liq} \quad (6)$$

here

$$A = \frac{(P_{op}+P_{buf})\cdot P_{buf}}{2P_0\cdot(P_{op}-P_{buf})} \quad (7)$$

From the last expression. the parameter Q_{slip} can be calculated based on the operating data of the gaslift well. Considering that $Q_{slip} = 0.785D^2 \cdot v_{rel}$ (D is the diameter of the lifting pipes). then the relative speed of the gas can also be determined:

$$v_{rel} = \frac{Q_{slip}}{0.785D^2} \quad (8)$$

Based on the data on the wells of the "Gunashli" field (Submersible Platform-15). using the pressure and other data on several gas lift wells. the real parameters of the multiphase gas-liquid flows in the lifters were calculated in the order mentioned above. and the results are given in table 3.

First. according to the formula (1). the gas-liquid mixture is calculated based on the worker ($P_{op} = P_{ann.sp}$). buffer pressure (wellhead pressure. $P_{buf} = P_{wh}$) and riser length (h) for wells № 98. 220. 235. 271 and 274. real density (ρ_{act}) is determined.

Table 3

The pressure on the wells in the Gunashli field (Submersible Platform-15) and values of the true parameters of the multiphase mixture in the riser

Well №	P_{wh}. atm	$P_{ann.sp}$.. atm	$P_{annulus}$. atm	ρ_{act}. kg/m^3	φ	A	Q_{slip}. m^3/day	V_{rel}. m/sec
98	18/19	20	30	20.37	0.977	171.0	90.6	0.25
220	34/38	90/92	156	466.04	0.471	41.56	525.4	1.45
235	46/64	96/100	142	336.40	0.618	77.08	282.8	0.78
271	17/20	49	53	264.51	0.700	21.53	1580.0	4.35
274	19/24	53	58	447.60	0.492	26.61	1271.9	3.50

Note: P_{wh}. $P_{ann.sp}$ and $P_{annulus}$ - wellhead. annulus. pipe respectively are the pressures behind it.

Taking into account the calculated true density of the mixture. the densities of the liquid and gas phase. the value of the true gas capacity of the multiphase mixture was determined for the wells according to the formula (2).

Taking into account that the liquid phase is small. the density of the liquid is ρ_m= 880 kg/m^3. and the density of the gas phase is $\rho_{gas}=1.2\ kg/m^3$.

Then. the part of the gas in the liquid phase that is subject to displacement (expenditure) was calculated according to the expression (5). Finally. according to the formula (8). the slippage (relative) speed of the gas phase was determined.

The values of the parameters reflecting the true characteristics of the multiphase flow calculated based on the macroscopic operating data are given in table 3. As can be seen from Table 3. the characteristics of the liquid-gas mixture in individual lifters of the studied gas lift wells are significantly different from each other due to the gas phase shift. and in some cases this difference is up to 20 times different.

Thus. in order to control the operation of gas lift wells. the possibility of estimating the real parameters of the multiphase flow in the riser based on the actual data of the well. taking into account the phase shift. was determined.

3. Conclusion

1. A new approach based on well operation data is proposed to determine the true characteristics of multiphase flows in gas lift (fountain) risers as well as in vertical pipes of underwater pipelines.

2. On the example of the wells of the "Gunashli" field (Submersible Platform-15) based on the actual operational data. the feasibility of estimating the real density. real gas capacity and phase shift of the gas-liquid flows in the risers and their suitability for engineering calculations have been shown.

Conflict of interest

The authors declare that they have no conflict of interest in relation to this research.

4. References

1. Guzhov A.I. Joint gathering and transportation of oil and gas// Moscow: Nedra. 1973. 280 p.
2. Sattarov R.M.. Kiyasbeyli T.N.. Ismayilov G.G. et al. Technique of hydraulic calculation of the optimal regime for the development of offshore underwater pipelines with the joint movement of oil and gas. Baku// AzINEFTECHIM. 1990. 20 p.
3. Chisholm D. Two-phase flows in pipelines and heat exchangers. Moscow// Nedra. 1986. 204 p.
4. Grichenko A.I.. Klapchuk O.V. Hydrodynamics of gas-liquid mixtures in wells and pipelines. Moscow: Nedra. 1994. 238 p.
5. Sow S. Hydrodynamics of multiphase systems// M.: Mir. 1979. 536 p.
6. Ismailov Sh.Z.. Suleymanov A.A.. Novruzova S.H. et al. Oil and Gas Well Production Technology// Baku. Elm. 2022. 540 p.
7. F. B. Ismayilova. Iskandarov E.X.. Babirov H. PROCEEDİNGS of Azerbaijan high texnikal educational institutions. Vol.18. Issue 07.2022. pp. 50-54.
8. Ismayilov G.G.. Ismayilova F.B.. Iskandarov E.X.. Adygozalova M.B. Multiphase technologies in oil and gas production// Baku. Elm. 2018. 300

Research on the possibility of hydrocarbon emissions control.

A.I.Babayev, N.I.Imanova, Z.A.Baghirova, T.H.Malikov

Scientific Research Institute of Geotechnological Problems of Oil, Gas and Chemistry, ASOIU, 20 Azadlig Avenue. Baku, AZ-1010 Azerbaijan

Abstract.

All processes in the chemical and petrochemical industry generally consist of a number of comparable standard processes, although the products produced may vary. In the chemical engineering industry and related industries, a typical process is a fundamental step in technology. For example, in the production of ammonia (NH3), gasification, reforming and synthesis of NH3

are typical processes that are interconnected and create a complete technology. Practically, the technological chain of methanol production also follows this sequence. Also the production of carbamide. The technology of individual production may consist of a large number of standard processes to obtain the desired product. However, the mechanisms for the formation of fugitive emissions in any state of aggregation practically differ little, except for the chemical composition of the emissions. As a result, the results of this study and methodology can be successfully applied to other installations and industries.
Key words: technology, processes, production, methanol, organized, unorganized emissions, ecology, thermal imaging control.
*Corresponding author. Tel.: +994 519489895
E-mail address: ziba.b84@gmail.com

1. Introduction

As technological installations know, emissions into the atmosphere are divided into 2 types: organized and unorganized. The analysis of fugitive emissions acquires particular importance after a long period of operation of the installation, after the elimination of major technological accidents, during the commissioning of new ones put into operation after major construction and fundamental technical refurbishment and reconstruction in order to avoid loss of resources and environmental pollution. Notes that the chemical industry is only a minor source of emissions for most pollutants (1-4). In this work, we will consider the possibilities of analyzing and calculating fugitive emissions in existing methanol production after long-term operation and relocation.

2. Conducting the experiment

Research was carried out at all potential sites (points) of fugitive emissions (leaks) on process pipelines, units, vessels and devices of auxiliary, main production and tank farms.

The inspection of “points” of potential leaks was carried out using thermal imaging control technologies. Experimental studies under operational conditions were carried out in accordance with the main provisions of the developed thermal imaging control technology. Before carrying out thermography, all necessary preparatory operations were completed. As a diagnostic equipment, a thermal imager of the FLIR GF320 type was used. The device is able to quickly survey large areas and detect the presence of hydrocarbon gas leaks in real time (5). Recently, intelligent thermal imaging equipment has been successfully used, which is an effective tool for monitoring any temperature changes in a variety of fields and industries, to ensure safety at production facilities in order to identify defects and prevent leaks of hazardous substances (6).

The number of examined “points” of potential leaks was first determined by analyzing process diagrams using working drawings. Their preliminary estimated number was 7579. Of these, 270 “points” relate to auxiliary production, 498 – to the tank farm, that is, containers for storing the finished product, raw materials and reagents, intermediate semi-finished products that are involved in the production process, waste obtained in the results of side reactions, which are further processed into target products (7).

3. Results and their discussion

Based on the results of the application of thermal imaging monitoring technologies on process pipelines, units, vessels and apparatuses of the entire production, 7579 possible suspected leak

points were analyzed. Out of a total of 7,579 points inspected, leaks were found in 29 points. Of these, 1 “point” related to the tank farm, the rest directly related to process equipment, communication pipelines, measuring circuit elements and actuators. All analyzes of fugitive emissions, namely their volumes, are calculated in kg for one year. Based on the results of the analysis and calculations, the total annual volume of fugitive emissions was established for the main components. The calculation results are shown in Figure 1.

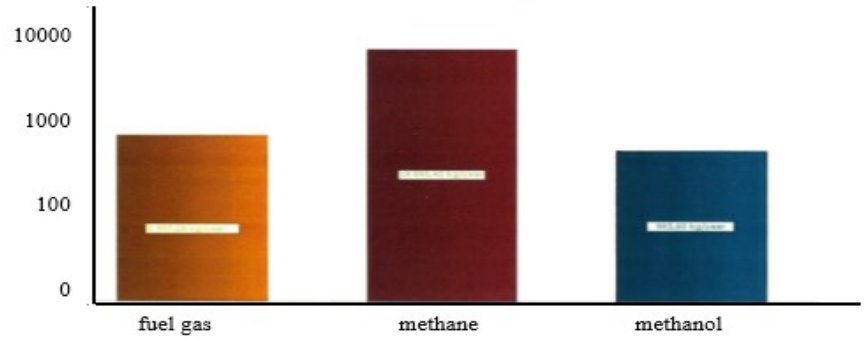

Fig. 1 Final estimated volume (mass fraction) of fugitive hydrocarbon emissions

If we calculate the volume of fugitive emissions of fuel gas - methane by type of element, then we can draw the following conclusions from the analysis data. Analyzes were carried out at 5188 "points", 24 of which were found to be leaking and only 4 of these "points" were repaired.
According to the analysis of fugitive methane emissions, several places of fuel gas leaks can be noted:
1) stuffing box - 1401.60 kg / year
2) threaded connections - 262.80 kg / year
3) other - 18331.03 kg/year
Total: 19995.43 kg / year.
Detection of leakage of fuel gas emissions - methane by type of element, was carried out using the thermal imaging method of photographing possible leakage points according to the technological scheme. The results of thermal imaging images of fuel gas leaks are shown in Figures 2, 3, 4, 5.

Ordinal number	Type of pipeline element fittings, apparatus,	unit
1	D-7 injector coupling (American)	Natural gas
Photograph of the object	thermal image	

Fig. 2 D-7 injector coupling (American)

Ordinal number	Type of pipeline element fittings, apparatus,	unit
2	Welded seam on the fuel gas line to the injector İ-5	Natural gas
Photograph of the object	thermal image	

Fig. 3 Welded seam on the fuel gas line to the injector I-5

Ordinal number	Type of pipeline element fittings, apparatus,	unit
3	Q-2 injector coupling	Natural gas
Photograph of the object	thermal image	

Fig. 4 Q-2 injector coupling

Ordinal number	Type of pipeline element fittings, apparatus,	unit
4	Threaded connection of the flexible injector connection A-7	Natural gas
Photograph of the object	thermal image	

Fig. 5 Threaded connection of the flexible injector connection A-7

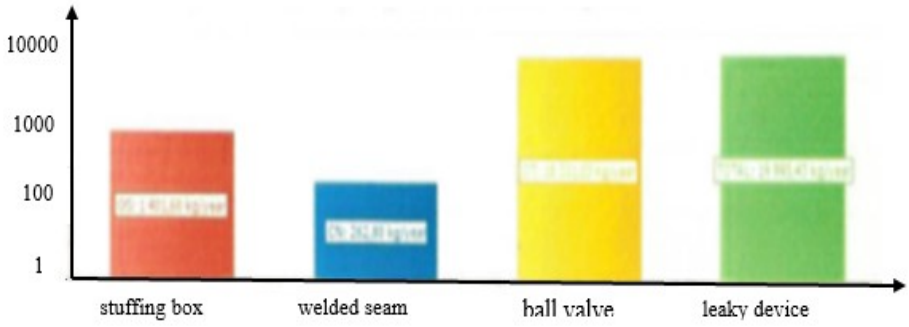

Fig. 6 Estimated volume (mass fraction) of fugitive emissions

And also according to the above analysis, it is possible to note specific places - equipment of fugitive emissions:

1) injector connection - 7992.42 kg / year:
threaded connection 1 – 7729.62 kg/year
threaded connection 2 – 262.80 kg/year
2) welded seam - 1927.20 kg / year
3) ball valve - 1401.60 kg / year
4) leaky device - 8674.21 kg / year
Total: 19995.43 kg / year.

A graphical representation of the results obtained is shown in Figure 7

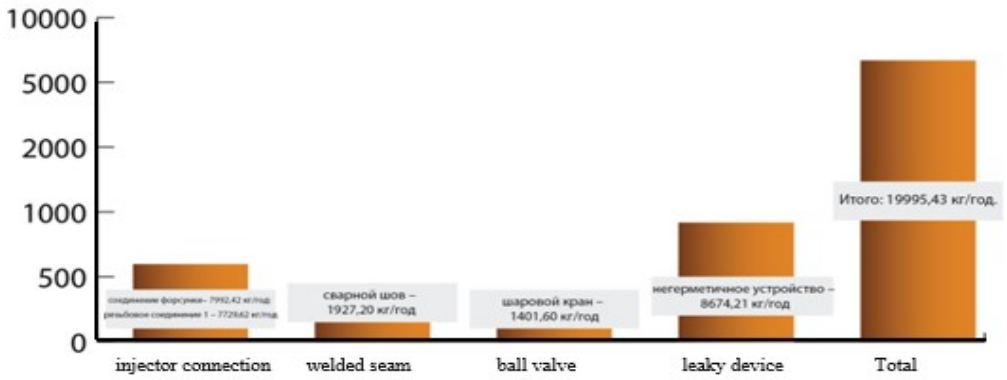

Fig. 7 Estimated volume (mass fraction) of unorganized fuel gas purifiers by position kg/year.

The second source of gaseous losses in the methanol production process is synthesis gas. It should be noted that gas synthesis technology differs in many respects from fuel gas technology. Accordingly, the checked control points are also comparatively smaller.
Analyzes were carried out at 601 “points”. Detection of mixed gas-gas leakage by element type was also carried out using the thermal imaging photography method with the possibility of replacing the leak according to the process flow diagram. The results of thermal imaging of synthesis gas leaks are shown in Figures 8, 9.

Ordinal number	Type of pipeline element fittings, apparatus,	unit
5	Threaded connection of the selection valve for the device pos.FE-2789 (HE-401)	syngas
Photograph of the object thermal image		

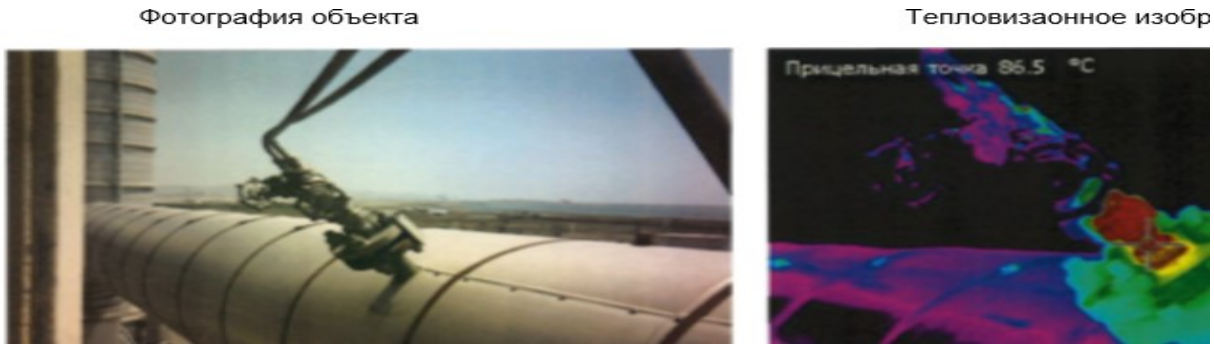

Fig. 8 Threaded connection of the selection valve for the device pos.FE-2789 (HE-401)

Ordinal number	Type of pipeline element fittings, apparatus,	unit
6	Threaded connection of the selection valve for the device pos.AT-18794 (R-401)	syngas
Photograph of the object thermal image		

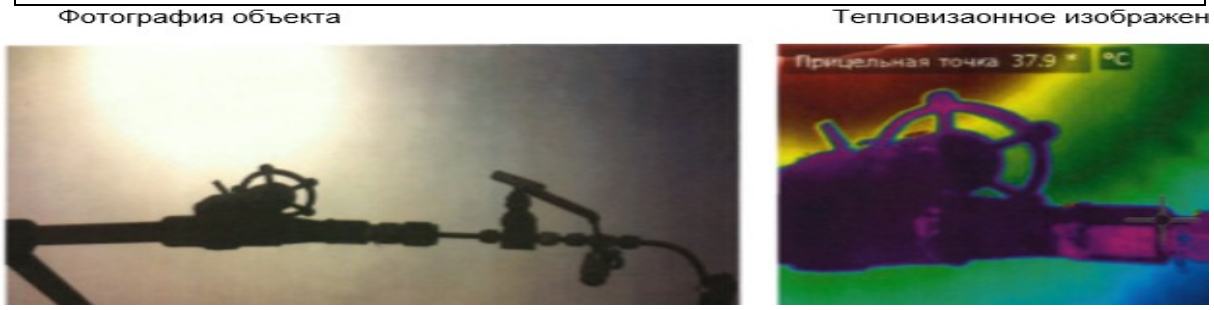

Fig.9 Threaded connection of the selection valve for the device pos.AT-18794 (R-401)

Based on the analysis of the estimated volume of fugitive emissions of synthesis gas by element type, the following results were obtained:
1) flange connections - 1471.68 kg/year
2) stuffing box – 525.60 kg/year
Total: 1997.28 kg/year.
A graphical representation of the results obtained is shown in Figure 10.

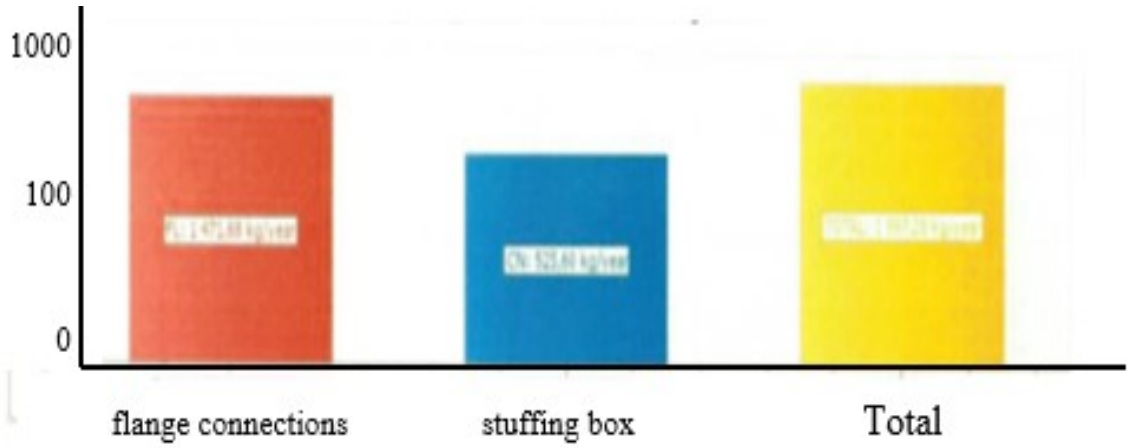

Fig. 10 Estimated volume (mass fraction) of fugitive emissions of synthesis gas kg/year.

A control analysis was carried out on a specific equipment position and connection point in the synthesis gas process loop and the following results were obtained:
1) flange connections - 735.84 kg/year
2) threaded connection - 525.60 kg/year
3) valve – 735.84 kg/year
Total: 1997.28 kg/year

A graphical representation of the results obtained for specific locations - fugitive emissions of synthesis gas equipment is shown in Figure 11:

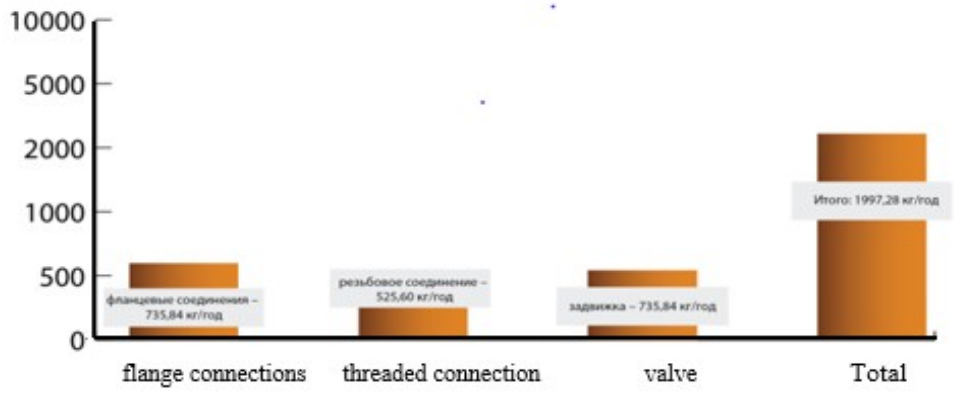

Fig. 11 Estimated volume (mass fraction) of fugitive synthesis gas emissions by position, kg/year.
As noted, the technological installation has 498 tank equipment. Taking into account the harmful properties of methanol, analyzes were carried out at 1790 “points”. It was installed in one place - equipment for fugitive methanol emissions:

1) locking cap – 963.60 kg/year.

The photo image of the detected pass point is shown in Figure 12.

Ordinal number	Type of pipeline element fittings, apparatus,	unit
7	Tank gauge cover 24TK-0024	methanol
Photograph of the object	thermal image	

Fig 12 Cover of the tank measuring device 24TK-0024

A graphical representation of the results obtained for specific locations - equipment for fugitive methanol emissions is shown in Figure 13.

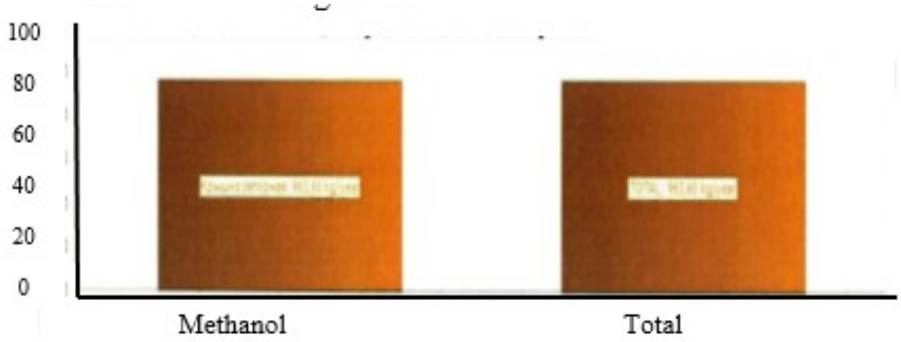

Fig. 13 Estimated volume (mass fraction) of fugitive methanol emissions by position, kg/year.

Particular attention must be paid to the drainage and transport communication hub. Because this system is quite highly mobile. During the day, connecting nodes undergo dynamic technological operations by connecting and disconnecting several times. This explains the high level of detected gaps.

Analysis of the above data shows that there is a high overall level of hydrocarbon losses and an extremely high level of hydrocarbon losses relative to the amount of fugitive emissions after a certain time of operation of the equipment. Based on this, after long-term operation of a production plant, it is necessary to conduct a control inspection of the technical condition of process equipment, communication pipelines, connecting units and seal tightness. Systematic qualification analysis of the state of unorganized emissions at a production enterprise also guarantees safety, explosion and fire safety, stable operation, and high economic efficiency.

4. Conclusions

According to the analysis results, it can be noted that the mass fraction of methane prevails and amounts to 19995.43 kg/year. The mass fractions of synthesis gas and methanol are 1997.28 kg/year and 963.60 kg/year, respectively. Consequently, the final calculation of the volume (mass fraction) of fugitive hydrocarbon emissions is 22956.31 kg/year. The number of inspected “points”

of potential leaks using thermal imaging control technologies on process pipelines, units, vessels and apparatuses of the entire production is 7579. Of the 7579 inspected “points”, 270 “points” relate to auxiliary production; 6811 - main production, 498 - tank farm.
In 498 tank equipment, analyzes were carried out at 1,790 “points” and only one was detected, and 6,811 points in the main production of 29 cases of fugitive emissions. It has been established that the main share of fugitive emissions comes from the methane technological communication system and logistics. Based on this, in the applied significance of this study, similar enterprises are recommended to systematize and strengthen control in the presence of such systems and components.

Conflict of interest

The authors declare that they have no conflict of interest in relation to this research.

4. References:

1. https://www.eea.europa.eu/ru/publications/rukovodstvo-emep-eaos-po-inventarizaciivybrosov-2016
2.https://www.eea.europa.eu/ru/publications/rukovodstvo-emep-eaos-po-inventarizaciivybrosov-2019
3. The science. Technology. Production-2017. “Applied science as a tool for the development of petrochemical production” // Materials of the International Scientific and Technical Conference dedicated to the Day of the Chemist and the 40th anniversary of the Department of Chemical Technological Processes of the branch of the Ufa State Petroleum Technical University in Salavat Ufa Publishing house USPTU 2017
4. Geological CO2 storage in Eastern Europe, the Caucasus and Central Asia: an initial analysis of potential and policies // UNITED NATIONS GENEVA, 2021 c2021 United Nations5. http://ptk-nk.ru/index/poisk_utechek_i_teplovizionnyj_kontrol/0-14
6. https://hikvision.ru/press/190617035746
7. A. I. Babayev Ecological Cybernetics of Oil Processing and Petrochemical Processes11th World Conference “Intelligent System for Industrial Automation” 7s

Influence of technological modes for manufacturing parts from plastic materials on the accuracy of their dimensions

N.A. Gasanova
Azerbaijan State Oil and Industry University,
Azerbaijan Republic, Azadlig Ave., Baku, AZ-1010 Azerbaijan,

Abstract. Constructions of oilfield equipment details (thread, cover, flange, etc.) can be made of various plastic materials. The influence of technological modes of casting on the quality of plastic parts of oilfield equipment is considered. In the manufacture of plastic parts from various compositions of press materials, the main technological factor affecting the quality of the parts is the casting regime. Based on the results obtained, modes are recommended for a specific brand of plastics used in oilfield equipment.

Keywords. plastic parts, technological parameters, casting temperature, injection molding, optimal cylinder temperature.
*Corresponding author. Tel.:
E-mail: haciyevanaila64@gmail.com

1. Introduction.

The nature of the course of physical and chemical processes, the formation of the structure and properties of plastics, mainly depends on the technological parameters of the manufacturing process of specific parts.

The mode of manufacturing parts from plastics during pressing and injection molding is determined by three components: temperature, residence time of the part in the mold and pressure. It should be noted that the accuracy of manufacturing plastic parts depends not only on fluctuations in the values of these main technological factors, but also on changes in their nominal values [1]. In the latter case, the issues of improving the accuracy of manufacturing parts should be addressed together with the issues of economics of production, increasing labor productivity.

The temperature at which casting takes place determines the cooling time of the material in the mold, the filling time, the required pressure, the initial temperature of the mold, and the final properties of the products. In the injection molding process, heat is consumed to heat the material in the cylinder, to transform the material into a viscous-flowing state, and partially goes into the environment.

2. Methodological part.

The choice of the optimal temperature of the heating cylinder in each case is determined depending on the characteristics of the processed material. Therefore, for each brand of material, it is necessary to set the optimum temperature of the cylinder, at which a high productivity of a homogeneous melt and the required quality of products are achieved.

The pressing temperature depends on the properties of the material and its initial state, as well as the configuration of the part and the dimensions of the part. It is economically beneficial to increase the pressing temperature, but this measure does not always have a positive effect on accuracy, since it causes an increase in part shrinkage [2].

The fluctuation of the values of the pressing temperature in production conditions is mainly due to the following reasons: uneven and unequal heating of the punch and matrix; uneven modes of operation of electric heating devices; different nature of heat transfer, which depends on the type of mold and its weight, ambient temperature, etc. Temperature fluctuations during pressing in removable molds turn out to be much larger, for which it is recommended that parts are pressed out on special heated plates in order to prevent mold cooling.

The pressure during molding of parts made of thermoplastic plastics is necessary for filling the mold cavity with the cast material, its compaction, as well as for the normal course of relaxation processes during cooling in the mold.

It has been established that the value of the optimal pressure on the casting depends on the brand of material, thickness and configuration of the parts.

Pressing pressure has little effect on the accuracy of plastic parts. Holding under pressure is designed to seal the part after filling the mold and prevent material from flowing out of it [3]. With a change in exposure under pressure, the amount of material entering the mold, the pressure in the

mold and the cooling rate of the part in it change, which ultimately has a certain effect on the quality of the parts.

The holding time under pressure is assigned depending on the type of binder resin and on the pressing temperature. This time depends on the type of mold, namely: when pressing in closed molds, it is longer than when pressing in open molds, since the hardening reaction is slowed down by the presence of moisture and volatile substances, the release of which is difficult. The holding time under pressure can be reduced by applying preheating, pre-pressing and holding pressure operations. The operation for pressing is performed when pressing on stationary molds in the manufacture without reinforcing parts. It consists in removing gaseous products from the mold cavity immediately after it is closed.

3. Results and discussion.

Pressure delay operation, i.e. observance of a pause between the moment the punch touches the press material and the moment the mold begins to close is made to prevent the flow of material with high fluidity from the mold cavity even before the material is completely compacted. Operations for pressing and holding pressure increase the accuracy of manufacturing plastic parts [4].

When injection molding thermoplastics, the main factors that determine the mode of manufacturing parts are: the temperature of the material cylinder, which determines the melting temperature of the mass supplied by pressure into the mold; the temperature of the mold, where the cooling of the mass and its curing take place; pressure in the material cylinder; mass injection pressure; pressure in the filled mold; injection speed; total time or duration of the casting cycle, which consists of the cooling time of the plastic part in the mold, the time the material is held in the mold under pressure, the mold closing time, and a number of other terms; design and dimensions of parts.

4. Conclusion.

In general, factors such as temperature, pressure and time affect the accuracy of injection molded parts in the same way as pressing and injection molding, but this influence is further enhanced by a very short manufacturing cycle and its full automation. Due to the high elasticity of plastics processed into parts by injection molding, both the absolute value of the pressure and fluctuations in the pressure value have a particular influence on the accuracy. The specific properties of injection molded plastics also explain the increased influence of molding temperature fluctuations on manufacturing accuracy. In practice, this temperature is equal to the temperature of the material cylinder.

Conflict of interest

The authors declare that they have no conflict of interest in relation to this research.

5. References

1. 1. Kerimov D.A. Scientific foundations and practical methods for optimizing the quality indicators of plastic parts of oilfield equipment// Doctor of Technical Sciences dissertation, abstract, Baku, 1985
2. 2. Kerimov D.A., Kurbanova S.K. Basics of designing plastic parts and molds//Baku: Elm Publishing House, 1997, 504 p.Kerimov D.A., Gasanova N.A., Determination of quality of

plastic details without disruptions. 13th International Conferen-ce on Theory and Application of Fuzzy Systems and Soft Computing — ICAFS-2018, Warsaw, Poland, Springer Nature Switzerland AG 2019, Advances in Intelligent Systems and Computing (AISC),2019, Springer, Cham., 2018., pp. 848-851

3. Gasanova N.A.: Behavior of Plastic Working in Oil-Field Equipment. International Journal of Innovative Research in Computer Science & Technology (IJIRCST), ISSN: 2347-5552, Impact Factor: 4.405, Google Scholar, Crossref, Publons. Vol-5, Issue-5, pp.371-375(2017). https://doi.org/10.21276/ijircst.2017.5.5.2

Predicting the flare temperature of binary mixtures according to data on activity coefficients

N.M.Abbasov*, R.Kh. Malikov, F.R. Cafarli

*Department of Industrial machines, ASOIU, 20 Azadlig Avenue. AZ-1010 Azerbaijan

Scientific Research Institute of Geotechnologocal Problems of Oil, Gas and Chemistry, ASOIU, 20 Azadlig Ave., Baku, AZ-1010 Azerbaijan

Abstract

A method for calculating the flash point from the results of simulating liquid–solid equilibrium at constant pressure using the Gibbs equation is discussed. A model is used to predict the flash point of the mixture based on the modified Le Chatelier equation, the Antoine equation and a model for estimating the activity coefficient.

The flammability hazard of liquids is primarily characterized by their flash point. The flash point is defined as the temperature at which a liquid evaporates and forms a flammable mixture with air. To measure the flash point, closed and open type devices are used. In closed-type devices, the state of equilibrium between the liquid and vapor components of the mixture is studied. Open type devices take into account the interaction of a mixture of flammable liquids with the atmosphere. The flash point of a mixture is a critical property, but experimental data for many mixtures are lacking and obtaining such data is expensive and time-consuming. Therefore, the development of mathematical models for analyzing the state of the environment under conditions of increasing risk of emergency situations is an important scientific and practical task. This paper examines the possibility of predicting the flash point in closed-type devices, i.e. the influence of atmospheric conditions is not taken into account in this approximation. Several models for predicting the flash point for mixtures of various types have been proposed previously.

Keywords: binary mixtures, flash point, boiling point, activity coefficients, solvation coefficient, association coefficient.

*Corresponding author. Tel.: + 994 503112553

E-mail address: malikov.rauf@mail.ru

1. Introduction

Safety in the production and storage of flammable liquids is one of the most important tasks, since dangerous situations often occur, such as explosions at gas stations, accidents during the transportation of flammable substances, etc. When assessing the fire hazard of liquids with a melting point of less than 50°C, a number of indicators of fire and explosion hazard are used: flammability group, flash point, ignition temperature, auto-ignition temperature, lower and upper concentration limits of flame propagation, ability to explode and burn when interacting with water, atmospheric oxygen and others substances, etc. These parameters are interconnected. For example, the flash point is linearly related to the boiling point: fp b t a bt = +, which depends on the ambient pressure. In this regard, the task of assessing the influence of pressure and temperature on the thermodynamic characteristics of mixtures of liquids is relevant. It is especially important to study the behavior at various temperatures, pressure, concentration, thermophysical parameters of the environment, etc. of such flammable liquid mixtures as fuel mixtures, brake fluids, antifreezes used for cooling internal combustion engines, coolants in heating and air conditioning systems. Along with this, it is necessary to solve the problem of heat transfer, which is divided into external or internal depending on the characteristics of the heat source and the shape of the heat accumulator. Thus, predicting the flash point is only part of the problem of studying fire and explosion safety conditions

Models developed for ideal solutions [4−6] are unsuitable for nonideal mixtures, which are most common. The imperfection of solutions is due to the interaction of molecules. The influence of liquid phase non-ideality on activity coefficients is taken into account by constructing appropriate thermodynamic models, which can be divided into two categories: models using experimental data and so-called a priori predictive models. To model the properties of a solution, it is necessary to be able to calculate the activity coefficients of the components of the mixture in the liquid phase.

2. Methodological part

Thermodynamic models NRTL, Wilson and UNIQUAC are often used, but in these models the binary interaction parameters are calculated from experimental data. Therefore, these models are not predictive. The UNIFAC model [12] is predictive, since it does not require experimental data to calculate the parameters of binary interaction. To assess the interaction, group contribution parameters are used [10, 13]. The general model for predicting the flash point of a mixture is known [1] and improved by Liu et al. [2] based on the modified Le Chatelier equation (1), Antoine equation (2) and a model for estimating activity coefficients [3]:

$$\sum_i x_i y_i P_i / P_{i,fr}^0 = 1; \qquad (1)$$

$$log P_i = A - B_i/(T + C_i), \qquad (2),$$

where x_i is the mole fraction of the i-th component in the liquid; γ_i is the activity coefficient of the component; P_i is the saturated vapor pressure of the i-th component of the mixture at a given temperature; P_i, 0 fp is the vapor pressure of pure combustible component i at its flash point, respectively.

The Le Chatelier equation $L = 1/\sum_i p_i/L_i$ is used to determine the explosion limit of a vapor mixture and is a formula for calculating the harmonic mean value, where L is the ignition limit of the mixture; L_i – flammability limits of individual components; pi is the contribution of individual components to the studied property of the liquid mixture. In particular, the equation allows us to determine the average pressure P_{fp} at which a flare can occur, i.e. at $L_i = P_{i,fr}^0$. Under

the condition of phase equilibrium of liquid and vapor, the partial pressure of the vapor of a component of a nonideal liquid has the form $p_i = x_i\gamma_i P_i$. The activity coefficient is introduced as a characteristic of the imperfection of the mixture. If the activity coefficient is equal to one, this means that the interactions between different or the same molecules are identical and the mixture is in an ideal state; if the activity coefficient is different from unity, the mixture is in a non-ideal state. In the case of an ideal solution, $\gamma_i = 1$, the partial pressure of a component is proportional to its fraction in the solution $p_i = x_i y_i P_i$, which is the formulation of Raoult's law. The Antoine equation is an approximate representation of the Clausius - Clapeyron equation for the equilibrium of the liquid and vapor phases and makes it possible to move from pressure to the temperature characterizing the flash point, and to find the dependence of the flash point on the composition. To calculate the flash point on the basis of equilibrium models, the activity coefficients of the components γ_i are determined for a given solution composition, then the vapor pressure of the mixture components $P_{i,fr}^{0}$ is found using the Antoine equation at the flash point of the pure components. The flash point T_{fp} for the mixture is found by solving Antoine's equation (2) and equation (1) together. Substituting the pressure P_i from the Antoine equation into the Le Chatelier equation makes it possible to calculate the flash point for the entire range of solution compositions, i.e. dependence T(x). The main problem is to determine the activity coefficients of the components of a non-ideal mixture. This problem can be solved if mathematical modeling methods are used.

Thermodynamic models of phase equilibrium of solutions From models of activity coefficients of the liquid phase, two types can be distinguished: 1) models used for non-polar systems, for example, mixtures of hydrocarbons, isomers, and homologues, which include regular solution theory (RST) and Flory-Huggins models; 2) models used for non-polar and polar systems. These models are commonly used to predict liquid phase activity coefficients and include the Van Laar equation, Wilson equation, NRTL, UNIQUAC equation, UNIFAC equation, etc.

Vidal et al. [13] combined the flash point prediction of Liu et al. [2] with the model UNIFAC to predict the minimum for highly nonideal solutions. Gmeling and Rasmussen calculated the flash point of binary systems using the UNIFAC model to estimate activity coefficients [10, 14]. At the minimum flash point of the mixture, the flash point may drop by several degrees, increasing the risk of explosion, which is often accompanied by a positive deviation of the liquid–vapor equilibrium from Raoult's law [9, 13, 15]. The maximum on the flash point behavior curve is associated with a negative deviation from Raoult's law, which leads to a decrease in the risk of explosion [16].

In the original UNIFAC model [12], the logarithm of the activity coefficient consists of the combinatorial and residual parts. To improve the performance of the original UNIFAC model predicting liquid–vapor equilibrium (VLE), liquid–liquid equilibrium (LLE) and excess enthalpies, several versions of the model were proposed [17−20].

The main disadvantage of the UNIFAC model and its versions is the need to create a database of group parameters of pure components and interaction parameters. The group contributions of these parameters are systematically improved by the UNIFAC consortium [21]. In [22], the flash point of mixtures is predicted (Liaw and Chiu flash point prediction model [3]); to calculate the behavior of the activity coefficients of the liquid phase, UNIFAC type models are used, which do not require experimental data to find the parameters of the binary system. In Fig. Figure 1 presents experimental data [22], as well as the results of calculating the activity coefficients and flash point temperature for the systems ethanol - butanol-1, ethanol - acetone. Various versions of the UNIFAC model and the NRTL model were used for the ideal ethanol -

butanol-1 system (Fig. 1, a) and the ethanol - acetone system with a positive deviation from ideality (Fig. 1, b). The phase behavior of mixtures becomes more complex if there is a large difference in their physical properties, types of polarity, or critical properties. As can be seen in Fig. 1, there is a significant scatter in the results of calculations of activity coefficients and flash point for different models.

One form of the equation relating various parameters of a system to internal energy can be written as

$$dU = TdS - PdV + \sum_{i=1}^{n} \mu_i dN_i, \qquad (3)$$

where U = f(S,V, N_1, N_2,…,N_n) is the internal energy of the phase as a function of entropy, volume and number of moles of components forming the phase; $\mu = {}_i (\partial U/\partial N_i)_{S\,V\,N,j\neq I}$ chemical potential of the i-th component; $T = (\partial U/\partial S)_{V\,N,j\neq i}$ − temperature; P= $(\partial U/\partial V)_{S,N\,J\neq i}$ − pressure.

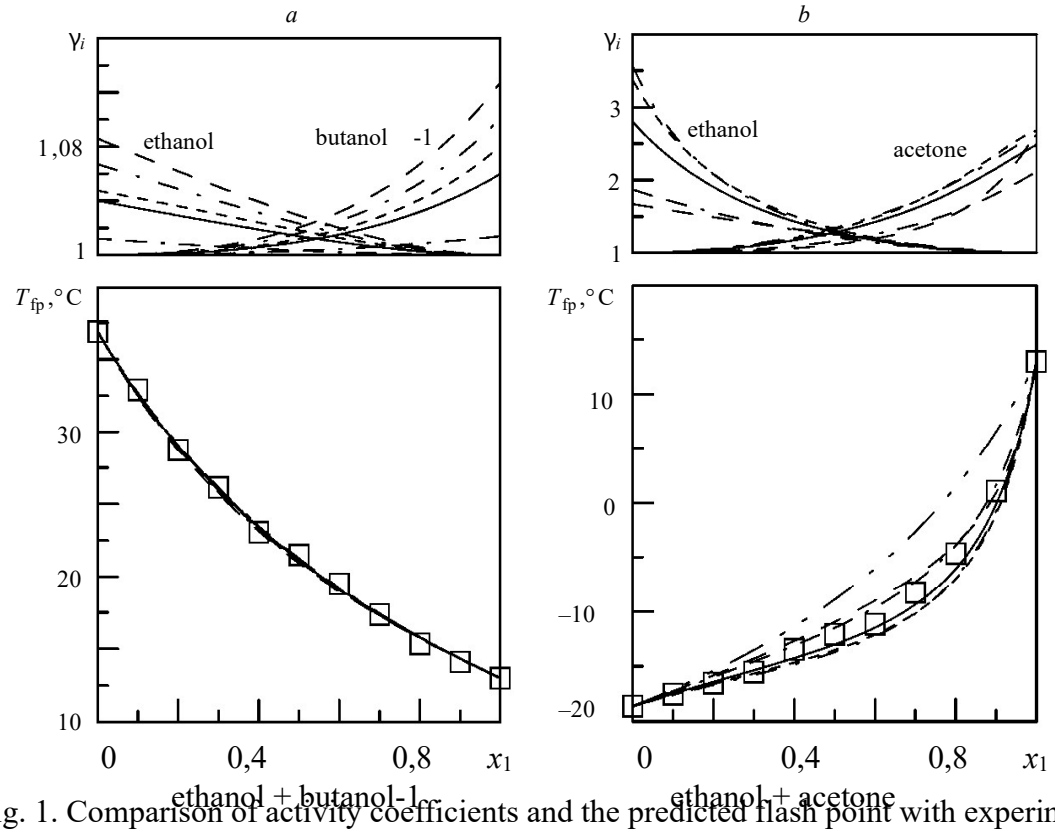

Fig. 1. Comparison of activity coefficients and the predicted flash point with experimental data [22] for an ideal solution ethanol - butanol-1 (a) and a solution with a positive deviation from ideality ethanol - acetone (b): " " - experimental data, " - " - original UNIFAC; "----" − UNIFAC DORTMUND; « — · — :» − UNIFAC Linghby; "— — —" – version of UNIFAC Bastos and others; "— — · —" − NRTL; "— --" – ideal solution

This paper discusses a method for calculating the flash point based on the results of simulating liquid–solid equilibrium at constant pressure. The relationship between the activity coefficients γ_i and the excess Gibbs free energy GE:

$$RT\sum x_i \ln \gamma = {}_i \; G^E.$$

Equation (3) can be written in another form using the Gibbs energy GE (P,T,x_1,x_2,.., x_n) as the characteristic function:

$$dG^E = -SdT + VdP + \sum^n_{i=1}\mu_i\, dx_i.$$

The equation can also be written as

$$-SdT + VdT - \sum^n_{i=1}x_i\, d\mu_i = 0,$$

where the transition is made from the number of moles of components to their molar fractions x_i. The difference between the equations of state of a binary system for the real and ideal equilibrium phases can be represented as [23]

$$-(H^E/RT^2)\, dT + (V^E/RT)\, dP = \sum^2_{i=1} x_i\, d\ln\gamma_i,$$

where γ_i is the activity coefficient of the component, i = 1, 2; H^E – enthalpy of mixing; V^E – excess volume; P – solution pressure; T – absolute temperature; R is the universal gas constant.

The Gibbs equation is used to represent phase equilibrium over a wide range of temperatures and pressures, and to calculate thermal and volumetric properties.

Thus, equation (4) allows us to find the activity coefficients of the components if the enthalpy of mixing and excess volume are known. If the formation of associates of molecules of pure components occurs, then the effective molar mass of the component in the solution can be calculated using the formula M' $\lambda_i M_i$, where M_i is the molar mass of the component before mixing, λ_i are correction factors. The average ratio of the number of molecules in associates of pure components $\lambda = \lambda_1/\lambda_2$ characterizes the stable structure of the solution. The difference between the coefficient λ and unity indicates the presence of a deviation from ideality in the binary system and the need to move to effective mole fractions to obtain thermodynamically consistent models.

In [24 − 27], a method for modeling phase equilibrium diagrams of liquid–solid and liquid–vapor in real solutions and the possibility of predicting the flash point of a binary liquid mixture is considered.

In most real solutions, the components interact, leading to the formation of molecular compounds of the AB type. The solvation coefficient $\lambda = \lambda_1/\lambda_2$ shows the ratio of the number of molecules A to the number of molecules B in the resulting molecular compound. Molecules of components A and B can also form clusters consisting of molecules of the same type. The ratio of the number of molecules of component A to the number of molecules of component B united into associates will be characterized by the association coefficient $k = k_1/k_2$. The association coefficient k1 shows how many molecules of component A in the liquid phase have combined into a cluster of type AA, similarly, the association coefficient k_2 shows how many molecules of component B in the liquid phase have combined into a cluster of type BB. Minimizing the excess Gibbs energy with respect to the solvation parameter λ leads to an equation that models the liquid–solid phase equilibrium diagram at P = const:

$$T(z_1) = [H_1^E z_1 + H_2^E(1 - z_1)]/[(H_1^E/T_1^0)\, z_1 + (H_2^E/T_2^0)(1 - z_1) -$$

$$- R(z_1 \ln z_1 + (1 - z_1)\ln(1 - z_1))], \qquad (5)$$

where T is the liquidus temperature; H_i^E − enthalpy and T_i^0 – melting temperature of the component forming the one-component phase, i = 1, 2; $z_1 = x_1/(x_1 + \lambda x_2)$, $z_2 = x_1/(x_1/\lambda + x_2)$ are the effective mole fractions of the components of the binary mixture.

The PCEAS (Phase Chart Eutectic and Azeotropic Systems) model proposed by the authors of this work [28] is based on minimizing the excess Gibbs energy using the solvation parameter λ, which characterizes the ratio of the number of molecules A to the number of molecules B in a molecular compound. Equation (5) allows us to find the dependence of the temperature of the

mixture on the composition at constant pressure. The PCEAS program makes it possible to calculate the liquid-solid equilibrium, as well as the liquid-vapor equilibrium at constant pressure or at constant temperature. The input data is the temperature T_i and the enthalpy of phase transitions H_i^0 of pure components. The program allows you to determine the average values of the solvation coefficient λ, as well as the association coefficient k, and calculate activity coefficients.

Phase equilibria liquid - solid and liquid - vapor in binary systems, as well as the dependence of the flash point on the composition of the solution were calculated at atmospheric pressure.

3. Results and discussion

Figure 2 presents the results of calculating the flash point temperature using the PCEAS model for the ideal ethanol - butanol-1 system (Fig. 2, a) and the ethanol - acetone system with a positive deviation from ideality (Fig. 2, b).

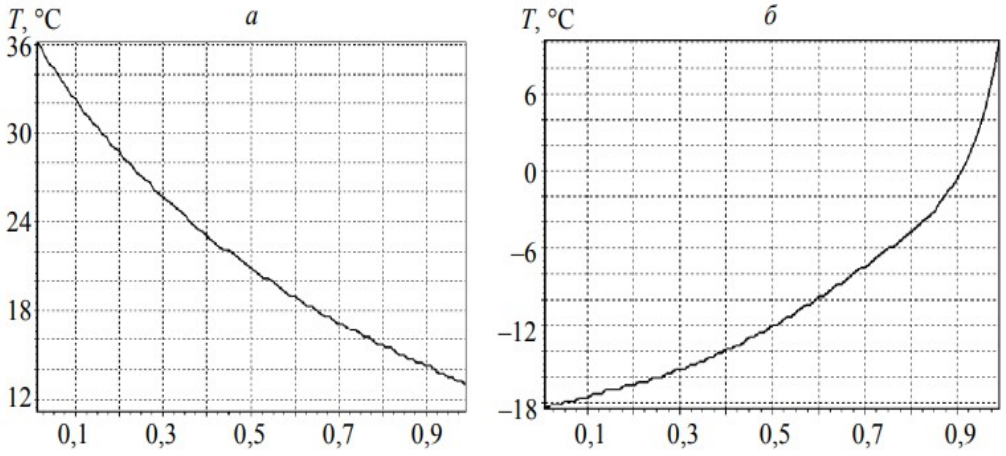

Fig. 2. Dependence of the flash point temperature on the composition of the solution according to the PCEAS model: a – for the ethanol – butanol-1 system; b – for the ethanol – acetone system

In Fig. Table 3 shows the results of calculating activity coefficients using the PCEAS model for the systems ethanol - butanol-1 and ethanol - acetone at normal atmospheric pressure. To predict the flash point of mixtures close to ideal, it is sufficient to use the activity coefficients of the liquid phase obtained from the results of modeling the liquid–solid equilibrium. The work [22] presents modeling results and experimental curves of the dependence of the flash point on the composition for systems with the formation of an extremum of the flash point. It is noted that existing thermodynamic models do not accurately describe such systems. The reason for this is insufficient attention to the processes of solvation and association in the liquid and vapor phases, as well as the consistency of thermodynamic data.

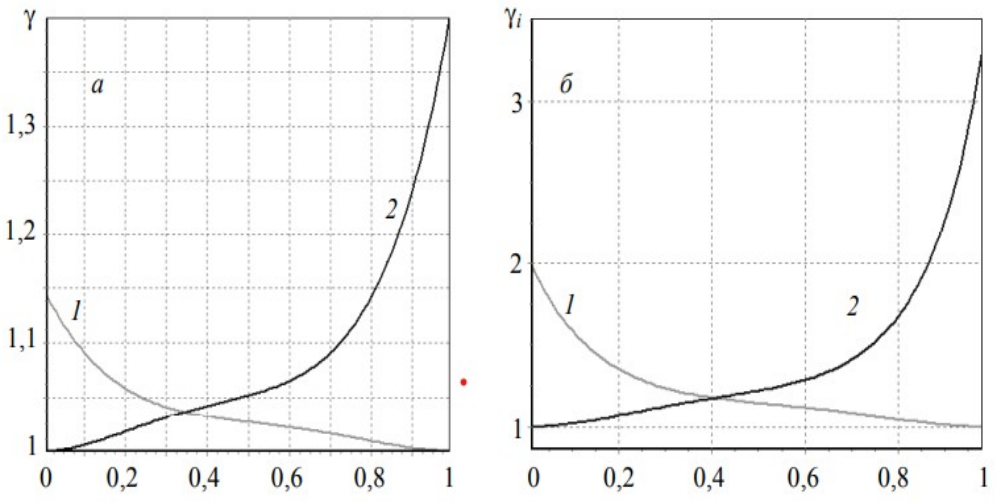

Fig. 3. Calculation of activity coefficients at P = 101.4 kPa using the PCEAS model for solutions: a – ethanol – butanol-1: cr. 1 – activity coefficient (ethanol), cr. 2 – activity coefficient (butanol-1); b – ethanol – acetone with a positive deviation from ideality, line 1 – activity coefficient (ethanol), line 2 – activity coefficient (acetone)

In Fig. 4, 5 show the calculation results and experimental data for systems with the formation of a minimum flash point [22].

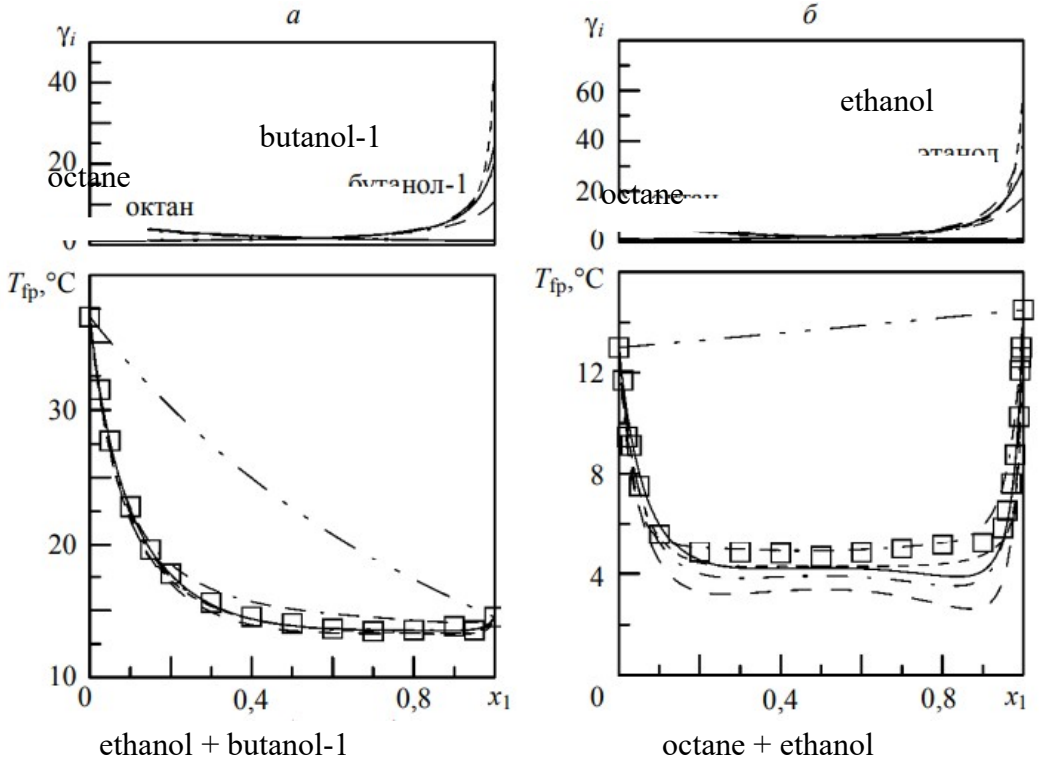

Fig. 4. Comparison of activity coefficients and predicted flash point with experimental data [3] for solutions with the formation of a minimum flash point octane - butanol-1 (a) and octane - ethanol (b): " " - experimental data, " - " - original UNIFAC; "----"– UNIFAC DORTMUND; « — · — :» – UNIFAC Linghby; "— — —" – version of UNIFAC Bastos and others; "— — · —" – NRTL; "— --" – ideal solution

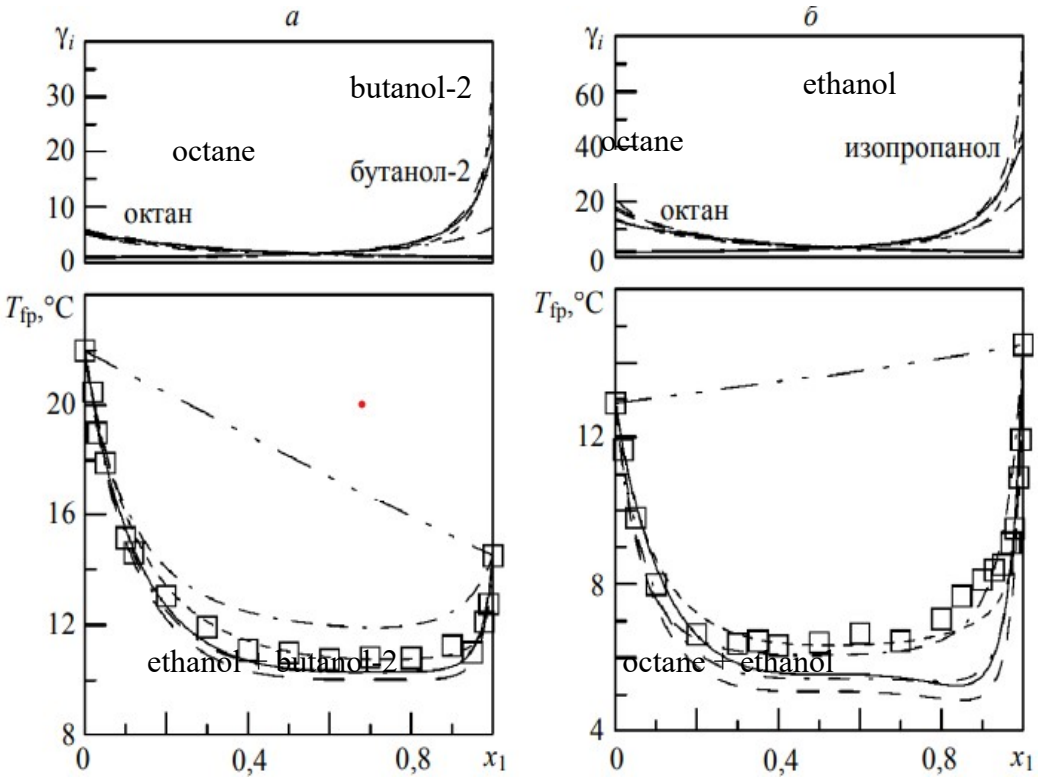

Fig. 5. Comparison of activity coefficients and predicted flash point with experimental data [22] for solutions with the formation of a minimum flash point octane - butanol-2 (a) and octane - isopropanol (b): " " - experimental data, " - " - original UNIFAC; "----" − UNIFAC DORTMUND; « ─ · ─ :» — UNIFAC Linghby; "─ ─ ─" – version of UNIFAC Bastos and others; "─ ─ ─" – NRTL; "─ --" – ideal solution

In Fig. 6. The results of calculating the boiling point and flash point temperature using the PCEAS model for an octane - butanol-1 solution with the formation of flash point extrema are presented.
In Fig. 7 – results of calculating the boiling point and flash point using the PCEAS model for the octane-ethanol system at normal atmospheric pressure.
In Fig. 8 – results of calculating the boiling point and flash point using the PCEAS model for the octane - butanol -2 system at normal atmospheric pressure.
In Fig. 9 – results of calculating the boiling point and flash point using the PCEAS model for the octane - isopropanol system at normal atmospheric pressure.

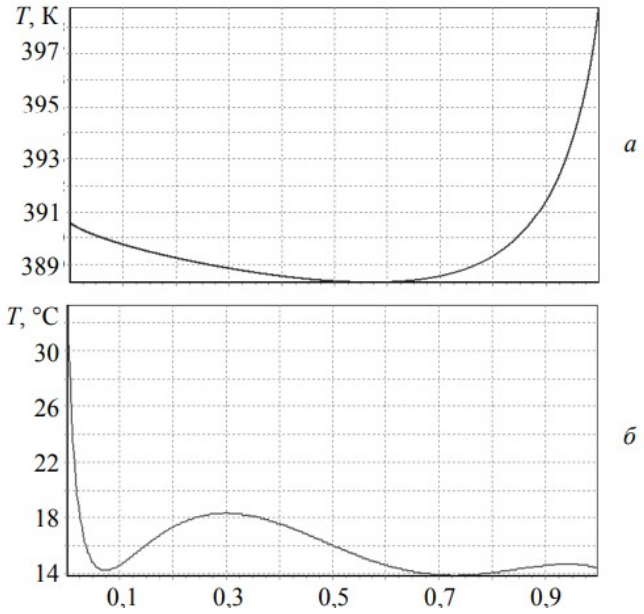

Fig. 6. Calculation of the boiling point and flash point temperature using the PCEAS model for a solution of octane-butanol-1 with the formation of flash point extrema: a – boiling point - calculation; b – flash point temperature – calculation

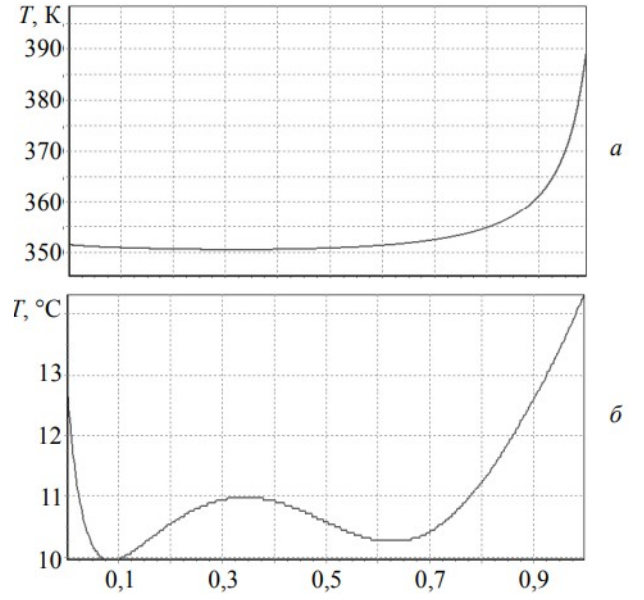

Fig. 7. Calculation of the boiling point and flash point temperature using the PCEAS model for an octane-ethanol solution with the formation of flash point extrema: a – boiling point - calculation; b – flash point temperature – calculation

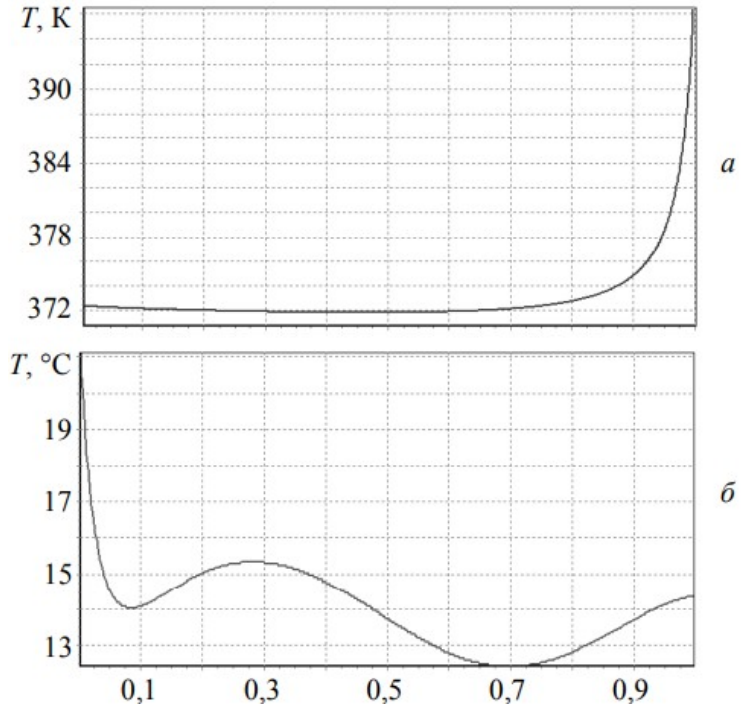

Fig. 8. Calculation of the boiling point and flash point temperature using the PCEAS model for a solution of octane - butanol-2 with the formation of flash point extremes: a - boiling point - calculation; b – flash point temperature – calculation

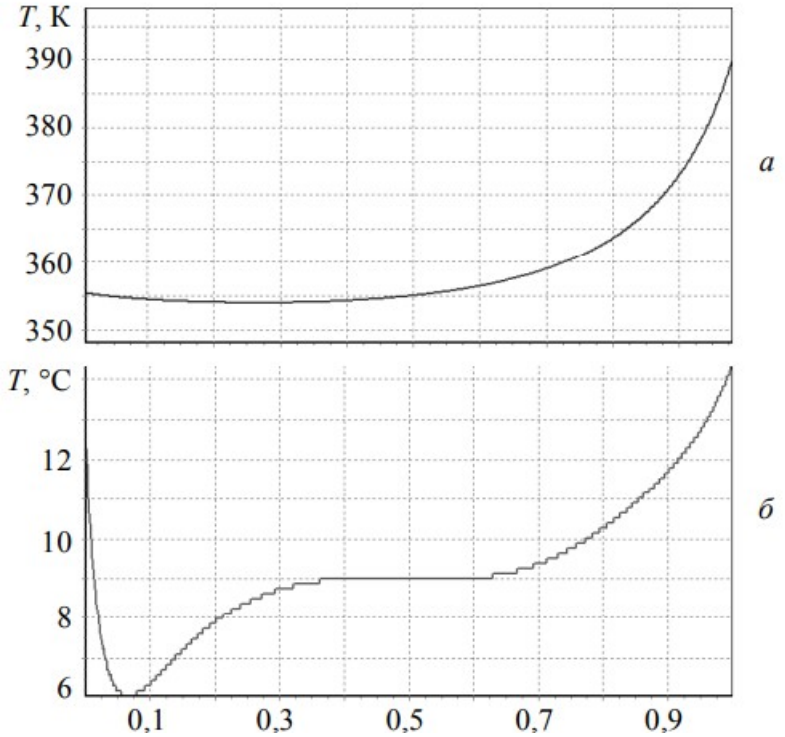

Fig. 9. Calculation of the boiling point and flash point temperature using the PCEAS model for an octane - isopropanol solution with the formation of a minimum flash point: a - boiling point - calculation; b – flash point temperature – calculation

4. Conclusion

A method for predicting the dependence of the flash point of binary flammable liquid mixtures on the composition of the solution is presented. The method is based on the use of mixture pressure data obtained using mathematical modeling of phase equilibrium under isobaric conditions. Predicting the flash point of a binary mixture requires data on the enthalpy and melting point, enthalpy and boiling point, and flash point of the pure components

Conflict of interest

The authors declare that they have no conflict of interest in relation to this research

5. References

1. Torsuev N.S. Limits of flammability of a mixture of vapors of volatile solvents // Journal of Chemical Industry. 2003. No. 22−23. pp. 1413−1414, (in Russia).
2. Liaw H.-J., Lee Y.-H., Tang C.-L., et al. A mathematical model for predicting the flash point of binary solutions // J. Loss Prev. Process. 2002. No. 15. P. 429–438.
3. Liaw H.-J. A general model for predicting the flash point of miscible mixture / H.-J. Liaw, Y.-Y. Chiu // J. Hazard Mater. 2006. No. 137. P. 38–46.
4. Affens W.A. Flammability properties of hydrocarbon solutions in air / W.A. Affens, G.W. McLaren // J. Chem Eng. Data. 2017. No. 17. P. 482–488.
5. White D. Flame spread on aviation fuels / D. White, C.L. Beyler, C. Fulper, J. Leonard // Fire Saf. J. 2007. No. 28. P. 1–31.
6. Garland R.W. Evaluating vent manifold inerting requirements: flash point modeling for organic acid-water mixtures / R.W. Garland, M.O. Malcolm // Process Saf. Prog. 2002. No. 21. P. 254–260.
7. Liaw H.-J. A model for predicting the flash point of ternary flammable solutions of liquid / H.-J. Liaw, C.-L. Tang, J.-S. Lai // Combust. Flame. 2004. No. 138. P. 308–319.
8. Liaw H.-J. A non-ideal model for predicting the effect of dissolved salt on the flash point of solvent mixtures / H.-J. Liaw, T.-A. Wang // J. Hazard Mater. 2007. No. 141. P. 193–201.
9. Catoire L. Estimation of closed cup flash points of combustible solvent blends / L. Catoire, S. Paulmier, V. Naudet // J. Phys. Chem. Ref. Data. 2006. No. 35. P. 9–14.
10. Gmehling J. Flash points of flammable liquid mixtures using UNIFAC / J. Gmehling, P. Rasmussen // Ind. Eng. Chem. Fundam. 2002. No. 21. P. 186–188.
11. Lee S.-J. The Lower Flash Points of Binary Systems Containing Non-flammable Component / S.-J. Lee, D.-M. Ha // Korean J. Chem. Eng. 2003. No. 20. P. 799–802.
12. Fredenslund A. Group-Contribution Estimation of Activity Coefficients in Nonideal Liquid Mixtures / A. Fredenslund, R.L. Jones, J. M. Prausnitz // AIChE J. 1975. No. 21. P. 1086−1099.
13. Vidal M. Prediction of minimum flash point behaviour for binary mixtures / M. Vidal, W.J. Rogers, M.S. Mannan // Process Saf. Environ. Prot. 2006. No. 84. P. 1–9.
14. Zabetakis M. G. Flammability Characteristics of Combustible Gases and Vapors // U.S. Dept of the Interior, Bureau of Mines, Washington, 2005.
15. Liaw H.-J. Binary liquid solutions exhibiting minimum flash-point behavior / H.-J. Liaw, T.-P. Lee, J.-S. Tsai, W.-H. Hsiao, M.-H. Chen, T.-T. Hsu // J. Loss Prev. Process. 2003. No.
16. P. 173–186. 16. Liaw H.-J. Binary mixtures exhibiting maximum flash-point behavior / H.-J. Liaw, S.-C. Lin // J. Hazard. Mater. 2007. No. 140. P. 155–164.
17. Weidlich U. A modified UNIFAC model. 1. Prediction of VLE, hE, and gamma Infinite / U. Weidlich, J. Gmehling // Ind. Eng. Chem. Res. 2017. No. 26. P. 1372–1381.

18. Gmehling J. A modified UNIFAC model. 2. Present parameter matrix and for different thermodynamic propertie / J. Gmehling, J. Li, M. Schiller // Ind. Eng. Chem. Res. 2003. No. 32. P. 178–193.
19. Larsen B.L. A modified UNIFAC group contribution method for prediction of phase equilibria and heats of mixing / B.L. Larsen, P. Rasmussen, A. Fredenslund // Ind. Eng. Chem. Res. 1987. No. 26. P. 2274–2286.
20. Magnussen T. UNIFAC parameter table for prediction of liquid-liquid equilibria / T. Magnussen, P. Rasmussen, A. Fredenslund // Ind. Eng. Chem. Process Des. Dev. 2001. No. 20. P. 331–339.
21. The UNIFAC Consortium / http://unifac.ddbst.de/ (accessed 2010)[electronic resource].
22. Liaw H.-J. Prediction of miscible mixtures flash-point from UNIFAC group contribution methods / H.-J. Liaw, V. Gergaud, Y.-H. Li // Fluid Phase Equilibria. 2011. No. 300. P. 70−82.
23. Kogan V.B. Heterogeneous equilibria. L.: Chemistry, 2016. 432 pp., (in Russia).
24. Esina Z.N. Mathematical modeling of the liquid–solid phase transition / Z.N. Esina, M.R. Korchuganova, V.V. Murashkin // Bulletin of Tomsk State University. Management, computing and information science. 2011. No. 3 (16). pp. 13−23, (in Russia).
25. Zakharov Yu.N. Phase transitions as a cause of disasters at coal and oil processing enterprises / Yu.N. Zakharov, Z.N. Esina, M.R. Korchuganova // Kuzbass-2: collection. articles. A separate issue of the Mining Informational and Analytical Bulletin (Scientific and Technical Journal). 2009. No. OB17. M.: Publishing house "Mountain Book". pp. 54−58, (in Russia).
26. Esina Z.N. Forecasting the flash point of binary liquid mixtures / Z.N. Esina, M.R. Korchuganova, V.V. Murashkin // Problems of environmental monitoring: collection. proceedings of the XI All-Russian conference with the participation of foreign scientists (October 24−28, 2011). Kemerovo: KemSU, 2011. pp. 177−182, (in Russia).
27. Esina Z.N. Mathematical modeling of phase transitions in real solutions: monograph. Kemerovo: Kemerovo State University, 2011. 228 pp., (in Russia).
28. Esina Z.N. Phase Chart Eutectic and Azeotropic System (PCEAS): Certificate of state registration of a computer program No. 2012618394 / Z.N. Esina, M.R. Korchuganova, V.V. Murashkin (RU) – No. 2012616324; application 07/25/2012; Registered in the Register of Computer Programs, Moscow, September 17, 2012 (in Russia).

Study of the designs of devices for centrifugal extraction

R.Kh. Malikov*, N.M.Abbasov, S.Mammadova

*Department of Industrial machines, ASOIU, 20 Azadlig Avenue. AZ-1010 Azerbaijan
Research Institute of Geotechnologocal Problems of Oil, Gas and Chemistry, ASOIU, 20 Azadlig Ave., Baku, AZ-1010 Azerbaijan

Abstract

This article provides an overview of centrifugal extractors of various configurations, their advantages are noted advantages and disadvantages. It is noted that, despite the variety of types of

extractors, there are few generalized studies on optimization presented in the scientific literature. Methods for increasing the efficiency and productivity of existing structures are proposed.

***Keywords**:* centrifugal extraction, devices optimization, sectional rotor, annular chamber.

*Corresponding author. Tel.: + 994 503112553
E-mail address: malikov.rauf@mail.ru

1. Introduction

The development of methods of separation and purification of substances is motivated by the needs of the petroleum, chemical and pharmaceutical industries. One of the promising methods of separation of mixtures is extraction.

Currently, many extractor designs have been developed that are used in various industries, which is explained by the variety of types of raw materials used and various technological requirements for extraction process. The choice of the optimal design of the apparatus for certain processes of the chemical, petrochemical industry should be based on a comparison of the technical and economic indicators of extractors with its performance, degree of separation, as well as various kinds of costs for its manufacture, operation and maintenance.

2. Methodological part

Extraction devices used in the chemical industry can be divided into several groups: differential contact, stepped and structures occupying an intermediate position. The first group includes, as a rule, column apparatuses, which are distinguished by a constant contact of phases and a smooth change in the concentration of the extracted component along the height of the apparatus. Their compactness, due to their vertical location, allows them to be used in conditions of limited production space, but as a result of longitudinal mixing caused by axial convective flows, turbulent pulsations and stagnant zones, it is possible to reduce the average driving force.

Multistage extractors are usually vertical columns divided by various contact devices into sections or so-called theoretical stages, at each of which the initial solution and extractant are repeatedly mixed and delaminated. The efficiency of these devices is estimated by the efficiency of individual stages or the height of the device equivalent to one equilibrium stage — the theoretical plate.

According to the type of process, extractors can be divided into periodic and continuous devices. In batch extractors, the process is usually carried out in a stationary layer, in which the filtration rate of the extractant, porosity and pressure drop, which creates a driving force, change over time. Often, to increase the filtration rate of the extract, the pressure drop in the apparatus is increased, which, in turn, leads to compression of the material layer in the apparatus and deterioration filtering. An excessive increase in the pressure drop can lead to the termination of the filtration of the extract in the layer. The same phenomenon is observed in continuous vertical type devices without the use of special transporting devices.

To devices occupying the intermediate position between step devices and devices of differential contact type include centrifugal extractors in which stirring followed by phase separation, occurs under the influence of centrifugal forces. How typically, the extractor rotor is set of perforated cylinders, spiral tapes, etc. Through contact devices that increase the phase contact surface to the periphery from the center moves the heavier phase, and more light phase - in the opposite direction, thus the extractant and the original solution move towards each other. Phase dispersion (and redispersion subject to recycling) - when passing through contact devices.

Among the devices for performing centrifugal extractions are distinguished in discrete-step (or chamber) and differential contact. Discrete-stage ones consist of individual workers volumes, in each of which phases moving countercurrent, first mixed, then are separated. In this case, the mass transfer process occurs under conditions close to constant contact moving towards one another phase flows; direction of movement is determined channels formed by internal devices rotor.

Centrifugal extractors are distinguished by significant productivity (flow rates can be several hundred m^3/h) and high efficiency (small number of theoretical stages), as well as short duration of phase contact, as a result of which mass transfer processes in the apparatus occur very intensively. The listed advantages make it possible to use these devices in the production of unstable compounds, when working with radioactive solutions and stable emulsions, and when separating systems whose components have similar densities. Centrifugal extractors are advisable use for systems that require little time phase contact or having a small difference specific gravity. When comparing performance column countercurrent extraction devices with centrifugal extractors, then in the first case the intensity is limited mainly by the rate of deposition or rise of droplets of the dispersed phase, and in the second, it is limited by the speed of movement of the droplets in the direction of the radius. Ponikarov I.I. and Bochchachev V.G. in their study [1] provide a comparative analysis of the rate of sedimentation of droplets in a liquid in a gravitational field, calculated approximately using the Stokes equation, and the speed of movement of droplets in a liquid in a field of centrifugal forces. From the analysis of the results obtained and comparison of these speeds, it follows that the speed of drops moving under the influence of centrifugal forces will be greater than their speed in the gravitational field. Thus, the centrifugal field has a number of important advantages compared to gravity, which represents present ample opportunities for intensification extraction process in the apparatus. A more detailed development of this advantage will make it possible to develop centrifugal extractors that can be successfully used for other extraction systems that occur without chemical reactions, and be competitive in comparison with gravity-type devices.

Currently, there are a large number of different designs of centrifugal equipment, most of which have found widespread application in various technological processes in the chemical, food and oil refining industries industries. However, the variety of types and types of existing contact devices centrifugal extractors complicates them somewhat correct choice and rational use. In view of this, work is required not only to categorize and classify devices, but also to generalize methods for optimizing the structure of radial flows inside the rotor, to correctly solve the problem of increasing the efficiency of devices and optimizing structural and technological parameters.

Quite often, researchers achieve increasing the efficiency of centrifugal extractors by changing the design of the nozzles used, installing additional internal devices in them that intensify the mass transfer process. However, such modifications, as a rule, complicate the design of the apparatus and are based on the “design considerations” of the designer without taking into account the influence of hydrodynamic parameters; they do not have universal application, but are suitable only for solving a particular problem of optimizing an apparatus of a certain design. When solving the problem of increasing efficiency, it is necessary to take into account that the angular velocity changes along the radius of the apparatus and the free cross-section of the nozzle increases, which leads to a decrease in holding capacity and affects the mass transfer coefficient. To reduce the influence of these effects, recirculation, countercurrent movement and multiple phase dispersion.

Continuous is considered the most effective extraction carried out in multi-stage extractors with countercurrent of the initial solution and extractant. In this case, the specified degree of

extraction is achieved with the lowest extractant consumption. If it is necessary to recirculate the extractant with a rotating rotor or increase the phase contact time in centrifugal extractors, an input and output unit is provided phases implemented in the form of suction tubes or disks (Fig.1). Disadvantages include longitudinal mixing, which has not yet been sufficiently studied. Currently, methods for studying this phenomenon are being considered and evaluation for different extractor designs.

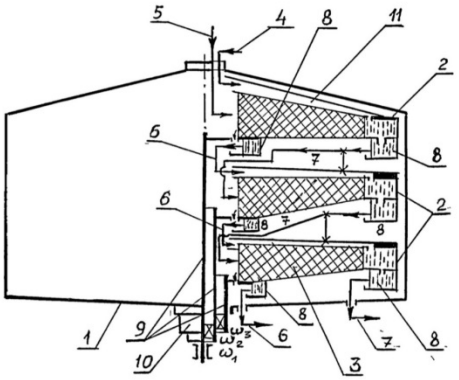

Fig. 1 – Schematic diagram of cascade extractor

The apparatus shown in Figure 1 consists of non-rotating housing 1; sectioned rotor 2 with nozzles 3; liquid input and output devices made in the form of tubes: for supplying light 4 and heavy phase 5 and sampling tubes, 6 and 7, respectively; overflow ring chambers 8; coaxial shafts 9 and bearing unit 10; circular slot for supplying the light phase to the periphery 11.

To create favorable conditions for phase selection from sections and improve separation, it is proposed to vary the speed of rotation of the sections and their sizes. Sections are provided with individual drives, the number of revolutions of which is determined from the condition of optimization of individual processes: extraction carried out at 1500-2000 rpm, separation – at 3000-5000 rpm, etc.

This design solution (cascade extractor) allows you to expand the range of processed liquid mixtures and implement a more efficient mode of movement of liquids in sections, resulting in increased productivity and efficiency of the apparatus.

The device shown in Figure 2 contains fixed housing 1 with cover 2; rotor 3 with cover 4; extraction container 5 with collar 6 and sleeve 7; a conical glass 8 and an extract collector 9, installed coaxially with the rotor 3. A gap is formed between the extraction container 5 and the conical glass 8 to drain the extract. On the outer surface of the sleeve 7 there are grooves 10 for draining the extract into the extract collector 9. The rotor cover 4 is made in the form of an annular chamber in which a suction tube 11 is located, connected to a fitting 12, movably fixed in the housing cover. Rotor 3 is equipped with a drive 13.

The technical solution to the problem posed to the authors is that the centrifugal extractor, in addition to a vibration-driven mixer, was additionally equipped with a conical glass installed with a gap between the extract collector and the extraction container, which made with a sleeve with grooves for draining the extract. In turn, the rotor cover was made in the form of an annular chamber equipped with a suction tube connected to the fitting, movably fixed to the housing cover. The extraction container is made with a collar, the annular channels of which form a labyrinthine device with a rotor lid, which further reduces the loss of extract during extraction with a suction tube.

It is worth noting that the intensification of the process extraction can be achieved by discrete-pulse energy input methods. Physical the essence of these methods is that the supplied energy is dissipated mainly near the surface of solid particles, and unproductive energy consumption outside these zones is minimal. Thus, mechanical vibrations provide continuous flow of liquid around solid particles with variable direction and magnitude of speed.

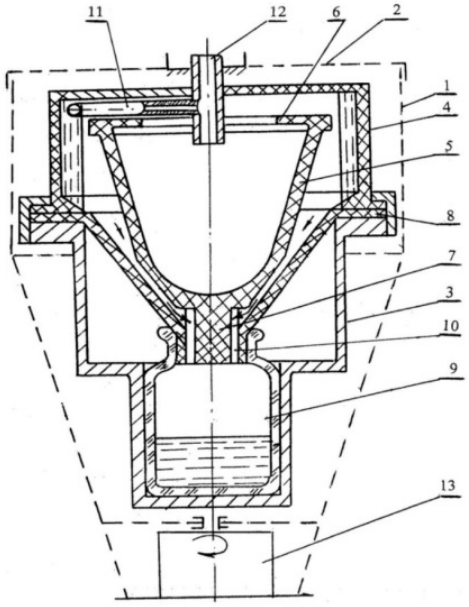

Fig. 2 - Schematic diagram of the extractor centrifuge

For creating vibrations, extractors with vibrating bodies and special vibrating devices installed in the apparatus itself are used. Latest they are used mainly in column or container type extractors. Experimentally it has been proven that the application of vibration
fields of different frequencies and amplitudes significantly accelerates mass transfer and increases the productivity and efficiency of the apparatus.

2. Conclusions

1. Currently researched and developed a large number of various equipment using centrifugal forces to intensify various mass transfer processes, ranging from the simplest mixing devices to the most complex multi-module designs of centrifugal extractors.
2. The theory and practice of various mixers, separators and centrifuges are widely covered in the existing scientific and technical literature, however there are scattered data on centrifugal extractors, both on designs and on the results of theoretical and experimental studies, and they are presented mainly in individual dissertations and scientific articles.
3. Particular attention in the works of researchers is paid to the most promising designs of centrifugal devices, ways to increase the efficiency of existing devices by profiling rotors, sectioning packed devices and the use of packed elements that ensure the creation of an optimal flow structure and increasing the productivity of the device, as well as various ways of supplying energy.

Conflict of interest

The authors declare that they have no conflict of interest in relation to this research

4. References

1. A.Yu. Politov, V.V. Dobrotvorsky, I.M. Balakin, III International Scientific and Technical Conference “Innovative Projects and Nuclear Energy Technology” NIKIET-2014, Moscow, 2014. (in Russia).
2. Yu.I. Shishatsky, E.I. Melnikova, S.Yu. Plyukha, E.V. Kuzmin, S.S. Ivanov, M.A. Samoilova, journal “Issues of modern science and practice”, V.I. Vernadsky University, 2, 40, (339-351), 2012. (in Russia).
3. N.S. Grishin, I.I. Ponikarov, S.I. Ponikarov, D.N. Grishin, Extraction in a field of variable forces. Hydrodynamics, mass transfer, apparatuses: monograph: in 2 parts. Part 2. Publishing house KNRTU, Kazan, 2016. 444 p. (in Russia).
4. A.A. Salin, N.S. Grishin, Bulletin of Kazan Technological University, 17.10, (167-168), (2014).
14. A.A. Salin, N.S. Grishin, S.I. Ponikarov, Bulletin of Kazan Technological University, 2014. (in Russia).

Hydrocarbon losses arising from phase transformations in field collection pipelines

E.Kh. Iskandarov, M.M. Hasanova, S.A. Ibadova

Azerbaijan State Oil and Industry University, 20 Azadlig Avenue. Baku, AZ-1010 Azerbaijan

Abstract

In offshore fields, the quality indicators of the well product are subjected to change when it passes the initial preparation stage at the collection points and is transported to the shore. Researches show that most of the problems that arise in the collection points of fields operated in marine conditions are related to multi-component and multiphase flows. Contamination from the inner surface of the pipeline due to the internal phase transformations of the pipeline causes an increase in the operation and energy costs of the collection transport system. Blockages are formed in underwater pipelines when the liquid and mechanical particles in the transported gas are separated and settle inside the pipe.

Keywords: Carbohydrogen mixtures, multiphase, phase transformations, condensation, carbohydorgen losses, inner pipe separation.

*Corresponding author. Tel.: +994 502146214

E-mail address: e.iskenderov62@mail.ru (E.Kh.Iskandarov)

1. Introduction

The movement of gas and liquid phases that is a stratified flow form actually takes place in the gas pipeline. Separation of the liquid phase of hydrocarbon mixtures also causes certain errors in the measurement of the consumption of the transported gas. Thus, the existing international standards for measuring gas consumption are based on its monophase principles [1,2,3,4]. On the other hand, the presence of a liquid phase in gas flows causes pressure and consumption pulses. These harmful pulses cause pipelines to deform and fail prematurely [5,6].

2. Methodological part

A visual inspection of the inner surface of the pipes showed that sediments are mainly collected in the lower part and partly in the upper part. (Figure 1.)

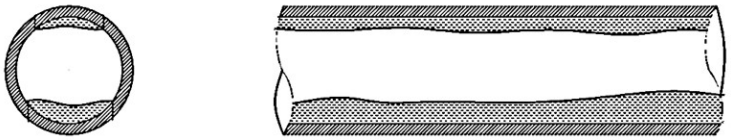

Figure 1. Accumulation of deposits in the gas pipeline

Operational experience shows that the occurrence of blockages in gas pipelines is mainly due to the following factors.

1. Incomplete drying of the gas
2. Occurrence of phase transformations with changes in thermodynamic conditions,

A visual inspection of the inner surface of the pipes showed that sediments are mainly collected in the lower part and partly in the upper part (Figure 1).

Water and heavy hydrocarbons contained in the gas condense during transportation and are adsorbed on the surface of mineral deposits in the inner part of the pipeline, forming layers of different strength on the inner surface of the pipelines.

Contamination of the inner surface of pipelines results in complications and costs. Thus, the throughput and productivity of the pipeline decreases. This results in losses of valuable raw materials [7,8,4,9,10].

Violation of the technological regime in the transportation process, non-compliance of the physico-chemical parameters of the gas with the current requirements, failure to timely remove the mechanical impurities of the liquid phase separated in the pipeline, cause hydrocarbon losses.

The operational experience of field technological pipelines of various purposes shows that even the deep separation implemented in transport systems cannot prevent the formation of a liquid phase in the gas pipeline. Although the free liquids (hydrocarbon condensate and water) contained in the gas are separated from the gas in primary processing units, water and hydrocarbon vapors in equilibrium enter the transportation system [13]. One of the reasons for the liquid phase to fall into the gas pipeline is related to the occurrence of phase transformations due to changes in the temperature and pressure of the transported gas. By performing the separation at sub-optimal temperatures and pressures below or above the maximum condensing pressure, the liquid in the separator is not falls apart and the remaining liquid subsequently sets apart in the pipeline at a lower temperature [11,12,13,14,10].

Thermobaric influences of the enviroment also cause thermodynamic parameters of the gas to change. As a result, hydrocarbon condensate and water vapors in its content condense and become liquid. Thus, the first reason for the drop of the liquid phase in the gas pipeline is the incorrect selection of the separation parameters. The second reason for the liquid to fall apart from the gas is related to the change of those parameters along the pipeline during transportation. Thus, at low temperatures, heavy hydrocarbons condense more intensively. The maximum drop in pressure in the gas pipeline due to condensation causes the gas to evaporate and pass into the gas phase due to an increase in moisture content. Gas drying ends up inside the pipeline. This process is called internal separation. But later, the gas phase is saturated with liquid, and with the next decrease in temperature, condensation of moisture occurs again. Therefore, in the high pressure zone, under certain conditions, "reverse condensation" or "reverse evaporation" processes occur. Since the

composition of the well product is constantly changing during the period of exploitation of the fields, the maximum condensation pressure determined for the initial stage of the field operation is not enough to separate the liquid phase from the gas in the separators at the later stages of development. At this time, as the temperature of the gas decreases, its composition becomes richer with water and heavy hydrocarbons [10,15,2,16,13,17,18].

The amount of hydrocarbons passing from the gas phase to the liquid phase as a result of phase transformations can be determined by the following expression:

$$x_i = \frac{z_i}{L + k_i V} \quad (1)$$

Here: Z_i and x_i - mole density of component i in the liquid phase in the mixture, respectively; and L. and V are the mole fractions of the components in the liquid and gas phase, respectively. K_i was the equilibrium coefficient:

$$K_i = \frac{y_i}{x_i} = \quad = \frac{(P\,d)_i}{P} \quad (2)$$

Here: Pd is the saturation pressure of the i-th component; P-is the pressure in the system.

From expression (2), the following expression can be written for the equilibrium state of the system:

$$y_i \cdot P = x_i \cdot (P_d)_i$$

If $=\sum x_i = 1$ is obtained as a result of solving the expression (1) by the method of gradual approximation, then the problem has been considered to be solved correctly.

Depending on the seasons of the year, an imbalance occurs between the volumes of gas transported to the shore as a result of phase transformations in underwater pipelines.

Calculations on phase transformations were performed on the basis of Pedlix-Kwong and Peng-Robinson equations of state:

$$P = \frac{RT}{V-b} = \frac{a}{T^{0.5} V(V+b)} \quad (3)$$

$$P = \frac{RT}{V-b} = \frac{a\,(T)}{V(V+b)+b(V-b)} \quad (4)$$

Here: P, T, V and R are the pressure, temperature, volume and universal constant of the gas, respectively, and a and b are coefficients.

Calculations are performed with two equations at the same time due to the fact that the Pedlich-Kwong equation gives more accurate results for relatively "dry" gases, while the Peng-Robinson equation of state gives more accurate results for "oily" gases.

3. Results and discussion

In order to investigate the thermodynamic reasons for the separation of the liquid phase in the gas pipeline, experiments and calculations were carried out using available literature sources data. The studies were conducted on the basis of the following primary data.

1. Temperature -10 °C.
2. Pressure P=2.0; 4.0; 6.0; 8.0; 10.0 and 12.0 MPa.

Amount of liquid phase precipitated per 100 moles of gas mixture (Mol/100 Mol)
(C_3H_8, C_4H_{10}, C_5H_{12}, C_6H_{14}, C_7H_{18}, C_8H_{18}) are assigned.

Figure 2 shows the dependence of the precipitated liquid phase on the presssure.

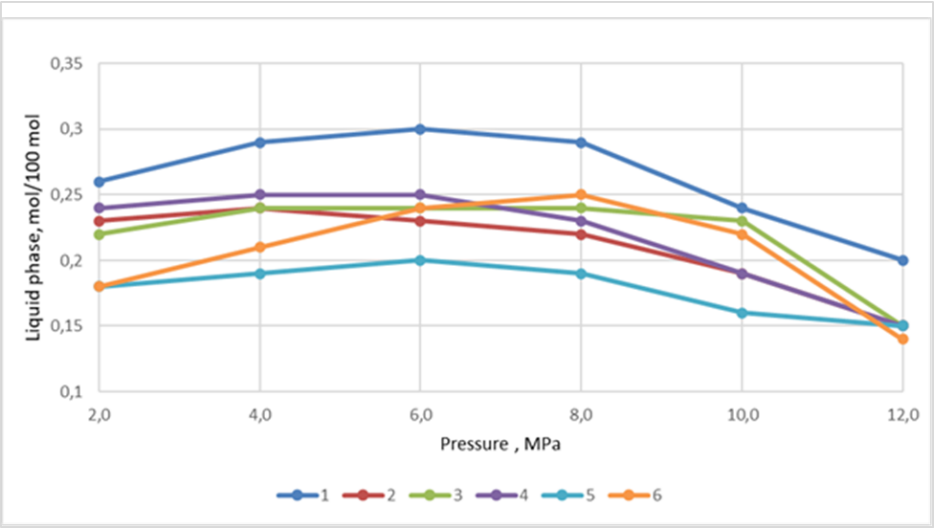

Figure 2. Amount of liquid phase precipitated at different pressures.

1- C_3H_8, 2- C_4H_{10}, 3-C_5H_{12}, 4- C_6H_{14}, 5-C_7H_{18}, 6- C_8H_{18}

As it can be seen from Figure 2, the maximum precipitation of the liquid phase due to condensation corresponds to the pressure value of 6.0 MPa (maximum condensation pressure). It is clear from Figure 2 that the amount of precipitated liquid is greater at higher values of pressure. This is due to the fact that gases such as methane, ethane, nitrogen and carbon in the gas change from higher pressures to the liquid phase. Thus, studies show that as a result of the imperfection of the separation process, water and gas vapors enter the gas pipeline and condense and cause various complications. Such complications caused by phase transformations lead to the need to remove the liquid phase accumulated in separate parts of the transport systems from the pipeline. In the oil and gas industry, various methods and devices are used for this purpose.

The values of gas "losses" due to liquid deposition in the pipeline varies depending on both pressure and temperature. In order to evaluate gas losses depending on pressure and temperature changes, the amount of condensed hydrocarbons was determined at selected points (for the samples taken) based on laboratory experiments. Figure 3 provides a 3D dependence showing the dynamics of changes in the calculated values of gas losses (in 1kg/1000m³) for samples under transport conditions, i.e. along the length of the gas pipeline.

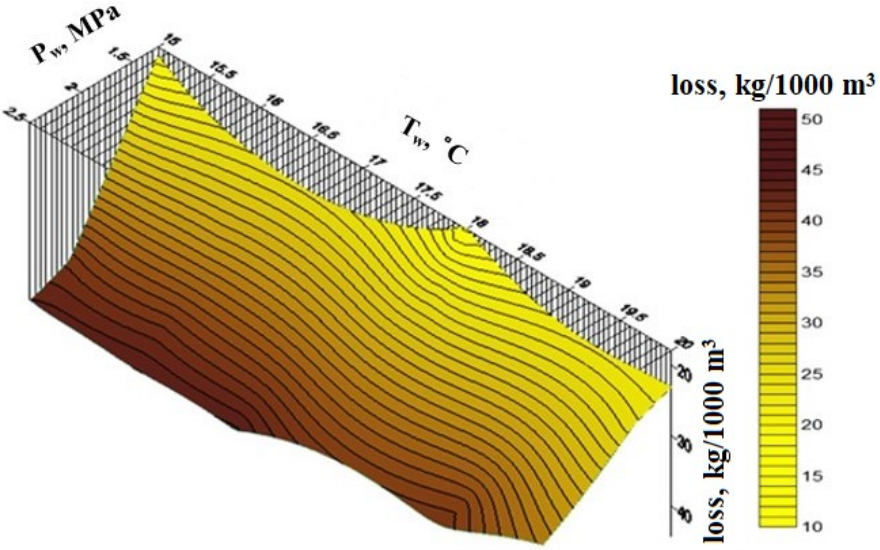

Figure 3 Changes in gas loss values depending on temperature and pressure in transport conditions

As it can be seen from Figure 3 gas losses per 1000 m³ of gas volume have different values with temperature and pressure changes. So, the dynamics of changes in dependence shows that, the amount of gas losses along the pipeline decreases with a drop in pressure. For example, in examples 1 and 8, a slight change in temperature (1 °C) is accompanied by a 2-fold decrease in pressure (from 2.5 to 1.3 MPa), so the loss of hydrocarbons per 1000 m³ of gas decrease from 44 to 18.0 kg. That is, pressure changes have a sharper effect on the dynamics of changes in gas losses compared to temperature.

4. Conclusion

Researches have shown that as a result of the imperfection of the separation process, water and heavy hydrocarbon vapors entering the gas pipeline condense in the pipeline and cause phase transformations. As a result, hydrocarbon losses occur. The conducted reports have shown that these losses are related to the condensation process caused by pressure changes along the pipeline, and it is possible to significantly reduce the losses caused by phase transformations by correctly setting the maximum condensation parameters at each stage of operation.

Conflict of interest

The authors declare that they have no conflict of interest in relation to this research.

5. References

1. Donald L. Katza Handbook of Natural Gas Engineering// Mc Graw-Hill Book Company, Lnc.New York, 2002, p.213. https://www.amazon.com/Handbook-Natural-Gas-Engineering-Chemical/dp/007033384X
2. E.Kh. Iskandarov. Control-diagnostic methods in the transportation and storage of oil and gas// Baku, "Science", -2023, p.327.
3. Gritsenko A.I., Klapchuk O.V., Kharchenko Y.A. Hydrodynamics of gas-liquid mixtures in wells and pipelines // Moscow: Nedra, - 1994, p. 279. https://journals.ucp.by/index.php/jcp/article/view/719
4. Gritsenko A.I., Sirotin A.M. et al. Energy-saving technologies in natural gas production // Moscow, - 1996, p. 235. https://www.dissercat.com/content/razrabotka-energosberegayushchikh-tekhnologii-podgotovki-gaza-valanzhinskikh-zalezhei-ureng
5. Gafar G. Ismayilov Vugar M. Fatalıyev Elman Kh. Iskandarov / Inverstigating the impact of dissolved natural gas on the flow characteristics of multicomponent fluid in pipelines // Open Phys., -2019; 17, - p.206-213 https://www.degruyter.com/document/doi/10.1515/phys-2019-0021/html
6. Sattarov R.M., Ismailov K.K., Efendiev N.G. Study of the movement of gas-saturated systems in pipes in the presence of phase transformations.// Azerb. Oil Economy, - Baku, - 1991, Nº 5, p.33-36. https://www.dissercat.com/content/issledovanie-dvizhenii-reofizicheski-slozhnykh-zhidkostei-v-trubakh-i-poristykh-sredakh
7. Aliev E.U. New scientific and technical direction in the field of gas classification. Baku,International Congress // "Energy, Ecology, Economy", - Baku, - 2003, p.29-33.
8. Aliev E.Y. et al. Gas separation in pipelines, // Baku: - 2006, Nafta-Pressl, p. 205
9. Korshak A.A., Shammazov A.M. Fundamentals of gas business. // M., Centre litNefteGaz, - 2007, p.560. http://fizikaplasta.ru/wp-content/uploads/pdfs/korshak.pdf

10. Kharchenko Yu.A. Justification of energy-saving technology of operation of gathering systems at offshore oil and gas fields // Oil economy, - Moscow: -2004, Nº7, - p.68-71. https://naukarus.com/obosnovanie-energosberegayuschey-tehnologii-ekspluatatsii-sistem - sbora-na-morskih-neftegazovyh-mestorozhdeniyah
11. Alekbarov Y.Z. Gasohydrodynamic effects in the separator-collector system in the process of gas preparation for transportation // Azerbaijan Oil Industry, Baku: -2010, No.7, -p. 45-49 https://ru.scribd.com/document/657248215/
12. Iskandarov E.Kh. Optimum technologies of collection and transportation of multiphase well products in offshore fields // News of the Azerbaijan Engineering Academy, - Baku: -2017, volume 9 #3 - p.92-100 https://www.ama.com.az/VOLUME9-N3.pdf
13. Gritsenko A.I., Klapchuk O.V., Kharchenko Y.A. Hydrodynamics of gas-liquid mixtures in wells and pipelines // Moscow: Nedra, - 1994, p.279. https://elib.gubkin.ru/#/
14. Mirzajanzadeh A.H., Kuznetsov O.L., Basniev K.S. et al. Fundamentals of gas production technology // Moscow: Nedra, - 2003, p.806 https://www.geokniga.org/books/4864
15. Hamami Bissor E., Yurishchev A., Ullmann A., Brauner N., 2020. Prediction of the critical gas flow rate for avoiding liquid accumulation in natural gas pipelines // International Journal of Multiphase Flow, vol. 130, 103361. https://www.sciencedirect .com/science/article/pii/S0301932220301063
16. Guzhov A.I. Joint collection and transport of oil and gas // Moscow: Nedra, - 1973, p. 280. https://www.studmed.ru/guzhov-ai-sovmestnyy-sbor-i-transport-nefti-i-gaza_ccb7aa0b 919.html
17. Lebedeva E.V., Sitenkov V.T. Justification of the mechanism of phase interaction in the gradient-velocity field // Chemistry and Technology of Fuels and Oils, - Moscow: 1999, No. 4, - p. 31-35. https://www.oil-info.ru/lit/Sitenkov/gidravlix.pdf
18. O. Y. Batalin, A. I. Brusilovsky, M. Y. Zakharov. Phase equilibria in natural carbon-hydrogen systems // Moscow, Nedra, 1992, p.272. https://www.geokniga.org/books/9339

Technology of reverse-osmosıs sweetenıng of seawater wıth permeate softenıng

Aliyeva O.O., Khalilov K.J.

Scientific Research Institute of Geotechnological Problems of Oil, Gas and Chemistry, ASOIU, 20 Azadlig Avenue. Baku, AZ-1010 Azerbaijan

Abstract

In energy production systems, the allowable concentration of hardness in feed water is 1-10 μg/l to ensure smooth operation of medium and high pressure (3.9-13.4 MPa) steam drum boilers. Calculations show that during reverse osmosis (RO) processing of Caspian Sea water, the hardness of sweetened water (permeate) is higher than required: depending on the prcentage of permeate (50-80%) and the selection of the membrane (99-99.8%), it varies between 0.23 mg/l and 2.1 mg/l. Therefore, softening of the permeate is required. Usually, the Na-cationization method is used for this purpose, and cationite regeneration is carried out with a 3-8% solution of external NaCl salt.

The article shows that in the softening of the permeate, the waste concentrate which is rich in NaCl and Na_2SO_4 salts of the RO process can be used instead of external NaCl salt for the

regeneration of the cationite. Their concentration reaches 3-4%. In this case, the ion-exchange process takes place in equilibrium conditions. Approximately 40% of KU-2 cationite which has total ion-exchange capacity of 1700 mq/l is used in the permeate softening process. The residual hardness concentration of the softened permeate is 0.5-33 μg/l, and when the selectivity of the membrane is taken as 99.4-99.8%, the hardness concentration drops to the required level of 0.5-10 μg/l.

The authors believe that the proposed method can be effective for obtaining softened permeates from ocean and other saline waters.

Research were conducted by analytical method and some simplifying conditions. Therefore, it is planned to verify the obtained results by experimental method in the future.

Keywords: sea water, desalination, reverce osmosis, Na-cationization, permeat, concentrate.
*Corresponding author. Tel.: +994 503550057
E-mail address olga_da@mail.ru (O.O.Aliyeva)

1. Introduction

One of the most important problems of modern times is the shortage of fresh water. The reason for this is the increase in the population, the change of the economic situation, the fact that the percentage of fresh water in the Earth's total water is very small (2.5%) and etc. It is known that the main part of natural waters (> 97%) is sea, ocean and other salty waters with a salinity of 3-50 g/l. "Fresh" water means waters with salinity less than 1 g/l [1,2].

Experience shows that one of the main ways to solve the fresh water problem is the desalination of salt water by different methods. This problem is becoming relevant for some regions of the Republic of Azerbaijan. Desalination of the Caspian Sea water has already been put on a practical level by the state.

Although various seawater desalination methods are used, the most widely used method is reverse osmosis (RO - reverse osmosis): 60-65% of desalinated water is processed by this method [1]. The principle of this method is process of filtering sea water through a special (semi-permeable - mainly permeable to water molecules) membrane with a pressure higher than the osmotic pressure. The reasons for the widespread use of the RO method are the following - its simplicity, low energy consumption, less space requirment and are modular, easy automation, etc. The main disadvantages of the method are the high residual water salinity (TDS – Total Dissolved Solids) of the received permeate: in the RO-process of Caspian Sea water (TDS=13 g/l) -100-120 mg/l, RO of ocean water in the process (TDS=35 g/l) - 400-600 mg/l; short service life of membranes (3-5 years), use of complex pre-treatment technologies to RO membranes from various deposits, etc. i. [3].

As a rule, the production of water with different purposes is carried out with the additional processing (post treatment) of the permeat received in RO units [4,5]. Mainly by further processing of RO permeate, water is prepared for the following purposes:

- Drinking water production;
- Production of demin water for heat energy production systems (steam boilers with different pressures, heating networks, etc.);
- for other purposes.

For example, in [6] preparing hot drinking water from RO effluent is considered. It is shown that when additional salts are added to the permeate (remineralization), formation of scale is

observed. İt was observed that water temperature, calcium concentration and two types of inhibitors have effect on formation scale. It was determined that at low water temperatures (20-25^{0}C) and when the concentration of Ca is 40-69 mg/l, scale does not form.

Research [4] discusses demin water preparation technologies for steam boilers by combining RO and ion-exchange methods. It is shown that the permeate treatment stage is selected and designed depending on the steam boiler pressure:

- for the preparation of make-up water of boilers of flat-flow and critical-to-high-pressure, as well as high-pressure steam-gas plants, in the first stage, permeate aeration (to get rid of CO_2 gas), in the second stage, complete desalination of permeate is carried out in mixed-effect filters loaded with cationite and anionite. Acidic (H_2SO_4) and alkaline (NaOH) solutions are used for filter regeneration. As a result, the specific electrical conductivity of water reaches the limit of 0.2 µSm/cm (TDS=0.4 mg/l);

- for the preparation of make-up water of boilers of laminar-flow and critical-to-high-pressure, as well as high-pressure steam-gas plants, in the first stage, permeate aeration (to get rid of CO_2 gas), in the second stage, complete desalination of permeate is carried out in exchange filters loaded with cationite and anionite. Acidic (H_2SO_4) and alkaline (NaOH) solutions are used for filter regeneration. As a result, the specific electrical conductivity of water reaches the limit of 0.2 µSm/cm (TDS=0.4 mg/l);

- deep softening (Na-cationization) of the decarbonized permeate is performed instead of complete desalination for the preparation of additional water of low, medium and high pressure drum steam boilers. The essence of the process is the exchange of Ca and Mg ions, which make up the hardness of water and lead to the formation of scale, to Na ions that do not form scale. In the process of Na-cationization, regeneration of the cationite filter is carried out with a 3-8% solution of NaCl salt.

Permeate conventional Na-cationization technology has the following disadvantages:

1. NaCl salt is purchased dry from an external system and requires certain costs.
2. A part of the RO permeate is used for the preparation of NaCl solution.
3. The spent regeneration solution formed in the regeneration process is formed and causes environmental damage as a result of its discharge into the environment.

Considering the indicated disadvantages of RO permeate softening technology due to external NaCl salt, an alternative approach is proposed and investigated in this paper. The essence of the proposal (hypothesis) is that instead of the regeneration solution made from external NaCl salt, the softening of the permeate is carried out using the concentrate of the RO process. As a result of the literature review, the authors did not come across any research work conducted in this direction.

The possibility that the RO process of seawater can be useful as a cationite regenerant comes from the fact that NaCl+Na_2SO_4 salts are the main components of all sea and ocean waters, and the concentration of these salts increases to 3-4% in the reverse osmosis process. However, unlike traditional technology, the concentration of hardness in the concentrate of the RO process is high. This worsens the technological performance of the Na-cationization process. But the degree of influence of this factor is not clear. Therefore, it is required to conduct appropriate research by analytical method.

Thus, the aim of the study is to investigate the efficiency of using the waste concentrate of that RO process instead of external NaCl salt as cationite regenerator for the softening of the

permeate formed in the RO desalination process of the Caspian Sea water by the Na-cationization method.

Research Me

Figure 1 shows the technological schemes of the reverse osmosis sweetening system with Na-cationization of the permeate.

Figure 1 shows the technological schemes of the reverse os
with Na-cationization of the permeate.

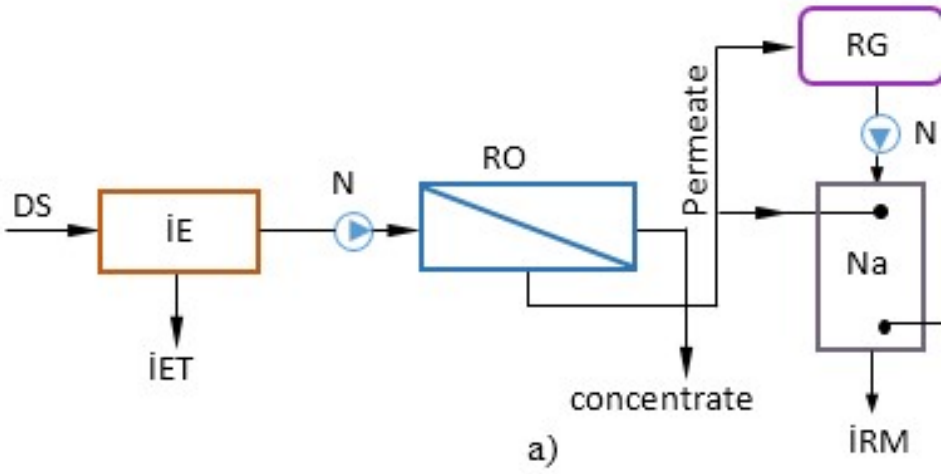

Figure 1. Technological schemes of reverse osmosis sweetening system with Na-cationization of permeate: a) traditional method, b) proposed method: DS-sea water; IE– pre-treatment , IET – waste of primary processing; YP – softened permeate; IRM – spent regeneration solution; RC - regeneration tank; N-pump.

In Figure 1,a, process of the RO-Na process with traditional method which use external NaCl salt, is shown. As can be seen from the scheme, sea water (DS) is purified from certain impurities in the initial treatment stage (IE-Pretreatment) and is fed to the RO module under high pressure. Here, seawater is separated into two parts: permeate (sweetened water) and concentrate, which has high salinity. The latter is thrown into the sea. Part of the permeate is fed to the regeneration tank (RC) to prepare the NaCl salt solution. Regeneration of the cationite charged to the Na-cationite filter is carried out by means of that solution. The processed regeneration solution (IRM) is discharged into the sea. In the regeneration process, the cationite changes to the Na-form. In the next step, the rest of the permeate is softened by passing it through a cationite filter: the main part of Ca and Mg ions in the permeate is replaced by Na ions. Softened permeate (YP) is used as make-up water of steam boilers. The second scheme (Fig. 1,b) is based on the proposed new method and, as can be seen from the figure, it is envisaged to use the concentrate of the RO process for the regeneration of the Na-cationite filter.

Analytical method was chosen as the research method of the proposed method. The study of the RO phase was carried out with the modern methodology presented in [3]. The Nikolski equation based on the law of mass effect was used in the study of the Na-cationization process of the permeate [7]. Main issues resolved:

- Determination of the concentration of Na, Ca and Mg ions in the obtained permeate and concentrate depending on the share of RO permeate and the selectivity of the membrane.

- Derivation of the formula for the specific consumption of Na-ions contained in the concentrate of the RO process (the ratio of the permeate to the hardness).

- Evaluation of the ion exchange capacity of the cationite and the residual hardness of the permeate during the softening process of the permeate.

In order to solve the problems, a computational model of the researched technology (Fig. 1, b) was developed and a computer simulation of this model was carried out. The residual hardness of the softened permeate was compared with the acceptable hardness of the feed water of different pressure steam boilers [8].

1.	Nominal pressure at the outlet of the boiler, MPa	3,9	9,8	13,8
2.	Total Hardness content of feed water, μg/l:			
	for liquid fuel boilers	≤5	≤1	≤1
3.	for other type fuel boilers	≤10	≤3	≤1

Researches were conducted on the example of Caspian Sea water (mg-eq/l): Na=136; Ca=16; Mg=60; Cl=140; SO_4=68; HCO_3 = 4. Total salinity- TDS=12.6 g/l.

2. Calculation Method

The calculation scheme of the RO module is given in figure 2.

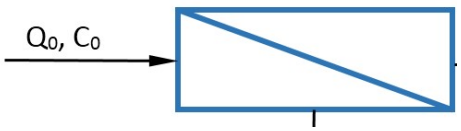

Fig. 2. RO-module calculation scheme

According to the calculation scheme, sea water with consumption Q_0 m^3/h is supplied to the membrane module and is separated into two parts during the treatment process: the permeate passing through the membrane (QP) and the residual concentrate (QK) that does not pass through the membrane. The concentration of salts in seawater is C0, in the permeate - CP, in the concentrate - CK. Then we can write the following material balance equations:

$$Q_0 = Q_P + Q_K \quad (1) \qquad Q_0 \cdot C_0 = Q_P \cdot C_P + Q_K \cdot C_K \quad (2)$$

If we take the amount of permeate β = QP / Q0, we can write the following expressions for the amount of Na, Ca and Mg ions:

$$G_{K,Na} = Q_0(1-\beta)\, C_{K,Na} \quad (3) \qquad G_{P,Ca} = Q_0 \cdot \beta \cdot C_{P,Ca} \quad (4)$$

$$G_{P,Mg} = Q_0 \cdot \beta \cdot C_{P,Mg} \quad (5) \qquad G_{P,Ca+Mg} = Q_0 \cdot \beta \cdot (C_{P,Ca} + C_{P,Mg}) \quad (6)$$

Here $G_{K,Na}$ - sodium in the concentrate of RO, $G_{P,Ca}$; $G_{P,Mg}$ and $G_{P,Ca+M}$ are the amounts of calcium, magnesium and hardness ions in the permeate, mg-eq; $C_{K,Na}$, $C_{P,Ca}$, $C_{P,Mg}$ - is the concentration of the corresponding ions, mg-eq/l. The concentration of each i ion in the concentrate and permeate can be calculated by the following formulas [3].

$$C_{i,K} = C_{i,0}\,(1-\beta(1-R))/(1-\beta) \quad (7) \qquad C_{i,P} = C_{i,OR}(1-R) \quad (8)$$

$$C_{i,OR} = 0{,}5(C_{i,0} + C_{i,K}) \quad (9)$$

Here $C_{i,0}$; $C_{i,K}$ and $C_{i,P}$ are the concentrations of any ions in seawater, concentrate and permeate, respectively, in mg-eq/l; $C_{i,OR}$ is the average concentration of ions in the water flowing over the membrane, mg-eq/l; R is the selectivity of the membrane.

Taking these into account, the formula for the specific consumption ($g_{Na,P}$) of sodium salts in the concentrate of RO and used for softening the permeate can be written as follows:

$$g_{Na,P} = G_{K,Na}/(C_{P,Ca} + C_{P,Mg}), \quad \text{mq-eq/mq-eq} \qquad (10)$$

If formulas (7)-(9) are taken into account in (10):

$$g_{Na,P} = (1-\beta)\,C_{K,Na}/(\beta(C_{P,Ca} + C_{P,Mg})), \quad \text{mq-eq/mq-eq} \qquad (11)$$

For the ion-exchange equilibrium process, using the relative concentrations for the system of different valence cations, the Nikolsky equation is written as follows [7]:

$$\frac{1-\theta}{\theta^{\lambda}} = B\frac{1-\varphi}{\varphi^{\lambda}} \qquad (12)$$

Here θ -is the share of Na ions in cationite; λ is the ratio of hardness and valence of Na ions, $\lambda=2/1=2$; φ is the amount of Na ions in water; $B = K^{\lambda}/h$, where K is the average value of concentration constants of ion pairs; h is the ratio of the total concentration of cations in water to the total ion-exchange capacity (E_T) of the cationite:

$$\varphi = \frac{C_{Na}}{C_{Ca}+C_{Mg}+C_{Na}} \qquad (13)$$

$$h = \frac{C_{Ca}+C_{Mg}+C_{Na}}{E_T} \qquad (14)$$

As a result of the general solution of formula (12), we get:

$$\theta = \frac{-\varphi^2+\varphi\sqrt{\varphi^2+4B(1-\varphi)}}{2B(1-\varphi)} \qquad (15)$$

Formula (15) calculates the amount of Na ions for the concentrate and permeate of the reverse osmosis unit in the cationite content: $\Theta_{K,Na}$ and $\Theta_{P,Na}$. Based on these, useful ion-exchange capacity of cationite according to hardness ions is determined - E_F:

$$E_F = E_T(\Theta_{K,Na} - \Theta_{P,Na}) = E_{K,Na} - E_{P,Na}\,, \text{mq-ekv/l}_K \qquad (16)$$

Here, lK is the volume of the cationite, l.

Since the calculation of the residual hardness of softened permeate by analytical method is a very complicated matter – [7], with some simplifications (taking into account the activity coefficient of ions in water and cationite, etc.) and taking into account that $C_{Ca+Mg,\,YP} << C_{Ca+Mg,\,P}$., softened permeate residual hardness - $C_{Ca+Mg,\,YP}$ (C_{YP}) can be calculated from the following formula:

$$C_{Ca+Mg,\,K}/(C_{Na,\,K})^2 = C_{Ca+Mg,\,YP}/(C_{Na,\,P}+(C_{Ca+Mg,\,P} - C_{Ca+Mg,\,YP}))^2 \qquad (17)$$

A program in Pascal language was developed to conduct the computer simulation of the calculation model. amount of permeate β= 0.5-0.8; the selectivity of the membrane was changed in the range of R= 0.990-0.998 (99-99.8%). The full ion exchange capacity of KU-2 cationite ET=1700 mg-eq/l was considered.

3. Analysis of Results

Image. Figures 3 and 4 show the influence of the amount of permeate and the selectivity of the membrane on the concentration of Ca, Mg and Na cations in the permeate and concentrate obtained in the RO process.

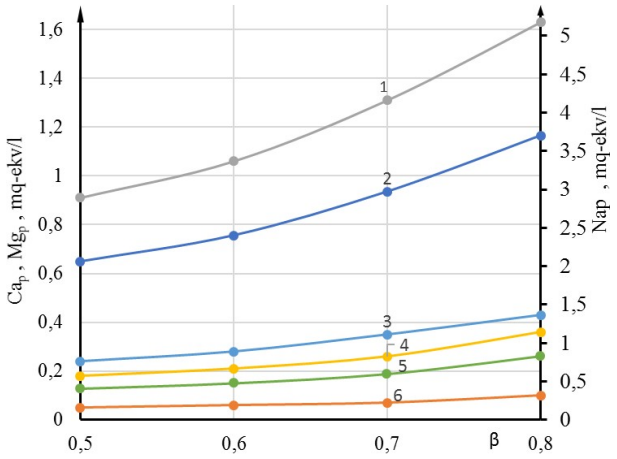

Fig. 3. Dependence of the concentration of cations in the permeate on the amount of the permeate and the selectivity of the membrane:
1,4- Mg_P; 2,5-Na_P; 3,6-Ca_P; 1,2,3 – R=99%;
4,5,6 – R=99,8%

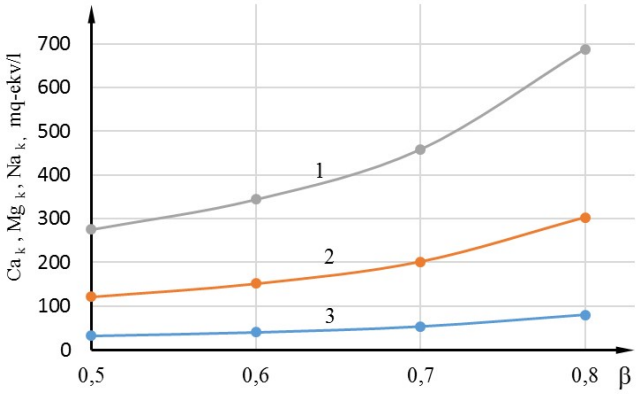

Fig. 4. Dependence of the concentrations of cations in the concentrate on the amount of the permeate and the selectivity of the membrane: 1- Na_K; 2- Mg_K; 3- Ca_K ; R=99,6%

Analysis of the first graph shows that increasing the amount of permeate (β) leads to an increase in the concentration of all three cations in the permeate at both levels of membrane selectivity. At values of β greater than 0.7, concentrations increase more rapidly. At 99% value of R, the total hardness of permeate increases from 1.2 mg-eq/l to 2.6 mg-eq/l. The concentration of sodium ions increases from 2.1 mg-eq/l to 3.7 mg-eq/l. This increase is explained by the fact that the increase in β decreases the amount of the concentrate, and since the amount of salts is constant, the salinity of the concentrate flowing over the membrane increases. Since the permeate is taken from that concentrate, the concentration of ions passing through the membrane, including cations, increases.

Regarding the effect of membrane selectivity, it can be seen from the graph that increasing this indicator from 99% to 99.8% decreases the concentration of cations. For example, at the

maximum value of β, the concentrations of Ca, Mg and Na ions decreases approximately the same level respectively 4.3, 4.5 and 4.6 times. Thus, the minimum and maximum values of permeate hardness in the study area are 0.23 and 2.1 mg-eq/l, respectively: the average is 1.16 mg-eq/l.

According to calculations, the selectivity of the membrane has little effect on the concentration of cations in the concentrate. Therefore, the graph of the corresponding dependence was brought for the average value of R (99.6%) - Fig. 4. According to the graph, the concentration of Na ions increases from 280 mg-eq/l to 700 mg-eq/l. If we convert these salts to equivalent NaCl salt, we get 1.6-4.1%. But the hardness of this solution is very high and on average it is 260 mg-eq/l.

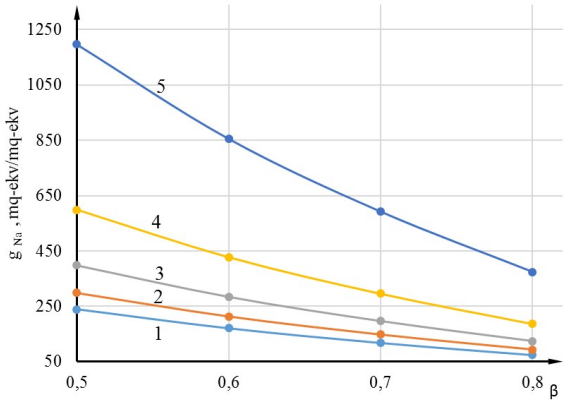

Fig. 5. Dependence of the specific consumption of Na-salts on the share of the permeate and the selectivity of the membrane: 1-R=99%; 2-99.2%; 3 -99.4%; 4-99.6%; 5- 99.8%

As shown above, the ratio of the amount of Na ions in the RO process concentrate to the sum of the amount of Ca and Mg ions in the permeate indicates the specific consumption of Na ions (g_{Na}) in the softening process. As can be seen from Fig. 5, the numerical value of this indicator depends on β and R. An increase in β decreases the specific consumption of Na ions, and an increase in R increases it.

Analysis of the graph shows that the increase of β, regardless of the value of R, reduces the specific consumption of Na ions by 3.2 times. The main result is that the absolute values of the specific consumption of Na ions are very high in all cases. Even minimal values (75-375 mg-eq/mg-eq) are on average 18 times higher than required (10-15 mg-eq/mg-eq in the conventional method). This is an indicator that the ion-exchange process is in equilibrium.

Graphs of the effect of β and R indicators on useful ion-exchange capacity of cationite and residual hardness of softened permeate are given in figure 6.

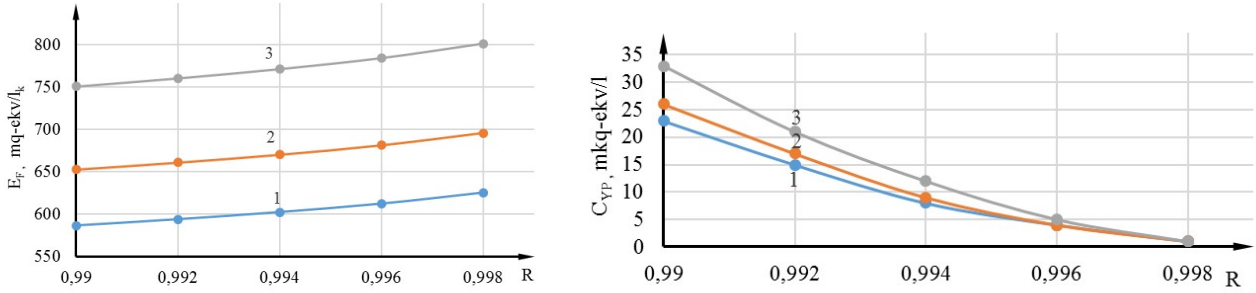

a) b)

Fig. 6. Influence of permeate fraction and membrane selectivity on useful ion exchange capacity (a) and residual hardness of softened permeate (b): β=0.6(1); 0.7(2); 0.8(3).

As can be seen from Fig. 6,a, the increase of input variables increases the useful ion-exchange capacity of cationite in the range of 580-800 mg-equiv/lK, which is 34-47% of the full ion-exchange capacity. But at a constant value of the amount of permeate, the absolute value of the increase in E_F is small - about 50 mg-eq/lK. The increase in EF is related to the fact that as the β and R indicators increase, the TDS of the RO concentrate, including the concentration of Na-salts, which is its main part, increases. It is known from the theory and practice of ion-exchange that as the concentration of the regenerant increases, the ion-exchange capacity increases and the residual hardness of softened water decreases. As can be seen from Fig. 6, b, the residual concentration of softened permeate (C_{YP}) varies in the range of -0.5-35 μg-eq/l. The smallest values are obtained at the maximum value of R, regardless of β. At small values of R, the increase of β decreases the residual hardness of softened permeate, for example, when R=99.2%, hardness decreases by 5 μg-eq/l. It can be seen from the figure that the selectivity of the membrane used in the RO unit is greater than 99.4% to ensure the residual concentration of the softened permeate in the range of 1-10 μg-eq/l. Permeate with a higher hardness value can be used in low-pressure steam boilers and medium-pressure boiler-utilizers.

If we compare the results presented in the last graph and the norm indicators of feed water of different pressure steam boilers, it can be seen that by choosing the selectivity of the membranes used in the RO process and the proportion of permeate, the required hardness of the permeate can be ensured.

5. Conclusion

1. On the example of Caspian Sea water, analytical studies show that the concentrate produced in this process can be used instead of external NaCl salt to soften the permeate obtained in the RO process by the Na-cationization method. With this method, it is possible to prepare make-up water for steam boilers operating at a working pressure between 3.9 and 13.4 MPa, which provides a scale free and has a concentration of less than 10 μg-eq/l. It is considered that the quality indicators of make up water of steam boilers should not differ from feed water.

2. From an economic and ecological point of view, this method is more convenient, because: a) costs incurred for the purchase of external NaCl salt are eliminated; b) a part of sweetened water is not used to prepare a working solution from dry salt; c) no additional salts are thrown into the environment, they consist only of seawater salts.

3. The authors believe that the permeate softening method of the RO process using its own concentrate can be used for the treatment of other saline waters, including standard ocean water with TDS=35 g/l.

4. Analytical research and number of simplifed conditions require experimental verification of the obtained results and are planned by the authors.

Conflict of interest

The authors declare that they have no conflict of interest in relation to this research.

5.References

1. Curto D., Franzitta V., Guercio A. A. Review of the Water Desalination Technologies. Appl. Sci. 2021. 11. 670.

2. Peter G. Youssef, Saad M. Mahmoud and Raya K. AL-Dadah // Seawater desalination technologies. International Journal of Innovation Sciences and Research. 2015. Vol.4. № 8, P.402-422.

3. Sergio G. Salinas-Rodríguez et. al. Seawater Reverse Osmosis Desalination. Assessment and Pre-treatment of Fouling and Scaling. IWA PABLISHING, 2021, 301 p4.

4. Hafiz Abdul Rehman1 and Kashif Ahmed. Reverse osmosis and ion-exchange water treatment for boilers- a brief review Sci.Int.(Lahore),27(6),6147-6151,2015

5. Пантелеев А.А., Рябчиков Б.Е., Хоружий О.В. Технологии мембранного разделения в промышленной водоподготовка. – М.: ДеЛи плюс, 2012 – 429 с.

6. A.H. Haidari et al. Scaling after demineralization of reverse osmosis permeate. Desalination .Volume 467, 2019, P. 57-63.

7. Солдатов В.С. - Теория и практика ионного обмена: современные аспекты. Минск. Белорусская наука. 2020, 599 с

8. В.Н. Воронов, Т.И. Петрова Водно-химические режимы ТЭС и АЭС.- М.: Издательский дом МЭИ, 2016. - 240 с.

Engineering solutions optimization aimed at mitigating risks

M.B. Mammadov, F.T. Rzayev

Encotec LLC – Engineering Institution/Company – Baku Azerbaijan

Abstract

Current Facilities for unloading, storage, preparation, transportation and offloading as a rule have design life to last of over 30 years, often 50 years. In reality very often facilities require life cycle extension as being still in demand after expiry of design life. Such an approach has become more in demand during recent decades as modern engineering more and more aims at optimizing the overall costs while engineering values, to achieve higher efficiencies.

During latest periods the occurring disastrous events are being observed with the aging facilities, like fires, explosions etc., which sometimes are ascribed to conspiracies, which however often are due to inadvertent attitudes to facilities and hazards those facilities may conceal. Risks are not properly identified and addressed, thus leading to artificial higher cost efficiency missing critical assessment criteria for brownfield engineering solutions.

This Article aims at structuring the approaches to safer engineering by dividing the process into stages each having its weight in consideration of extension of facility's longevity. Such approach will significantly minimize risks of hazardous events during exploitation of facility beyond their design life. This will be through staged approach, evaluation of threats at each stage and developing solutions at various levels of approach.

Keywords: oil and gas, optimization, design life, hazards identification, risk assessment, critical parameters, efficiency engineering

1. Introduction

The contemporary situation with the industrial facilities and their engineering systems being under operation, requires a significant change in the attitude to their upgrades and maintenance. This is the result of the quick progresses in engineering fields and very often the crucial and sometimes step

changes in various fields occur within the design life of the facility. Accordingly, service life of some equipment may expire and even replacement by the same model may not be possible as equipment has already been replaced by newer versions.
Such a situation requires that an active interaction of the operating and engineering team with the systems under operation takes place within all service life of the system and periodic reassessments and revalidations of various parts of the system take place.
This new tendency requires developing and using new approaches and tools of analyses to be applied to the system that enable the team to effectively identify the potential gaps, threats and risks to operation and launch corresponding processes to prepare and realize the necessary changes, updates, upgrades and integration to bring the system back into the safe mode of operation.
It is necessary to note that despite a diversity existing in the systems, equipment, operation etc., there are some similarities that allow to generalize approaches and theorize in order to have more developed concept of the contemporary requirements to operations of the systems.
This Chapter summarizes the extensive experience of the authors in the area of the upgrades, modifications and modernizations of the engineering systems in the facilities under operation, which required multidiscipline approach, multidiscipline thinking and uniting of efforts of various engineering disciplines in order to achieve the best or optimal result.
The general approaches in this field embrace variety of engineering disciplines as well as such tools and processes like those to identify the potential threats, evaluation of risks to operation, identifying the range of solutions and evaluation of their comparative efficiencies, value engineering, development selection criteria and others.

2. Methodologies involved in such approach

Generally speaking, engineering is oriented towards problem solving. Modern engineering is focused on optimization and polishing of the conventional and nonconventional approaches for problem solving.
Development and application of the optimization methodologies starting from conceptual stage of upgrade in modern large scale engineering systems is not just necessary but an absolute must. Technology, engineering/tools and advanced methodologies are widely developed and applied for solving of the largescale problems and projects. Modern engineering is accelerated, very flexible and combine optimized qualitative and quantitative solutions' mechanism.
New applications and software interconnects knowledge and statistical data with mathematic models at the level of the artificial intelligence and eliminates the time and scale limitations in problem solving. Margins of cost and time applied for achieving quality can be easily controlled and optimized shortly and accurately.
Motto of the modern engineering is – "quality and safety can easily be achieved at optimized cost and maximum efficiency".
For this reason, engineering process is split into various stages starting from high levels of design up to detailed approaches.
Each level gradually has become quite independent of others and develops its own tools for solving engineering problems. Significant differences nowadays require different skills of engineers to develop in order to effectively and efficiently solve problems that occur within existing operations.
Accordingly, companies develop their own structures in order be able to fit into one or more sectors down the stream of levels where engineering is needed.

The differences between various stages are quite uncertain generally. To define those in a more precise way. Encotec company developed the comparison table (Table1) where these differences are cleared out and assist to select the right approach to problem solving.

Table 1

No	Criteria	Appraise / Select Projects Typical format		Define / Execute stage projects Typical format	
		Level/Rates	**Main Features**	**Level/Rates**	**Main Features**
1	Uncertainty/Risk level	High Uncertainty / Risk	Risk identification, analyses based on policies and techiques (risk matrix, levelling, ranking etc). Engagement with other work groups and third parties to reduce uncertainties. Identification of Risk level as per Annex 3 Risk Matrix of GDP 3.1-0001 and propose risk reduction solutions. Develop and implement risk mitigation plans.	Low Uncertainty / risk	Follow Requirements Implementation of risk reduction recommendations and solutions. Follow risk mitigation plans
2	Project Definition level	0% - 25%	Decision making, engineering solutions, benchmarking, development analyses and optimisation of alternatives, market screening for innovative/alternative solutions. Undertake risk / costs / Hazard assessment and select an optimal solution.	15% - 100%	Systems, procedures, specifications, flow charts, project controls

3	Project Estimating accuracies and method	+/- 60% to +/- 20%	Requires high level estimating techniques, capacity, benchmarking, judgement or analogy and analysis. Focus on reliability and value engineering, economic assessment (CAPEX / OPEX, NPV, IRR etc.)	+/- 20% to +/- 10%	Focus on details Unit cost based on detailed Take-off
4	Manhours	X	Requires capacity to define the uncertainty and propose solutions	5X - 50X	Require Strong Management of multiple / multidiscipline works
5	Project Execution	Development of requirements	Communication / Coordination	Follow Requirements	Project management led
6	Project planning level	level 1 - level 2	Capacity to skip over details and prioritise	Level 3 - level 5	Delving into many details
7	Average experience of involved engineering staff. Qualification requirements.	10 years plus	Approach based on experience, expertise and risk analyses. Versatile, with diverse experiences, capability of broad,'out-of-box' thinking, qualities of leaders, strong analytical capabilities	below 10 years	Skill based approach. Specialisation, skills development, focus on instructions
8	Project Quality	Expression of goals	Define requirements, roles and responsibilities,	Achievement of goals	Measurement of KPIs, criticalities, quality assurance / control
9	Operations Experience input	Major	Engagement with Operations work groups to identify operation requirements, based on experience.	Minor to Medium	Compliance and/or verification of Operation experience requirements

10	HSE impact	Establishment	Identification and evaluation of HSE risks as per Risk Framework – HSE Impact Levels. Identification of Risk level as per Annex 3 Risk Matrix of GDP 3.1-0001 and propose risk reduction solutions. Input into ESIA and health impact assessment process	Application	Implementation of risk reduction recommendations and solutions. Incorporate into design and execution (third parties and subcontractors)
11	SOW/engineering completion %	1-10%	Conceptual Engineering / Scoping Study / Opportunity Phase	10-100%	Detailed engineering/Final design/Installation deliverables

3. Outcomes and discussion

Efficiency has been major problem standing in front of the engineering during decades. To achieve efficiency, to measure it and combine the outputs of the successes and failures to develop tools to be applied to the problem solving required certain knowledge, experience and efforts and were not always providing required results.

Decades before, concepts/solutions were engineered to last for long as tendency in change and innovation was so slow that it could take decades of developments to integrate new ideas into the industry. Rapid growth and development of technology nowadays enable new features and solutions for the green field and brown field engineering. Modern engineer has to consider multiple aspects and growth tendencies while developing a solution as it has to be enough flexible to be partially/fully replaceable and upgradable.

The appropriate tools usually need to be developed to enable uncovering such ‘mystic’ areas as uncertainties, risks, multiple opportunities, expected expenditures and their assessments, etc. etc.

Tools and measures applied by modern engineering does not cover only engineering but also extend to financial and management aspects of the projects. Such an extend in recent decades has brought solutions as:

Modular blocks

Large operation range equipment packages;

Plug and play equipment requiring minimum or no integration efforts;

Low cost high durability materials;

High efficiency and comparatively low cost modern solutions/packages due to standardized manufacturing process;

Solutions optimized from weight, dimensions and transportability point of views;

Optimized from project management point of view.

Based on the practice and experience of the world wide engineering, most of the conventional approaches scarify 1-2 out of 3 fundamental design elements. These elements are cost, time and quality.

Widely applied even today conventional engineering methodologies enable double or in some cases triple of the capacities actually required. Multiple life extension projects of the facilities built in 80th and 90th has been carried out and within these project via application of modern tools it has been revealed that original design offers way too longer design life from what original cope required.

Such margins of course brought benefit at later stages of the facility life time by providing solid bases for life extensions. But, these pre-installed margins should be controlled and accurate. Such can be achieved via clear identification of scope and expectation considering the rapid growth of technology and change of demands.

Dealing with the existing operations and working to improve/optimize those is associated with certain risks of achieving adverse results. This is due to the interference with the operating area and current operations going on. Eliminating or mitigating risks at stage of engineering brings benefit to aforementioned key criteria - cost, time and quality.

An example of the risk analyses and its report are provided in the Table 2. Example of Sensitivity Analyses and decision based on sensitivity to risk / assumptions is provided in the Table 3.

Table 2

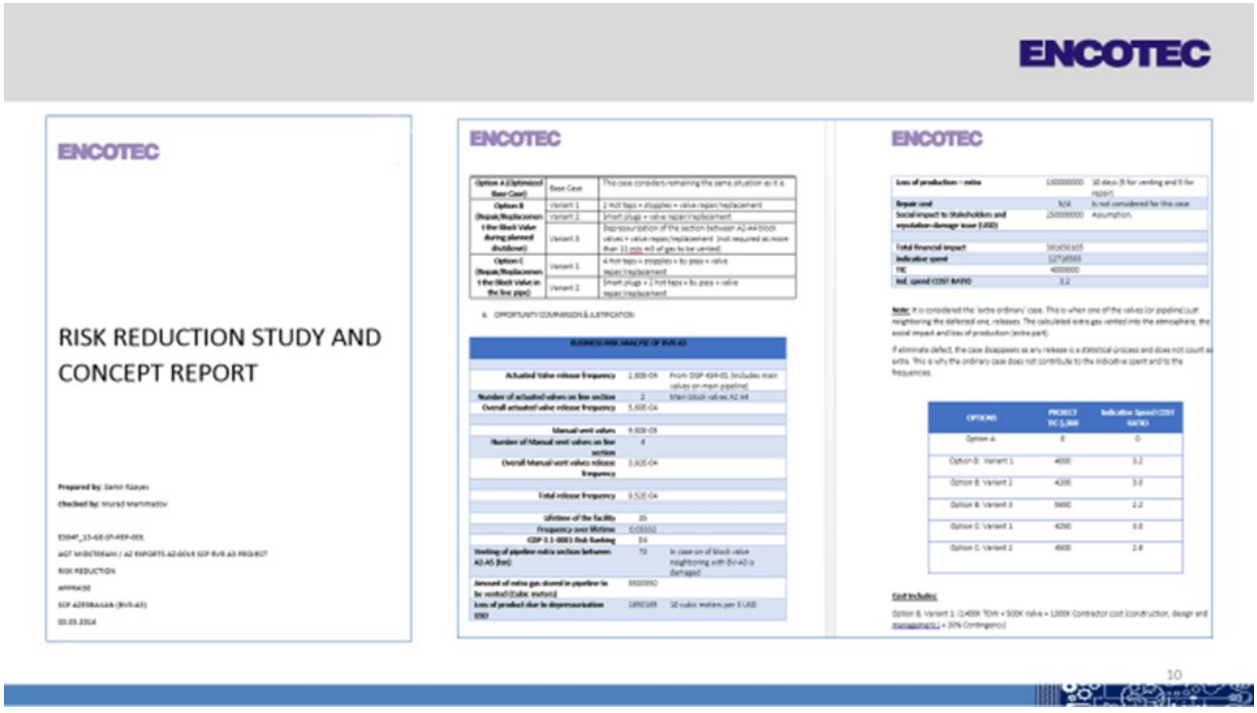

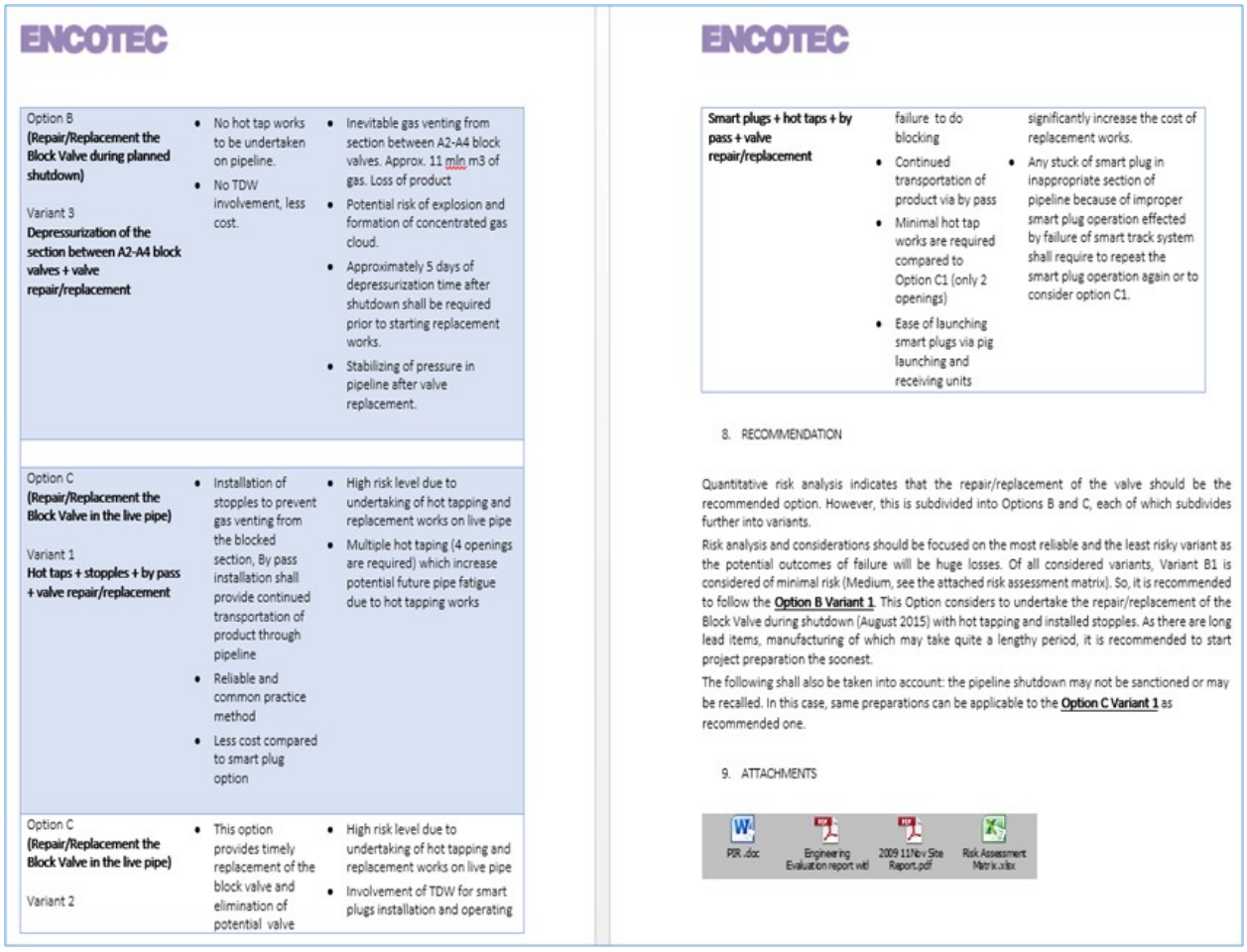

ENCOTEC

Option B **(Repair/Replacement the Block Valve during planned shutdown)** Variant 3 **Depressurization of the section between A2-A4 block valves + valve repair/replacement**	• No hot tap works to be undertaken on pipeline. • No TDW involvement, less cost.	• Inevitable gas venting from section between A2-A4 block valves. Approx. 11 mln m3 of gas. Loss of product • Potential risk of explosion and formation of concentrated gas cloud. • Approximately 5 days of depressurization time after shutdown shall be required prior to starting replacement works. • Stabilizing of pressure in pipeline after valve replacement.
Option C **(Repair/Replacement the Block Valve in the live pipe)** Variant 1 **Hot taps + stopples + by pass + valve repair/replacement**	• Installation of stopples to prevent gas venting from the blocked section, By pass installation shall provide continued transportation of product through pipeline • Reliable and common practice method • Less cost compared to smart plug option	• High risk level due to undertaking of hot tapping and replacement works on live pipe • Multiple hot taping (4 openings are required) which increase potential future pipe fatigue due to hot tapping works
Option C **(Repair/Replacement the Block Valve in the live pipe)** Variant 2	• This option provides timely replacement of the block valve and elimination of potential valve	• High risk level due to undertaking of hot tapping and replacement works on live pipe • Involvement of TDW for smart plugs installation and operating

ENCOTEC

Smart plugs + hot taps + by pass + valve repair/replacement	failure to do blocking • Continued transportation of product via by pass • Minimal hot tap works are required compared to Option C1 (only 2 openings) • Ease of launching smart plugs via pig launching and receiving units	significantly increase the cost of replacement works. • Any stuck of smart plug in inappropriate section of pipeline because of improper smart plug operation effected by failure of smart track system shall require to repeat the smart plug operation again or to consider option C1.

8. RECOMMENDATION

Quantitative risk analysis indicates that the repair/replacement of the valve should be the recommended option. However, this is subdivided into Options B and C, each of which subdivides further into variants.

Risk analysis and considerations should be focused on the most reliable and the least risky variant as the potential outcomes of failure will be huge losses. Of all considered variants, Variant B1 is considered of minimal risk (Medium, see the attached risk assessment matrix). So, it is recommended to follow the **Option B Variant 1**. This Option considers to undertake the repair/replacement of the Block Valve during shutdown (August 2015) with hot tapping and installed stopples. As there are long lead items, manufacturing of which may take quite a lengthy period, it is recommended to start project preparation the soonest.

The following shall also be taken into account: the pipeline shutdown may not be sanctioned or may be recalled. In this case, same preparations can be applicable to the **Option C Variant 1** as recommended one.

9. ATTACHMENTS

PIR .doc | Engineering Evaluation report wit | 2009 11Nov Site Report.pdf | Risk Assessment Matrix.xlsx

All aforementioned are aimed at full or partial elimination of the obstacles preventing engineering to achieve high efficiency.

One has to understand that efficiency is relative understanding and what is efficient today will become in-efficient shortly.

4. Conclusion

The area of providing solutions to the emerging problem during existing operations is not studied to the degree adequate to its occurrence nowadays. Only a few publications are dedicated to this and the demand is quickly growing. The multiple and multidiscipline character of the emerging problems complicates development of unified tools and approaches.

At the same time, at the current stage some important tools have been developed that enable effective solutions to the problem being identified, developed and managed.

The most important issues are defining the problem and identifying all uncertainties associated with it, further to which start dealing with uncertainties and their management. The general tools are Identification of the type of uncertainty, considering approaches to uncertainty and developing alternative options as solutions, analysis of alternative options and their ranking, risk analysis for each alternative option, analysis of various scenarios related to alternative options, cost analysis, constructability analyses etc., summarizing analyses of considered options and selecting the most applicable against certain criteria developed specifically for the project.

Along with this, the risk management approach is a very important tool of the process as ignoring risks may create serious deficiencies in the proposed solution up to an overall project failure.

The stated approaches to conceptual level of the engineering approaches to the solution are supported by examples from the practical work of Encotec LLC enabling successful project development and a significant tool to making right decision on all stages of the project.

Conflict of interest

The authors declare that they have no conflict of interest in relation to this research.

5.References

1. Frank Peter Helmus (Prof. Dr.-Ing. Frank Peter Helmus University of Applied Sciences Osnabrück Engineering). Book - Process Plant Design (In Germany) https://elmoukrie.files.wordpress.com/2022/06/process-plant-design-project-management-from-inquiry-to-acceptance-frank-peter-helmus.pdf
2. Gerbert van Weige - Front end loading in the O&G Industry 2008
3. Herve Baron. O&G Engineering guide -. (3rd edition) November 2018
4. David G. Carmichael. Problem Solving for Engineers – 1st edition 2013
5. Harris R. Greenberg and Joseph J. Cramer Risk Assessment and Risk Management for the Chemical Process Industry: Stone and Webster Engineering Corporation
6. Maureen Hassall, Paul Lant - Fundamentals of Risk Management for Process Industry Engineers 1st edition 2023

Possibility to eliminate accidents in oil and gas wells occurring with glass fibre rods with the help of a rod head designed for them.

R.Narimanov[1] S. Hajiyeva[2],

[1]Training master department of "Materials Science and Processing Technologies" Azerbaijan State University of Oil and Industry, Azerbaijan.
[2]Assistant department of "Materials Science and Processing Technologies" Azerbaijan State University of Oil and Industry, Azerbaijan. Email

Abstract

The operation of oil and gas wells with sucker rod deep well pumping units takes place in aggressive conditions of the oil and gas production field. This leads to accidents arising with deep well pump rods of these units. The report talks about the possibility of eliminating accidents arising with glass fibre rods, which differ from metal, steel rods by their physical and mechanical properties. These rods are the most important part of a deep-water pumping unit. It is noted that in order to eliminate accidents with deep-well pumping units it is necessary to develop a catching tool rod-header. The diameters of these rods used in production are specified. It is noted in the report that fibreglass rods are made in order to save metal, as well as these rods are anticorrosive in comparison with metal rods. The disadvantage of fibreglass rods is their relatively low strength (σ) compared to metal, steel rods and their smoother surface, which is less able to be effectively gripped by the rod head. The report explains the process of eliminating a fibreglass rod accident with this catching tool. Continuing the lowering of the rod-header there is a gripping inside the tool body by the surface of the coupling or body of the fibreglass rod by gripping elements, spiral parts and collet. The efficiency of the process of gripping of the glass fibre rod depends on what, as a

result of this, it is possible to eliminate the accident in a well with oil and gas producing deep well pumps with the help of the rod head developed for glass fibre rods.

Keywords: fibreglass rods, downhole rod pumping unit, accident elimination, rod header.
*Corresponding author. Tel.: + 994 506139897
E-mail: Rustam.narimanov.73@inbox.ru; id: haciyeva_1987@list.ru

1. Introduction

Downhole sucker rod pumping units are one of the main operating equipment for oil and gas production. The operation of these units takes place in aggressive conditions of producing oil and gas wells. The most responsible unit of the pumping unit is the pumping rod string. For oil and gas production, apart from metal steel rods, fibreglass rods are used. In terms of physical and mechanical properties glass fibre rods differ from metal rods. During operation of the wellbore, these rods are subjected to loads and stresses. A certain period of operation in downhole conditions leads to ageing and mechanical wear of glass fibre rods. As a consequence, the glass fibre rods are likely to break, resulting in a well pump abandonment accident. For this purpose it is necessary to eliminate the accident for further operation of oil and gas producing wells, i.e. to extract the remaining fibreglass rod from the wells. For this purpose a catching tool for fibreglass rods is developed. These rods are made of fibreglass material in order to save metal. The disadvantage of fibreglass rods is their relatively low strength (σ) compared to metal and steel rods and their smoother surface, which is less easy for the rod catcher to grip effectively. Consequently, there is a question of the possibility of accident elimination in oil and gas producing wells with fibreglass rods. That is, to solve this issue, it is necessary to consider and take into account the design features of the developed rod header, as well as its technical characteristics of the gripping unit and components.

2. Methodological part

The topic of the report is based on the method of critical analysis in oil and gas well remediation of accidents in oil and gas wells, arising with glass fibre rods with the help of the developed for them rod-header. Taking into account the disadvantage of glass fibre rods, i.e. their relative low strength (σ) in contrast to metal and steel rods and their smoother surface, which is less amenable to effective gripping by the rod head, as follows from this, the possibility of liquidation of accidents occurring with glass fibre rods is logically considered. The design of the developed catching tool of the rod header is given according to the outer diameters of glass fibre rods Ø16, Ø19, Ø22, Ø25 mm, i.e. its general view and the glass fibre rod itself. The process of effective gripping of the rod-header by its main working parts spiral and collet is described and analysed on this basis. According to the method of critical analysis, the possibility of elimination of accidents in oil and gas wells, arising with fibreglass rods, depends on the reliable process of engagement of the smooth surface of the body or coupling of the fibreglass rod with notches of the inner surface of the gripping elements of spiral and collet parts. The same reliability of the grip on the body of the glass fibre rod is possible at fixation and compressive forces (Fcj.), i.e. from large elastic properties of these gripping elements (parts). Having notches on the inner surface of the parts sproul and collet cover the whole diameter of the coupling end or the body of the fibreglass rod. It follows that in order to securely grip the emergency fibreglass rod, it is necessary to take into account, as a factor, the technological fit (e.g. H4; h4) between the smooth surface of the body or end of the coupling of the fibreglass rod (shaft system (e.g. h4)) and the inner surface with notches of the gripping elements, i.e. spiral and collet (bore system (e.g. H4)). And analyzing, it is possible to say that at gripping by the inner surface with notches of a spiral or a collet and a smooth cylindrical surface of a body or an end of a coupling of a fibreglass rod, a tight fit is formed, which promotes reliable gripping of an emergency object, i.e. this rod and makes possible liquidation of an accident occurring with these rods in a well with the help of a catching tool developed for them, i.e. a rod header.

3. Main part

Oil and gas production by downhole deep well sucker rod pumping units, i.e. their operation, takes place in unfavourable conditions of the oil and gas production field. Oil and gas fields at their operation by deep well rod pumps, in addition to the usual metal steel rods, glass fibre rods are used. The physical and mechanical properties of glass fibre rods differ sharply from metal rods. Deep well pumping rods are subjected to static and dynamic loads and stresses during operation in production wells. Being the most critical connection of this unit, the fibreglass rod string is also subjected to these loads and stresses. As a consequence, during a certain period of operation of the fibreglass rod string, its ageing and mechanical wear occurs. During this process there is a possibility of glass fibre rods breakage, resulting in an accident associated with the deep well pump remaining in the well. It is necessary to eliminate the accident for further operation of oil and gas producing wells. In this case we mean the elimination of the accident with fibreglass rods. For this purpose it is necessary to develop a catching tool, a rod header for glass fibre rods. It is known that metal rods with diameters Ø16, Ø19, Ø22, Ø25 mm are used in production. (Fig.1). These rods are made of fibreglass material in order to save metal and improve technical performance.

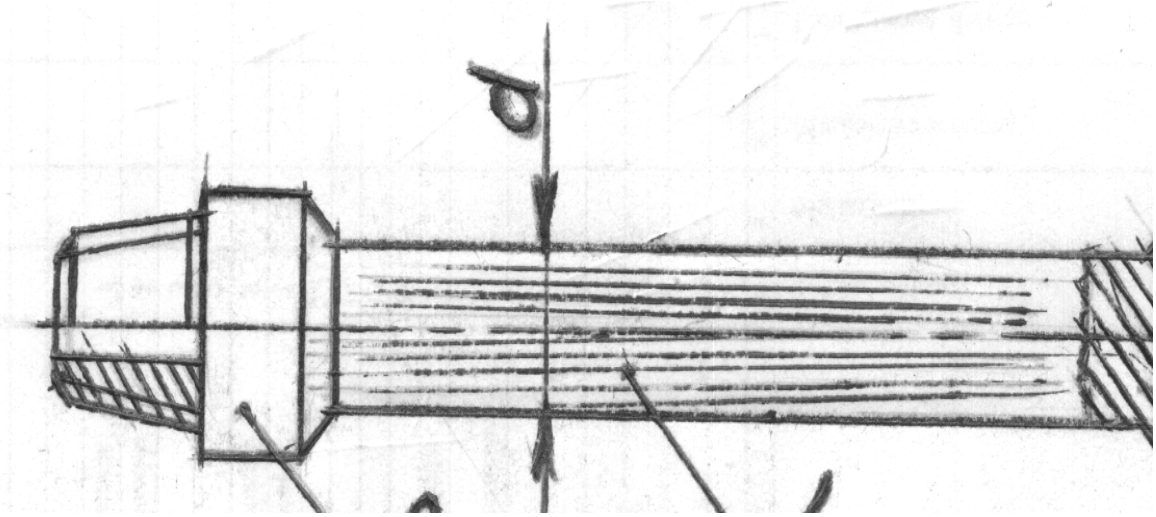

Fig.1 General construction of glass fibre rod: 1- glass fibre body (body) of the rod; 2- metal nipple end of the rod; 3- metal coupling end of the rod.

Compared to metal rods, fibreglass rods are economical to manufacture and anti-corrosive. The downside of fibreglass rods is their relatively low strength (σ) compared to metal steel rods and their smoother surface, which is less easy to grip effectively with a rod-header. The process of liquidation of an accident with fibreglass rods, consists of the operation of lowering the catching tool of the rod catcher on the string suspension of rods into the emergency well with the emergency object, fibreglass rod, its capture by the body of the rod catcher and extraction from the well. The construction of the rod head (Fig.2) consists of a cylindrical body.

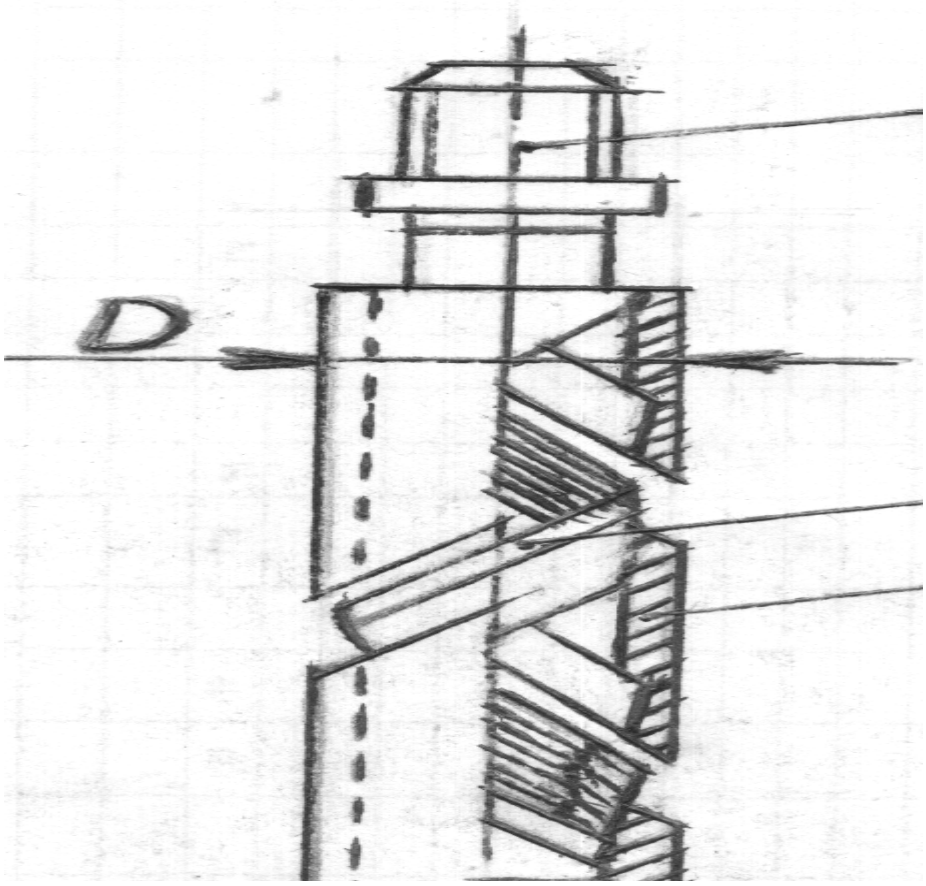

Fig.2 Assembly design of the rod-header for glass fibre rods: 1- body; 2- gripping element (detail)-spiral; 3- place of connection of the rod-header with the string of rods suspension for lowering into the emergency well.

In the upper part of the casing there is a place for connection to the rod string suspension for lowering the rod header into the well. The rod head body has a lateral spiral window with a spiral conical surface mating with it to hold the spiral and collet gripping elements (spiral and collet parts). The spiral gripping element with a spiral conical surface on the outside and notches on its inner surface is used for gripping both the body and the head of the boom. After lowering the rod-header into the well, its lower part of the body in the form of a funnel passes the end of the coupling or the head of the fibreglass rod inside the tool body. As the rod head continues to descend, the inner notched surface of the spiral or collet gripping element grips inside the tool body by the surface of the coupling or fibreglass rod body. In general, after the process of grasping the surface of the coupling or body of the glass fibre rod, the effectiveness of this grasping, as well as the possibility of eliminating the accident, that is, the extraction of the emergency object of the glass fibre rod depends on a reliable process of engagement of the smooth surface of the end of the coupling or body of the glass fibre rod with notches on the inner surface of the gripping elements, spiral and collet. Also fixation and compressive force (ability), i.e. from the large elastic properties of these gripping elements (parts), makes it possible to securely grip the body or end of the coupling of the glass fibre rod. The gripping elements of the boom catcher cover with their inner surface with notches over the entire diameter of the coupling end or body of the fibreglass rod. As follows, in order to securely grip the emergency rods, it is necessary to take into account, as a factor, an index of technological fit (e.g. H4; h4) between the smooth surface of the body or coupling end of the fibreglass rod (shaft system (e.g. h4)) and the notched inner surface of the gripping elements of the helix and collet (bore system (e.g. H4)). That is, the interference fit formed by the gripping surface

of the inner surface with notches of the helix or collet and the smooth cylindrical surface of the body of the coupling end of the fibreglass rod, contributes to the reliable gripping of the emergency object, i.e. the fibreglass rod, and makes it possible to eliminate accidents in a well with oil producing rod deep well pumps with the help of a catching tool, i.e. a rod head designed for fibreglass rods.

4. Results and discussion

The paper presents a schematic diagram of the fibreglass rod (Fig.1) and a schematic diagram of the rod catcher tool as an assembly drawing (Fig.2). The construction of the boom catcher and its parts is described. It clearly indicates the emergency object and the catching tool. The diameters of the metal (fibreglass) rods used in production are indicated accordingly. Operation of fibreglass rods takes place in unfavourable conditions of oil and gas production field and wells. Being the most critical connection of a downhole deep well pumping unit, the fibreglass rod string is subjected to static and dynamic loads and stresses. As a consequence, at a certain period of operation of the fibreglass rod string, the fibreglass rods age and wear out. This leads to the probability of glass fibre rods breakage, resulting in an accident associated with the abandonment of the deep well pump in the well. It is necessary to eliminate the accident, for further operation of oil and gas producing wells. With the help of the developed, for catching (capturing) the emergency object, remaining in the well fibreglass rod, rod-header (Fig.2), the liquidation of the accident is carried out. As a result, for reliable gripping of the smoother surface of the body or coupling of glass fibre rods in comparison with metal rods, it is necessary to have reliable meshing (high value of the coefficient of friction force at meshing) with notches of the inner surface of the gripping elements, i.e. parts of the spiral or collet rod-header. Also the possibility of reliable gripping of the body or coupling of the fibreglass rod, will be at fixation and compressive forces, i.e. from the large elastic properties of these gripping elements. When the notches on the inner surface of the spiral or collet parts are gripped, they cover the entire diameter of the end of the coupling or body of the fibreglass rod. The result of covering these parts indicates a process fit factor (e.g. H4;h4) between the smooth surface of the body or coupling end of the fibreglass rod (shaft system (e.g. h4)) and the notched inner surface of the gripping elements of the helix and collet (bore system (e.g. H4)). A tight fit is formed when the spiral or collet gripping elements are gripped by the notched inner surface of the smooth cylindrical surface of the body or end of the fibreglass rod coupling. This contributes to a reliable grip of the emergency object, i.e. fibreglass rods and as a result makes it possible to eliminate the accident with the help of the developed rod-header.

5. Conclusion

The operation of a downhole rod pumping unit takes place under unfavourable conditions in the oil and gas production field. The downhole pumping rod column is the most critical connection of this unit. Oil and gas producing wells during their operation by deep well pumps, in addition to the usual metal, steel rods, glass fibre rods are used. These rods differ sharply from metal rods by their physical and mechanical properties. In conditions of operation of glass fibre rods in oil and gas producing wells their ageing and mechanical wear occurs. This process contributes to probable breakage of glass fibre rods. This leads to an accident associated with leaving the deep well tubing pump in the well. It is necessary to eliminate the accident with fibreglass rods. For this purpose it is necessary to develop a catching tool, a rod head for fibreglass rods according to their outer diameter. At accident elimination the rod catcher is lowered on the string suspension of rods into

the emergency well with the emergency object, i.e. fibreglass rod. According to the specified design of the rod-header (Fig.2), its main gripping element is the spiral and collet parts located in the tool body. The end of the body or coupling of the fibreglass rod, when lowering the rod head, goes through the funnel inside the body of the rod head and the internal surface with notches of the gripping elements of the spiral and collet of this rod is captured. It is covered with its inner surface with notched gripping elements, over the entire diameter of the end of the body or coupling of the fibreglass rod. The body of the glass fibre rod has a smoother surface compared to metal, steel rods. Consequently, the possibility of accident elimination, i.e. extraction of the emergency object of the glass fibre rod from the well depends on the reliable process of engagement of the smooth surface of the end of the body or coupling of this rod with notches of the inner surface of the gripping elements, i.e. spiral and collet. That is to say, having a high coefficient of friction between these surfaces, the possibility of retrieving the fibreglass rod remaining in the borehole is more likely. Fixation and compressive force, i.e. from the large elastic properties of these gripping elements also makes it likely that the smooth surface of the body or end of the coupling of the fibreglass rod can be grasped and extracted from the well. Engagement of the gripping elements by their internal surface with notches along the entire diameter of the coupling end or body of the fibreglass rod indicates the factor of technological fit between these surfaces. The tight fit formed between these surfaces makes it possible to eliminate the accident with fibreglass rods with the help of a rod-header designed for them.

Conflict of interest

The authors declare that they have no conflict of interest in relation to this research

6. References

1. Mamedov Z.E. "Express-method of calculation of equal-strength two-stage rod string"// ANT, № 4-5, p.87, 2007.
2. Dzhabbarov R.D., Hasanov A.P. "Complex of downhole equipment and tools for emergency wells" // ANT, No.7, p.45. 2006 г.

Modeling and optimization of the process hydrotreating of diesel fuel

N.M.Abbasov*, A.A. Məsimov

* Research Institute of Geotechnologocal Problems of Oil, Gas and Chemistry, ASOIU, 20 Azadlig Ave., Baku, AZ-1010 Azerbaijan
Department of Industrial machines, ASOIU, 20 Azadlig Avenue. AZ-1010 Azerbaijan

Abstract

The main approaches to the development of a reactor unit for the hydro desulfurization of diesel fuels are considered, taking into account the reactivity of the organosulfur components that make up diesel fuel and the formation of pseudocomponents conditionally combining a group of organosulfur components. As the concentration of easily or difficult-to-hydrogenate sulfur-containing components in raw materials increases, the role of a substance limiting the quality of diesel fuel purification may shift from an easily hydrogenated to a difficult-to-hydrogenate

pseudocomponent and vice versa. The efficiency of operation of five variants of the reactor unit of hydrotreating plants is compared. It is shown that from the point of view of minimizing the loading of the catalyst, the two-reactor scheme of the hydrotreating process with separate supply of low-boiling and high-boiling fractions of straight-run diesel fuel to the reactors is optimal. The necessity of determining the temperature boundary of their division, taking into account the qualitative and quantitative composition of these fractions by organosulfur substances, is substantiated.
Keywords: hydrotreating, diesel fuel, mathematical modeling and optimization of hydrotreating, kinetics of chemical reaction, organosulfur substances
*Corresponding author. Tel.: + 994 506139897
E-mail:

1. Introduction

Hydrotreating of diesel fuel is one of the largest-tonnage petrochemical processes. The specificity of the process lies in the fact that its implementation is carried out in the presence of a number of adverse factors [1]. These include:

– carrying out the process at very high pressures of 3-8 MPa;

– low content of organosulfur compounds in the feedstock – 1.5–0.8 wt. %, as a result of which hydrotreating as a chemical process occurs at very low rates of desulfurization reaction;

– the process as a whole is carried out in the most difficult to implement three-phase system: liquid-phase raw materials, hydrogen-containing gas, bifunctional solid catalysts that ensure the implementation of homolytic and heterocyclic reactions [2, 3];

– a large number of various organophosphorus compounds, which significantly complicates the formation of mathematical models of the process;

– simultaneously with hydro desulfurization, a large number of additional reactions involving hydrogen (hydrodeazotization, hydronitration of aromatic hydrocarbons) occur;

– strict requirements for the quality of diesel fuel, limiting the sulfur content;

– gradual deactivation of the catalyst, which leads to instability of the operation of hydrotreating plants.

While low requirements for the quality of diesel fuel were ensured by reducing the total sulfur content as a result of hydrotreating by 5-10 times, it did not matter that different organosulfur components of raw materials have different hydrogenation rates.

This made it possible to use in calculations a quasi-homogeneous scheme of the desulfurization process as a whole [4, 5] according to the scheme of the generalized reaction:

$$RS + H_2 \rightarrow HC + H_2S,$$

where RS, H_2, HC, H_2S are, respectively, the total organosulfur substance, hydrogen, hydrocarbon, hydrogen sulfide.

In this case, due to the fact that hydrogen is introduced into the hydrotreating process in large excess (consumption of hydrogen-containing gas 200-800 m^3/m^3 of raw materials), the desulfurization reaction could be considered as a pseudo-first-order reaction and the kinetics of hydrotreating was described by the equation:

$$\frac{dC_{RS}}{d\tau} = -KC_{RS},$$

where C_{RS} is the concentration of a generalized set of organosulfur components in the reaction system, τ is the reaction time, and K is the reaction rate constant, which, due to accepted assumptions, is effective.

As the requirements for the quality of diesel fuel became stricter and the level of permissible sulfur content decreased by standards from Euro-3 (350 million^{-1}) to Euro-5 (10 million^{-1}), the schemes of reactor units of the hydrotreating plant began to improve with the transition from single reactors to more complex systems: two-reactor schemes with series and parallel reactors, three-reactor schemes, reactors with several layers of catalysts of different selectivity, the use of a recycle of purified raw materials, etc. [6-14].

At the same time, they began to delve into mathematical models of hydrotreating.

The degree of activity of sulfur compounds in hydrogenolysis reactions varies and decreases in the series: mercaptans > sulfides > thiophenes > benzothiophenes > dibenzothiophenes. At the same time, the most difficult-to-hydrogenate compounds of the thiophene series are concentrated mainly in heavy fractions boiling above 330°C. With an increase in the temperature of the process, the degree of hydrogenation of sulfurous and unsaturated the dehydrogenation of naphthenes increases, however, at values above 420°C, the effectiveness of the target reactions decreases markedly due to the transition of the process to the diffusion zone, but the rate of cracking reactions increases, provoking the formation of coke, and the catalyst itself begins to sinter with the destruction of the porous structure. Therefore, the main attention is paid to the formation of mathematical models of hydrogenation kinetics in the temperature range 320-380°C [15-20] with alternative approaches to solving the problem. The first approach is to identify an extremely complete set of organosulfur components of diesel fuel and develop a database of possible reaction routes, for example, [21] describes 38 hydrogenation reactions of organosulfur components with the number of carbon atoms in a molecule from 2 to 12, belonging to the following groups of substances: mercaptans, sulfides, disulfides, thiophenes, benzothiophenes, dibenzothiophenes.

However, it is quite problematic to implement kinetic experiments to obtain the physicochemical characteristics of reactions necessary for modeling the process, primarily the constants of the Arrhenius equation (activation energy and preexponential multiplier) due to the microconcentrations of many components in the reaction mixture.

The second approach consists to a certain extent in formally combining the components of one group of organosulfur substances into a conditional pseudocomponent, but at the same time the calculated constants of both the Arrhenius equation and the reaction rate constants themselves are effective and do not allow an objective analysis of the reaction process to be formed. For example, in [15], the study of the desulfurization process of diesel fuel was performed using the following conditional pseudocomponents: combined sulfides, combined ethylbene-zothiophenes, combined propylbenzothiophenes, combined butylbenzothiophenes, dibenzothiophene, combined methyldibenzothiophenes and combined ethyldibenzothiophenes, and in [22]

A different grouping was used: combined aliphatic and non-heterocyclic sulfurcontaining components, including thiols, sulfeeds and thiophenes, benzothiophene, combined benzothiophenes, including alkyl chains from 1 to 5 carbon atoms, dibenzothiophene, combined dibenzothiophenes, including alkyl chains from 1 to 5 carbon atoms, while in the course of mathematical modeling of hydrotreating, far from equivalent compositions of raw materials are taken into account, including organosulfur components (Table 1).

From the standpoint of the direct use of mathematical models for the control of industrial hydrotreating reactors, more The second direction is rational, however, a detailed analysis of the process is necessary, taking into account the organosulphurization components that limit the depth of hydrodesulfurization of diesel fuel.

2. Methodological part

It is obvious that ensuring the depth of purification of diesel fuel to the required permissible level of sulfur content is determined not by the total content of organosulfur components in the fuel being cleaned, but by a combination of two factors: the concentration and reactivity of the most characteristic impurities [21-23] combined into pseudocomponents. An increase in the concentration of any pseudocomponent leads to an increase in the duration of hydrotreating and, accordingly, a proportional increase in the loading of the catalyst into the reactor. Availability in raw materials hydrotreating of a hard-to-hydrogenate pseudo-component also leads to an increase in the duration of hydrotreating and an increase in the loading of the catalyst into the reactor.

Figure 1 shows variants of generalized schemes of the chemistry of the hydrotreating process with a different number of conditional pseudocomponents.

Table 1. The content of pseudocomponents in diesel fuels

Pseudocomponent		The proportion of the pseudocomponent in organosulfur substances, wt. %	
		according to [15]	according to [22]
Combined aliphatic and heterocyclic sulfur-containing components, thiols, sulfides, thiophenes		-	3.2
Benzothiophene		-	11.5
Combined methylbenzothiophene		-	14.1
Combined ethylbenzothiophenes		21.5	17.9
Combined propylbenzothiophene		34.8	20.5
Combined butylbenzothiophene		33.2	23.2
Combined pentylbenzothiophenes		-	
Dibenzothiophene		7.9	2.6
Combined methyldibenzothiophene		2.4	6.4
Combined ethyldibenzothiophenes		0.1	

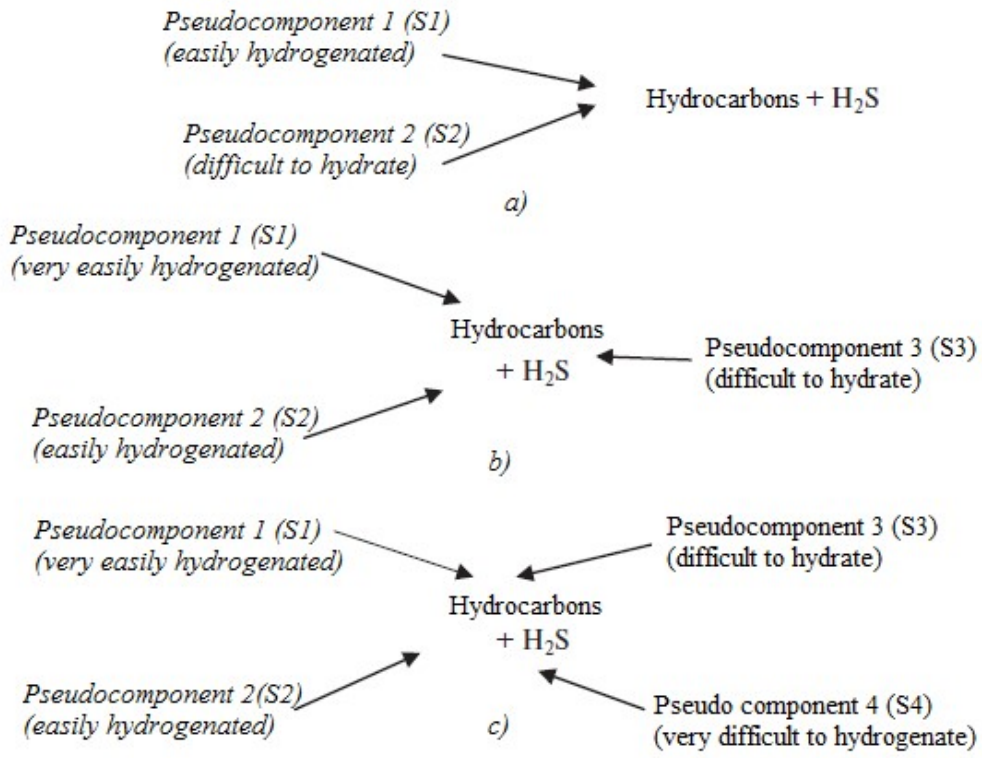

Fig. 1. Generalized schemes of the hydrotreating process with the number of pseudo-components two (a), three (b) and four (c) according to [22].

The model of the kinetics of the hydrotreating process, for example, for four pseudo-components has the form of a system of equations:

$$\left.\begin{aligned}\frac{dC_{S1}}{d\tau} &= -K_1 C_{S1}\\ \frac{dC_{S2}}{d\tau} &= -K_2 C_{S2}\\ \frac{dC_{S3}}{d\tau} &= -K_3 C_{S3}\\ \frac{dC_{S4}}{d\tau} &= -K_4 C_{S4}\end{aligned}\right\}$$

$$C_{RS} = C_{S1} + C_{S2} + C_{S3} + C_{S4},$$

where C_{Si} and K_i are, respectively, the concentration of the organosulfur pseudocomponent and the rate constant of the i–th reaction.

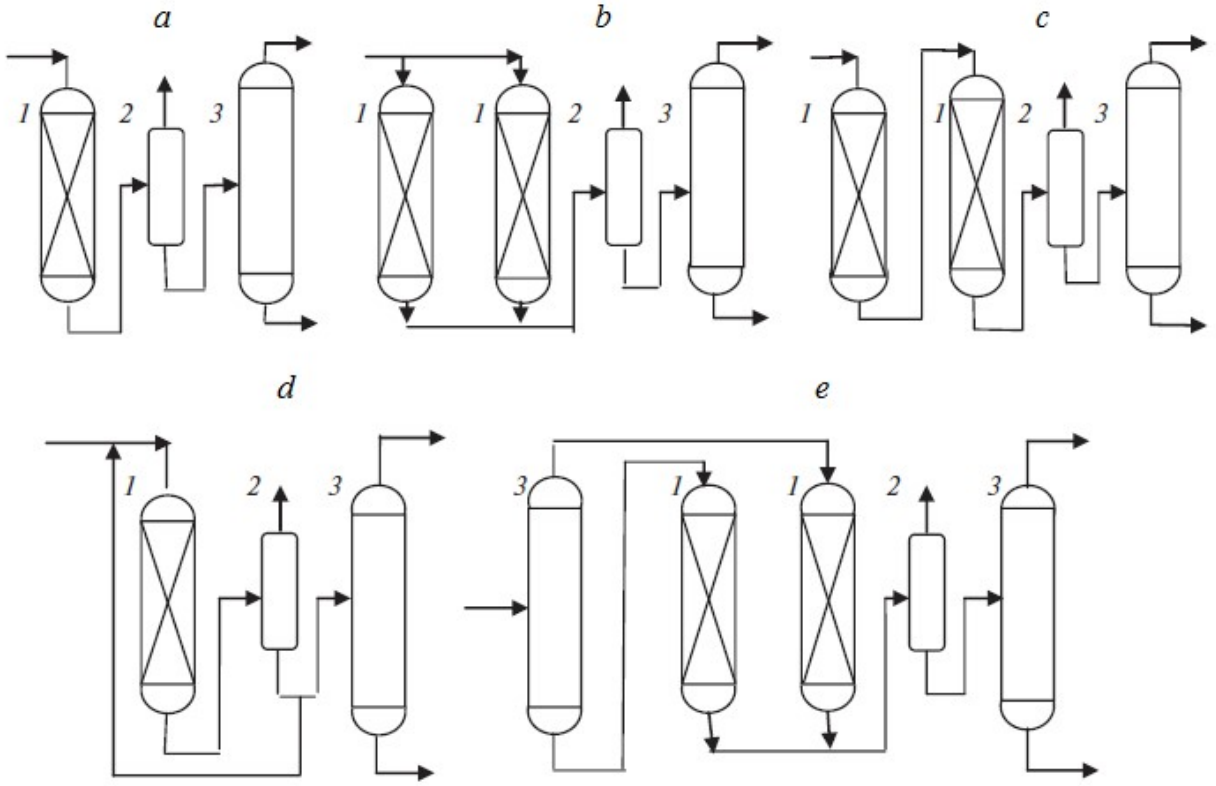

Fig. 2. Schematic diagrams of reactor units: (a) – single–reactor unit [24], (b) – two–reactor unit with parallel feed of raw materials [25], (c) – two-reactor unit with sequential feed of raw materials [25, 26], (d) – single-reactor unit with recirculation of purified diesel fuel [27], (e) – a two–reactor unit with preliminary fractionation of raw materials [28]; 1 – reactor, 2 – separator, 3 – distillation column.

The variety of hardware design of the reactor unit of hydrotreating plants (Fig. 2) requires a fairly detailed analysis from the standpoint of minimizing the loading of the catalyst to obtain high-quality diesel fuel. Since the reactors are structurally the same in all circuits, when solving the task, it was assumed that the ideal displacement regime is implemented in the reactors from the standpoint of hydrodynamics and isothermicity of the process was assumed to simplify calculations, since with constant depth of hydrotreating and other things being equal, the temperature profile in the height of the catalyst layer in reactors of different circuits should be almost the same.

To compare different reactor systems of hydrotreating stem (Fig. 2), mathematical modeling of the hydrodesulfurization process of 250 m^3/h of diesel fuel with a sulfur content of 6000 mg/kg (6000 mln^{-1}) was performed at a volumetric feed rate of 2 h^{-1} and the accepted effective rate constant of the hydrodesulfurization reaction of 2 h^{-1} [15], that, with constant technological parameters (temperature, pressure, flow rate of hydrogen-containing gas), it was possible to correctly consider a rather complex catalytic hydrotreating process as a quasi-homogeneous reaction of the first order. Calculations the differential equations of the model were performed by the Runge–Kutta method with the determination of the required contact time of the reaction mixture with the catalyst. The efficiency of the reaction system in ensuring the final concentration of sulfur in purified diesel fuel from 500 to 10 mg/kg was estimated by the total volume of the catalyst in the

reaction system, represented by a single reactor, two parallel reactors, two sequentially operating reactors and a single a reactor with a purified diesel fraction fed into it as a recycle after separation of hydrogen-containing gas, which was supposed to shorten the duration of the reaction by reducing the sulfur concentration at the reactor inlet.

The calculations showed (Table. 2) that the volume of the catalyst in a single reactor, and in a parallel and sequential reactor system, necessary to achieve a given residual sulfur concentration in diesel fuel, is the same and the configuration of the installation scheme is determined only by technical limitations.

The supply of a recycle of purified diesel fuel from the separator to the reactor is irrational, since this technique leads to an increase in the reaction volume, all other things being equal (Fig. 3, Table. 2), since, despite a slight decrease in the duration of the hydrodesulfurization process, the actual flow rate of the cleaned stream increases significantly due to the additional recirculation contribution.

Calculation of several options for the hydrotreating process of model diesel fuel with a total sulfur content of 1000 mln^{-1}, but with different the content of easily and difficult-to–hydrogenate conditional pseudocomponents with reaction rate constants of 20 and 5 h^{-1}, respectively, showed that for a process implemented in a single reactor, as the concentration of difficult-to-hydrogenate sulfur-containing pseudocomponents in raw materials increases, the role of limiting the quality of diesel fuel purification gradually shifts from an easily hydrogenated to a difficult-to-hydrogenate pseudocomponent (Fig. 4, Table 3).

To switch from the degree of hydrotreating of raw materials from 95% (residual sulfur content of 50 $million^{-1}$) to 99% (residual sulfur content of 10 $million^{-1}$), it is necessary to double the duration of the process and, accordingly, the loading of the catalyst into a single reactor (Table 2).

The greatest interest is from the standpoint of minimizing the loading of the catalyst into hydrotreating reactors The original scheme (Fig. 2,d) is presented, which was proposed in [28, 29] and considers the preliminary separation of the initial diesel fuel into light (180-300°C) and heavy (300-360°C) fractions with their separate hydrotreatment in two reactors to the required depth of hydrodesulfurization, which made it possible to increase the depth of hydrotreatment of diesel fuel at the L-24-6 RNPZ unit without changing the loading of the catalyst into the reactors [29].

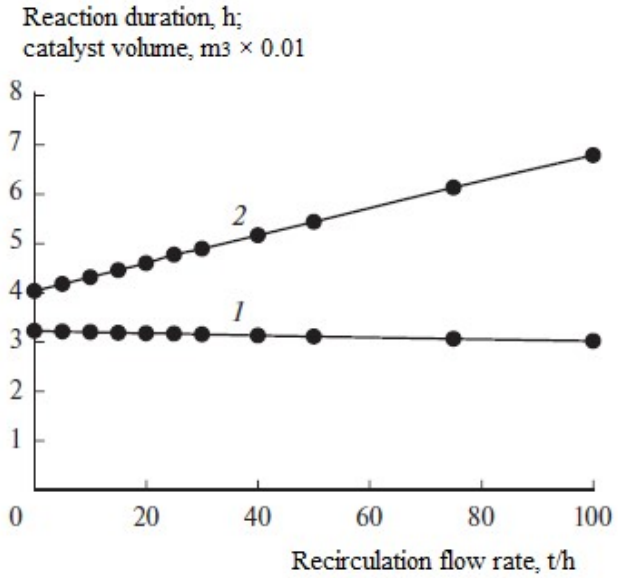

Fig. 3. Dependence of the reaction duration (1)

and the volume of the catalyst (2) on the recirculation flow rate at the residual sulfur concentration in diesel fuel 10 million^{-1}.

Table 2. Modeling of various reaction systems for hydrotreating diesel fuel

The reaction system	Recirculator flow rate, t/h	Final sulfur concentration, mg/kg	Reaction time, h	Volume of the catalyst, m^3
Diagrams of Fig. 2a, 2b, 2c – one reactor, two serial or two parallel reactors	0	2000	0.550	68.8
Diagrams of Fig. 2a, 2b, 2c Diagrams of Fig. 2a, 2b, 2c Diagrams of Fig. 2a, 2b, 2c Diagrams of Fig. 2a, 2b, 2c	0	500	1.245	155.6
Diagram fig. 2d – reactor with recirculation	10	500	1.220	164.7
Diagram fig. 2d	30	500	1.175	182.1
Diagram fig. 2d	50	500	1.130	197.7
Diagram fig. 2d	10	350	1.400	189.0
Diagram fig. 2d	30	350	1.350	209.2
Diagram fig. 2d	50	350	1.310	229.2
Diagram fig. 2d	10	50	2.370	319.9
Diagram fig. 2d	30	50	2.325	360.4
Diagram fig. 2d	50	50	2.285	399.8
Diagram fig. 2d	10	10	3.175	428.6
Diagram fig. 2d	30	10	3.130	485.1
Diagram fig. 2d	50	10	3.085	539.8

The disadvantage of this two-reactor scheme is the rigid temperature limit of 300°C separation of the initial diesel fuel into light and heavy fractions, since the efficiency and depth of hydrotreating are influenced not only by the reactivity of organosulfur substances, but also by their concentration (Table 3). For a detailed analysis of the effect of both the reactivity and concentration of organosulfur substances and the search for the optimal boundary for dividing raw materials into light and heavy fractions, mathematical modeling of the hydrotreating process of straight-run diesel fuel with boiling limits of 180-365°C, which potentially contains more than 30 organosulfur components (mercaptans, sulfides, disulfides, thiophenes) was performed by analogy with [22] were grouped in four conditional pseudocomponents contained in four narrow fractions and characterized by conditional reaction rate constants, The values of which are taken in proportion to the corresponding rates of hydrodesulfurization reactions of various classes of organosulphurization components (Table 4).

During the mathematical modeling of the hydrotreating process, the concentrations of four pseudocomponents (respectively C_1, C_2, C_3, C_4) varied and the reaction time and the required

volume of the catalyst for four variants of the process were determined, provided that the concentration of sulfur in the final hydrogenate does not exceed 10 mln^{-1}. In the first variant, all the raw materials in the amount of 100 m^3/h are supplied to one reactor, in other variants, the raw materials are pre-fractionated in a distillation column into light and heavy fractions, each of which includes specific narrow fractions and pseudo-components according to Table 5, separately entering the first and second reactors, respectively (Table 5).

In all series of calculations, a change in the volume of the catalyst loaded into the reactor was observed block, when redistributing light and heavy fractions of the initial diesel fuel over two reactors with a minimum volume at a certain temperature boundary of the separation of raw materials in the distillation column.

Table 3. The effect of the share of the hard-to-hydrogenate component Z in the total amount of sulfur-containing substances in model diesel fuel on the hydrotreatment of raw materials to the level of 95 and 99%

Parameters	Z, mass. %					
	0.20	0.15	0.10	0.07	0.05	0.03
Sulfur content in raw materials, mln^{-1}:						
– general	1000	1000	1000	1000	1000	1000
– easily hydrated	800	850	900	930	950	970
– difficult to hydrate	200	150	100	70	50	30
Sulfur content in hydrogenate, mln^{-1}:						
– general	50	50	50	50	50	50
– easily hydrated	2.54	6.19	14.43	22.43	20.09	36.76
– difficult to hydrate	47.45	43.81	35.36	27.57	20.90	13.24
The duration of the process (c) until the degree of purification is reached						
– 95% (S_{extr} = 50 million^{-1})	1035	886	744	670	627	589
– 99% (S_{extr} = 10 million^{-1})	2200	1950	1600	1400	1200	100

Table 4. Characteristics of model diesel fuel

The number of the narrow fraction	Boiling limits of the narrow fraction, °C	Fraction content in raw materials, wt. %	The number of organosulfur components in the fraction	Pseudo component number	Conditional constant reaction rates of hydrodesulfurization, h^{-1}
1	180-240	50	14	1	15
2	240-320	25	14	2	9
3	320-350	10	3	3	5
4	350-365	15	2	4	1

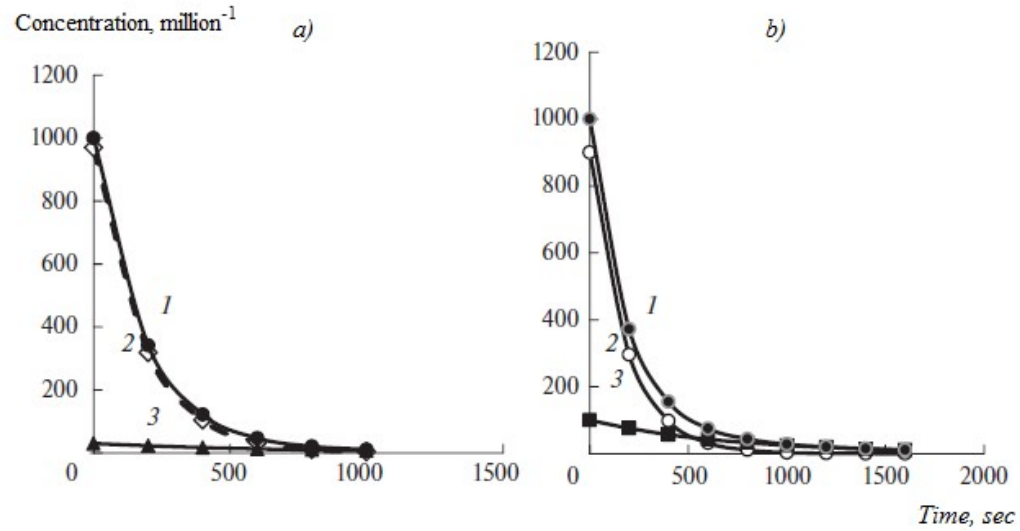

Fig. 4. Examples of calculating the kinetics of hydrotreating model diesel fuel with the proportion of a difficult-to-hydrogenate component in the total amount of sulfur-containing substances Z = 0.03 (a) and 0.1 (b): 1 – the total content of organosulfur substances; 2 – easily hydrogenated substances; 3 – difficult-to-hydrogenate substances.

The simulation results showed that as the concentration of hard-to-hydrogenate organosulfur substances in heavy fractions increases, the temperature boundary of the division of raw materials into light and heavy fractions shifts to a zone of lower temperatures. For example, with an increase in the concentration of the most difficult–to-hydrogenate pseudocomponent 4 from 500 (Table 5, series of experiments C) to 20,000 million^{-1} (Table 5, series of experiments B), the optimal boundary of the division of light and heavy fractions, which reduces the total volume of the catalyst in two reactors, shifts from the zone between components 2 and 3 (320°C) per zone between components 3 and 4 (350°C). The simulated systems for the concentration of organosulfur substances are quite typical for hydrotreated diesel fuels, for example, for straight-run diesel fuel from the diesel fuel hydrotreating plant G-43–107M/1 (fraction 180-365°C) with a total sulfur content of 24800 mln^{-1} when divided into fractions 180-320 °C (78 wt. %) and 320-365°C (22 wt. %) the total sulfur content in these fractions was 21700 and 32700 mln^{-1}, respectively.

It is characteristic that under optimal process conditions, the volumes of the catalyst loaded into each of the reactors are close to each other, which makes it possible to form a reaction unit of a hydrotreating plant from two identical reactors, compensating for some underloading or overloading of the catalyst compared to the required additional temperature control in each of the reactors.

Thus, the optimal position of the temperature boundary of the division of the feedstock into light and heavy fractions is determined simultaneously by the concentration and rate of reactions hydrodesulfurization of organosulphurization of organosulphurization components, while the temperature boundary of the division of raw materials can shift both upwards and downwards depending on the composition of organosulphurization impurities in the raw materials, while minimizing the criterion of optimality of the hydrotreating process, which can be taken as the minimum total loading of the catalyst into two reactors, characterizing the efficiency of the process [30].

When dividing the initial diesel fuel into two fractions, it is desirable to consider complexes of organosulfur substances in the form of at least four to six pseudo-components distributed in

corresponding narrow fractions, which together form two hydrotreated fractions. It should be noted that when characterizing raw materials by organosulfur components, six pseudo-components ensure acceptable accuracy of process modeling hydrotreating [31]. Naturally, an increase in the number of pseudo-components leads to an increase in the volume of experiments conducted to generate the initial data necessary for mathematical modeling of the hydrotreating process. At the same time, it is necessary to form model mixtures using expensive samples of specific organosulfur components. The optimization problem is much easier to solve if non-specific groups of homologues of organosulfur components are considered as pseudocomponents, as proposed in the hydrotreating of the entire raw material stream in [15, 22, 31], since organosulfur components that are fundamentally different in structure and reactivity may have similar boiling points (for example, 2-phenylthiophene and h-undecyl mercaptan have boiling points of 256 and 257°C, respectively), and consider the pseudocomponent as a set of organics to determine the parameters of the Arrhenius equation for the hydrodesulfurization reaction of this fraction of the initial diesel fuel in total sulfur from several experiments at different process temperatures.

3. Results and discussion

The loading of the catalyst with separate feeding into two reactors of light and heavy fractions is 2-3 times less than when feeding raw materials into one reactor or two sequentially or parallel reactors (Fig. 5), and as the concentration of organosulfur substances in the raw materials increases, this ratio increases.

Since the fractionation of the feedstock into light and heavy fractions requires additional energy consumption for heat supply and irrigation in the distillation column and subsequent heating of the resulting light fraction, compensating for the heat removal in the distillation column for the preparation of two fractions of raw materials, it is in principle possible to exclude this column from the scheme of the hydrotreating plant to obtain two fractions of diesel fuel with a given temperature the boundary of the fraction division directly at the primary oil refining plant [32]. In this case, the energy consumption for The hydrotreating unit will be even slightly lower compared to common schemes (Fig. 3a–3d) due to the receipt of two sufficiently hot fractions with a temperature of 150-200°C to the hydrotreating unit.

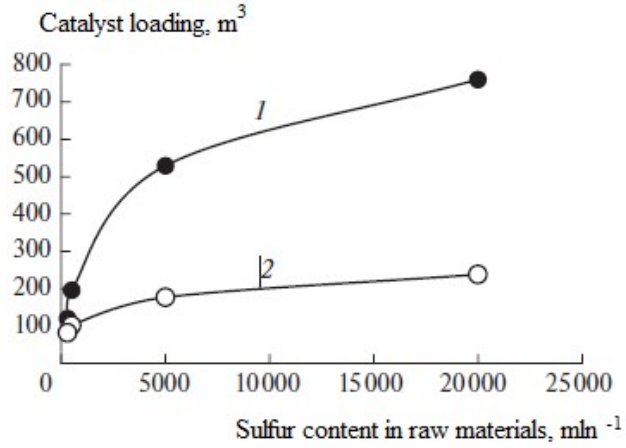

Fig. 5. The dependence of the catalyst loading into the reactor system of the hydrotreating plant on the sulfur concentration in the initial diesel fuel:
1 – a single reactor, two reactors operating in series or in parallel, 2 – the supply of light and heavy fractions of raw materials separately into two reactors.

Table 5. The results of modeling the operation of a two-reactor hydrotreating scheme for diesel fuel consisting of four pseudo-components

Option number	Pseudocomponents in the reaction mixture		The residence time of the product in the reactor, h		Catalyst loading, m^3			Sulfur concentration at the reactor outlet, mln^{-1}	
	Reactor 1	Reactor 2	Reactor 1	Reactor 2	Reactor 1	Reactor 2	Total	Reactor 1	Reactor 2
A	The concentration of pseudocomponents, $million^{-1}$: $C_1 = 12000$, $C_2 = 8000$, $C_3 = 3000$, $C_4 = 5000$								
1	1,2,3,4	-	5.29	-	529.50	-	529.50	9.99	-
2	**1,2,3**	**4**	**1.14**	**5.29**	**97.24**	**79.43**	**176.67**	**9.99**	**9.99**
3	1,2	3,4	0.74	5.29	55.65	132.40	188.05	9.78	9.99
4	1	2,3,4	0.47	5.29	23.50	264.50	288.00	9.87	9.99
B	The concentration of pseudocomponents, $million^{-1}$: $C_1 = 5000$, $C_2 = 10000$, $C_3 = 15000$, $C_4 = 20000$								
1	1,2,3,4	-	7.59	-	760.0	-	760.0	9.99	-
2	**1,2,3**	**4**	**1.46**	**7.59**	**124.1**	**113.9**	**238.0**	**9.95**	**9.99**
3	1,2	3,4	0.76	7.59	58.4	189.9	248.3	9.91	9.99
4	1	2,3,4	0.41	7.59	20.6	379.9	400.5	9.88	9.99
C	The concentration of pseudocomponents, $million^{-1}$: $C_1 = 20000$, $C_2 = 5000$, $C_3 = 2000$, $C_4 = 500$								
1	1,2,3,4	-	1.96	-	196.00	-	196.00	9.89	-
2	1,2,3	4	1.07	1.96	90.95	29.40	120.35	9.37	9.89
3	**1,2**	**3,4**	**0.70**	**1.6**	**52.50**	**49.00**	**101.50**	**8.93**	**9.89**
4	1	2,3,4	0.51	1.96	25.50	98.00	123.50	8.98	9.89
D	The concentration of pseudocomponents, million–1: $C_1 = 30{,}000$, $C_2 = 3000$, $C_3 = 300$, $C_4 = 100$								
1	1,2,3,4	-	1.20	-	120.0	-	120.0	9.84	-
2	1,2,3	4	0.80	1.20	68.0	18.0	96.0	7.01	9.83
3	**1,2**	**3,4**	**0.70**	**1.20**	**52.5**	**30.0**	**82.5**	**6.11**	**9.83**
4	1	2,3,4	0.60	1.20	30.0	60.0	90.0	4.05	9.83

4. Conclusion

For a comparative analysis of the efficiency of the reactor unit of diesel fuel hydrotreating plants by mathematical modeling, the loading of a catalyst into the reactor unit is considered as an optimality criterion, all other things being equal a process with the representation of a set of organosulfur components of raw materials in the form of several conditional pseudo-components. Of the considered options for the hardware design of the reactor unit in the form of a flow reactor, a reactor with recirculation of a part of the hydrotreated fuel, two reactors with sequential and parallel operation of reactors and two separately operating reactors with loading of light and heavy fractions of pre-separated raw diesel fuel, the lowest catalyst loading is provided in the last two-reactor version, while amounting to 70 to 30% compared to other options.

To substantiate the temperature boundary of the division of hydrotreating raw materials into light and heavy fractions, it is necessary to pre-divide the raw materials into 4-6 narrow fractions, in each of which the set of organosulfur components is considered as a pseudo-component, for which the kinetic characteristics necessary for the computational analysis of the hydrotreating process are experimentally determined.

Conflict of interest

The authors declare that they have no conflict of interest in relation to this research.

5. References

1. Akhmetov S.A. Technology of deep processing of oil and gas// Ufa: Gelem, 2002.

2. Orochko D.I., Sulimov A.D., Osipov L.N. Hydrogenation processes in oil refining// M.: Chemistry, 1971 (in Russian).

3. Kaminsky E.F., Khavkin V.A. Deep oil refining: technological and environmental aspects// M.: Tekhnika, 2001(in Russian)..

4. Tanatarov M.A., Akhmetshina M.N., Faskhutdinov R.A., Voloshin N.D., Zolotarev P.A. Technological calculations of oil refining installations// M.: Chemistry, 1987 (in Russian)..

5. Krivtsova N.I., Ivanchina E.D., Zanin I.V., Landl Yu.I., Tataurshchikov A.A. Kinetic patterns of transformation of sulfur-containing compounds in the process of hydrotreating the diesel fraction of oil // Izv. Tomsk Polytech. Univ. 2013. No. 3. P. 83.6. *Song C.* An overview of new approaches to deep desulfurization for ultra-clean gasoline, diesel fuel and jet fuel // Catal. Today. 2003. V. 86. № 2. P. 213(in Russian).

7. Gavrilov N.V., Durov O.V., Sorokin Yu.B., Syrkin A.M. Determination of the reasons for the increase in sulfur content in the hydrotreating product of reforming raw materials // Bashk. chem. and. 2008. T. 15. No. 2. P. 110 (in Russian)..

8. Ivanova L.S., Ilaldinov I.Z. Design of a diesel fuel hydrotreating unit // Vestn. Kazan. technol. Univ. 2013. T. 16. No. 7. P. 229 (in Russian)..

9. Kanashevich D.A., Fedushchak T.A., Petrenko T.V. Hydrodesulfurization of the diesel fraction in the presence of catalysts obtained using mechanochemical activation. Izv. Tomsk Polytech. Univ. 2010. T. 317. No. 3. P. 58.10.

10. *Solmanov P.S., Maximov N.M., Eremina Yu.V.,Zhilkina E.O., Dryaglin Yu.Yu., Tomina N.I.* Hydrolight coking gas oil // Pet. Chem. 2013. V. 53. № 3. P. 177. [*Солманов П.С., Максимов Н.М., Еремина Ю.В.,Жилкина Е.О., Дряглин Ю.Ю., Томина Н.И.* Гидроочистка смесей дизельных фракций с бензином и легким газойлем коксования // Нефтехимия. 2013. Т. 53. № 3. С. 199.]

11. Nagiev R.S., Chernov E.B. Development of modern domestic carriers for hydrotreating catalysts based on γ-Al2O3 // Bashk. chem. and. 2015. T. 22. No. 2. P. 38.

12. Rudenko A.V. Increasing the efficiency of the diesel fuel hydrotreating process // Actual. problem humanist natural Sci. 2014. No. 5-1. P. 25.

13. Fomichenko I.V., Uskach Ya.L. Improving the process of hydrotreating diesel fuel // International. and. adj. fundam. research 2010. No. 8. P. 145.

14. Tomina N.N., Pimerzin A.A., Moiseev I.K. Sulfide catalysts for hydrotreating oil fractions // Ross. chem. and. 2008. T. 52. No. 4. P. 41.

15. Krivtsova N.I., Krivtsov E.B., Ivanchina E.D., Golovko A.K. Kinetic patterns of hydrodesulfurization of the diesel fraction // Fundam. research 2013. No. 8. P. 640.

16. *Li H., Yang J., Weng H., Wang J.* Kinetic study of liquidphase hydrodesulfurization of FCC diesel in tubular reactors // China Pet. Process. Petrochem. Technol.2015. V. 17. № 2. P. 1.

17. Velikov S.V., Pokrovskaya S.V., Bulavka Yu.A. Kinetic patterns of the process of hydrodesulfurization of diesel fuel at the L-24/6 installation // Vestn. Polotsk Univ. Ser. V. Industry. Appl. Sciences. Chem. technol. 2014. No. 11. P. 153.

18. *Nakano K., Ali S.A., Kim H.-J., Kim T., Alhooshani K.,Park J.-I., Mochida I.* Deep desulfurization of gas oil over NiMoS catalysis supported on alumina coated USY-zeolite // Fuel Process. Technol. 2013. V. 116.P. 44.

19. *Shokri S., Marvast M.A., Tajerian M.* Production of ultra low sulfur diesel: simulation and software development // Pet. Coal. 2007. V. 49. № 2. P. 48.

20. *Al-Zeghayer Y.S., Jibri B.Y.* Kinetics of hydrodesulfurization of dibenzothiophene on sulfide commercial CoMo/γ-Al2O3 catalyst // J. Eng. Res. 2006. V. 3. № 1.P.38.

21. *Афанасьева Ю.И., Кривцова Н.И., Иванчина Э.Д.,Занин И.К., Татаурщиков А.А.* Разработка кинетической модели процесса гидроочистки дизельного топлива // Изв. Томск. политех. унив. 2012. № 3.С. 121.

22. *Tang X., Li S., Yue C., He J., Hou J.* Lumping kinetics of hydrodesulfurization and hydrodenitrogenation of the middle distillate from Chinese shale oil // Oil Shale.2013. V. 30. № 4. P. 517.

23. Lebedev B.L., Loginov S.A., Kogan O.L., Lobzin E.V., Kapustin V.M., Lugovskoy A.I., Rudyak K.B. Study of the composition and reactivity of sulfur compounds in the process of hydrodesulfurization at an industrial plant // Neftepererab. petrochemical 2001. No. 11. P. 62.

24. Manovyan A.K. Technology of primary processing of oil and natural gas. M.: Chemistry, 2001.

25. Rudin M.G., Somov V.E., Fomin A.S. Oil Refiner's Pocket Guide. M.: TsNIIT-Eneftekhim, 2004.

26. Solodova N.L., Terentyeva N.A. Hydrotreating of fuels. Kazan: KSTU, 2008.

27. Tarakanov G.V., Nurakhmedova A.F., Popadin N.V., Tarakanov A.G. Method for hydrotreating diesel fuel. Pat. 2323958 Russian Federation. 2008.

28. Loginov S.A., Lebedev B.L., Kapustin V.M., Lugovskoy A.I., Kurganov V.M., Rudyak K.B. Development of a new technology for the hydrodesulfurization process of diesel fuels // Neftepererab. petrochemical 2001.No. 11. P. 67.

29. Loginov S.A. Improving the technology of industrial production of high-quality diesel fuels. dis. ...cand. tech. Sci. Ryazan: Ryazan Oil Refinery, 2002.

30. Samoilov N.A. Prospects for mathematical modeling and optimization of diesel fuel hydrotreating // Materials of the IV All-Russian (with international participation) symposium “Current problems of the theory and practice of heterogeneous catalysts and adsorbents”. Ivanovo, 2019. P. 379.

31. *Bannatham P., Teeraboonchaikul S., Patirupanon T., Arkardvipart W., Limtrakul S., Vatanatham T., Ramachandran P.A.* Kinetic evaluation of the hydrodesulfurization process using a lumpy model in a thin-layer reactor //Ind. Eng. Chem. Res. 2016. V. 55. № 17. P. 4878.

32. Mnushkin I.A., Samoilov N.A., Zhilina V.A. Method for hydrotreating diesel fuel. Pat. 2691965 Russian Federation. 2019.

Study of the composition of petroleum products extracted from oil-contaminated soil using the spectrometric method.

K.M. Ismailova, N.A. Yusubova

Research Institute of Geotechnological Problems of Oil, Gas and Chemistry, ASOIU, Azadlig Ave. 20, Baku, AZ-1010 Azerbaijan

Abstract

Oil-contaminated soils undergo various transformations, depending on the composition and duration of exposure to the pollutant, which leads to changes in the soil structure and even the component composition of the oil. This paper presents the results of a study of soil samples with a high content of oil fractions. From the results, it follows that oil-contaminated soils under the influence of the environment undergo significant structural changes, namely, agglomeration, with the formation of long hydrocarbon chains and indestructible complexes. This must be considered when developing methods for cleaning soils from oil pollution.

Key words: oil-contaminated soil, petroleum hydrocarbons, volatile components, spectrum, chromatography

*Corresponding author. Tel.:+994707719992

E-mail address : kamala.i@mail.ru

1.Introduction

The reason for separating oil pollution into separate types is the complex composition of oil (hundreds of different hydrocarbon compounds and heterocyclic compounds containing nitrogen, oxygen, sulphur, and trace elements) and its simultaneous entry into the environment. Strong toxicants to vegetation are volatile aromatic hydrocarbons contained in oil and some water-soluble fractions of oil. Oil and oil products in direct contact with plants act mainly as powerful herbicides [1]. In soils, oil and oil products exist in several forms: in pores, gas and liquid in a state of high mobility, free or dissolved in aqueous or aqueous emulsion phase; in pores and cracks, in a free, stationary state, acting as a viscous or solid binder between soil particles and aggregates; in a sorbed state, bound on soil particles, including soil humus compounds; in the surface layer of soil or soil in the form of a dense organomineral mass. The qualitative and quantitative changes that occur during the long-term presence of foreign organic compounds in the soil and the mechanisms of their redistribution have not yet been fully studied.

When oil comes to the surface of the earth, it finds itself in qualitatively new existing conditions. Geochemical processes penetrate a well-aerated environment from anaerobic conditions, where it undergo various physical and chemical changes [2]. Oil components can rearrange under the influence of diffusion and capillary forces through saturation, hydrogenation, or dissolution of soil pores in water. Crude oil can be transported and transformed by evaporation, adsorption, and sedimentation. Under the influence of various atmospheric influences and chemical transformations, various hydrocarbon fractions of oil and petroleum products can be converted into asphaltenes. In this case, oil and its derivatives acquire a bituminous structure, which is difficult to decompose.

Asphaltenes and high molecular weight polycyclic aromatic hydrocarbons tend to accumulate in soil. Due to the absence of polar groups on the molecules, these substances are extremely hydrophobic. They can be absorbed by organic matter, trapped in micropores, and form

stable compounds in the soil, which contributes to their low biodegradability [3]. As a result of oil pollution, intrasoil heterogeneity in the distribution of pollutants occurs.

Soil contamination with oil leads to a sharp change in its properties: the soil becomes hydrophobic, and therefore its agrophysical and especially water-physical properties change dramatically. Light fractions of oil have a particularly strong phytoxic effect [4].

The effect of oil on living soil organisms is largely determined by its concentration. In low concentrations, oil has a stimulating effect on soil biota since it is an energy substrate for a large group of microorganisms and contains substances that stimulate plant growth and development. Severe soil contamination with oil is accompanied by an acute toxic effect of oil on living organisms, especially in the initial period after contamination [5].

As a result, when choosing a solvent, it is necessary to take into account the complex chemical composition of both the substance being determined—the petroleum product—and the object being studied—the soil. Impregnation of soil mass with oil leads to changes in the chemical composition, properties, and structure of soils. First of all, this affects the humus horizon; the amount of carbon in it increases sharply, but the properties of soils as nutrient substrates for plants deteriorate. Petroleum products cause the formation of a stable hydrophobic film, thereby disrupting the recycling and exchange of nutrients through the soil. In the soil profile, it is possible to change redox conditions and increase the mobility of humus components and several microelements [6].

4. Research method

To study the negative impact of long-term oil pollution on the soil cover, we conducted laboratory studies of a certain composition and concentration of oil products. These studies were based on chemical methods: extraction using organic solvents, calcination to determine volatile components, and gas-liquid chromatography [7]. We took two samples of oil-contaminated soils of varying degrees from the Balakhanyneft field. Samples were taken from the well area at two different locations from the well, with a sample collection date of April 4, 2023. We studied the processes of extracting petroleum products from samples using different solvents: benzene, n-hexane, toluene, and chloroform.

We examined the resulting samples of petroleum products after extraction using gas-liquid chromatography, since it is the most promising, with simultaneous decoding of the chemical composition, which allows us to determine the individual components in a mixture of petroleum products. Therefore, we examined samples of extracted petroleum products using a gas chromatograph with a flame ionization detector, and the separation efficiency of the mixture components was high [8].

5. Results and discussion

For the most complete information about the isolated petroleum products, we carried out additional research on the analysis of petroleum products using a modern physical and chemical method, such as nuclear magnetic resonance. The NMR spectra of the samples we prepared, presented below, were taken to obtain approximate information about the composition of petroleum products extracted from the soil and more precisely, to assess the integral intensity of the signals to obtain the number of protons belonging to various functional groups.

To do this, we prepared two samples of petroleum products extracted from contaminated soil using chloroform as a solvent. The first sample was obtained by the long-term stirring of this soil in chloroform, with further evaporation of the solvent by heating. We obtained a second similar

sample with minimal stirring and evaporation without heating. Based on the NMR spectra of these samples, it can be concluded that the aliphatic part of the mixture is many times greater in composition than the aromatic compounds.

Figure 1. NMR spectrum of the first sample

The broadened signals in the spectrum of the first sample in the region of 0.74–1.1 ppm relate to the signals of the methyl, methylene, and methine groups of alkanes and cycloalkanes. The broadened signals in the region of 2.12–2.5 ppm refer to the signals of methyl, methylene, and methine groups associated with the benzene ring. The broadened signals in the region of 6.85–7.2 ppm belong to the signals of aromatic protons.

Figure 2. NMR spectrum of the second sample.

As can be seen from the spectrum of the second sample, the broadened signals in the region of 0.89–1.21 ppm relate to the signals of the methyl, methylene, and methine groups of alkanes and cycloalkanes. The broadened signals in the region of 2.16-2.53 ppm refer to the signals of methyl, methylene, and methine groups associated with the benzene ring. The broadened signal at 7.08 ppm refers to the signal of aromatic protons.

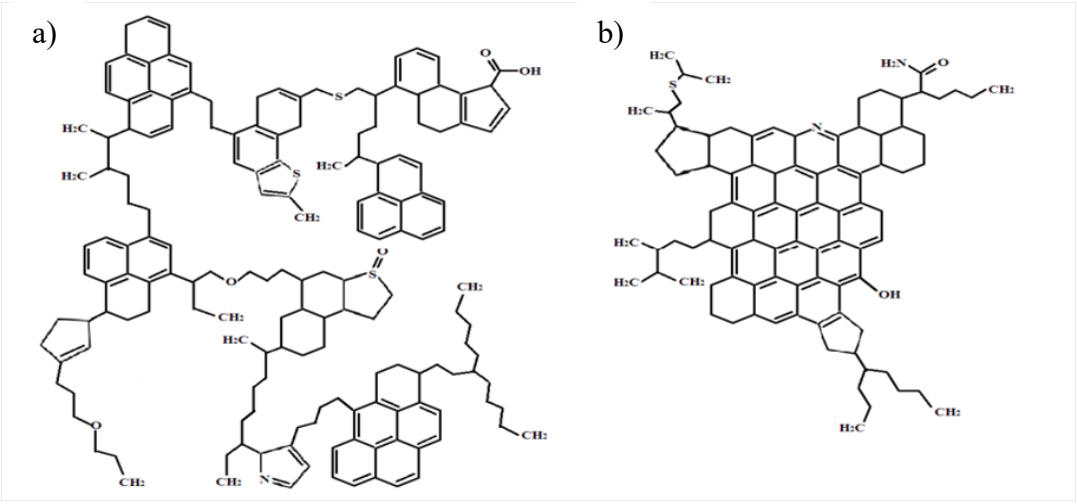

Figure 3. Asphaltenes structures

Considering the above examples, it can be assumed that different asphaltenes may be present in the mixture. However, more accurate information about the composition of the mixture can be obtained from mass spectroscopic analysis data.

6. Conclusion

A study of petroleum products extracted from oil-contaminated soil was carried out using the nuclear magnetic resonance method. The obtained spectra confirm that the composition of oil absorbed into the soil undergoes strong changes over a long period of time. The aliphatic part of the petroleum product mixture is many times greater than the aromatic components. The results obtained confirm the data of the gas-liquid chromatography study with flame ionization.

Conflict of interest

The authors declare that they have no conflict of interest in relation to this research.

References

1. Macaulay, B. M., Rees, D.(2014) Bioremediation of oil spills: a review of challenges for research advancement Annals of environmental Science.T. 8. C. 9-37.

2. Babaev, E. R. (2018). Conversion characteristics of hydrocarbon composition of Apsheron peninsula oils in their microbiological degradation in soil. Territorija Neftegas, (6), 104-112. (in Russian).

3. Macaulay, B. M., Rees, D. (2014). Bioremediation of oil spills: a review of challenges for research advancement. Annals of environmental Science, 8, 9-37.

4. Rakhmanova, G. F., Sharonova, N. L., & Degtyareva, I. A. (2016). Influence of nanosorbent on the biodegradation process of contaminated gray forest soil. Vestnik Kazanskogo tekhnologicheskogo universiteta, 19(5), 149-152. (in Russian).

5. Kathleen A. Theoharides, Martin Suberg.(2019) Method for determination of extractable petroleum hydrocarbons (EPH). Massachusetts Department of Environmental Protection. Solid Waste Bureau. Commonwealth of Massachusetts. Executive Office of Energy and Environmental Affairs. Revision 2.

6. Francisco Cláudio de Freitas Barrosa, Luiz Constantino Grombone Vasconcellosb, Técia Vieira Carvalhoc, Ronaldo Ferreira do Nascimentoa (2014)Removal of petroleum spill in water by chitin and chitosan The Electronic Journal of Chemistry. № 6 (1). P. 70–74.
7. Babayev A.I., Hasanov G.S., Ismailova K.M., Gakhramanova Z.O., Sadygova N.A., Huseynova A.R.(2023) Reseach on the composition of petroleum products extracted from oil-contaminated soils using the method of express gaz chromatograthy with flame ionization, Transactions of Azerbaijan Institutes of Technology, Publisher SSRN [https://www.scopus.com/record/display.uri?eid=2-s2.0-85168094322&origin=resultslist&sort=plf-f&src=s&sid=cf4ab28ccf4f49a6902b232d62a9f9a2&sot=a&sdt=a&s=DOI%2810.1016%2Fj.scitotenv.2023.167117+%29&sl=37&sessionSearchId=cf4ab28ccf4f49a6902b232d62a9f9a2]
8. Babayev A.I.,Gakhramanova Z.O.,Sadygova N.A.,Ismailova K.M.,Aliyev E.N. Research and development of technology for purification of oil polluted soils by physical and chemical methods (2022) Scientific Proceedings, Baku ,Volume 22 no.1 pp.104-108

Novel adsorbents on the bases of functionalized chitosan and magnetite nanoparticles for removal of organic pollutants and heavy metal ions from water

Z.O. Gakhramanova[b], S. A. Mammadhanova[a] , S. S. Hasanova[a,b] ,N. S. Bayramova[b].

[a] Azerbaijan State Oil and Industry University, 20 Azadlig Ave., Baku, AZ1010, Azerbaijan

[b] Scientific Research Institute of " Geotechnological Problems of Oil, Gas and Chemistry", ASOIU, 20 Azadlig Ave., Baku, AZ 1010 Azerbaijan

Abstract
This paper reports about the successful functionalization of low molecular weight chitosan with 2,2-(ethane-1,2-diylbis(oxy))dibenzaldehyde and further conjugation of obtained gel with Fe_3O_4 nanoparticles. The functionalization of chitosan with dialdehyde occur through condensation reaction of chitosan amino group with carbonyl groups of dialdehyde that brings to the imine linkage that tithing the chitosan chains. The structure of prepared gel have been proved by NMR and FTIR spectroscopies. The morphology and composition of prepared conjugated gel@Fe_3O_4 have been studied by XRD and TEM analysis methods.
Keywords: Chitosan, 2,2-(ethane-1,2-diylbis(oxy))dibenzaldehyde, adsorption, Fe04, nanostructure, gel.
Corresponding author. Tel. 0555503579
Email address sibel.aliyeva2002@gmail.com

1. Introduction

The development of oil and petrochemical industry moving to the next level however exerts serious influence on the environment, pollution of water basins and greenhouse effect. One of the global problems at the moment is the leakage of oil and oil products leading to serious environmental problems. Enterprises aimed at oil transportation and oil and gas complexes are the most frequent water polluters [1]. As a result of poisoning by organic compounds and heavy metals, abiotic components including marine life and plants are killed, leading to the destruction of the ecosystem [2].
Currently, various methods of water purification have been developed and successfully applied. Among them there are such methods as: gravity sedimentation [3] and corrugated plate interceptors

[4],chemical pretreatment (coagulation-flocculation)[5], centrifugal separation using hydrocyclone [6], gas flotation [7,8] and dissolved gas flotation. Recently, biological water treatment processes using membrane bioreactor [9,10] as well as biotechnological water treatment methods have received much attention. One of the simplest and most effective methods of water purification is filtration using various porous materials such as ion-exchange polymers, resins, sand, clay, silica [11] ultrafiltration [12,13]; nanofiltration [14] and reverse osmosis [15,16]

The development and application of new materials as adsorbents is an urgent task in view of the increasing problems of ecological character, the use of biodegradable and biocompatible materials is very much in demand. Recently, there have been many reports in the literature that chitosan and its derivatives can be successfully used as adsorbents for the purification of polluted water [17].

Another promising material as adsorbents are nanomaterials. Recent advances in nanotechnology also present nanomaterials as effective adsorbents for the treatment of polluted water. The recent studies reported about advances of magnetite nanoparticles and nanocomposites applications in water remediation from organic pollutants [18].

Taking in consideration above mentioned we carried out the synthesis and characterization of chitosan derivatives on the bases of chitosan and dialdehyde with further conjugation with Fe3O4 nanoparticles [19,20].

2. Experimental part

Reagent and materials

Chitosan (Mol wt=50,000 Da), salicylaldehyde, 1,2-dibromethane, were obtained from Sigma-Aldrich, acetic acid(100%), ethanol(95%), (DMSO-d6, d, ppm), CTAB, K_2CO_3, distillated water, $FeCl_3 \cdot 6H_2O$, $FeCl_2 \cdot 4H_2O$, NH_4OH(10%) were purchased from Merck.

Synthesis

Synthesis of 2,20-(ethane-1,2-diylbis(oxy))dibenzaldehyde.

The process stared with dissolving of 38.3 moles salicylaldehyde in 20 mL of DMSO followed by the addition of 37.7 moles of K_2CO_3. Then after the addition of 1.2-dibromoethane, we heated on a water bath for 3 hours followed by cooling for 3 hours with ice. After the time is over, it should be filtered, washed with distilled water and dried at ambient

Synthesis of gel on the base of chitosan and dialdehyde

In a round bottom flask we put 0.0016 mmol of chitosan and add 50 ml of acidified water. After 3 hours of stirring, at the temperature of 40℃ , added a solution of 0.18 mmol of dialdehyde in 10 mL of ethanol. The reaction was continued for 3 hours at constant stirring. Prepared gel was analyzed by FTIR, XRD and TEM methods.

Synthesis of magnetic nanoparticles

The process was performed in molar ratio of Fe^3 :Fe^{2+} as 2:1. In a round bottom flask we dissolved 27 mmol of $FeCl_3 \cdot 6H_2O$ in 50 mL distillated water followed by addition 13.4 mmol of $FeCl_2 \cdot 4H_2O$. The reaction was carried out in the nitrogen atmosphere and continued by stirring and heated to 60°C. After a 3 hours, we added 50 ml of NH_4OH 10% and stirred until the color of the solution turned black and pH of solution 9. Then 0.002 mmol of CTAB in 10 ml of distillated water added to the solution of formed magnetic nanoparticles for stabilization. After stirring we filtered and dried stabilized magnetic nanoparticles at the temperature of 70℃ for 2 hours.

Synthesis of gel@Fe3O4 nanoparticles

The 0.8 g of magnetic nanoparticles in 50 ml deionized water was exposed to an ultrasonic bath for 30 min. Then the sonicated mixture of magnetic nanoparticles slowly was added to the 60 ml of gel , with further stirring at 40 °C for 60 min.

3.Characterization

FTIR spectroscopy

The synthesized structure of chitosan derivative and gel@Fe3O4 nanoparticles have been analyzed by FTIR spectroscopy method. The spectra have been recorded FTIR spectrophotometer Thermo^{TM} Scientific^{TM} Nicolett iS20, using an attenuated total reflectance (ATR) accessory intherangeof4000–450cm1.

NMR spectroscopy

The NMR experiments were performed on a BRUKER FTNMR spectrometer AVANCE 300 (Bruker, Karlsruhe, Germany) (300MHz for ^{1}H and 75 MHz for ^{13}C) with a BVT 3200 variable temperature unit in 5 mm sample tubes using Bruker Standard software (Top Spin 3.1). Chemical shifts were given in ppm (d) and were referenced to internal tetramethylsilane (TMS). Multiplicities are declared as follows: s (singlet), d (doublet), t (triplet), q (quadruplet), and m (multiplet). Coupling constants J are given in Hz. The experimental parameters for ^{1}H are as follows: digital resolution=0.23Hz, SWH=7530Hz, TD=32K, SI= 16K,901pulse-length=10ms, PL1=3dB, ns=4, ds=2, d1=1s and for ^{13}C as follows: digital resolution=0.27Hz, SWH= 17985Hz, TD=64K, SI=32K,901pulse-length=9ms, PL1= 1.5dB, ns=1000, ds=2, d1=3s. The NMR-grade DMSO-d6 (99.7%, containing 0.3% H2O) was used for the solutions of synthesized compounds.

Transmission electron microscopy (TEM).

The TEM analysis of the nanostructures gel and gel@Fe_3O_4 was performed on a TEM JEOL-1400 (Japan) at 80–120kV. The ultrasonicated solution of gel in ethanol was placed on a carbon-coated grid and dried at ambient conditions.

X-Ray powder diffraction analysis (PXRD).

XRD analysis was performed under ambient conditions on a Rigaku Mini Flex 600 XRD diffractometer, equipped with Cu Ka radiation, to study the crystalline structure of the synthesized Fe3O4 nanoparticles and gel@Fe3O4. The samples were scanned in the Bragg angle range of 10^0–80^0 at 2 θ, 15 mA. The Williamson-Hallmethod was used to calculate the crystallite size.

7. Results and discussion

One of the promising materials is chitosan obtained by hydrolytic deacetylation of natural chitin, which is a structural component of the skeletons of all crustaceans and insectivores. Due to the presence of amine and hydroxyl groups in the macromolecule of chitosan such adsorption properties of binding heavy metal ions, organic pollutants and antimicrobial, but also being a natural polysaccharide it shows such properties as biocompatibility and biodegradability. Chitosan and its modifications are already being used for water purification. It is chemically modified in a variety of ways, including coupling with other polymers or inorganic materials, complexation and crosslinking to reduce its solubility in acidic media and to increase its chemical stability and flexibility. The best known crosslinkers for linking chitosan chains are formaldehyde, epichlorohydrin, glutaraldehyde, and tripolyphosphate [21]. Chitosan in hydrogel form is also used as an adsorbent for pollutant removal [22] . Therefore, scientists combine chitosan with polymeric materials such as polyethylene glycol [23], polyvinyl alcohol (PVA, bentonite [24] and zeolite [25]). The authors of [26] reported of chitosan-polystyrene-Zn nanocomposites by precipitation method and after characterization, they likened the efficiency of nanocomposite in nitrate ion removal by

batch and steady-state precipitation methods. A lanthanum encapsulated chitosan-kaolin composite was proposed by Thagira Banu et al. to remove nitrate ions from wastewater [27].
In view of the above, we have functionalized 50,000 Da chitosan with 2,2-(ethane-1,2-diylbis(oxy))dibenzaldehyde. The dialdehyde was synthesized by us previously based on salicylic aldehyde and 1,2-dibromoethane. The reaction scheme is presented below.

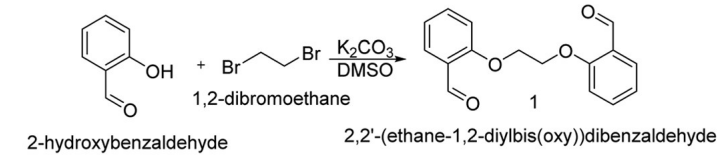

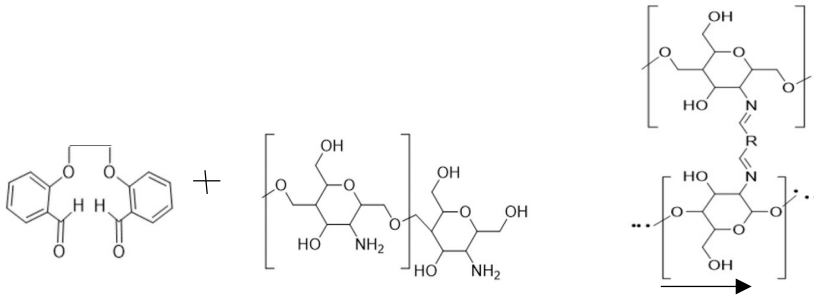

Then we modified the obtained gel with magnetite nanoparticles. Fe3O4 nanoparticles were obtained by chemical coprecipitation reaction of Fe+2 and Fe+3 iron salts. The obtained nanoparticles were stabilized with CTAB molecules and analyzed by NMR, FTIR, XRD. The morphology and composition of prepared nanostructures were investigated by transmission electron microscopy.

The structure of obtained dialdehyde have been proven by NMR spectroscopy. ^{1}H NMR spectrum (Fig.1a) of compound 1: (DMSO-d6, d, ppm), 4.57s (4H, 2OCH2), 7.077.12t(2H,Ar,J=9Hz),7.31–7.34d(2H,Ar,J=9Hz),7.64–7.69t (4H,Ar,J=9Hz),10.29s(2H,COH).^{13}C NMR spectrum of compound 1: (DMSO-d6,d,ppm),67.87(2OCH2),114.61 (2CH, Ar), 121.58 (2CH, Ar), 124.97 (2C, Ar), 128.02 (2CH, Ar), 136.85(2CH,Ar), 161.28(2C,Ar), 189.60(2COH).Found,%:C 71.04;H5.11.C16H14O4.Calculated,%:C71.11;H5.19.

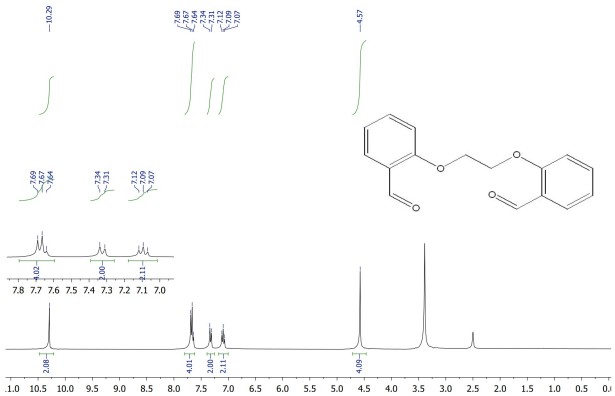

Fig 1(a) ^{1}H NMR spectra of 2,2-(ethane-1,2-diylbis(oxy))dibenzaldehyde

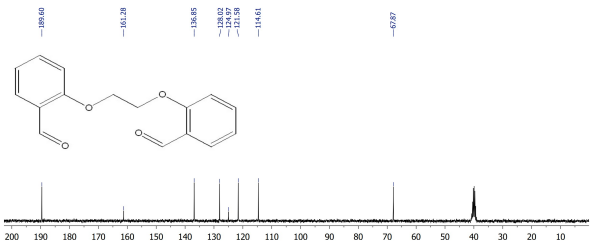

Fig 1(b) ^{13}C NMR spectra of 2,2-(ethane-1,2-diylbis(oxy))dibenzaldehyde

The functionalization of chitosan with synthesized dialdehyde led to preparing of the gel, that further was conjugated with Fe3O4 NPs. The figure 2 presents the FTIR spectra of pristine gel and gel@Fe3O4. As it can be seen from the spectra C–H stretching of aromatic ring pick reveal at 2364 cm^{-1} and C=C stretching of benzene ring at 1515 cm^{-1} . The 1636 cm^{-1} peak corresponds to imine bond (CH=N stretching) ,the 542 cm^{-1} peak represent Fe–O stretching

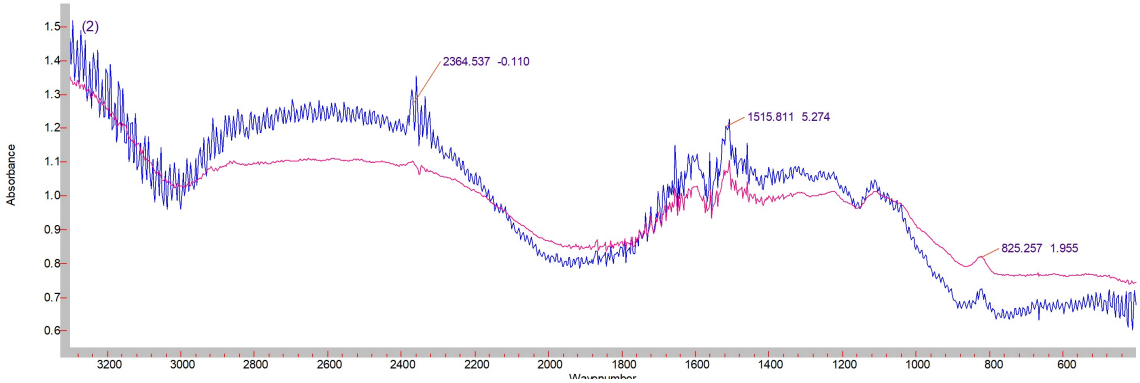

Figure 2. FTIR spectra of gel (red line), nanostructures gel@Fe3O4 (blue line)

The morphology of the gel and gel@Fe_3O_4 is presented by TEM images has been shown on the Figure 3. The TEM images of pristane gel Figure 3(a) reveals crumbly morphology of chitosan functionalized with dialdehyde. The Figure 3(b) represents the morphology of the gel conjugated with Fe_3O_4 nanoparticles. The dark regions on the spectra demonstrates the agglomeration of the Fe_3O_4 in the body of the gel.

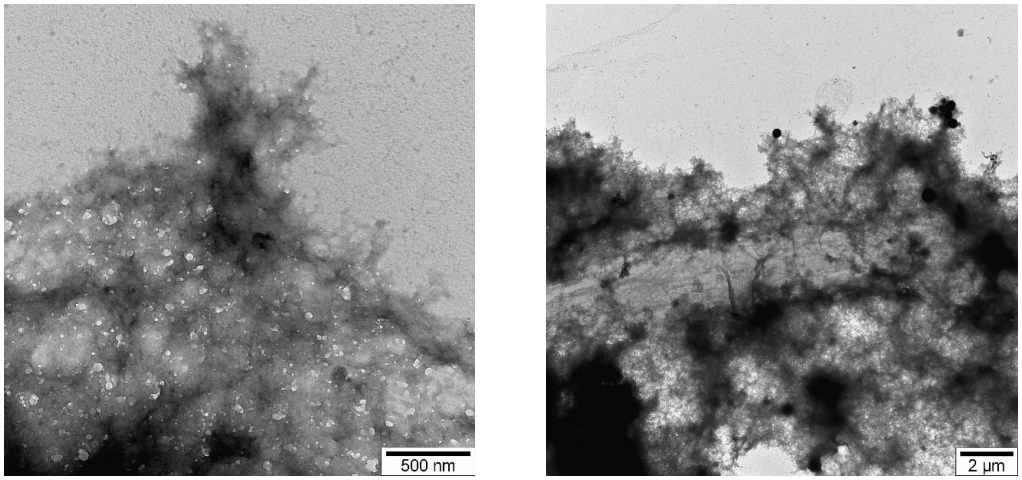

Figure 3(a) TEM image of the pristine gel; (b) TEM image of the gel@Fe_3O_4

The analyzed sample (green line) can be referred to gel@Fe3O4 nanoparticles of cubic structure because the presence of characteristic peaks at 30.131, 38.5361, 43.171, 59.071, 63.751. All these

peaks correlate with the standard pattern of Fe_3O_4, indexed in the ICDD (PDF-2/Release 2011 RDB) DB card number 01-075-0449 for the magnetite phase. The red line is the XRD spectra of chitosan indicating the standard peak 20.65 that showing crystalline form of biopolymer. The blue line is the XRD of gel that showing how the sharp peak became more gentle, indicating that the modification produced a more amorphous structure.

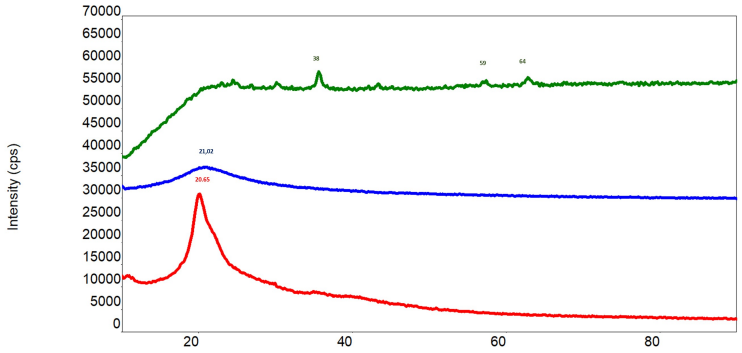

Figure 4. XRD pattern of gel

8. Conclusion

The synthesis of Schiff base and nano-ensemble were obtained by reaction of nucleophilic substitution followed by condensation of chitosan with 2,2-(ethane-1,2-diylbis(oxy)) di-benzaldehyde and further conjugation with nano magnetite. This modification of gel and gel@Fe_3O_4 were confirmed by several methods including TEM, NMR, FTIR, XRD spectroscopy. FTIR and XRD spectra showed that biopolymeric nano-ensemble underwent significant changes in comparison with chitosan. These changes included formation of imine fragment and changing the crystalline structure into the amorphous respectively. Modification of gel@Fe_3O_4 allowed for increasing in intra- and inter-molecular cavities further improving adsorption properties. The obtained structures have a great potential as adsorbent that can be used for treatment of oil-contaminated water from organic impurities and heavy metals.

Conflict of interest

The authors declare that they have no conflict of interest in relation to this research.

5.Refernses

1- Camilo Zamora-Ledezma, Daniela Negrete-Bolagay, Freddy Figueroa, Ezequiel Zamora-Ledezma, Ming Ni, Frank Alexis, Victor H., 2021. Guerrero Heavy metal water pollution: A fresh look about hazards, novel and conventional remediation methods//Environmental Technology & Innovation 22-101504.https://doi.org/10.1016/j.eti.2021.101504.

2- Jonny Beyer, Anders Goksøyr, Dag Øystein Hjermann, Jarle Klungsøyr, 2020. Environmental effects of offshore produced water discharges: A review focused on the Norwegian continental shelf// Marine Environmental Research, 162 (2020) 105155, https://doi.org/10.1016/j.marenvres.2020.105155 .

3- Stewart, M., Arnold, K., 2009. Emulsions and oil treating equipment. In: Emulsions and Oil Treating Equipment// Elsevier, pp. 107e211. http://dx.doi.org/10.1016/ B978-0-7506-8970-0.00003-7

4- Drewes, J., Cath, T., Xu, P., Graydon, J., 2009. An Integrated Framework for Treatment and Management of Produced Water// El-Gohary, F., Tawfik, A., Mahmoud, U., 2010

5- El-Gohary, F., Tawfik, A., Mahmoud, U., 2010. Comparative study between chemical coagulation/precipitation (C/P) versus coagulation/dissolved air flotation (C/ DAF) for pre-treatment of personal care products (PCPs) wastewater// Desalination 252, 106e112. http://dx.doi.org/10.1016/j.desal.2009.10.016.

5-Husveg, T., Rambeau, O., Drengstig, T., Bilstad, T., 2007. Performance of a deoiling hydrocyclone during variable flow rates. Min. Eng. 20, 368e379. http:// dx.doi.org/10.1016/j.mineng.2006.12.002

7- Al-Shamrani, a. a., James, a, Xiao, H., 2002. Destabilisation of oil-water emulsions and separation by dissolved air flotation// Water Res. 36, 1503e1512. http:// dx.doi.org/10.1016/S0043-1354(01)00347-5.

8- Al-Zoubi, H., Al-Thyabat, S., Al-Khatib, L., 2009. A hybrid flotationemembrane process for wastewater treatment: an overview// Desalination Water Treat. 7, 60e70. http://dx.doi.org/10.5004/dwt.2009.726.

9- Izahrani, S., Mohammad, A.W., 2014. Challenges and trends in membrane technology implementation for produced water treatment: a review. J. Water Process Eng. 4, 107e133. http://dx.doi.org/10.1016/j.jwpe.2014.09.007.

10- Kose, B., Ozgun, H., Ersahin, M.E., Dizge, N., Koseoglu-Imer, D.Y., Atay, B., Kaya, R., Altınbas, M., Sayılı, S., Hoshan, P., Atay, D., Eren, E., Kinaci, C., Koyuncu, I., 2012. Performance evaluation of a submerged membrane bioreactor for the treatment of brackish oil and natural gas field produced water// Desalination 285, 295e300. http://dx.doi.org/10.1016/j.desal.2011.10.016.

11- Angelova, D., Uzunov, I., Uzunova, S., Gigova, A., Minchev, L., 2011. Kinetics of oil and oil products adsorption by carbonized rice husks// Chem. Eng. J. 172, 306e311. http://dx.doi.org/10.1016/j.cej.2011.05.114

12- Li, X., Wang, L.L., Yang, Y., You, H., Zhang, W.C., Qin, X.H., Wang, X.F., 2013. Thin film nanofibrous composite ultrafiltration membrane for oil removal from oilfield wastewater// Adv. Mater. Res. 669, 99e102, 10.4028. www.scientific.net/AMR. 669.99.

13- Lipp, P., Lee, C.H., Fane, A.G., Fell, C.J.D., 1988. A fundamental study of the ultrafiltration of oil-water emulsions// J. Memb. Sci. 36, 161e177. http://dx.doi.org/ 10.1016/0376-7388(88)80014-0.

14- Franco, C.A., Nassar, N.N., Cortes, F.B., 2014. Removal of oil from oil-in-saltwater emulsions by adsorption onto nano-alumina functionalized with petroleum vacuum residue// J. Colloid Interface Sci. 433, 58e67. http://dx.doi.org/10.1016/ j.jcis.2014.07.011.

15- Mohammadi, T., Kazemimoghadam, M., Saadabadi, M., 2003. Modeling of membrane fouling and flux decline in reverse osmosis during separation of oil in water emulsions// Desalination 157, 369e375. http://dx.doi.org/10.1016/S0011- 9164(03)00419-3.

16- Mondal, S., Wickramasinghe, S.R., 2008. Produced water treatment by nanofiltration and reverse osmosis membranes// J. Memb. Sci. 322, 162e170. http://dx.doi.org/10.1016/j.memsci.2008.05.039.

17-Mina Keshvardoostchokami , Mahyar Majidi , Abbasali Zamani , Bo Liu. 2021. A review on the use of chitosan and chitosan derivatives as the bio-adsorbents for the water treatment: Removal of nitrogen-containing pollutants// Carbohydrate Polymers 273, 118625. https://doi.org/10.1016/j.carbpol.2021.118625.

18-Angela M. Gutierrez, Thomas D. Dziubla and J. Zach Hilt. 2017. Recent advances on iron oxide magnetic nanoparticles as sorbents of organic pollutants in water and wastewater treatment// De Gruyter.1-7,DOI 10.1515/reveh-2016-0063

19- Souad A. Elfeky, Shymaa Ebrahim Mahmoud, Ahmed Fahmy Youssef. 2017. Applications of CTAB modified magnetic nanoparticles for removal of chromium (VI) from contaminated water// Journal of Advanced Research,35, https://doi.org/10.1016/j.jare.2017.06.002
20- Gordana Hojnik Podrepšek, Željko Knez and Maja Leitgeb, 2020, Development of Chitosan Functionalized Magnetic Nanoparticles with Bioactive Compounds, 10, 1913, https://doi.org/10.3390/nano10101913
21-Zhang, L., Zeng, Y., & Cheng, Z. (2016). Removal of heavy metal ions using chitosan and modified chitosan// A review. Journal of Molecular Liquids, 214, 175–191. https://doi. org/10.1016/j.molliq.2015.12.013
22-Zheng, Y., & Wang, A. (2009). Enhanced adsorption of ammonium using hydrogel composites based on chitosan and halloysite// J. Macromol. Sci. A, 47, 33–38. https:// doi.org/10.1080/10601320903394421
23- Rajeswari, A., Amalraj, A., & Pius, A. (2016). Adsorption studies for the removal of nitrate using chitosan/PEG and chitosan/PVA polymer composites// Journal of Water Process Engineering, 9, 123–134. https://doi.org/10.1016/j.jwpe.2015.12.002
24- Haseena, P. V., Padmavathy, K. S., Rohit Krishnan, P., & Madhu, G. (2016). Adsorption of ammonium nitrogen from aqueous systems using chitosan-bentonite film composite// Procedia Technology, 24, 733–740. https://doi.org/10.1016/j.protcy.2016.05.203
25- Misganaw Golie, W., & Upadhyayula, S. (2017a). An investigation on biosorption of nitrate from water by chitosan based organic-inorganic hybrid biocomposites// International Journal of Biological Macromolecules, 97, 489–502. https://doi.org/ 10.1016/j.ijbiomac.2017.01.066
26-Keshvardoostchokami, M., Babaei, S., Piri, F., & Zamani, A. (2017). Nitrate removal from aqueous solutions by ZnO nanoparticles and chitosan-polystyrene-Zn nanocomposite: Kinetic, isotherm, batch and fixed-bed studies// International Journal M. Keshvardoostchokami et al. Carbohydrate Polymers 273 (2021) 118625 12 of Biological Macromolecules, 101, 922–930. https://doi.org/10.1016/j. ijbiomac.2017.03.162
27- Thagira Banu, H. A., Karthikeyan, P., Vigneshwaran, S. V., & Meenakshi, S. (2020). Adsorptive performance of lanthanum encapsulated biopolymer chitosan-kaolin clay hybrid composite for the recovery of nitrate and phosphate from water// International Journal of Biological Macromolecules, 154, 188–197. https://doi.org/10.1016/j. ijbiomac.2020.03.074